On the Synthesis and Utilization of *geminal*-Dimethyl Hydroporphyrins and Tetraphenylethylenes in Photodynamic Therapy

A thesis submitted by

Harry Charles Sample, M.Chem. (Hons.), M.R.S.C.

Trinity College Dublin, The University of Dublin

A thesis submitted to Trinity College Dublin, The University of Dublin, for the degree of

Doctor of Philosophy

30th June 2022

Under the supervision of Prof. Dr. Mathias. O. Senge

and co-supervision of Dr. Lígia C. Gomes-da-Silva

I dedicate this to myself. It's nearly four years of blood sweat and tears.

A love of science and making compounds that nobody has before got me through this.

Spite is not the best motivator.

Proving people wrong should not have to become a hobby.

Learn from my mistakes.

Declaration

I declare that this thesis has not been submitted as an exercise for a degree at this or any other university and it is entirely my own work.

I agree to deposit this thesis in the University's open access institutional repository or allow the Library to do so on my behalf, subject to Irish Copyright Legislation and Trinity College Library conditions of use and acknowledgement.

Where work was carried out jointly, this is duly acknowledged in the text wherever included.

Signed: 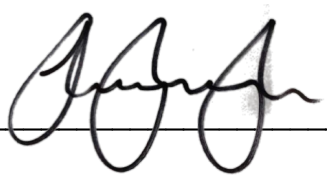

_____ (Harry Charles Sample)

June 2022 Trinity College Dublin

I. Summary

Chapter 1 introduces the main concepts of this thesis: photodynamic therapy (PDT), chlorins and photosensitizer arrays. In the case of PDT multiple topics are discussed, namely, the qualities of an ideal photosensitizer, the photochemical processes which facilitate cytotoxicity, different classes and generations of photosensitizers, and its applicability to cancer. Chlorins are introduced as the close relative to porphyrins they are. Initially, their spectroscopic differences are discussed. Following on from this, their natural origins, leading into their synthesis both from porphyrins and *via de novo* syntheses. The subject of chlorins in PDT is discussed, and why there is a need for a *geminal*-dimethyl hydroporphyrins. Lastly, the theory and prior utilization of photosensitizer arrays in PDT is discussed.

Chapter 3 focuses on the synthesis of *gem*-dimethyl hydroporphyrins **3.36a** and **3.36b**, along with their photophysical analyses to determine their suitability as PSs in PDT. This chapter provides some of the basic science that is not currently present surrounding *gem*-dimethyl hydroporphyrins. Their photophysical properties were indicative of this class of compound being a suitable core for PS generation in PDT.

Chapter 4 builds on the results presented in Chapter 3. Upon the knowledge that this core is suitable for PS generation, the system must be made more applicable to PDT through the implementation of bioconjugation handles, and more generally the implementation of motifs that aid the solubility of this class of compounds in aqueous media. Western half **4.72** was synthesized according to literature procedures, and throughout the sequence we present crystal structures of synthetic intermediates. Collection of multiple crystal structures along the synthetic pathway of organic compounds is something we believe to be good practice to assist data science investigations and offers potential insight into the electronic structure of intermediates. Further to this, we observed an unexpected diastereomeric resolution in **4.65**, an uncharacterized yet known by-product in this synthesis. Eastern half **4.71** was designed with two orthogonal bioconjugation strategies, one novel and the other sparsely utilized. With the aim of solubilizing these systems in aqueous media, the synthesis of alkyne **4.69** was attempted. Unfortunately, its synthesis was unsuccessful. We sought to broaden our study and compare the

synthesized chlorins to a series of analogous porphyrins. Photophysically all compounds presented typical spectra for their class; however, we were unable to determine a system for successfully determining the singlet oxygen quantum yield of all the desired species. *In vitro* evaluation of these five compounds exhibited stark contrasts regarding the solubility of these species, furthermore the lack of fluorescence of certain systems rendered multiple candidates non-suitable as PSs for PDT. Of the three most suitable candidates, two where chlorins. This work is the first example of *geminal*-dimethyl chlorins being utilized as PSs in PDT. Further to this it highlights the utility of sparsely substituted tetrapyrroles in PDT, however it further compounds the discussion of synthetic arduousity *vs.* photodynamic efficacy.

Chapter 5 deals with a different strategy of enhancing the efficacy of PDT. Instead of enhancing the efficacy of a single PS, Chapter 5 surrounds the generation of novel PS arrays for PDT. The scaffold utilized was 1,1,2,2-tetraphenylethylene, given its myriad application and general utility through the phenomenon Aggregation Induced Emission (AIE). We utilized BODIPYs as our PS of choice, given their synthetic ease, and well-studied utility as PSs in PDT. Through varying the distance between the TPE and BODIPY cores differing responses were observed in every property analysed. We find that the addition of an ethynyl-linker enabled the retention of the AIE phenomenon and presented the subsequent array with more possible applications in the future. Regardless, both arrays synthesized were shown to suitably generate singlet oxygen, exhibiting their utility as PSs for PDT.

II. List of Publications

1. Z. Melissari, H. C. Sample, B. Twamley, R. M. Williams, M. O. Senge, Synthesis and Spectral Properties of gem-Dimethyl Chlorin Photosensitizers, *ChemPhotoChem*, **2020**, *4*, 601–611.

2. C. J. Kingsbury, H. C. Sample, M. O. Senge, Crystal structures of 4-bromo-2-formyl-1-tosyl-1Hpyrrole, (E)-4-bromo-2-(2-nitrovinyl)-1-tosyl-1Hpyrrole and 6-(4-bromo-1-tosylpyrrol-2-yl)-4,4-dimethyl-5-nitrohexan-2-one, *Acta Crystallogr., Sect. E* **2021**, *77*, 341–345.

3. H. C. Sample, G. Emandi, B. Twamley, N. Grover, B. Khurana, V. Sol, M. O. Senge, Synthesis and Properties of BODIPY Appended Tetraphenylethylene Scaffolds as Photoactive Arrays, *Eur. J. Org. Chem.* **2021**, *29*, 4136–4143.

4. H. C. Sample, M. O. Senge, Nucleophilic Aromatic Substitution (S_NAr) and Related Reactions of Porphyrinoids: Mechanistic and Regiochemical Aspects, *Eur. J. Org. Chem.* **2021**, *2021*, 7–42.

Notes on Publications

Chapter 1 contains details from publication 1.

Chapter 2 contains details from publication 2.

Chapter 3 contains details from publication 3.

Other Publications

5. S. Y. Yap, H. Savoie, I. Renard, B. P. Burke, H. C. Sample, S. Michue-Seijas, S. J. Archibald, R. W. Boyle, G. J. Stasiuk, Synthesis of a porphyrin with histidine-like chelate: an efficient path towards molecular PDT/SPECT theranostics, *Chem. Commun.* **2020**, *59*, 11090–11093.

III. Acknowledgements

The acknowledgements section of any thesis should aim to thank all the people that have aided in the presentation of the resulting document. This is one of the few pieces of writing to which third party alterations cannot be enforced (but people can help by pointing things out, i.e., a spelling mistake, or one of many grammatical errors). Thus, this section will be rather lengthy, unapologetically so. Misty eyes incoming?

To begin, I have to go back to, well, the beginning. Not the Big Bang, that is beyond the remit of this work and, frankly, too nebulous (credit to Anthony for that one, vide infra). My career in academia started under the supervision of Professor Ross W. Boyle. Sad to say, I only became aware of the achievements he had been responsible for until midway through my Ph.D. The first meso-iodination and first intramolecular fusion of porphyrins, amongst multiple others. In my eyes, he's the Professor that had conjugated nearly every biological moiety to porphyrins. He ran his group to feel more like a family than anything else. I learnt so much from him, and his lab, lessons both brutal and exceptional. Without him, a lot of things would've been unimaginably different. I certainly wouldn't have found POLYTHEA. Thank you for everything; for giving me every chance, sharing every resource, and caring about my interests.

Throwback to July 2018, Penela. Where is that, anyway? It is where it all began. To this day, I have never delivered a presentation in such a warm room. If memory serves, I decided, rather unwisely, on a white shirt during that presentation. To this day, I'm amazed and grateful beyond words that the selection committee deemed me to be the correct candidate for one of these positions. They selected me to be ESR #6, and complete a thesis entitled 'Synthetic strategies for photo-sensitizers targeting', under the supervision of Prof. Dr. Mathias O. Senge, and Dr. Lígia C. Gomes-da-Silva. Every student wishes to be supervised by a world leader in their respective field – and I am lucky enough to have been supervised by two.

Lieber Mathias, ich weiß nicht, wie es dir geht, aber ich hatte definitiv Tage, an denen ich daran gezweifelt habe, ob ich es jemals so weit schaffen würde. Du hast dich bei diesem Projekt sehr weit aus dem Fenster gelehnt – es sei denn, du wolltest

noch einmal zurück zu deinen Wurzeln. Ist dies nur ein seltsamer Zufall oder war dies beabsichtigt? Grüne Lösungen müssen aber auf jeden Fall im Senge-Labor bleiben. Wir sind sicher nicht immer einer Meinung gewesen, aber wir konnten diese Differenzen schlussendlich überwinden. Du hast wirklich seltsame Ideen, fantastisch, aber seltsam. Ich kann es kaum erwarten, sie umgesetzt zu sehen. Ross hatte Recht, es hat mir Spaß gemacht, unter deiner Aufsicht zu arbeiten. Wer weiß, welche grün-blauen Monstrositäten wir ohne COVID und einige TPEs erschaffen hätten können. Bis zum nächsten Mal, vielen Dank Mathias.

Cara Lígia, uma vez químico sintético, sempre químico sintético? Acho que não. Pegaste num químico sintético e fizeste dele algo diferente. Foste tu quem tomou as decisões importantes e quem guiou o meu caminho. Fizeste a mudança de PC3 para 4T1, e eu apreciei incrivelmente a tua atitude sempre séria. Eu fiz PDT no teu laboratório, assunto sobre o qual eu tenho lido nos últimos seis anos, finalmente o concretizei. Eu perdoo-te por rires de 90% das minhas tentativas de falar português, e perdoo-te por rires do meu inglês extremamente expressivo. Se mantiveres alguma memória do tempo que passei no teu laboratório, espero que elas te façam sorrir exatamente do jeito que "oh, that's nice paper!" fez. Até a próxima e muitíssimo obrigado, Lígia.

To my fellow POLYTHEA ESR's: Emma Robbins, Zoi Melissari, Dr. Dáire Gibbons, Dr. João Simões, Bhavya Khurana, Dr. Nidia Maldonado-Carmona, Claire Donohoe, Piotr Gierlich, and Manuel Gallardo-Villagran; It's been a hell of a bumpy road. We (inadvertently) did a Ph.D. during a global pandemic. Crazy, but we thrived. We've been dotted all-over Europe for the past couple of years, and whilst it is unfortunate that we haven't all been able to spend as much time together, it's been a joy working alongside you all. A strange sense of comradery has befallen us; we are forever united through POLYTHEA.

To the group that hosted me for the first three years of this Ph.D.: Dr. Alina Meindl, Dr. Asterios Charisiadis, Dr. Christopher J. Kingsbury, Dr. Elisabeth Sitte, Dr. Ganapathi Emandi, Dr. Gemma Locke, Dr. Grant Strachan, Dr. Jessica O'Brien, Karolis Norvaiša, Dr. Keith J. Flanagan, Dr. Marc Kielmann, Dr. Marie Roucan, Dr. Nitika Grover, and Dr. Susan Callaghan; you are a diverse group, with backgrounds as wide reaching as your knowledge is deep. I learnt an immeasurable amount from

all of you – even if more of it was the history of British colonialism than how to safely use air sensitive reagents, for example. Joking aside, I've taken away differing mentalities in how I perform my work, and live my life as a result of our time together – in a good way.

To the current Senge group: Dr. Grant Strachan, Karolina Urbańska, Sophie Maguire, and Liam Cribbin; an incredible cohort who have kept the bar high and present a wonderful atmosphere for the group as it reforms and expands, I wish you all every success in L7.23. I look forward, with high hope and great expectations, to seeing the work that emanates from these new minds in the coming months and years.

To the others that have helped, again an enormous thank-you. John, I'm happy you enjoyed running the somewhere between 200 and too many spectra on some of my compounds. I hope the UGs liked them more than I did. Manuel, thank you for keeping the spectrometers running, in hindsight we should've crowdfunded for you to get an office in TBSI. Gary, I'm sorry my samples didn't fly. Thank you for your patience and continually endeavouring to get them to do so. Brendan, thank you for running my crystals, my first published one came from you, lest we forget. Thank you for fuelling/aiding my genuine interest in crystallography. Thanks for taking the time others wouldn't; it is more than admirable, to say the least.

It would be unfair to not credit others I have met at Trinity. I'm fortunate to have friends dotted all over the sixth and seventh floors of TBSI, along with main campus. Realistically, there are too many of you to name, but you all know who you are. Discussing everything from Kasha's rule to sulphur-containing reagents, and diastereomerism. You would never steal my work. Needless to mention the out of work activities – hampered somewhat by COVID, I spent one of my Christmases with some of you, and many other nights in the pubs of Dublin besides. Thank you for the companionship, the banter, the shoulder to cry on, and many other things besides. I hope that in years to come I can return the favours received.

I can't forget my time in Amsterdam, a truly joyous six weeks of my life made all the more pleasurable by the members of the Molecular Photonics Group. It's always a joy being able to pass on colloquial English to non-native speakers, it's quite frankly 'Unbelievable Jeff'. I'm still amazed I was trusted to use multi-million-euro laser set

ups alone, and I did so without correcting my own vision! Incredible! My time there would have been a disaster had it not been for the MolPhot group, and particularly Zoi (my other half, see Chapter 1) and Dàire: a huge thank you to both of you, and of course to Dr. René M. Williams, this all happened under your watch so 'heel erg bedankt'.

Speaking of spending time in different places, 'un grande merci beaucoup' to Dr. Benoit Habermeyer and the rest of the PorphyChem team. Thank you for hosting me, assisting me, and showing me what industry can be: it doesn't all have to be APIs. To this day, I've yet to hold 1 kg of TPP again. That's cool.

The last stop on this winding, and unpredictable road: Laboratório Fotobiologico da Universidade de Coimbra. This place provided the tranquillity, wine, coffee, and rissóis necessary to write this 'masterpiece'. There's little else I can say in addition to what I said to Lígia earlier. But there are extra acknowledgements to be had. Fábio, our photophysical wizard, I know that, reading this, you'll protest that your inclusion in this is unnecessary. I, and multiple others, beg to differ. So, to the man who gave PDT correction factors, and gave me a multitude of laughs every other day – 'muito obrigado'. To Claire, Piotr & Luís, you have all equally tolerated my inexperience and stupid questions (I know you said they weren't stupid at the time, but your facial expressions hide little) and helped me present the data I have. From telling me 'No, it's not that bad!' to 'O.K. yeah that isn't great', it's been one hell of an experience (a positive one, don't worry).

My social media escapades may have often received scoffs from colleagues, even those I've been able to help through social media. This thank-you goes to the #ChemTwitter community, and all those I've spoken to from it. Thank you for being a place to rant, to ask for help/assistance/guidance; for teaching me and entertaining me. Thank you for pictures of gigantic columns, crystals (both physical and resolved structures), anything vaguely colourful and insightful. #ChemTwitter can produce some utter dumpster fires, we all know this. But it is a community where we can all network and (if little else) admire some nice ChemScrapes.

To conclude the social media-based acknowledgements, a substantial thank you goes to the #AcademicMentalHealth community and Dr. Zoë J. Ayres. Watching this community evolve, I have learnt a lot about how to manage myself, and how to be

a better colleague. It's not something I am ashamed of admitting; I wish I'd learnt it earlier. I hope that if there are any prospective students reading this, they realize that that community is out there and that they utilize it to the greatest extent.

Last, but not least, family and friends. To Mum, Helen, Georgina, and Fudge, thank you for all listening to my rants, or just listening, really. Nobody warned me just how difficult this would be, and they probably didn't warn you either. Honestly, I'd have preferred that you didn't know how hard it was – but I guess you do. Mum, your 'Do you need to column it again?' comments will be forever etched in my brain. Helen, my second parent realistically, you've always championed me from the side-lines. Georgina, you've always reminded me to send birthday cards, Christmas cards, and let me rant no end. Fudge, you've been the cutest fluffball to exist. I know you can't read. But it would've been unfair to exclude you. You've all helped me, as a good family should. Thank you.

To finish, thank you Anthony. Doing our Masters together, you know I would've loved us to both go on and do Ph.D.'s. The movie nights and occasional hung-over mornings, the not-so-occasional screaming at insoluble porphyrins and lab-wide Metal fuelling our days. Having gone through this Ph.D., I can say I'm glad you didn't. You always had the intellect to do it, just not the self-belief. But you've seen how this has nearly broken me, and I couldn't have watched the same happen to you. It might not have, but the thought doesn't bear thinking about. Thank you for listening, for being an amazing friend. I'm sorry I wasn't a better one, just know I am forever grateful for you being here throughout this. Having written and re-read this, I can hear the Yorkshire modesty from here. Shh.

Not as long as I thought, que surpresa.

IV. List of Abbreviations and Acronyms

[X]	Concentration of species *X*
$^1O_2$	Singlet Oxygen (typically the $a^1\Delta_g$ state)
A	Absorbance
Ac	Acetyl
ACQ	Aggregation Caused Quenching
AIE	Aggregation Induced Emission
ALA	δ-aminolevulinic acid
APCI	Atmospheric Pressure Chemical Ionization
aPDT	Antimicrobial Photodynamic Therapy
APF	Aminophenylfluorescin
ARMD	Age Related Macular Degeneration
Bchl	Bacteriochlorophyll
bipy	2,2'bipyridine
BPDMA	Benzoporphyrin Derivative Monoacid Ring A
c	Speed of light
calcd.	Calculated
CAS	Chemical Abstract Services
cat.	Catalytic
CCDC	Cambridge Crystallographic Data Centre
Chl	Chlorophyll
COF	Covalent Organic Framework
CT	Charge Transfer
CuAAC	Copper(I) Catalysed Alkyne-Azide-Cycloaddition
DBPF	1,3-Diphenylbenzoisofuran
DBU	1,8-Diazabicyclo[5.4.0]undec-7-ene
DCTB	*trans*-2-[3-(4-*tert*-butylphenyl)-2-methyl-2-propenylidene]-malononitrile
DDQ	2,3-Dichloro-5,6-dicyano-1,4-benzoquinone
dec.	Decomposed
DHE	Dihydroethidium
DIPSI	Decoupling in the Presence of Scalar Interactions

DMF	*N*,*N*-Dimethylformamide
DMSO	Dimethyl sulfoxide
DPM	Dipyrromethane (see *Nomenclature*)
DSSC	Dye Sensitized Solar Cell
EDG	Electron Donating Group
EGFR	Epidermal Growth Factor Receptor
em	Emission
eq.	Equivalents
Et	Ethyl
EWG	Electron Withdrawing Group
exc	Excitation
FGS	Fluorescence Guided Surgery
g	Mass in grams
gem	Geminal
h	Time in hours
H_2TPC	17,18-dihydro-5,10,15,20-tetrakis(phenyl)porphyrin
H_2TPP	5,10,15,20-tetrakis(phenyl)porphyrin
HMBC	Heteronuclear Multiple-Bond Correlation
HOMO	Highest Occupied Molecular Orbital
Hp	Hematoporphyrin
HpD	Hematoporphyrin Derivative
h	Planck's Constant
HPPH	2-[1-hexyloxyethyl]-2-devinyl pyropheophorbide-a
HPS	1,1,2,3,4,5-Hexaphenylsilole
HRMS	High Resolution Mass Spectrometry
HSQC	Heteronuclear Single Quantum Correlation
I	Intensity
IC	Internal Conversion
IC_{50}	Inhibitory Concentration 50
*i*Pr	Isopropyl
ISC	Intersystem Crossing
IUPAC	International Union of Pure and Applied Chemistry
J	Coupling Constant (Hz)

L	Volume in Litres
LD_{50}	Lethal Dose 50
LE	Locally Excited
LED	Light Emitting Diode
LUMO	Lowest Unoccupied Molecular Orbital
M	Molar Concentration Units
m	Distance in meters
m.p.	Melting Point
m/z	Mass to Charge Ratio
m-CPBA	*meta*-Chloroperoxybenzoic Acid
Me	Methyl
Mes	Mesityl, or 2,4,6-trimethylphenyl
mg	Mass in milligrams
MHz	Mega Hertz
mL	Volume in millilitres
mM	Concentration in millimolar
MOF	Metal Organic Framework
mol%	Mole percentage
m-THPC	17,18-dihydro-5,10,15,20-tetrakis(3-hydroxyphenyl)porphyrin
n.d.	Not Determined
NBS	*N*-bromosuccinimide
*n*Bu	*n*-Butyl
NIR	Near Infra-Red
NMR	Nuclear Magnetic Resonance
NOE	Nuclear Overhauser Effect
NOESY	Nuclear Overhauser Effect Spectroscopy
OEP	2,3,7,8,12,13,17,18-octaethylporphyrin
OLED	Organic Light Emitting Diode
OTf	Triflate
P	Power (W)
PACT	Photo antimicrobial Chemotherapy
PDI	Photodynamic Inactivation

PDT	Photodynamic Therapy
PEG	Poly(ethylene glycol)
Ph	Phenyl
PL	Photoluminescence
pO_2	Partial Pressure of Oxygen
PPIX	Protoporphyrin IX or 2,7,12,18-tetramethyl-3,8-divinyl-13,17-porphyrin dipropionic acid
PPIX DME	Protoporphyrin IX Dimethyl Ester or Dimethyl 2,7,12,18-tetramethyl-3,8-divinyl-13,17-porphyrin dipropionate
PS	Photosensitizer
p-Tol	*para*-Tolyl or 4-methylphenyl
p-TsOH	*para*-Toluenesulfonic acid
PXRD	Powder X-Ray Diffraction
Q	Quartet
Q-TOF	Quadrupole Time of Flight
quant.	Quantitative
r.t.	Room Temperature
Recryst.	Recrystallized
R_F	Retention Factor
RIR	Restricted Intramolecular Rotation
RIV	Restricted Intramolecular Vibration
ROS	Reactive Oxygen Species
S	Singlet
SCXRD	Single Crystal X-Ray Diffraction
SDT	Sonodynamic Therapy
SEM	Standard Error Mean
S_n	Singlet State
SOC	Spin-Orbit Coupling
SOMO	Singly Occupied Molecular Orbital
SOQY	Singlet Oxygen Quantum Yield
SPAAC	Strain Promoted Alkyne-Azide-Cycloaddition
SPECT	Single Photon Emission Computed Tomography
T	Triplet

TBAF	Tetra(*n*-butyl)ammonium Fluoride
TFA	Trifluoroacetic acid
THF	Tetrahydrofuran
TICT	Twisted Intramolecular Charge Transfer
TIPS	Tri(isopropyl)silyl
TLC	Thin Layer Chromatography
TMPi	2,2,6,6-Tetramethylpiperidine
TMS	Trimethylsilyl
T_n	Triplet State
TNT	2,4,6-trinitrotoluene
TOCSY	Total Correlation Spectroscopy
TPE	1,1,2,2-Tetraphenylethylene
TPM	Tetraphenylmethane
$TPPF_{20}$	5,10,15,20-tetrakis(2,3,4,5,6-pentafluorophenyl)porphyrin
Ts	Tosyl, or *para*-Toluenesulfonyl
TsCl	*para*-Toluenesulfonyl chloride
µL	Volume in units of microliters
µM	Concentration in units of micromolar
UV	Ultra-Violet
v/v	Volume to Volume Ratio
vic	Vicinal
vis	Visible
W	Watts
WHO	World Health Organization
λ_x	Wavelength of process *x*
τ_Δ	Singlet Oxygen Lifetime (s)
≈	Approximately
α/Cα	α-position (see Nomenclature)
Å	Angstrom
Ax(λx)	Absorption of species X at wavelength x
β/Cβ	β-position (see Nomenclature)
Δ	Change in
δ	Chemical shift (ppm)

ε	Molar Extinction Coefficient (M-1cm-1)
meso/Cm	meso-position (see Nomenclature)
meta	1,3-disubstituted aromatic system
ortho	1,2-disubstituted aromatic system
para	1,4-disubstituted aromatic system
SOQY or ϕ_{Δ}	Singlet Oxygen Quantum Yield
ϕ_{F}	Quantum Yield of Fluorescence

V. Nomenclature

The nomenclature in the presented thesis is in line with nomenclature in the requisite fields, and inherently therefore different to CAS and IUPAC numbering systems, in some cases. Presented in Figures I and II below is the nomenclature that will be used throughout.[i,ii,iii]

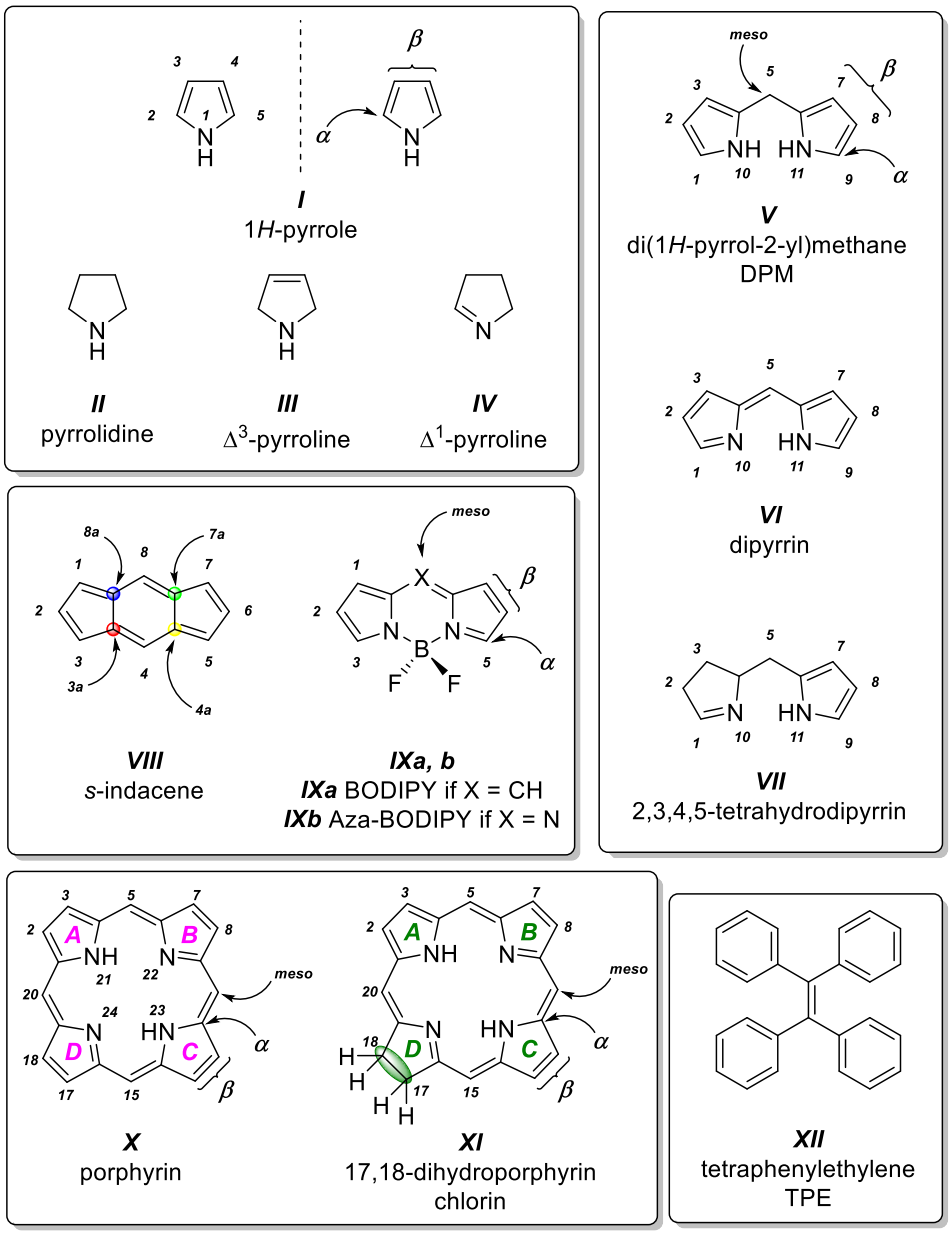

Figure I. Nomenclature of relative motifs used throughout the thesis. Positive and negative charges on the *N*[4a] and *B*[4] respectively are implied in **IXa,b** and have been excluded for clarity.[i,ii,iii]

The nomenclature of pyrroles, and pyrrolidines, remains unchanged from undergraduate level organic chemistry. The introduction of differing pyrrolines being

the only major distinction, with the Δ^1 species (**IV**) exhibiting a double bond between N^1-C^2 whereas the Δ^3 species (**III**) exhibits a double bond between C^3-C^4. The C^2 and C^5 positions of pyrrole (**I**) are labelled as the alpha/α-positions and the C^3 and C^4 positions are labelled as the beta/β-positions.

Non-direct linking of two pyrrole units produces a variety of species – obviously upon experimental conditions, *vide infra*. The joining of two pyrrole moieties, each by the α-positions, to a methane (-CH_2-) bridge yields di(1*H*-pyrrol-2-yl)methane (**V**). In the case of **V**, this is actually the name of the compound presented but more typically this class of compounds is referred to as 'dipyrromethanes' (abbreviated to DPM). In this case, the free α-positions are the 1 and 9 positions whereas the β are the 2,3,7 and 8 positions.

If the linkage is instead a methene (-CH-) bridge, the name changes to dipyrrin (**VI**). Older literature may refer to this class of compounds as 'pyromethenes'. This name will not be used herein, it is provided purely for historical context. Whilst **V** is symmetrical, **VI** is not and thus the numbering system in changes due to the higher oxidation state of one of the *N*-atoms, and thus the numbering starts on this ring (possessing the imine functionality) in an anti-clockwise fashion. Regardless of dipyrrin, or DPM, the 5-position is labelled as the 'meso' and the labelling for the types of pyrrolic positions (α and β) remains continuous. Lastly, **VII** is a motif that will be heavily discussed herein, a 2,3,4,5-tetrahydrodipyrrin.

DPMs and dipyrrins can be transformed into boron-dipyrromethenes or, more typically, BODIPYs (**IXa**). These 'BF_2-chelates' of dipyrrins take their name and nomenclature from the *s*-indacene scaffold (**VIII**). The expanded name for 'BODIPY' is 4,4-difluoro-4-bora-3a,4a-diaza-*s*-indacene. An analogous system is the Aza-BODIPY (**IXb**). Whilst not directly synthetically accessible from DPMs, nor dipyrrins, there is still a tricyclic heteroaromatic core, i.e., they are highly analogous.

Tetraphenylethylene, **XII**, and derivatives thereof are in contrast rather simplistic moieties, in terms of nomenclature at least, and thus warrant no discussion but are presented for completeness.

The structure of the simplest porphyrin (occasionally called 'tetraphyrin[1.1.1.1] where the numbers donate the amount of carbon atoms between two pyrrolic units), porphine, is represented as **X** (Figure I) in the metal free form (or free base) for

clarity. The four pyrrole rings are labelled *A*, *B*, *C*, and *D* starting in the top left, proceeding in a clockwise fashion around the macrocycle. In all cases herein, the *A*-ring of the tetrapyrrole will represent the 'true pyrrolic ring'. *meso*-positions are labelled as the 5, 10, 15 and 20 positions respectively, with the 2, 3, 7, 8, 12, 13, 17, and 18 positions as the β. The NH-units in the core are labelled first, i.e., 21 and 23 respectively with imines at 22 and 24 positions, travelling around the inner core in once again a clockwise fashion. As to retain the [18]π electronic pathway of these tetrapyrroles, the α-positions must remain undisturbed and fully conjugated, however for completeness these are numbered 1, 4, 6, 9, 11, 14, 16, and 19.

The numbering for porphyrins and hydroporphyrins differ minimally in this thesis, but greatly within the confines of IUPAC and CAS numbering. Other numbering schemes are not presented herein as to mitigate confusion. The numbering for the following discussions is analogous to that presented in Figure I.

Porphyrins which have been reduced are broadly labelled 'hydroporphyrins', in an analogous manner to the comparison between furan and tetrahydrofuran (THF). If a single meso position is reduced, the compound is named a phlorin (**XVI**, Figure II). If two meso positions are reduced, the species is then a porphodimethene, either a 5,10- or 5,15-species (**XIII** and **XIV** respectively). Further reduction of *meso* positions yields a porphyrinogen, **XVa**, an intermediate ubiquitous in porphyrin syntheses. If instead, the meso-positions are not merely reduced but possess non-H atoms, then the structure is termed a calix[4]pyrrole, **XVb**. These species can be grouped as '*meso*-reduced hydroporphyrins'.

What has yet to be addressed is the fact that a phlorin (**XVI**) is also a dihydroporphyrin, and in this case tautomerization can occur between phlorins and chlorins (**XI**) (green highlight, Figure II). This relationship 'links' the two otherwise vastly different sets of hydroporphyrins.

Naturally occurring β-reduced hydroporphyrins are typically represented with the first reduced ring in the lower left-hand corner, per historic convention. Literature in this field still follows the same convention, i.e., dictates that the reduced ring is in fact the *D*-ring, and that is what is presented herein.[iv]

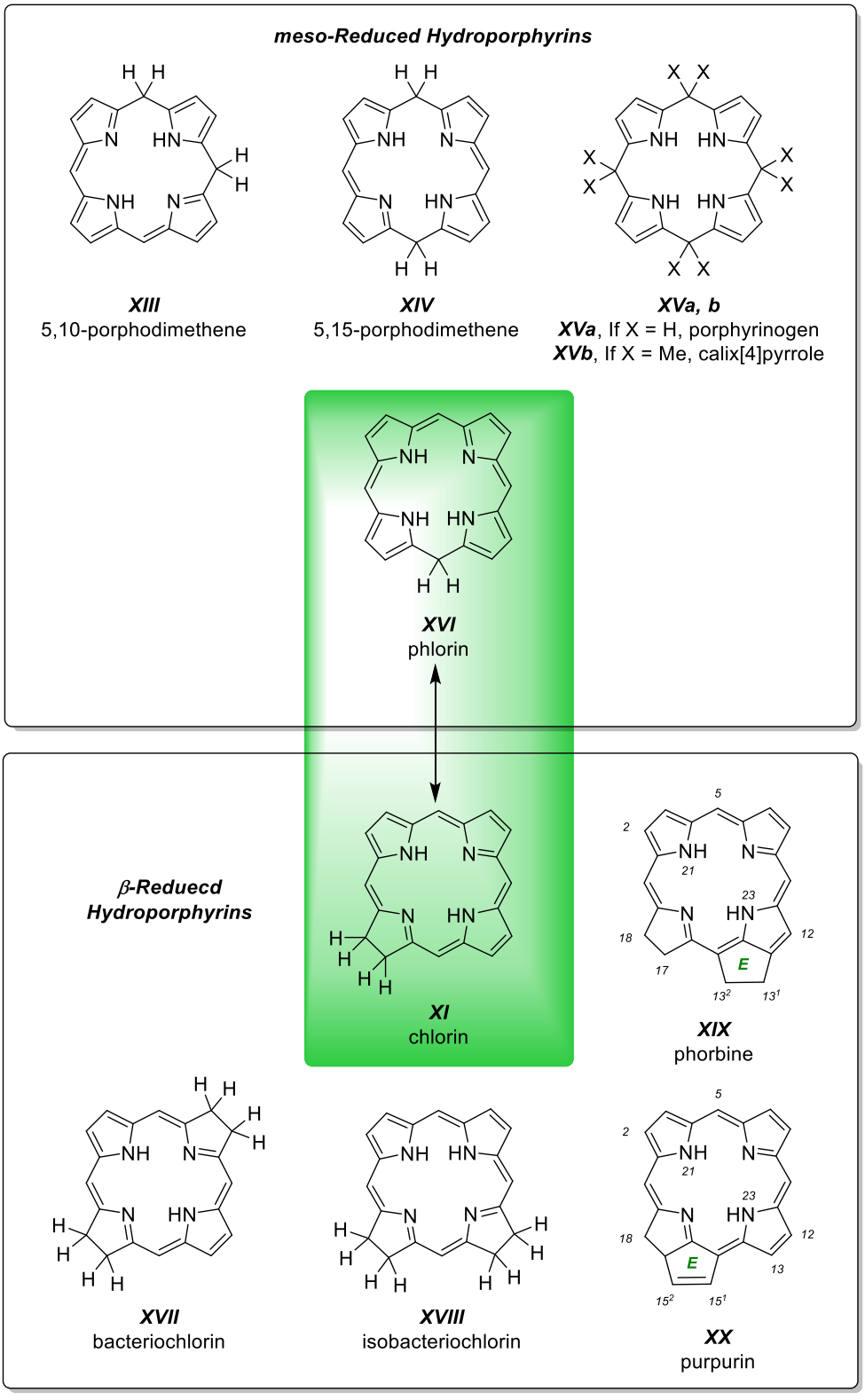

Figure II. Nomenclature of meso- and β-reduced hydroporphyrins, displaying the tautomeric relationship between phlorins (**XVI**) and chlorins (**XI**).

Reduction of a porphyrin at the β-positions yields a chlorin, **XI**, which is drawn in the/as the *D*-ring with the reduction occurring at the 17 and 18 positions – in spite

of CAS & IUPAC nomenclatures. Reduction of the subsequent β-positions in the *B*-ring (12 and 13 positions) then yields a bacteriochlorin, **XVII**, Figure II. Lastly, reduction of two adjacent pyrrole rings yields an iso-bacteriochlorin, **XVIII**. Presentation of the structures of isobacteriochlorins is inconsistent and varies between publications with apparent reduction of the *B*- and *C*- or *C*- and *D*-rings. Regardless, the relationship between reduction of rings adjacent, or opposite, to one another defines their properties and name therefrom.

Other structure types of great importance when discussing natural hydroporphyrins are phorbines (**XIX**), and purpurins (**XX**). The term purpurin has multiple definitions, *vide infra*, however in this thesis purpurins refer to 17,18-dihydrocyclopenta[*op*]porphyrins. Phorbines are further reduced, and are instead 13^1,13^2,17,18-tetrahydrocyclopenta[*mn*]porphyrins, where the 13^1 and 13^2 positions are part of the exocyclic *E*-ring (Figure II, bottom). For purpurins, the exocyclic ring (again labelled as the *E*-ring) possesses the 15^1 and 15^2 positions.[ii,iii]

The aim of this section is to introduce the reader to the nomenclature presented in the thesis herein and it is not intended to replace the wealth of literature already surrounding the subject. The readers are directed to the appropriate references.[i,ii,iii,iv]

VI. Table of Contents

1. Introduction

1.1 – Photodynamic Therapy (PDT)

1.1.1 Photodynamic Therapy: A Brief Walk Through A Photosensitive Past

Photodynamic therapy (PDT) is a treatment characterized by the administration of a photo-active dye, photosensitizer (PS), and light of a suitable wavelength with the aim of destroying diseased or unwanted tissue, such as tumours.[1,2] The use of a PS with the aim of destruction of bacteria,[3,4] fungi,[5] or viruses,[6] however, whilst utilizing identical concepts, typically comes under the headings of photodynamic antimicrobial chemotherapy (PACT), or photodynamic inactivation (PDI).

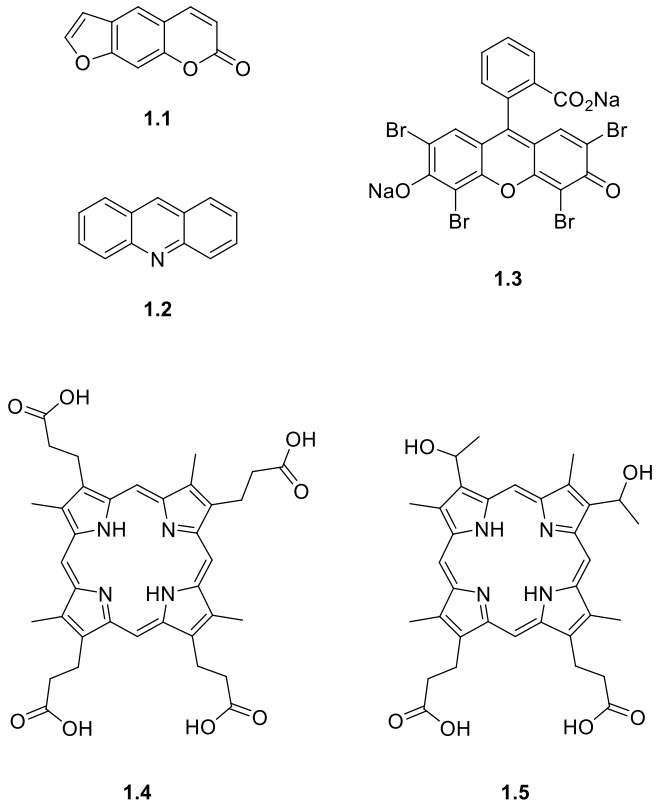

Figure 1.1: Structures of historically relevant compounds in PDT and PDI.

Understandably an abstract concept at first, however, PDT has been utilized since the building of the Great Pyramids of Giza. The Ancient Egyptians orally consumed plants growing on the banks of the River Nile, *Ammi majus*, containing psoralens (**1.1**, Figure 1.1) in their treatment of vitiligo.[7] This utilization of psoralens for the treatment of vitiligo is now accepted worldwide.[2] In 1900, Raab described the killing of *Paramecia* upon incubation with acridine dyes (**1.2**) and irradiation.[8] In the first example of oncological PDT, von Tappeiner treated a skin cancer with topically

applied eosin (**1.3**) and visible light.[9] In the same year, Finsen displayed the treatment of *Lupus vulgaris* through the photodynamic inactivation of *Mycobacterium tuberculosis*, *via* photosensitization of endogenous coproporphyrin III (**1.4**).[10,11,12] For this work, he was awarded the 1903 Nobel Prize in Physiology or Medicine "whereby he has opened a new avenue for medical science".[13] In one of the most infamous incidents in the history of PDT, Meyer-Betz self-administered 200 mg of hematoporphyrin (**1.5**), whereupon he experienced extreme photosensitivity for 8–10 weeks post treatment.[14] The true list of historical events in the world of, more loosely, phototherapy would constitute an encyclopaedia all of its own; however, comprehensive lists have been presented previously.[15]

1.1.2 Photodynamic Therapy: Underlying Principles

At its very core, PDT requires three elements to be successful:

1. A suitable PS
2. Light which can excite the PS
3. Molecular dioxygen (O_2)

A seemingly simple list at first glance, if one of these conditions is not fulfilled PDT is subpar or entirely unsuccessful. Given the depth and history of PDT, criteria for a perfect PS for oncological applications have been listed multiple times previously;[16,17]

A. Strong absorption in the red/near-infra-red (NIR) part of the electromagnetic spectrum (600 nm < λ < 800 nm)

B. High quantum yield of triplet formation (where $E(T_1) > 94.7$ kJ mol^{-1})

C. High singlet oxygen quantum yield (SOQY or Φ_Δ)

D. Low dark toxicity

E. Simple formulation of the drug and long shelf life

F. Selective tumour uptake and rapid clearance from the body

G. Facile synthesis of a single isolable molecule from readily available starting materials

H. Options for facile derivatization to introduce improvements

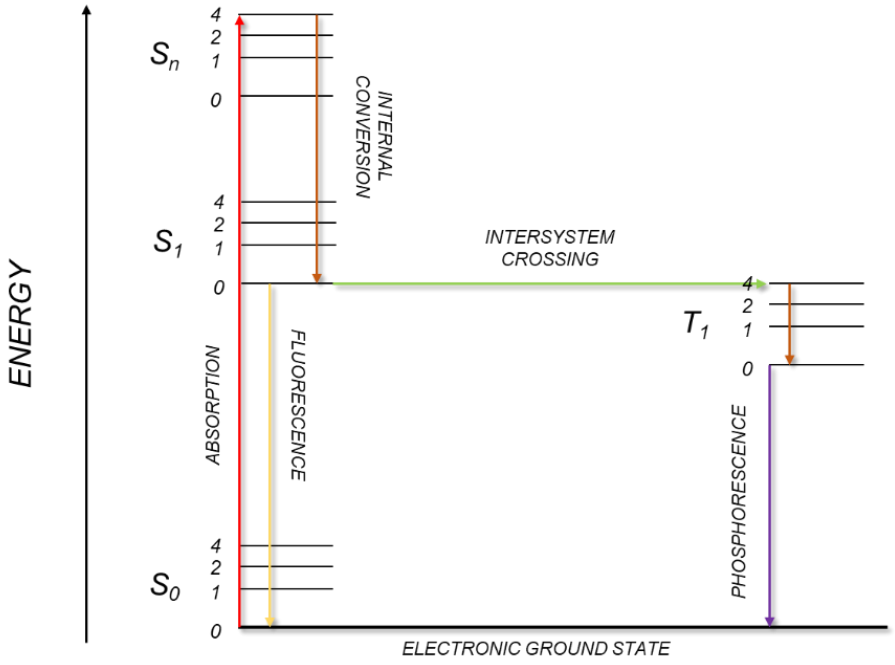

Figure 1.2. Simplified Jablonski diagram displaying the main photochemical processes occurring upon excitation of a PS; absorption (red arrow), internal conversion (bronze arrow, IC), fluorescence (yellow arrow), intersystem crossing (green arrow, ISC) and phosphorescence (purple arrow). Vibrational levels are shown to allow visualization of internal conversion. Rotational energy levels, and non-radiative decay pathways have been omitted for clarity.

Given the truly interdisciplinary nature of PDT, these requirements can all be influenced at different points in the development of the drug. For example, *A*, *B*, and *C* can only be determined *via* detailed photophysical analyses. *D*, *E*, and *F* require detailed biological evaluation. Lastly, *G* and *H* are influenced by the synthetic chemist/s that designed the molecule in question. It must be noted herein that there are distinct differences in requirements for PSs which are to be utilized in PDT for cancer, as opposed to PACT.[18]

Light which can excite the PS is arguably the most essential criteria (Figure 1.2), except the necessity for a PS. Without generation of the excited state of the PS, there is no PDT, instead there is dark cytotoxicity. There are two types of photochemical reaction that can occur from the first triplet excited state (T_1) of a PS. Without molecular oxygen, generation of excited state radical PSs can cause cellular death via Type I reactions. In contrast, Type 2 reactions occur via an energy transfer from the T_1 state with molecular oxygen to produce singlet oxygen (Figure

1.3). It must be noted that whilst the wavelength of absorption of a PS is an important topic in anti-cancer PDT, for PACT this consideration is of lesser importance, and instead the efficiency of the generation of the T_1 state takes importance.

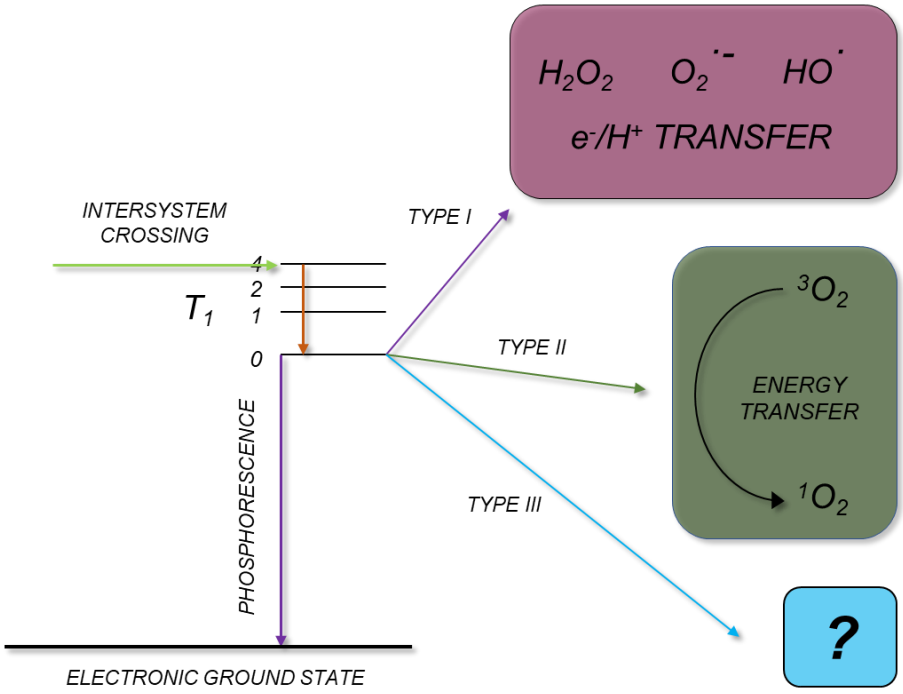

Figure 1.3. Reactions that occur from the first excited triplet (T_1) state of the PS which result in $^1O_2$ (type II) and other ROS (type I) that can cause intracellular damage and eventually lead to cell death. The species in question are highlighted in coloured boxes for each different process.

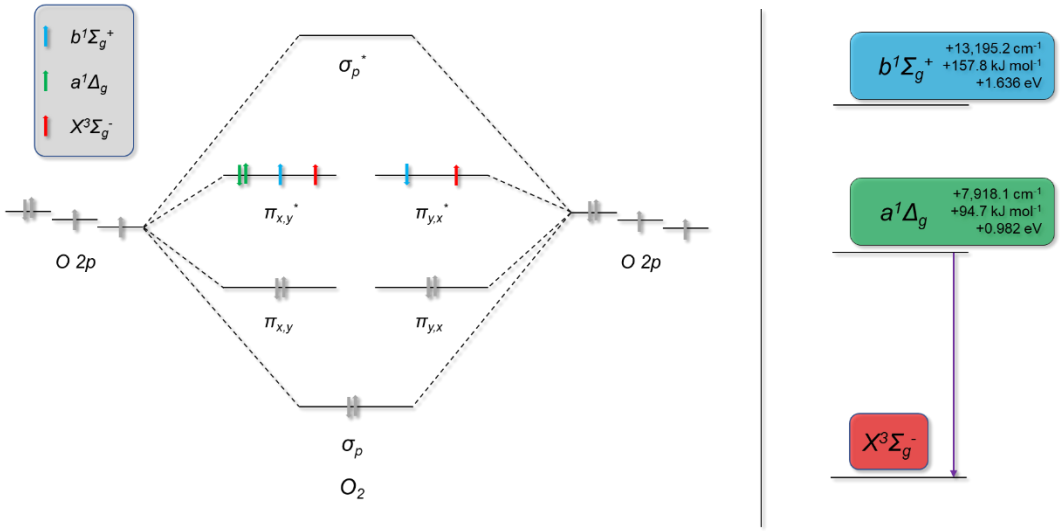

Figure 1.4 Molecular Orbital diagram for molecular dioxygen displaying the electronic configurations of the 3 possible electronic states; ground state $X^3\Sigma_g^-$ (red), and excited states $a^1\Delta_g$ (green) and $b^1\Sigma_g^+$ (blue). The a → X transition has been highlighted in purple for clarity, *vide infra*. Values presented herein are for an unperturbed O_2 molecule.[19]

One of the most toxic components of PDT is derived from the article necessary for life: molecular dioxygen.[20] The oxygen that living things use to respire, and plants produce in photosynthesis is something arguably forgotten about on a daily basis. A peculiar molecule in some ways – existing preferentially in a spin-triplet ground state ($X^3\Sigma_g^-$), research on O_2 and energetic states thereof began with the Schumann-Runge bands.[21] The initial definition of the energy levels we know of within O_2 today was given by Mulliken in 1928,[22] and further updated, again by Mulliken, in 1932.[23] Eventually, Mulliken won the Nobel Prize in 1966 “for his fundamental work concerning chemical bonds and the electronic structure of molecules by the molecular orbital method”.[24]

As observed in Figure 1.4, O_2 has two low-lying excited states: the $a^1\Delta_g$ and the $b^1\Sigma_g^-$ which are at 94.7 kJ mol^{-1} and 157.8 kJ mol^{-1} above the ground state respectively (for an unperturbed O_2 molecule).[19] In both gas and solution phases it is observed that the a ← b transition is much faster than the X ← a transition,[25] and thus, typically when referring to ”singlet oxygen” in PDT the reactive species being referred to is the $a^1\Delta_g$ state. Described by Kasha as “the electronic transition that is most forbidden in nature”,[26] the half-life of the *a* state has been reported in the range of 64–72 mins in the unperturbed molecule. Both a and b states of $^1O_2$ are highly reactive, and there are classical examples in both chemical and biological settings which exemplify this (Scheme 1.1).

Whilst it may seem that $^1O_2$ appears to be a “wild” species, with an inherent inability to be tamed, it has been successfully used in a multitude of syntheses. The first report of the use of $^1O_2$ in a synthetic context was in the Foote-Wexler reaction, for the oxidation of olefins, furans, and cyclopentanones.[27] The seminal publication exemplified the ”ene”, [4+2] and, [2+2] reactivity of $^1O_2$ observed and utilized since.[27,28] Whilst $^1O_2$ has been observed to oxidize olefins, it has also been utilized in the oxidation of thioethers to sulfoxides,[29] and phosphines to phosphine oxides, (Scheme 1.1).[30] Although a catalogue of results exists for the use of $^1O_2$ in chemical syntheses, it is described as ”still a relative newcomer”.[28]

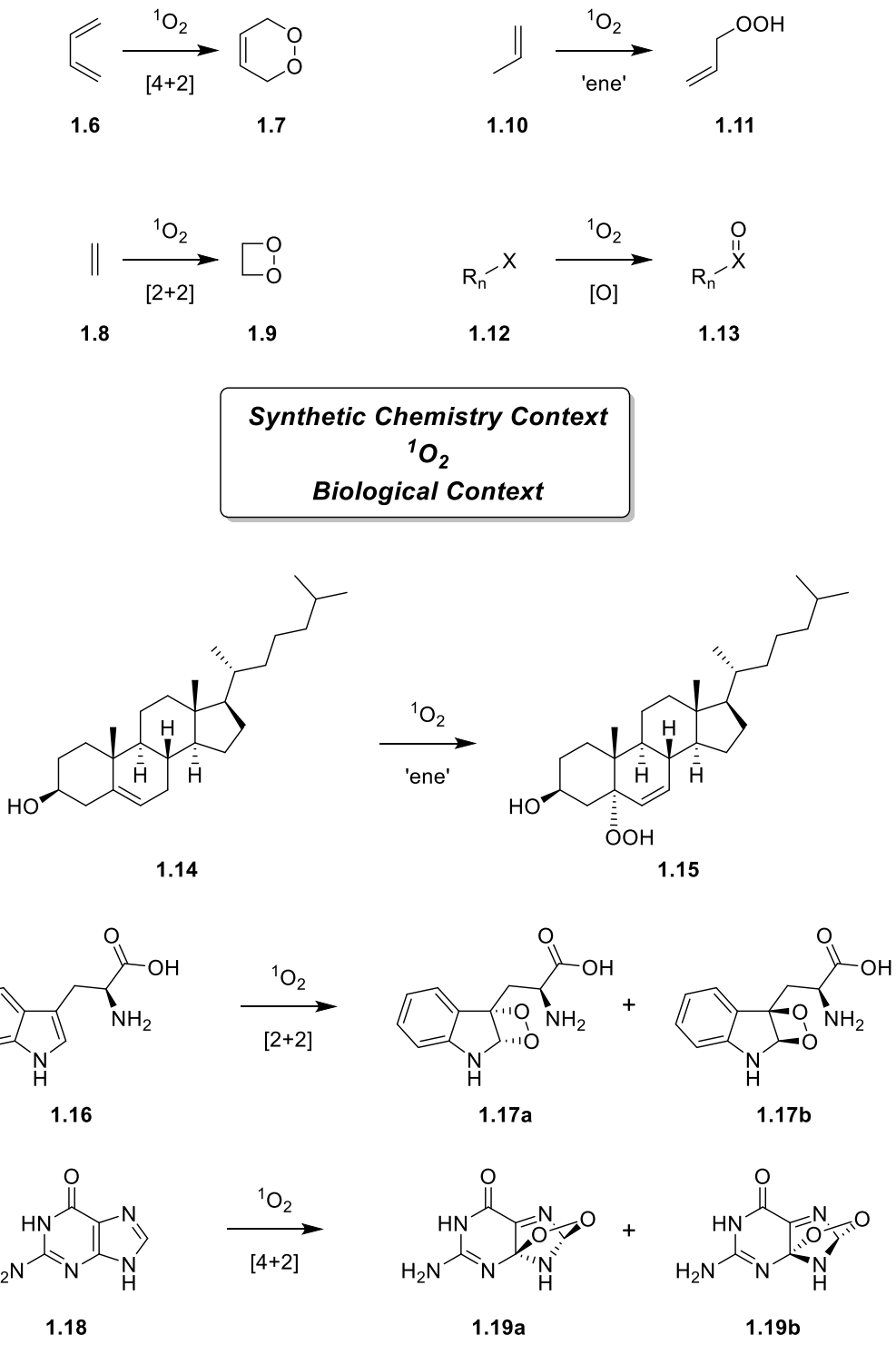

Scheme 1.1.Reactions of $^1O_2$ with synthetically useful reactions (top, **1.6** → **1.13**) and observed reaction products from PDT induced $^1O_2$ sensitization (bottom, **1.14** → **1.19b**). X = S, P, and R = alkyl, aryl.[27,28,29,30,36,36,37]

In the context of PDT, however, there is a desirability for the $^1O_2$ to remain untamed, and damage cellular components, or organelles, within its close vicinity. The distance travelled by $^1O_2$ within the cell is difficult to calculate. Factors including the

diffusion coefficient of $^1O_2$, D, and the lifetime of $^1O_2$, τ_Δ, amongst others. In a very broad assumption, it could be proposed that the distance $^1O_2$ can travel (d) is equal to:[31]

$$d = \sqrt{30\tau_\Delta D} \quad \ldots\ldots\ldots\ldots \boldsymbol{Eq.1.1}$$

Realistically, cells are not homogenous and thus equation 1 is an improper method to determine $^1O_2$ distance travelled. Instead, photobleaching experiments and extrapolation of data from model systems indicate τ_Δ = 10–320 ns.[32,33] The distance travelled by $^1O_2$ has been proposed to be 10–55 nm by Dysart and Patterson.[34]

Different parts of the cell will contain different molecules, in the broadest sense, and these different types of molecules undergo differing reactions with $^1O_2$. Three typical examples of PDT-induced $^1O_2$ sensitization include the reactions of cholesterol, tryptophan, and guanine. Cholesterol undergoes an “ene” type of reaction to produce the 5α-OOH adduct,[35] **1.15**, as shown in Scheme 1.1. In contrast, tryptophan undergoes a [2+2] reaction with $^1O_2$ to form mixtures of adducts **1.17a** and **1.17b**,[36] and a similar stereoselectivity issue is observed upon the reaction of guanine with $^1O_2$ yielding **1.19a** and **1.19b**.[37] This, therefore, indicates that destruction of cellular material/components occurs – independent of the region in which $^1O_2$ is produced. Recently, Senge and Callaghan exemplified the ability to control and thus successfully utilize $^1O_2$ for PDT.[38,39] Through the utilization of *N*-substituted 2-pyridones on the meso-positions of their porphyrins, they were able to capture $^1O_2$ via [4+2] cycloaddition, and release it upon heating the system to 40 °C.[39]

From the prior discussion regarding $^1O_2$, it is evident to see the ”Achilles’ heel” of PDT is hypoxia. Hypoxia is the term used to describe tissue with an insufficient oxygen supply, regardless of the reason for the low oxygen content. With a lack of oxygen, there is a lack of reactive oxygen species (ROS), i.e., $^1O_2$, superoxide and peroxide radicals and ions. In 2010, Allison and Sibata proposed a Type III mechanism for PDT, i.e., oxygen independent PDT, a system in which the excited state of the PS can effectively transfer energy to cellular organelles/biological material and facilitate cellular death therefrom.[40]

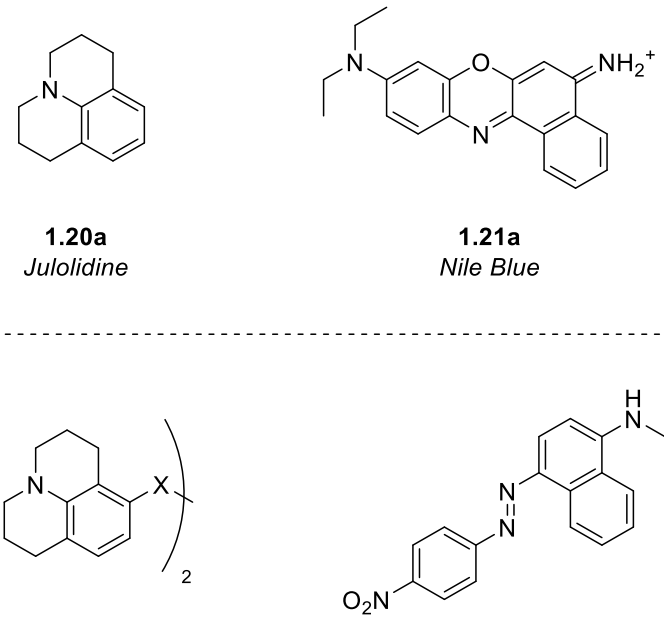

1.20a
Julolidine

1.21a
Nile Blue

1.20b, X = S
1.20c, X = Se
1.20d, X = Te

1.21b

1.22a, X = O
1.22b, X = S
1.22c, X = Se
1.22d, X = Te

Scheme 1.2 Synthesis of Type-III PSs (**1.22a**-**d**)via the combination of the julolidine core (**1.20a**) with the Nile Blue framework (**1.21a**) and subsequent heteroatom swapping as to improve the singlet oxygen quantum yield, Φ_{Δ}.[41,42] Sulphate counterion for **1.21a** omitted for clarity.

Recently, the first examples of a series of PSs capable of this Type-III mode of action were reported. This set of PSs were designed using desired properties present in two separate motifs; the julolidine moiety (Scheme 1.2, **1.20a**) is a sterically bulky electron donating amine which itself has a wealth of uses,[43,44,45] and Nile Blue (Scheme 1.2, **1.21a**) a visible dye (λ_{max}(EtOH) = 626 nm) which is once again a well-used system.[46] The authors utilized, what they call, the “door-bolt” mechanism,

whereby due to the steric bulk of the julolidine unit the synthesized probes cannot fit in the space between the double strands present in DNA, but they can fit into a ”spacious RNA pocket”.[41] This selectivity coupled with heightened RNA levels in cancer cells can therefore, loosely, be described as selectivity. Coupled with this, the swapping of the oxygen atom to a heavier analogue in the Nile Blue core (or more generally the phenoxazine motif) decreases the S_1-T_1 energy gap, heightening ISC, and enabling further reactivity from the T_1 excited state (through heightened T_1 population) enabling further cellular damage.[42] Whilst this is a promising initial report, further research must be done in order to understand the true action of the PS in these instances, and if it is possible to incorporate this Type-III reactivity into pre-existing PS-core structures as to remove the blight to PDT that hypoxia is.

1.1.3 Photodynamic Therapy: Classes of Photosensitizer (PS) – The PS Zoo

Given the criteria set out at the beginning of Section 1.1.2, it is evident to see that multiple types of compounds can fulfil at least some of these criteria and subsequently trailed for their efficacy concerning PDT. Within the introduction multiple PS family types have already been introduced.

Tetrapyrrolic PSs (**1.4** and **1.5**, Figure 1.1 as well as **1.23**, **1.24**, **1.25**, **1.26**, Figure 1.5) possess many defining characteristics that make them suitable PSs. Namely, this class of chromophores are extraordinarily absorbent in the visible region and are able to generate $^1O_2$. The syntheses of these can vary anywhere from exceedingly simple to extraordinarily difficult. To generate symmetric porphyrins, chlorins, bacteriochlorins or phthalocyanines may take only one (porphyrin, phthalocyanine) or two steps (chlorin, bacteriochlorin). Unfortunately, it is likely that symmetric tetrapyrroles of this nature are unsuitable for PDT for multiple reasons. Such is the extent of their success that the majority of publications on the subject surround PSs of these cores. A discussion on the syntheses of the cores of **1.23** and **1.24** along with their utility as PSs will be presented *vide infra*.

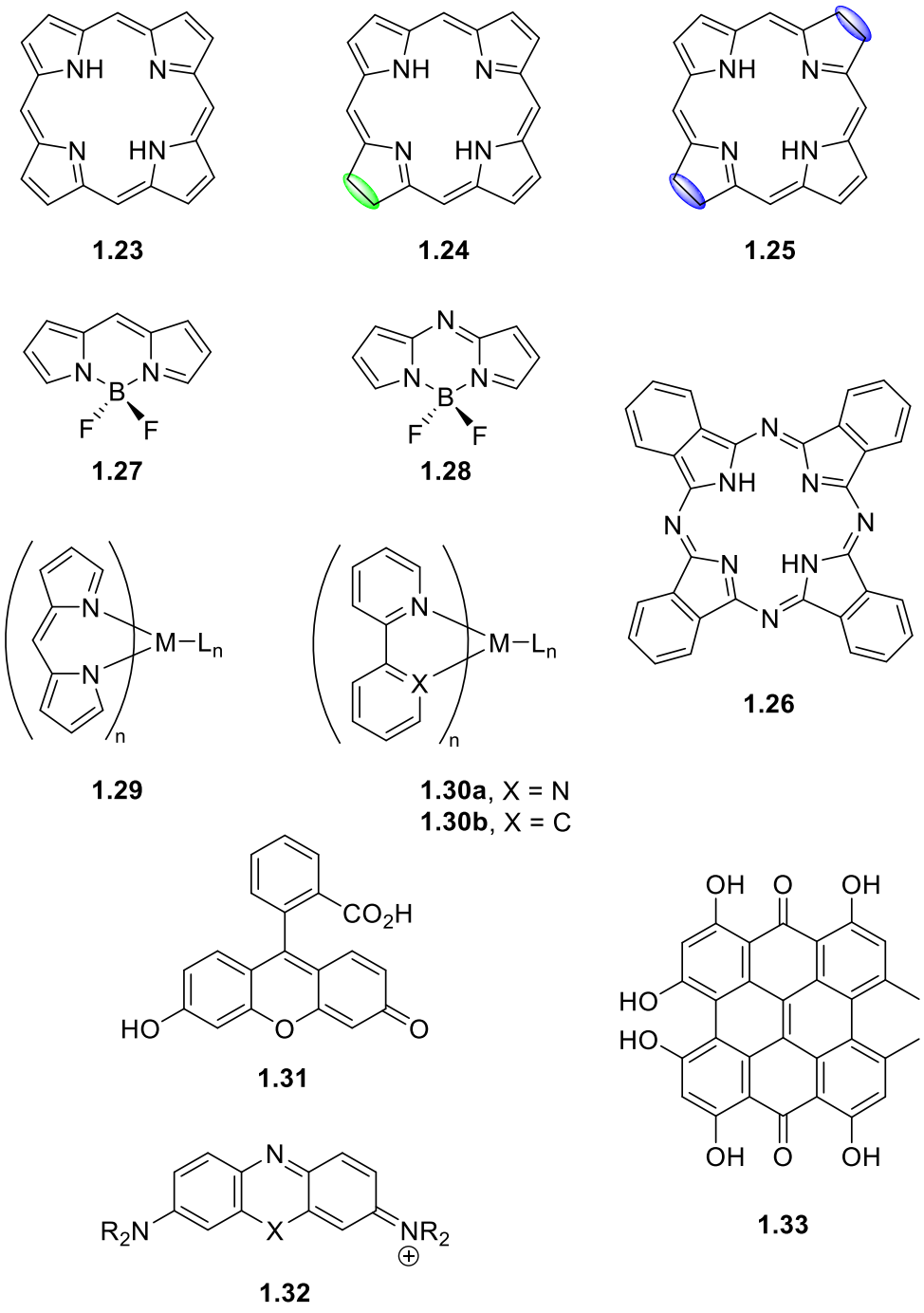

Figure 1.5. Core structures of common PS families: porphyrin (**1.23**), chlorin (**1.24**), bacteriochlorin (**1.25**), phthalocyanine (**1.26**), BODIPY (**1.27**), aza-BODIPY (**1.28**), (dipyrrinato)metal complexes (**1.29**), metal-bipyridine/phenylpyridine complexes (**1.30**), xanthene dyes (**1.31**), phenoxazine/phenothiazine (**1.32**), and hypericin (**1.33**). Porphyrin, chlorin, bacteriochlorin, and phthalocyanine have been shown as their free base structures. All compounds have been shown with minimal substitution for clarity. For **1.32**, R = alkyl.

BODIPY (**1.27**) and Aza-BODIPY (**1.28**) cores can be grouped given that they are both heteroatomic variants of the *s*-indacene core (for clarification see

Nomenclature) and differ mostly in their syntheses. Whilst BODIPYs can be synthesized in either 1- or 2-pot procedures consisting of only three steps each, Aza-BODIPYs require the synthesis, and isolation of three intermediates, and are synthesized over four steps. As a result of the meso-*N* in **1.28**, the substitution patterns obviously vary, but the same groups can be effortlessly installed. Both **1.27** and **1.28** undergo proto-deborylation in acidic media. The major difference between the two structure types is a (roughly) 100 nm change in the wavelength of absorption, with aza-BODIPYs exhibiting a longer wavelength of absorption dependent upon the electronic nature of the substituents along with solvatochromism.

Phthalocyanine (**1.26**, Pc) and derivatives thereof are tetrabenzo[*b,g,l,q*]-5,10,15,20-tetraazaporphyrins. Synthesized through the tetramerization of phthalonitriles (or other analogous materials e.g., phthalonitriles, diiminoisoindoles) their complexity more often than not arises from the modification of the original phthalonitrile. These compounds have an intense absorption in the red region of the spectrum. Recently, their characteristics and promise as PSs for PDT was outlined in great detail.[47]

Metal dipyrrinato complexes (**1.29**) are similar to BODIPYs (**1.27**), however, differing in the moiety being chelated by the dipyrrin ligand. Dipyrrins alone are typically yellow in both solid and solution state, and present an absorption band of low intensity around 450 nm. The recent developments in the field of dipyrrinato metal complexes was recently summarized.[48,49]

Metal polypyridyl and phenylpyridyl complexes (**1.30a**,**b**) have recently found some success in PDT. Notably the development of TLD1433,[50] a heteroleptic polypyridyl-dipyrido[3,2-a:2′,3′-c]phenazine ruthenium(II) complex, has gone someway to rattle the PDT community, as the first ruthenium complex to successfully enter clinical trials. Further to the field of this class of compounds in PDT, in recent years the Gasser group have continually pushed the field of $[Ru(bipy)_3]^{2+}$ PSs for PDT.[51] In 2020, Senge & Wiehe examined the utility of heteroleptic (dipyrrinato)iridium(III) complexes towards *S. Aureus*, amongst other bacterial strains, and multiple complexes were found to be promising PACT agents.[52]

Xanthene dyes (**1.31**) are more typically used as fluorescent tags in the modern day, as opposed to PSs,[53] excluding their use in blood sterilization,[54,55,56] despite the initial breakthrough with the use of eosin (**1.3**) in the clinic. In saying this however, rose bengal has found distinct popularity for aPDT in particular.[57] Analogous to xanthenes are rhodamines, and these again have been greatly investigated in recent years as fluorescent probes, as well as some investigation into their PDT efficacy.[58] In a similar vein, phenoxazine/phenothiazine PSs (**1.32**) have found greater applicability to aPDT than the oncological variant. Notable in this category are methyl- and toluidine-blue which are both routinely analysed with regards to their utility against Gram-positive and Gram-negative bacteria.[59]

Arguably a distinctly different structure, hypericin (**1.33**) is a naphthodianthrone. Despite first appearances, it is naturally produced by plants in the genus *Hypericum*, particularly *Hypericum perforatum*.[60] Its phototoxicity has been well studied, and efforts are ongoing to synthesize derivatives that modify its solubility and enhance its capability as a PS.[61,62]

There are points to be drawn from these structure types even from an initial glance: lower molecular weight/smaller systems are more likely to be internalized by any cancer cells to a higher degree than larger motifs. Further to this is the principal of heavy metal toxicity. Despite the success of TLD1433, *vide supra*, it is the only ruthenium-based drug to make any headway in PDT. Another point can be drawn from the UV-Visible absorption spectra of these compounds.

Compounds **1.21**, **1.26**, **1.31**, and **1.34**–**1.39** present genuine examples of PS core structures (Figure 1.6). Whilst it could be seen that this is an ill-though-out mixture of synthetic dyes and biologically relevant pigments, the utility of protoporphyrin IX dimethyl ester (**1.37**, or PPIX DME) has been unequivocally stated previously.[63,64] Chlorophyll *a* is lesser used, but other chlorins derived from natural pigments, e.g., chlorin e_6 have found great applicability to PDT. Compound **1.39** presents possibly an even more successful core structure with TOOKAD® being used for low-risk prostate cancer.[65] Solvatochromism between compounds and spectra can be disregarded for the statements which follow.

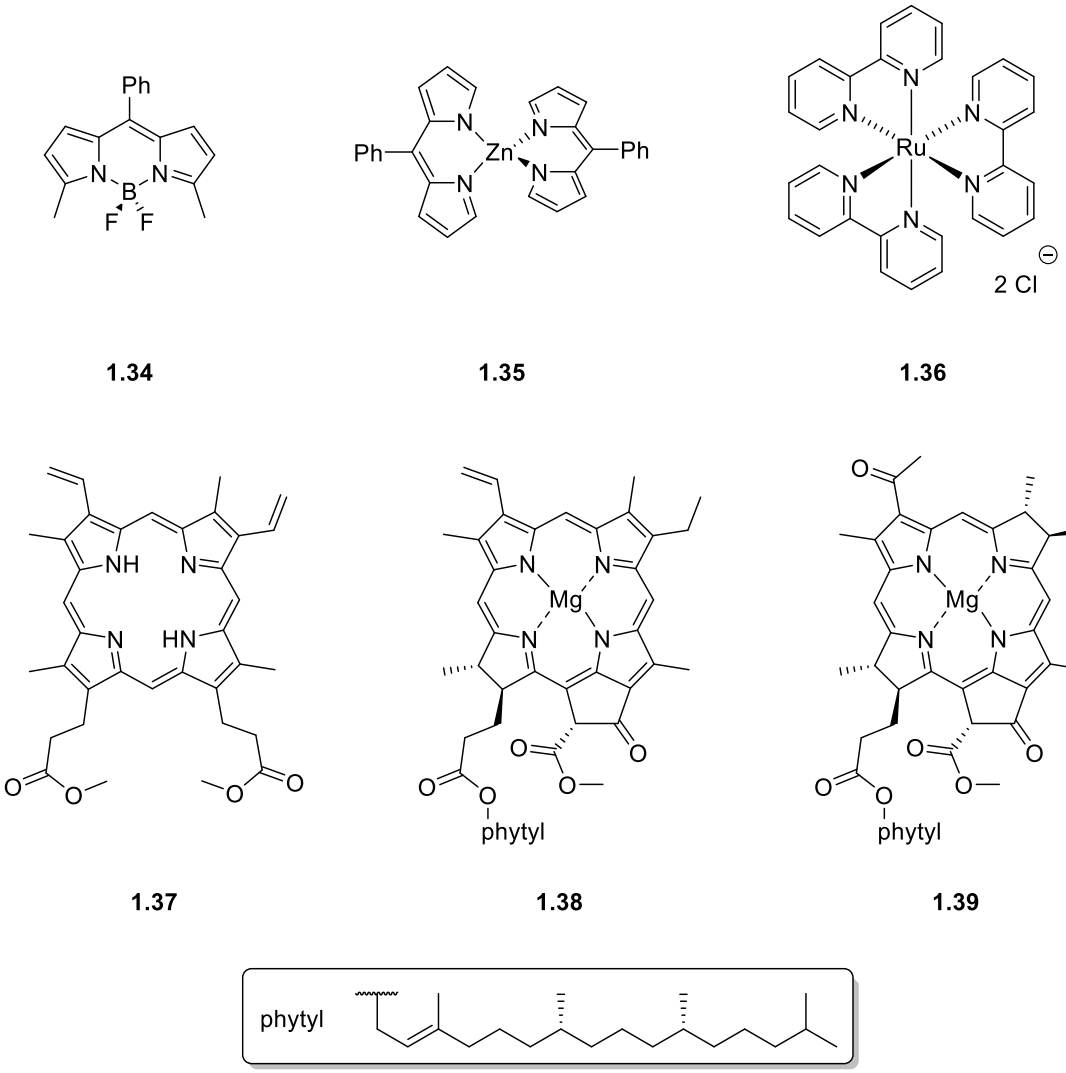

Figure 1.6. Structures of compounds for which the UV-Visible spectra are presented below in Figures 1.8 and 1.9; 3,5-bis(methyl)-8-phenyl-BODIPY (**1.34**), bis(5-phenyldipyrrinato)zinc(II) (**1.35**), ruthenium(II) tris(2,2'-bipyridine) dichloride (**1.36**), protoporphyrin IX dimethyl ester (**1.37**), chlorophyll *a* (**1.38**), and bacteriochlorophyll a (**1.39**). The structures of **1.21**, **1.26** and **1.31** are presented in **Scheme 1.2** and **Figure 1.5** respectively.

When considering PDT for oncology, it is worthy of note that solid tumours tend to mimic healthy tissues in their structure and thus are rarely a single layer, but instead three-dimensional structures with heterogeneous regions regarding exposure to oxygen and nutrients.[66] Assuming a tumour with no regions of hypoxia, and equal distribution of PS throughout the tumour (an ideal scenario), administration of light of differing wavelengths would treat different parts of the tumour. As depicted in Figure 1.7, the wavelength dependence of tissue penetration is a stark reminder that other chromophores will interfere with the PDT response.

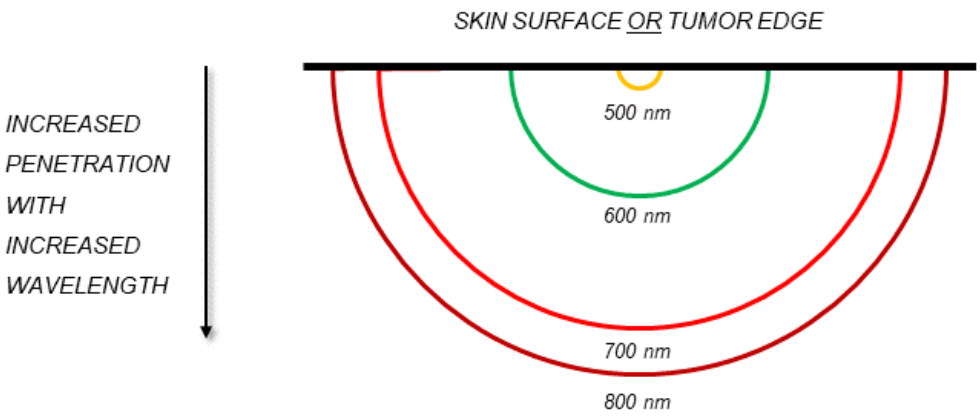

Figure 1.7. Wavelength dependent penetration of light through biological tissue. 800 nm light will reach a maximum of 1.0 cm depth. Depths extracted from ref.[1]

Considering Figure 1.7, we can see that the longer the wavelength of absorption of PS, the deeper the penetration of the light used. This enables activation of more PS molecules throughout the tumour, inducing greater cellular damage, and more tumour treatment. However, we can also observe that this is not a linear relationship between wavelength of light and depth of penetration. The maximum depth of penetration is at 800 nm where the depth reached is *ca*. 10 mm, after this point the absorption of water detracts from PS activation. There are great gains to be had by increasing the wavelength of absorption from 500 nm → 600 nm, but the gain is even larger still in the change from 600 → 700 nm.

Figures 1.8 and 1.9 are segregated in such a way to exhibit PS of non-porphyrinoid and porphyrinoid types. If we consider Figure 1.8, the longest wavelength of absorption is for **1.21** at 628 nm; otherwise, the values range from 445 nm (**1.36**) to 503 nm (**1.34**). Evidently, PSs based on these core structures would only be able to treat very small, or surface tumours.

At first glance, the same issue could be posed to **1.27**, and **1.37**–**1.39** in Figure 1.9. It is correct that these compounds show intense absorptions in the region of 300–450 nm; however, these are not the sole absorptions of these compounds. The majority of them show multiple intense absorptions > 650 nm.

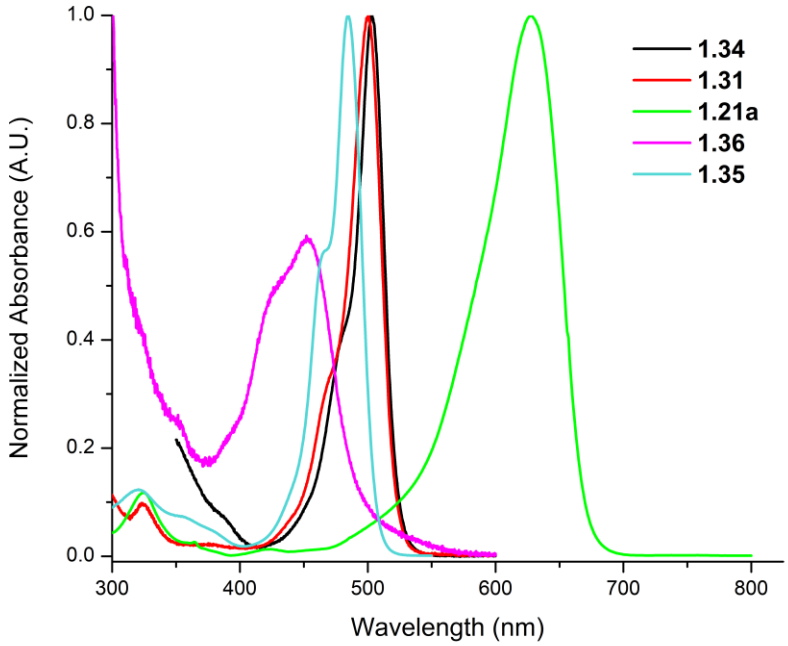

Figure 1.8. UV-Visible absorption spectra for a variety of non-porphyrinoid PSs; **1.21** (ethanol), **1.31** (ethanol, basic), **1.34** (toluene), **1.35** (toluene) and **1.36** (water). All data was taken from PhotoChemCAD.[71,72] Absorption spectra were normalized to the absorption peak of greatest absorption in the range of 300–825 nm.

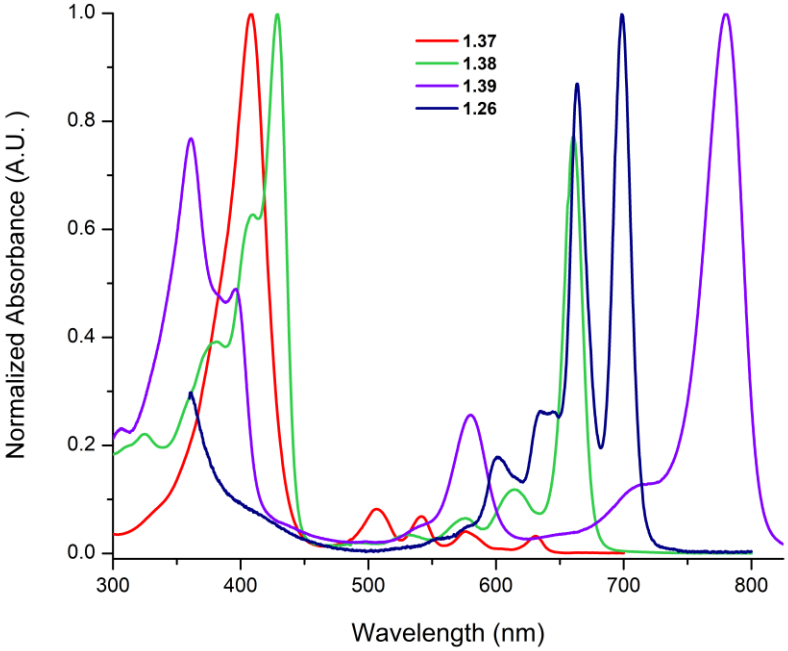

Figure 1.9 UV-Visible absorption spectra for a variety of porphyrinoid PSs; **1.26** (chloronaphthalene), **1.37** (chloroform), **1.38** (diethyl ether), **and 1.39** (toluene). All data was taken from PhotoChemCAD.[71,72] Absorption spectra were normalized to the absorption peak of greatest absorption in the range of 300–825 nm.

A greater discussion on the reasons behind this will be presented in Section 1.2.1, *vide infra*. Thus, these compounds have the capability to treat deeper tumours, larger tumours, or more generally a larger amount of tumour (assuming equivalent efficacy across PS core structure, i.e., the ideal scenario).

For this discussion, sonodynamic therapy (SDT) has been excluded,[69] and whilst interstitial PDT is greatly helping remedy the issue presented in Figure 1.7,[70] this cannot be a sole excuse to not increase the wavelength of absorption of a PS.

Thus, with the desire to minimize the number of treatments for the patient, it is advantageous to eliminate as much of the tumour as possible. The most successful way of doing this then is by ensuring as much of the tumour (containing PS) is irradiated at once – and the best way to do this is to ensure that the PS utilized has the longest wavelength of absorption possible.

1.1.4 Photodynamic Therapy: Generations of Photosensitizer (PS)

Classes and generations of PSs are two different things. The term “classes” represents merely the differing structural types at play. Discussion of generations of PSs becomes rather more troublesome, given there is no formal definition of the differing generations. To outline this concept more accurately, it makes more sense to discuss it from a historical perspective.

Although in Section 1.1.1., the phototoxicity Meyer-Betz experienced was initially claimed to be the result of the hematoporphyrin (Hp), it was found by Schwartz that Hp had rapid clearance from the body and thus could not have resulted in such extended phototoxicity.[73] Instead, porphyrin-oligomers resultant from Nencki’s isolation of Hp, from blood, were responsible for the prolonged phototoxicity.[74] Schwartz’s preparation enriched the generation of these oligomers, through the treatment of Hp, or PPIX, first with sulfuric acid in acetic acid, then strong alkali - and this was labelled hematoporphyrin derivative (HpD).[73] Lipson continued experimenting with HpD *in vivo,*[75,76,77] and eventually successfully treated a women exhibiting breast cell metastasis with HpD through selective irradiation of the tumour field.[78] This was the inaugural and seminal work cementing PDT as a cancer therapy. Clinical trials with differing formulations of HpD begun in the 1970s.[79,80,81]

Dougherty endeavoured to remedy the concerns from Schwartz's results with ultrafiltration in the mid-1970s to yield Photofrin II®.[82,83] Again, further purification in the 1980s by QLT PhotoTherapeutics and American Cyanamid, including the development of lyophilization (freeze drying) yielded the final drug Photofrin® which has not changed since the late-1980s.

Herein lies the issues with Photofrin®: nobody truly knew what the active ingredient(s) were. Initial analyses via mass spectrometry in the 1980s suggested that Photofrin® was mostly dimers, and thus that it was these yielding a phototoxic response.[84] However, more recent experiments have identified a nonamer,[85] and gel permeation chromatography suggests that the median for this mixture is instead trimeric.[86] It is postulated that the majority of the linkages between the porphyrins are ethereal, from the 3- and 7-positions of the porphyrin core, but ester linkages were also confirmed by Kessel.[87] People have also proposed meso-meso linked porphyrin dimers. High performance liquid chromatography (HPLC) of Photofrin® was found to yield a broad profile.[88] The lack of knowledge surrounding the composition of Photofrin is further complicated by the lack of knowledge surrounding the phototoxicity profiles of the individual components. Presumably, ether and ester linked bisporphyrins would act as two individual PSs, unless π-π co-facially stacked. Meso and/or β- β linked bisporphyrins typically present vastly differing photophysical properties to porphyrins, and whether oligo-porphyrins present phototoxicity given their greatly lessened solubility is another factor entirely.

Photofrin® is a first-generation PS for PDT, but HpD was the first, first generation PS for PDT. A large amount of drug development in PDT thus initially aims to overcome the flaws of these drugs, but first and foremost; utilize a single, isolable, compound that can be fully characterized. That, in itself, is as close to a formal definition of a second-generation photosensitizer as exists. The addition of active targeting moieties to this system generates a third-generation system.

An example of a prominent second-generation PS is **1.40**, 5,10,15,20-tetrakis(3-hydroxyphenyl)chlorin a.k.a. *m*-THPC, Temoporfin or Foscan®. It is used for the treatment of squamous cell carcinoma of the head and neck.[90] Originally synthesized by Bonnett et al. in 1989,[91] **1.40** has gained attention in recent years as a promising third-generation PS,[92] following suitable modifications.

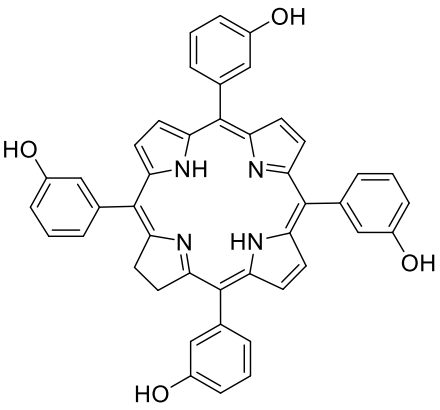

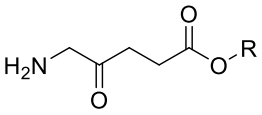

1.41a, R = H
1.41b, R = CH_3
1.41c, R = C_6H_{13}

1.40

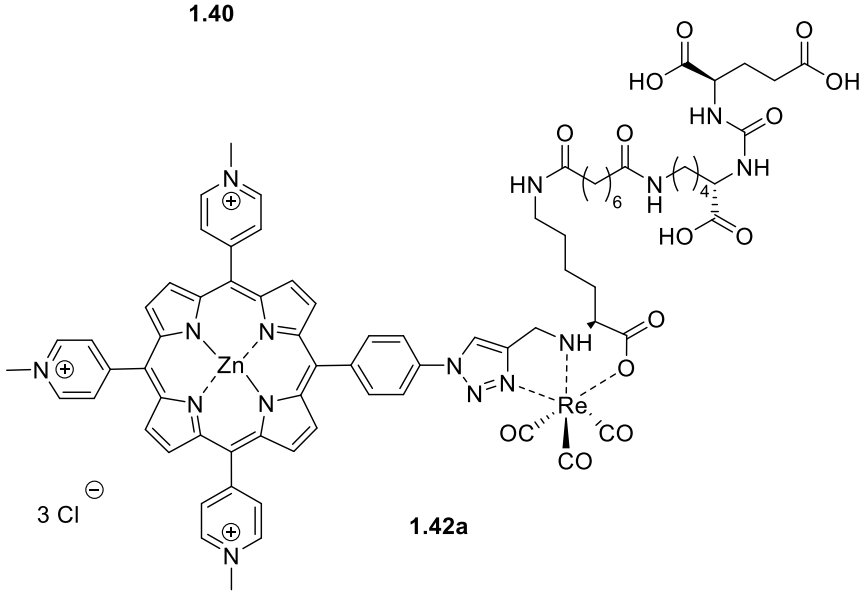

1.42a

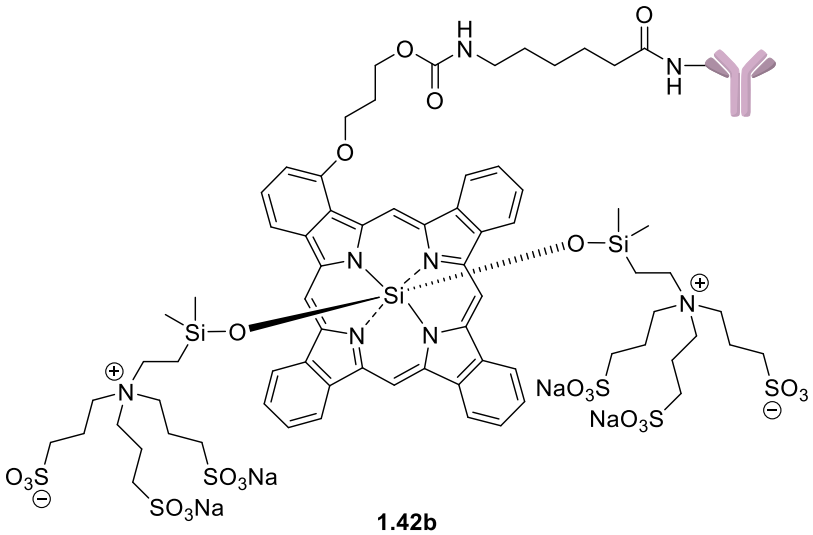

1.42b

Figure 1.10. Structures of second-generation PSs *m*-THPC (**1.40**), δ-aminolevulinic acid (**1.41a**) and its methyl and hexyl ester (**1.41b** and **1.41c**, respectively) derivatives, along with third-generation PS (**1.42a**) synthesized by Yap et al.[89] and cetuximab sarotalocan (**1.42b**).[100]

The topical application of δ-aminolevulinic acid (**1.41a**) to a tumour surface yields the enzymatic production of endogenous protoporphyrin IX (PPIX) which act as a PS in only the region of application i.e., the desired region. Given that the rate limiting step in the conversion of protoporphyrin IX into heme is insertion of iron (*via* ferrochelatase),[93] this means that all of the generated PS is consumed and presents little to no phototoxicity after 24 h.[94]. It was found that the utilization of methyl (**1.41b**) and hexyl (**1.41c**) esters of the acid yielded a much greater PDT response, as the increased lipophilicity of these drugs enabled greater penetration of the dermis, and for **1.41c** a 50-100-fold increase in rate of conversion to protoporphyrin IX.[95] It is these compounds that form the basis of Day-Light PDT which consists in the use of sun as a light source.[96]

In 2020, Yap et al.[89] presented the synthesis of **1.42a**; a porphyrin-amino acid conjugate with a targeting amino acid side chain. The introduction of this targeting moiety transforms the thoroughly utilized porphyrin,[97] from a second-generation to a third-generation PS system. This targeting moiety was found to increase the photodynamic efficacy in DU145-PSMA cells when compared to DU145 cells. Concomitant with this, the addition of the $Re^{I}(CO)_3$ (”cold” radioactive surrogate for $^{99m}Tc^{I}$) core through the administration of Schibli’s ”Click-to-Chelate” principle,[98] yields an imaging modality through single photon emission computed tomography (SPECT). This presents a third generation, theranostic,[99] PS system.

In September 2020, the first antibody-PS conjugate received regulatory approval.[100] Cetuximab saratolcan (**1.42b**) received approval for the treatment of advanced and recurrent head and neck cancer. Its PS component is based on the water-soluble silicon(IV) phthalocyanine, IR700, in this instance modified only slightly to enable bioconjugation. In the instance in question, it is conjugated to cetuximab, an epidermal growth factor receptor (EGFR) inhibitor. This 3rd generation PS exhibits a long wavelength of absorption (λ_{abs} = 690 nm), and high affinity for EGFR-expressing tumour cells, whilst sparing the tumour microenvironment and surrounding healthy tissue.

Evidently, there are many multiple examples of PS systems of all generations. Recently, the current state of third-generations PSs was summed up elegantly by Gierlich et al.[101]

1.1.5 Photodynamic Therapy: Cancer

In the current day and age, the most prevalent use of PDT, excluding dermatology with treatments for e.g., actinic keratoses,[102] is in an oncological setting. Whilst the classical definition of oncology refers to ”tumours and boils”,[103] herein we shall refer to cancerous tumours.

Cancer is a general term for multiple diseases resulting from uncontrollable division of cells, of nearly any type and from almost any part of the body, as a result of DNA damage or mutations. Whilst we typically refer to cancerous tumours as solid groups of neoplastic tissue, not all cancers exhibit themselves in this manner: namely blood cancers, i.e., leukaemia’s. Cancers can be classified as benign (harmless, in of themselves) or malignant (harmful). Cancers can also spread, and form new tumours in different parts of the body, in a process called metastasis. Of all deaths from cancer, 90% of these are a direct result of a metastatic cancer.

Cancer is a leading cause of death worldwide, along with; strokes, ischaemic heart disease, and diarrheal diseases.[104] In 2020, the World Health Organization (WHO) estimates cancer to be responsible for nearly 10 million deaths. The most common cancers, in terms of new cases in 2020, were breast, lung, colon and rectum, prostate, skin (non-melanoma), and stomach.[105]

There are multiple differing treatments for cancer, the choice of which is typically dependent on multiple factors including the size and location of the tumour. Resection (surgical removal) is the primary method of treatment for the majority of isolable solid tumours. Chemotherapy is the treatment of cancer through the administration of chemotherapeutic drugs. This treatment modality works *via* the killing the most rapidly dividing cells, a defining feature of cancer. Radiotherapy is the utilization of ionization radiation to eradicate the tumour, but it can also be used in a palliative care regime. For this discussion, we will exclude palliative care.

With such a variety of treatments available, it begs the question as to why PDT should be the new modality for cancer therapy.

- PDT is a non-invasive treatment (excluding interstitial PDT) subsequently minimizing post-treatment infections which can be deadly post-surgical resection.

- Chemotherapy is a treatment which affects the whole body, with dreadful side effects as a result of the destruction of healthy cells as well as cancerous ones. In contrast, PDT involves irradiation of a specific region of tissue, containing the PS, mitigating systemic side effects.
- Whilst radiotherapy is non-invasive and does have a targeting aspect, albeit spatial, inherently built in as a result of advances in computed tomography (CT), side effects stem from radiation-induced toxicity.
- In contrast to radiotherapy and chemotherapy, resistance cannot be developed to PDT
- Given the inherent mechanisms of PDT, it is possible to stimulate anti-tumour immunity, a promising avenue of research for the future of PDT.
- In a world where the cost of living is continually spiralling out of control, PDT does not require special facilities. There are no necessary radiation facilities, and given the lack of toxicity prior to irradiation there are no particular measures necessary in preparation of the drug prior to administration, in contrast to chemotherapy.

All this is to say that whilst there are multiple methods, all of which can eradicate cancerous cells, differing cancers cannot all be treated in the same manner and in more cases than not, underlying health conditions of the patient may mean that one treatment is preferential over another. A prime example would be incompatibilities between elderly patients and general anaesthesia for surgical resection of the tumour mass.

Thus, in a world which strives for ever more personalized medicine, a greater option of available cancer treatments makes for a world with a greater cancer survival rates.

1.2 – Chlorins

1.2.1 Chlorins *a.k.a.* Dihydroporphyrins

Porphyrins are the red pigments of life, with their etymology deriving from the Greek ‘πορπφνρα’ (porphura) meaning ‘purple’.[106] We have already elaborated how they can be used as PSs, and in Nomenclature their structure was labelled and named. Porphyrins make our blood red, and are responsible for the function of the P450 group of enzymes,[107] amongst many other things besides.

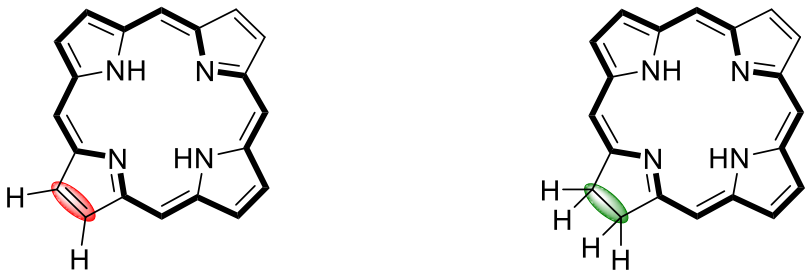

1.44
porphyrin
[18+4]**π**
D_{2h} (M = 2H)
D_{4h} (M = M^{II})

1.45
chlorin
[18+2]**π**
C_{2v} (M = 2H, M^{II})

Figure 1.11. Core structures of the simplest porphyrin and chlorin in their free base forms (for clarity), with the 18π-electron system shown in bold, along with the number π of electrons and symmetry of each system.

Chlorins are only slightly different, with the etymology of ‘chlorin’ deriving from, the Greek ‘χλωρός’ (chloros) meaning ‘green’ (and chlorophyll being ‘χλωρός’ + ‘φύλλον’ (phyllon) meaning leaf). Chlorins are also tetrapyrroles, structures with four pyrrole rings joined together in a ring linked by methene (-CH=) bridges. They are another of “natures annulenes”.[108] In the simplest and most analogous comparison, the difference is only an extra two hydrogen atoms, added across a C_β-C_β double bond; hence, the name dihydroporphyrins. Instead of red, they are the green pigments of life, responsible for photosynthesis. Despite the growing worldwide population, chlorins are still the most abundant class of tetrapyrrole on Earth.[109] .

The biggest difference comes from the names of the structure types, and their symmetries. As listed in Figure 1.11, the symmetry of the porphyrin macrocycle changes upon the core substituent. If the porphyrin is free base (i.e., no metal centre), the core exhibits a D_{2h} point group, and installation of a metal centre

increases that symmetry to D_{4h} point group. In contrast, regardless of the centre of the chlorin core, the symmetry approximates to a C_{2v} point group.

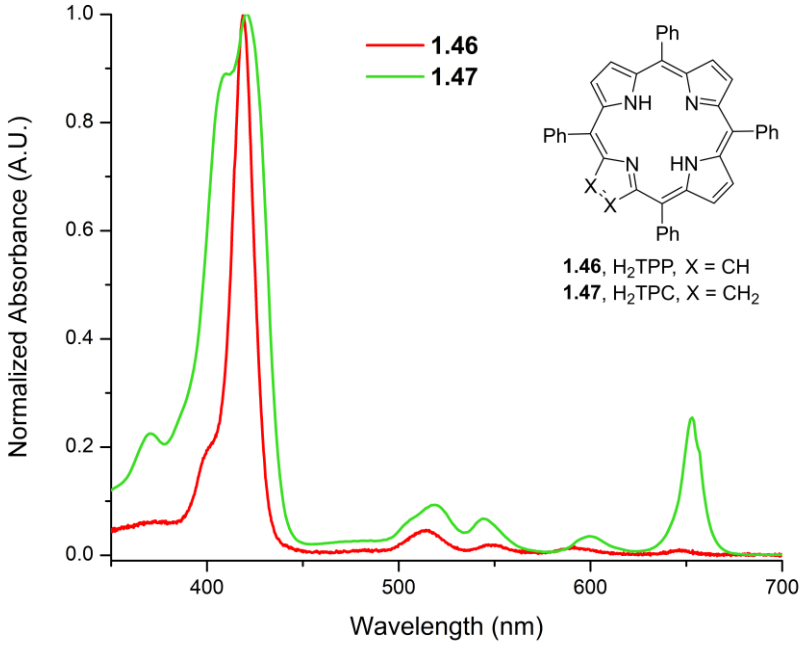

Figure 1.12. UV-Visible spectra of 5,10,15,20-tetraphenylporphyrin (**1.46**, H_2TPP) and 5,10,15,20-tetraphenyl-17,18-dihydroporphyrin (**1.47**, H_2TPC) in toluene, normalized at the peak of highest intensity. All data was taken from PhotoChemCAD.[71,72]

Presented in Figure 1.12 are the UV-Visible absorption spectra of porphyrin **1.46** and chlorin **1.47**, otherwise analogous aside from two hydrogen atoms. The spectrum of **1.46** (red, Figure 1.12) is dominated by an intense absorption at c.a. 419 nm. This band is named "Soret" after the man who discovered it.[110] Aside from this, there are four peaks of much lower intensity in the range of 500–670 nm. In contrast, the spectrum of **1.47** (green, Figure 1.12) shows two bands between 400–450 nm, at ca. 405 and 420 nm. Aside from these, there are multiple absorptions between 500–630 nm, at which point there is an absorption of much greater intensity around ca. 650 nm.

The origin of the intense absorption, in the case of **1.44,** is the combination of two $a_{1u} \rightarrow e_{.g.,}$ transitions, which are called "B" transitions. As a result of the degeneracy of the $e_{.g.,}$ set of orbitals, these transitions are equivalent, and become additive to produce a Soret band ($B_x + B_y$). In the case of **1.45** the e_g orbitals are no longer

degenerate, and thus the two transitions are of differing energies; hence, the splitting of this band.[111]

The Q-transitions (Q for quasi-allowed) in the spectrum of **1.44** arise from $a_{2u} \rightarrow e_{g}$., transitions, thus yielding one for each x and y direction. However, this does not explain why there are four transitions, instead of two. It is vibrational overtones of these bands which yield the second set of two Q-bands: $Q_y(1,0)$, $Q_y(0,0)$, $Q_x(1,0)$, and $Q_x(0,0)$, see Frank-Condon principle. As the symmetry is increased from D_{2h} to D_{4h} upon metallation of the porphyrin core, the x and y axes become degenerate and this yields two Q-bands: Q(1,0) and Q(0,0).

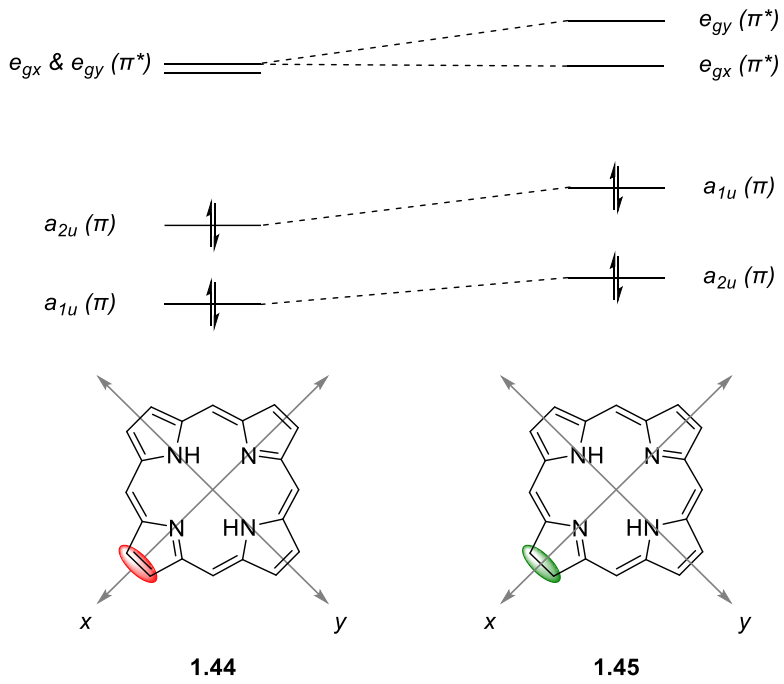

Figure 1.13. Structures of **1.44** and **1.45**, displayed with x and y axes along with the molecular orbitals (HOMO-1, HOMO, LUMO, LUMO+1) responsible for the transitions observed.

In the case of **1.45**, the ”Q-transitions” are actually allowed due to reduced symmetry. These Q-bands are mostly poorly defined, and alternating with vibrational overtones as the x-axis is surveyed.[112] The $Q_y(0,0)$ band, however, is the outlier. It arises from the $a_{1u} \rightarrow e_{gx}$ transition and is strongly allowed.[113,114,115,116]

1.2.2 Chlorins in Nature: The Omnipresent Tetrapyrroles

The setting in which most are familiar with chlorins is likely to be the plants in the garden. These chlorins are chlorophylls, and they are found in the chloroplasts of oxygenic photosynthetic organisms (Figure 1.14, **1.38**, **1.48**–**1.51**).

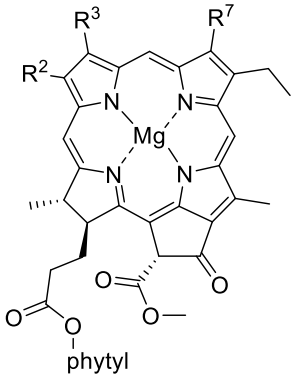

1.38, **1.48 - 1.51**

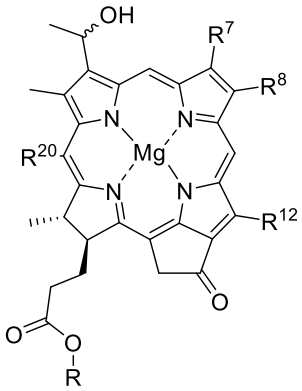

1.52 - 1.55

$R^2 = R^7 = CH_3$, $R^3 = CH{=}CH_2$, **1.38**, Chl *a*
$R^2 = CH_3$, $R^3 = CH{=}CH_2$, $R^7 = CHO$, **1.48**, Chl *b*
$R^2 = R^7 = CH_3$, $R^3 = CHO$, **1.49**, Chl *d*
$R^2 = CHO$, $R^3 = CH{=}CH_2$, $R^7 = CH_3$, **1.50**, Chl *f*
$R^2 = CH_3$, $R^3 = R^7 = CHO$, **1.51**, Chl *g*

$R^7 = R^{12} = R^{20} = CH_3$, $R^8 = C_2H_5$, **1.52**, Bchl *c*
$R^7 = CH_3$, $R^8 = R^{12} = C_2H_5$, $R^{20} = H$, **1.53**, Bchl *d*
$R^7 = CHO$, $R^8 = R^{12} = C_2H_5$, $R^{20} = CH_3$, **1.54**, Bchl *e*
$R^7 = CHO$, $R^8 = R^{12} = C_2H_5$, $R^{20} = H$, **1.55**, Bchl *f*

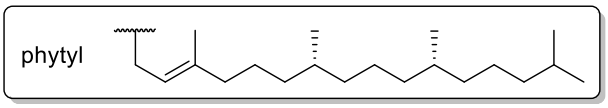

Figure 1.14. Structures of naturally occurring chlorins: chlorophylls *a*, *b*, *d*, *f*, and *g* as well as originally incorrectly labelled bacteriochlorophylls *c*, *d*, *e*, and *f*.

Further to these, are bacteriochlorophylls (**1.52**–**1.55**). These are isolated form photosynthetic bacteria. In total, there have been numerous natural chlorophylls isolated and found, albeit some incorrectly named (**1.52**–**1.55**, Figure 1.14), in contrast to bacteriochlorophylls *a*, *b*, and *g* which are true bacteriochlorins. In all cases, there is an extra ring, the E-ring. This nomenclature is displayed in Figure 1.15.

Chlorophyll *a* (Chl *a*) is the pigment responsible for the green colour present in the majority of plants, and is present in both photosystems I and II. Chl *b* is the second most abundant and is identified as an “accessory pigment”, and is not found in reaction centres. These were both discovered in 1817 by Pelletier and Caventou,[117,118,119] but it wasn’t until Stokes’ work c.a. 50 years later that realized

the extract of Pelletier and Caventou contained two compounds.[120] Eventually, these were separated by Tswett,[121] however some accredit this accolade to Willstätter and Isler.[122] As with natural porphyrins, the correct structure was initially proposed by Fischer in 1940, albeit with the omission of stereochemistry.[123] Multiple years and research groups eventually contributed to the understanding that led to Fischer's result. The structure of Chl *a* was unequivocally assigned through, arguably, one of the greatest total syntheses of all time from Woodward and co-workers.[124] Interestingly, this occurred before the first assigned NMR spectra of either Chl *a* or Chl *b* had been reported. Whilst no crystal structures of chlorophylls containing the phytyl chain exist, Strouse's 1975 structure of ethyl chlorophyllide *a* dihydrate is presented below,[125] along with the numbering system and structure of phorbines.

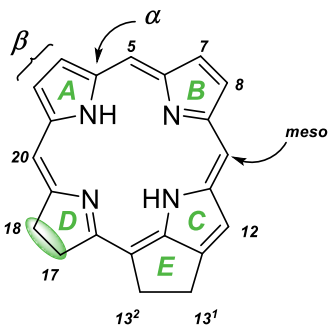

1.56

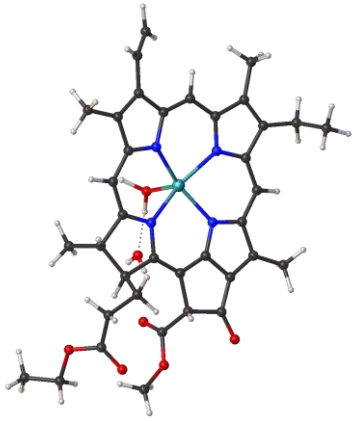

1.57

Figure 1.15. Left: structure of phorbine (**1.56**) along with Lindsey's numbering system (see Nomenclature, *vide supra*) and ring labelling and right: Strouse's 1975 crystal structure of ethyl chlorophyllide *a* dihydrate (**1.57,** CCDC No. 1101397),[125] atoms represented as spheres. Image generated from Olex2.[126]

Chl *d* was isolated form the photosystem I reaction centre complex of *Acaryochloris marina*, in which the ratio of Chl *d*:Chl *a* was found to be 180:1.[127] Originally thought to be a possible artifact, it was confirmed as a main-player in global photosynthesis when it was found in both sea- and freshwater sediments upon administration of near infra-red (NIR) light.[128,129]

Chl *g* is somewhat a strange one. Isolated in low yield from *Acaryochloris marina*, again, upon the introduction of the chlorophyllide *a* oxygenase gene. The structure of Chl *g* was assigned at 7-CHO-Chl *d*, and instead this was named Chl *g*.[130]

Chl *f* has been left until last as it was the most recently discovered. Initially isolated in 2010 upon culturing cyanobacteria under red light,[131] it has now been isolated from multiple *bacteria* in both Australia,[132] and Japan.[133] Its structure, which is essentially 2-formyl-2-demethyl-Chl *a*, was fully assigned by Scheer in 2013.[134] It is the most red-absorbing chlorophyll with $\lambda(Q_y)$ = 707 nm (methanol, $\log_{10}\varepsilon$ = 4.85).[135]

Of course, Chl chemistry is steeped in history, and rather a vast subject. Thus, this short summary includes a miniscule percentage of the work in the field, which has been continually catalogued fastidiously elsewhere.[i,ii,136]

The bacteriochlorophylls presented have lesser known about them, in reality. Bacteriochlorophylls (Bchls) *c*, *d*, and *e* were isolated in the 1960s & 70s, from photosynthetic bacteria,[137] and whilst Bchl *f* had been predicted, its existence came only recently, and was as a result of a deliberate mutation.[138]

1.2.3 Chlorin Syntheses: Nobody Said It Was Easy

Clearly, nature has had some fun in its syntheses of hydroporphyrins. Derived from primordial soup, engineered by enzymes over millennia to yield the biologically active cofactors we have today. Whilst scientists can extract Chls, their synthetic chemistry is somewhat arduous, and unpredictable. Understandably, chemists desire to make hydroporphyrins of their own for multitude reasons. Modification of the chlorin periphery can enable studies of; the spectral properties of these molecule, self-assembly properties in biologically important settings, and the design of architectures which support artificial photosynthesis.[ii] Of course, the application of these molecules to PDT is also of great interest, *vide infra*. To explain how they can, we must revert back to porphyrins, briefly.

It must be made clear that whilst some modifications of the porphyrin core result in molecules with “chlorin-like” UV-Visible absorption spectra, these molecules will not be included in this thesis. Notable examples in this subject include the majority of

Brückner's breaking and mending work – desymmetrization of the macrocyclic core has yielded a shifted wavelength of absorption.[139]

Syntheses of hydroporphyrins can be split into two broad categories: *A*. synthetic manipulation of porphyrins to yield chlorins, and *B*. outright chlorin syntheses. Thus, an initial recap on porphyrin syntheses is necessary.

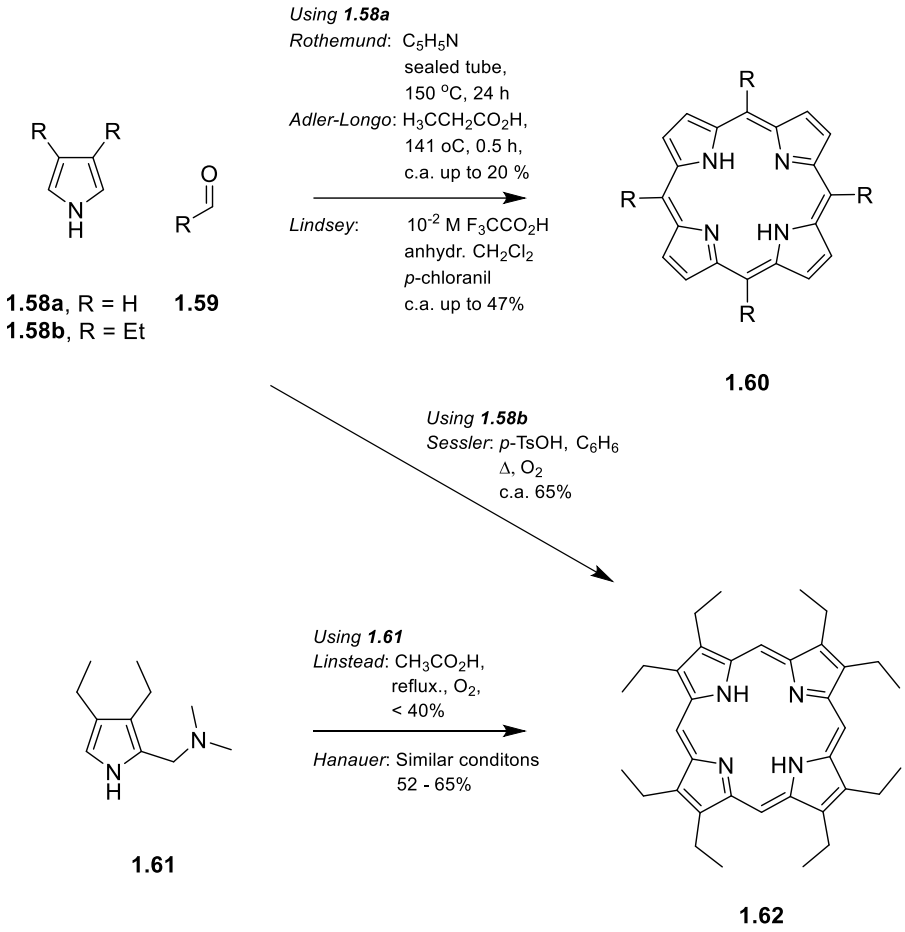

Scheme 1.3. Synthesis of synthetic porphyrin workhorses; A_4-porphyrins through Rothemund,[140,141] Adler-Longo,[142] and Lindsey syntheses,[143] with R = alkyl, aryl and octa-β-substituted octaethylporphyrin *via* Linstead,[149] Hanauer,[150] and Sessler's methods.[152]

The first synthetic chlorins were devised from synthetic porphyrins. Synthetic chemistry of non-natural porphyrinoids began with Rothemund's synthesis,[140,141] followed by Adler-Longo,[142] and eventually Lindsey rounded up the A_4-syntheses in 1986 (Scheme 1.3).[143] These syntheses all consisting of a pyrrole-aldehyde condensation yielding the simplest meso-substituted porphyrins. As the years have gone on, other methods have been developed to yield porphyrins of differing substitution patterns.[144] Whist it is entirely feasible to do mixed Adler-Longo or

Lindsey porphyrin condensations, separation of differing porphyrins can be excruciatingly tiresome. With advents in dipyrromethane chemistry came the MacDonald [2+2] condensation,[145,146] and organolithium chemistry from Senge yielding porphyrins of mixed substitution patterns,[147] to name other milestones.

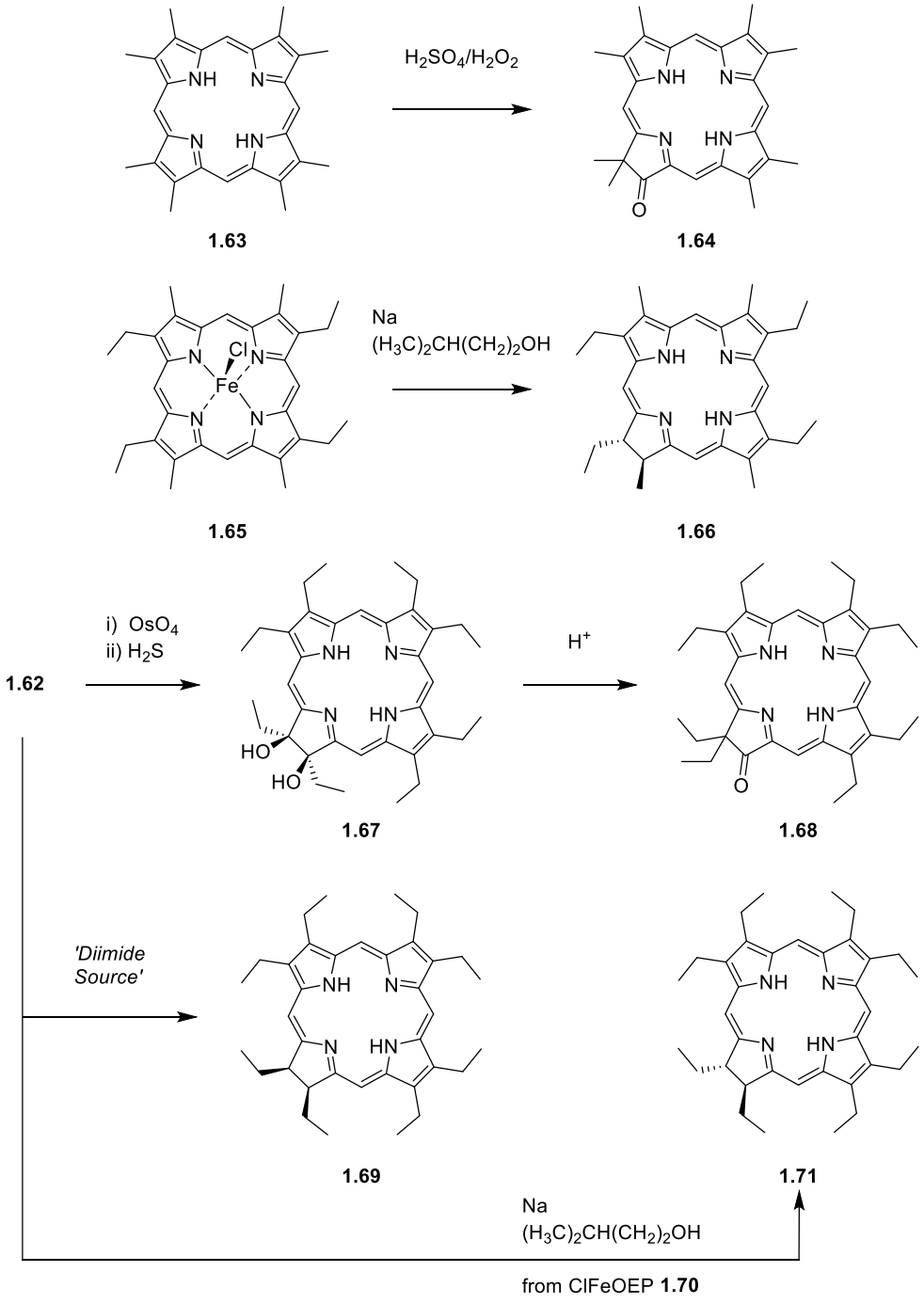

Scheme 1.4. Methods for generation of chlorins from porphyrins utilizing Na/isoamyl alcohol or osmium tetroxide and their rearrangements to oxochlorins.[158,159,160,161,162,163]

Further to the meso-substituted porphyrins, β-substituted porphyrins present another synthetic workhorse to the tetrapyrrole community. Key to this field is 2,3,7,8,12,13,17,18-octaethylporphyrin (**1.62**). The synthesis of which has been modified continually; initially synthesized by Fischer in 1937,[148] refined by Linstead,[149] refined then by Whitlock and Hanauer,[150] and then by Dolphin.[151] The synthesis of **1.62** was then made practical by Sessler,[152] however the contributions of Inhoffen to this field should not go un-noted.[153,154] Together, the tetra-meso and octa-β substituted porphyrins have become the workhorses for the synthetic tetrapyrrole community.

It was found that in all Rothemund, Adler-Longo and Lindsey porphyrin syntheses, the respective chlorins are also by-products. Between 1943–1946, Calvin and co-workers isolated H_2TPC, (**1.47**) upon investigation of the Rothemund synthesis. It was found that chelation of zinc enabled greater stability of, and hence isolation of H_2TPC and further experimentation therefrom.[155,156,157]

In 1927, Fischer et al. yielded 17,18-dihydro-2,3,7,8,12,13,18,18-octamethyl-17-oxo-porphyrin (**1.64**, Scheme 1.4) upon the treatment of octamethylporphyrin **1.63** with sulfuric acid in hydrogen peroxide *a.k.a.* ”piranha solution”.[158] In the 1930s, again Fischer treated various porphyrins with elemental sodium in isoamyl alcohol to yield *trans*-etiochlorin I (**1.66**) and II, along with *trans*-octaethylchlorin (**1.71**).[159,160,161] It was then Inhoffen who utilized osmium tetroxide to generate *vicinal*-dihydroxy chlorins (**1.67**) which themselves could be rearranged into 17-oxo-18,18-disubstituted chlorins (**1.68**).[162,163]

Modern attempts at chlorin synthesis typically rely on milder conditions still. Initially the Whitlock diimide reduction, first presented in 1969,[164] utilized *p*-toluenesulfyonyl hydrazide, **1.72,** in hot pyridine with added potassium carbonate. This resulted in the formation of the chlorin (**1.47**) and bacteriochlorin, as well as returning some starting porphyrin (**1.46**). Whilst stereochemistry of the reduced ring is not an issue for consideration when meso-substituted porphyrins are the starting materials in question, in the case of **1.62**, this procedure was found to generate only the *cis*-isomers. Little has been modified from the original procedure, and the area which has received the greatest attention is the diimide source (Scheme 1.5).

With the advent of **1.75**, the reaction could be undertaken in neutral conditions at only slightly elevated temperatures.[165] This not only made the reaction safer but also increased the possible substrate scope, through the lack of use of strong bases. **1.77**, however requires mild acidic treatment at room temperature.[166] Thus, the use of diimide reductions vastly expanded the generation and availability of chlorins to the synthetic chemist.

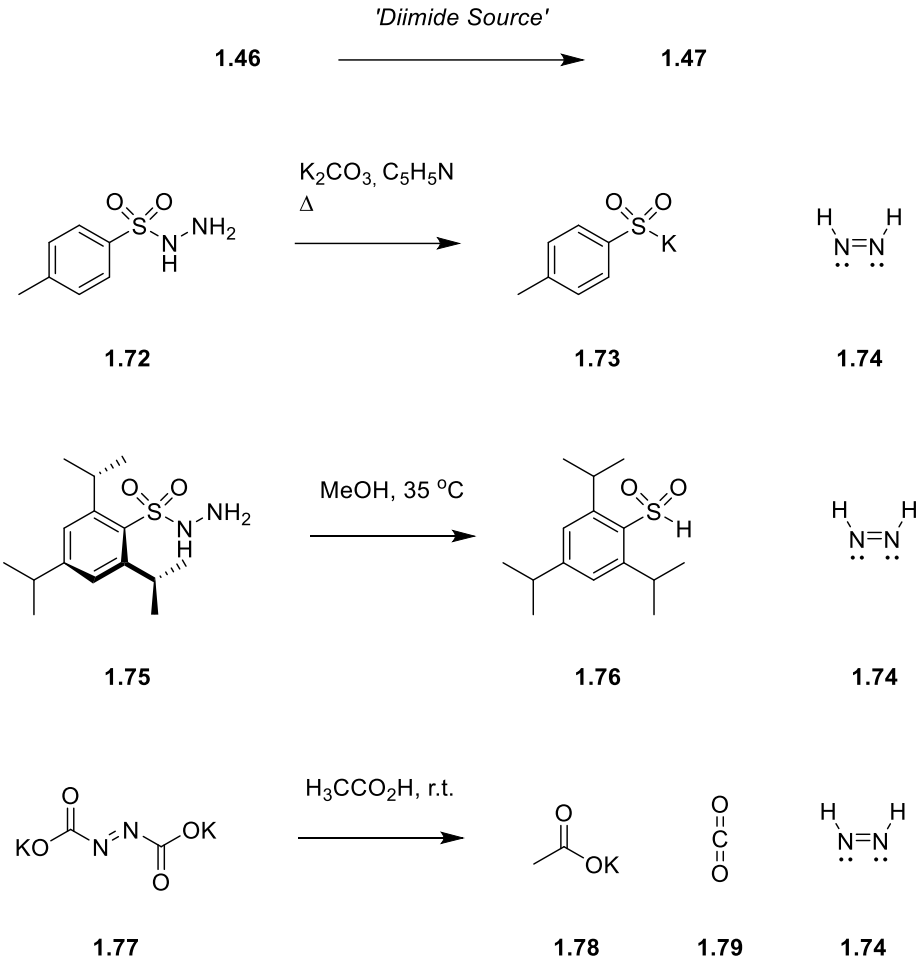

Scheme 1.5. Evolution of diimide source from the original Whitlock diimide reduction for the conversion of porphyrins to chlorins and bacteriochlorins, utilizing the conversion of **1.46** to **1.47** as prime example.[164,165,166]

One other common method for generation of chlorins is cycloaddition. In 1997, Cavaleiro and co-workers presented the reaction of tetraarylporphyrins with *o*-benzoquinodimethane which yielded naphtho[2,3-*b*]porphyrins,[167] exemplifying the reactivity of the C_β-C_β double bonds as dienophiles in Diels-Alder reactions. Only two years later, they presented the reaction of tetraarylporphyrins with azomethine ylide (**1.82**, Scheme 1.6) yielding *N*-methylpyrrolidine fused chlorins (**1.84**),[168] and

isobacteriochlorin bis-adducts as a result of a 1,3-dipolar cycloaddition reaction. Other cycloadditions have been performed across C_β-C_β double bonds with; pentacene,[169] azomethine ylides derived from proline derivatives,[170] nitrile oxides,[171] and methylpyrazoles,[172] amongst other dienophiles.

As shown throughout, natural tetrapyrroles contain a variety of substituents which take multiple steps to append to typical synthetic porphyrins. An example of which being the vinyl group. In 1994, Smith and co-workers treated a series of natural porphyrin dimethyl esters (including PPIX DME, **1.37**) first with dimethyl acetylene dicarboxylate, **1.85**, in which a [4+2] cycloaddition where the C_β-C_β and 3-vinyl moiety acted as the diene and **1.85** as the dienophile.[173] Resulting conversion of the 1,4-diene to the 1,3-diene with DBU and partial hydrolysis yields the drug we know of today as benzoporphyrin derivative mono-acid Ring A (BPDMA, **1.86a** and **b**). The structural assignment was confirmed by the authors through both crystallographic assessment and NOE experiments.

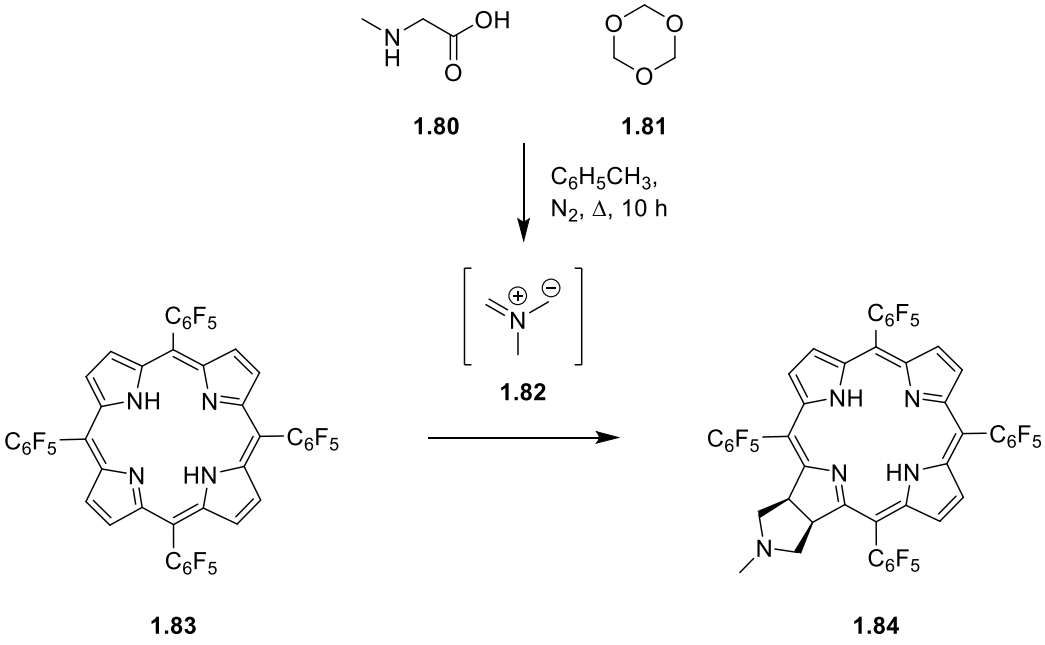

Scheme 1.6. Cavaleiro and co-workers' reaction of azomethine ylide with $TPPF_{20}$ (**1.83**) to yield an *N*-methylpyrrolidine fused chlorin.[168]

Two structures of BPDMA, **1.86**, are presented due to conflicting rules of nomenclature. Moss states the *A*-ring of a tetrapyrrole must be drawn in the top-left corner and as a pyrrole.[i] Convention states the reduced ring must be drawn as the *D*-ring in the bottom left corner. The majority of the literature surrounding this drug

constitutes ***A*** as drawn in Scheme 1.7, and whilst this does show the involvement of the 3-vinyl group in this reaction, it violates both statements. From here on out thus, the representation ***B*** will be used for BPDMA.

From cycloaddition to cyclization. In 1986, Morgan and Tertel reported the synthesis of **1.90**.[174] Whilst technically the structure type is a "purpurin" (not a 1,2,4-trihydroxy-9,10-antheaquinone), first identified by Conant and Moyer the term has become a word used for a tetrapyrrole with an electron withdrawing meso group.[175] For further definition on nomenclature, the readers are referred to Nomenclature, *vide supra*.

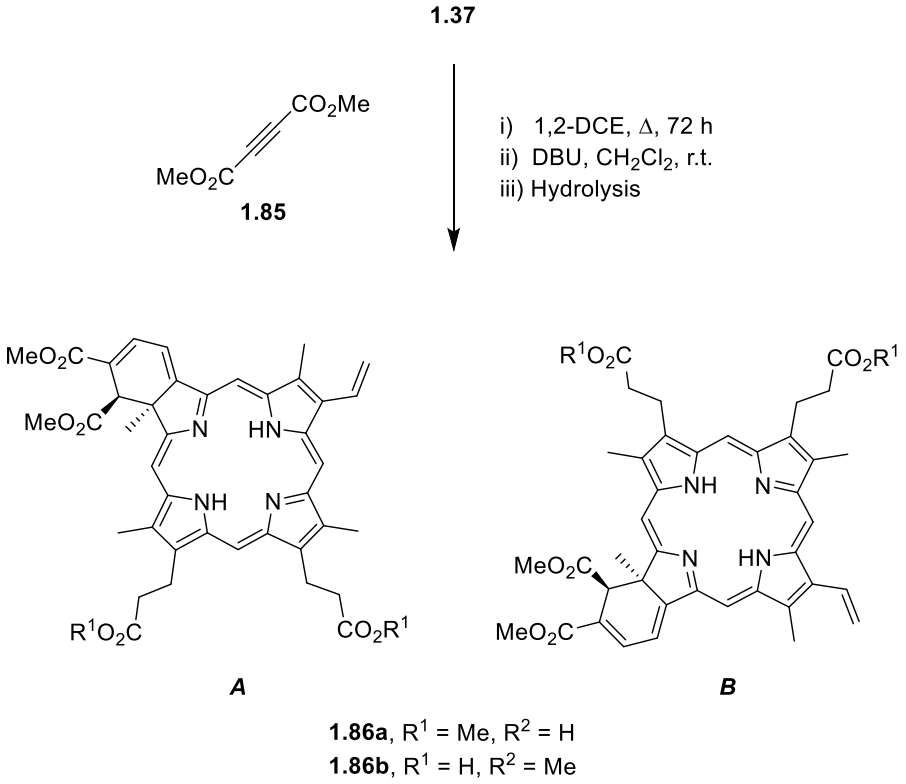

Scheme 1.7. Reaction of PPIX DME (**1.37**) with dimethylacetylene dicarboxylate (**1.85**), and subsequent steps, to yield Benzoporphyrin Derivative Monoacid Ring A (**1.86**) with two representation of the structure, see text.[i,173]

Etioporphyrin I (**1.87**, Scheme 1.8) underwent metallation, meso-formylation,[176] Wittig reaction and finally demetallation to yield **1.88**. Heating a solution of **1.88** in glacial acetic acid in the presence of air yields **1.89**. Subsequent metallation with tin(II) chloride yields tin(IV) etiopurpurin **1.90**. The importance of this compound in PDT will be discussed *vide infra*.

Thus, the toolbox of the synthetic chemist is vast when it comes to non-natural chlorins. Natural chlorins have presented more of a challenge, in contrast to the natural porphyrins which were synthesized by Fischer prior to even the Rothemund porphyrin synthesis.

The greatest example of natural chlorin syntheses, and one of the great total syntheses, must be Woodward's synthesis of chlorophyll *a*.[124] Misleadingly labelled as Woodward's synthesis, it comprised work over multiple decades, and studies of many chemists before the first team he assigned to this project.

Woodward's synthesis initially generated *A*-*D* and *B*-*C* halves. From there the intermediate generation of purpurins (both traditional, and meso-formyl hydroporphyrins) led to chlorin e_6 trimethyl ester, which could be turned into Chl *a* through the use of "well-trodden paths".[177]

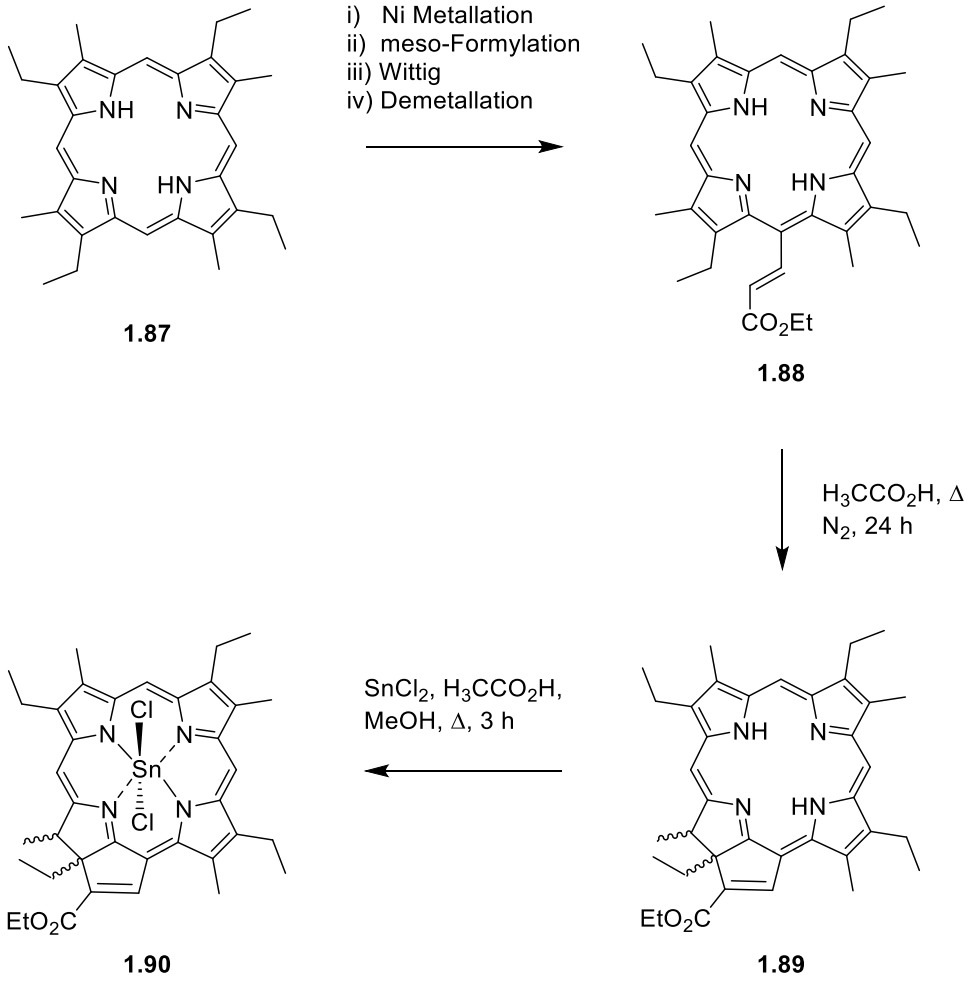

1.87 **1.88** **1.89** **1.90**

Scheme 1.8.Synthesis of tin(IV) etiopurpurin (**1.90**) from etioporphyrin I as reported by Morgan and Tertel.[174,176]

As noted prior – Woodward's synthesis relied on the generation of separate 'halves' which were then combined to yield the tetrapyrrolic intermediates. Looking at the chlorin core, there are two ways it can be divided to yield 'halves' (Scheme 1.10). The two methods bisect the core from top to bottom yielding East-West halves (Scheme 1.10, left), whereas disconnecting from left to right yields North-South halves (Scheme 1.10, right). Aside from these methods, construction of the chlorin core may occur in a stepwise fashion, appending one ring to another and passing through a tricyclic intermediate.

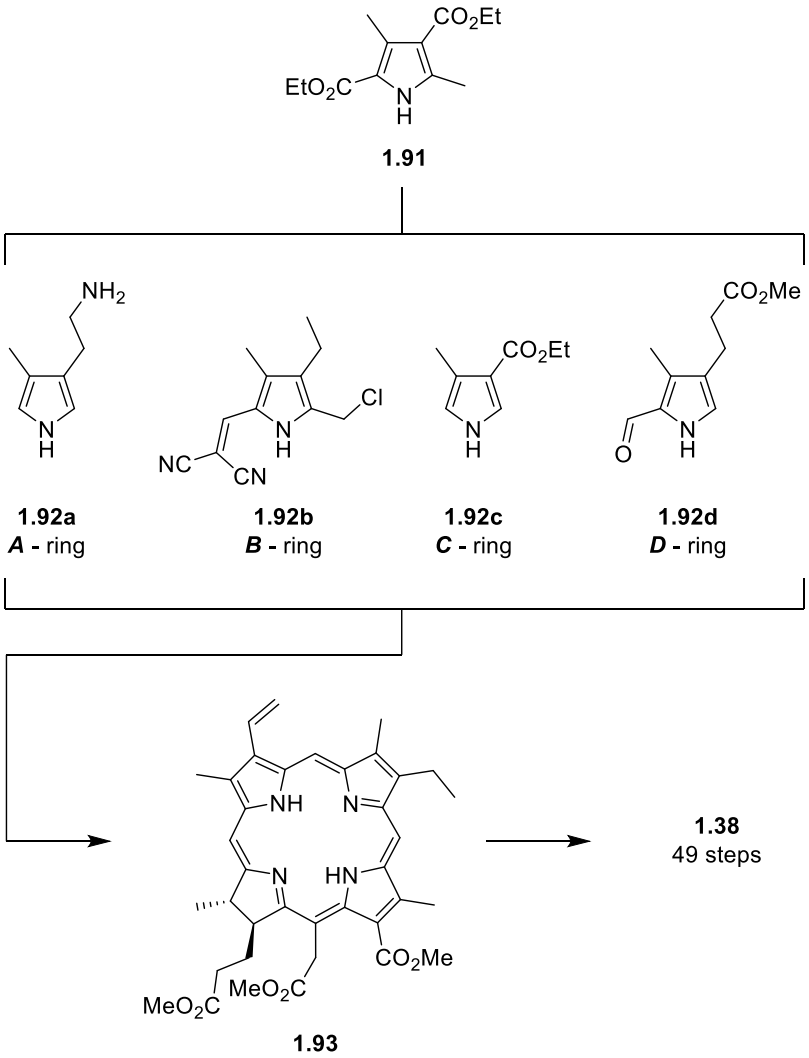

Scheme 1.9. Simplified scheme of Woodward's synthesis of Chl *a* (**1.38**) from Knorr's pyrrole **1.91,** passing through chlorin e_6 trimethyl ester **1.93**, as a relay point.[124,178]

Biologically relevant tetrapyrroles tend to contain little-to-no meso substituents, e.g., C^{15} substitution in Chls, and meso-methyl groups in BChls and vitamin B_{12}, and often are octa-β-substituted, in stark contrast to a large proportion of synthetic porphyrins

used today. In this case, there is one modern day synthesis which appears perfectly suited to this type of systems.

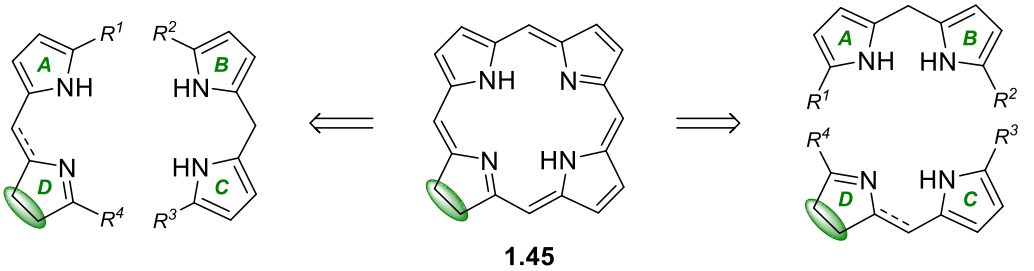

Scheme 1.10. Retrosynthetic disconnection of chlorin **1.45**, displaying the East-West method and North-South Method.

Jacobi's synthesis of chlorins is unique, for multiple reasons. As will become evident, *vide infra*, it differs in the initial generation of *C*-*D* and *A*-*B* halves, i.e., the implication of a North-South route. While the *A*-*B* half employs more typical and well established dipyrromethane chemistry, the *C*-*D* half does not, (Scheme 1.11).[179,180]

For clarity, all rings are presented in the same orientation as displayed for **1.45** with the *D*-ring represented with the green highlight, with the half containing the reduced ring presented as a hydro-dipyrrin and the other half presented as a dipyrromethane. Groups R^1–R^4 are oriented such that R^1 is appended to the *A*-ring and R^4 to the *D*-ring, with two of those groups being able to provide the meso carbon atoms necessary to yield the final tetrapyrrole.

Initially beginning with a pre-functionalized pyrrole and a pent-4-ynoic acid containing a *geminal* dimethyl group, the pseudo-Sonogashira coupling yields pyrrole-enelactam **1.96**.[181] From this, the route differs depending on the groups that are necessary to append to the α-positions of the dipyrrins. Subsequently, the conditions for this reaction differ greatly from the majority of porphyrin and hydroporphyrin syntheses – merely a percentage of trifluoroacetic acid in dichloromethane (Scheme 1.12).[182]

This route has been used to synthesize multiple methyl-propionate appended chlorins, i.e., side chains of distinct similarity to those found in nature.[183] This method has not yet been applied to Bonellin (Scheme 1.13).

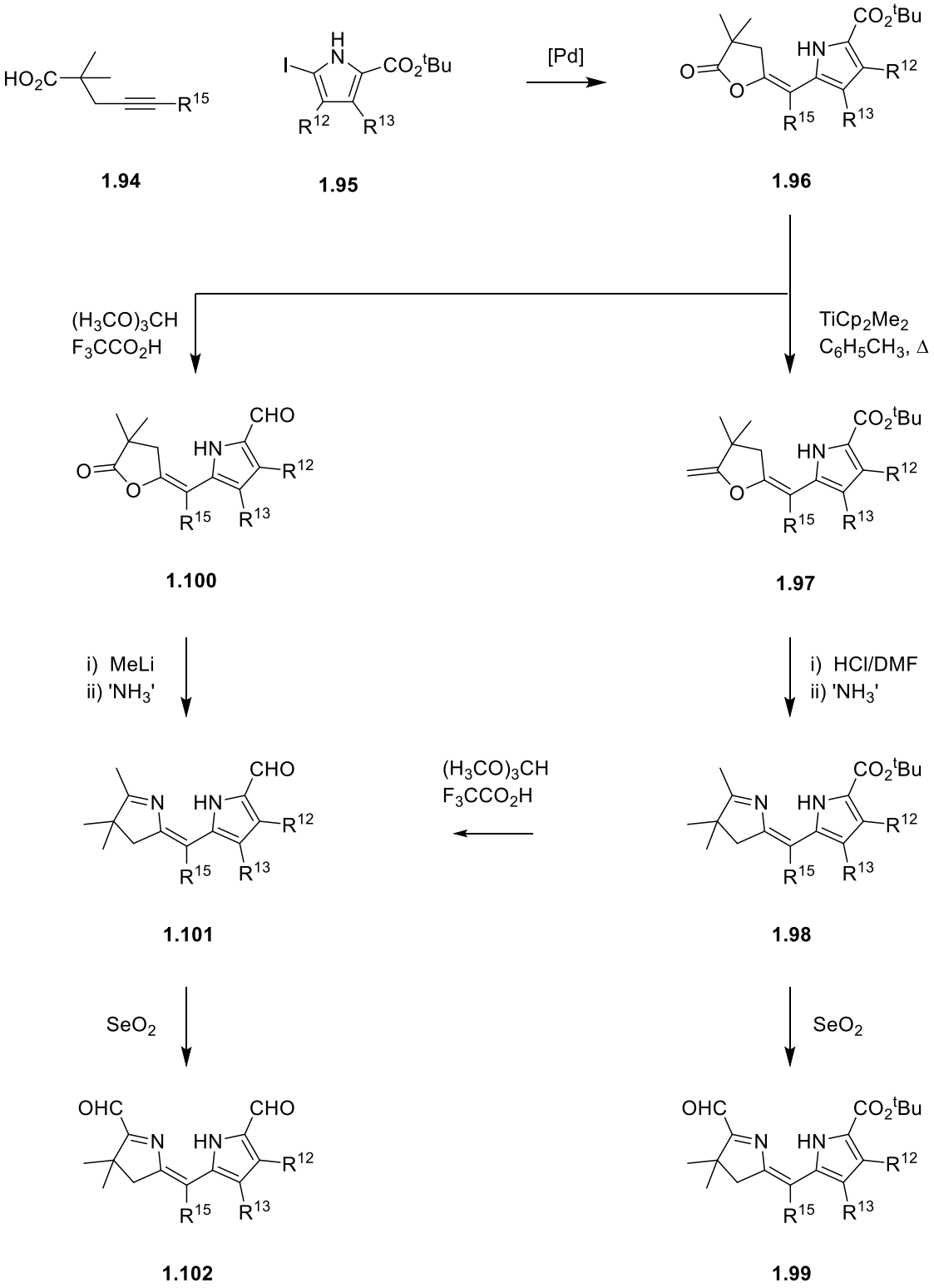

Scheme 1.11. Jacobi's construction of a *C-D* half for chlorin synthesis. R^{12}, R^{13}, R^{15} = alkyl, aryl.[179,180,181]

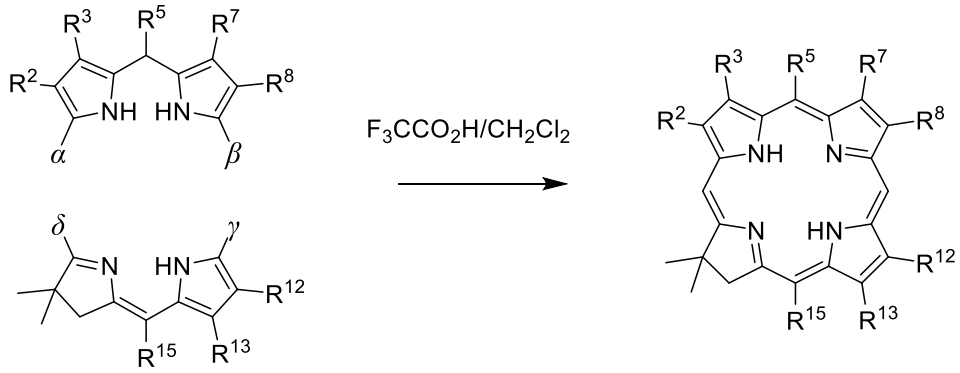

1.103-1.107 *Top*
1.99 or **1.102** *Bottom*

1.108

Scheme 1.12. General Scheme representing Jacobi's construction of chlorins from *A*-*B* and *C*-*D* halves.[182]

Bonellin is a naturally occurring tetrapyrrole continuing a *geminal* dimethyl moiety, **1.109**. It is produced by the green spoon worm, *Bonellia viridis*, (class *Echiura*, phylum *Annelida*).[184] It is found in the North-Eastern Atlantic ocean, as well as the Mediterranean sea. Among marine biologists, it is noted for displaying "exceptional sexual dimorphism" and the toxicity of the pigment within its skin.[185] Bonellin allows us to compare two (again) very different routes to hydroporphyrins. The two syntheses of (±)-bonellin dimethyl ester were presented by F. P Montforts, and A. R. Battersby.

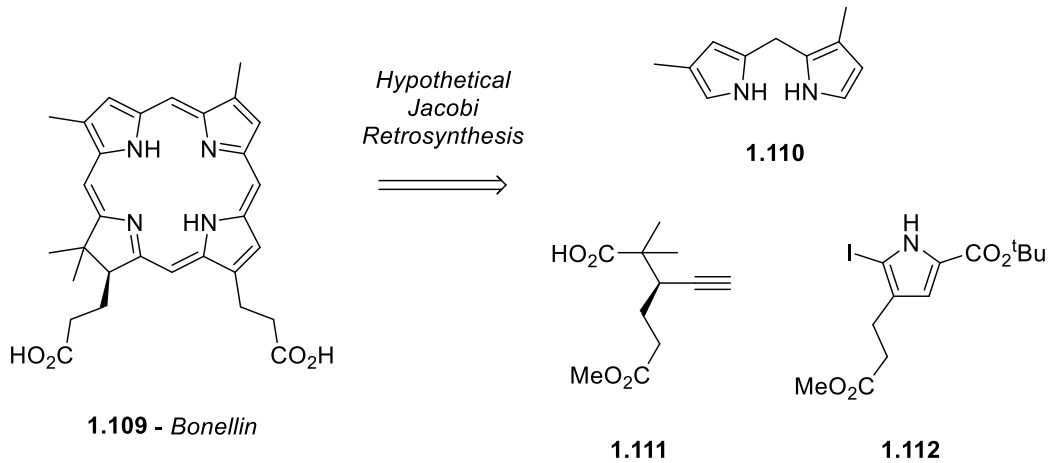

1.109 - *Bonellin*

1.110

1.111

1.112

Scheme 1.13. The structure of Bonellin and retrosynthetic analysis as if it were to be synthesized through a Jacobi style chlorin synthesis.

Whilst chronologically, Montforts synthesis was the last to be presented, its complexity warrants its initial discussion. For this synthesis, Montforts took a [3+1]

approach, a method he first reported in 1981 with the synthesis of 17,18-dihydro-18,18-dimethyl 2,3,7,8,12,13-hexamethyl-porphyrin.[186]

Each ring was meticulously prepared, some utilizing a mere bromination (ring *A*, **1.114**, Scheme 1.14),[187] or oxidation (ring *B*, **1.116**) whereas ring *C* required three steps; starting from Hagemann's ester **1.119**, derivatization to the enol ether, followed by ozonolysis, aldehyde deprotection and finally intramolecular cyclization in the presence of an ammonia source to yield 2-pyrrolone **1.120**. *D*-ring precursor **1.117** was carried over from another giant of total synthesis; vitamin B_{12}.[188,188,190,191,192] Subsequently, treatment of **1.117** with Lawessons' reagent, and conversion into the pyrrolidine-ylidene upon treatment with a brominated allylic malonate yields the *D*-ring.

The *B*,*C*-half **1.121** was generated upon condensation of *B*- and *C*-ring counterparts **1.116** and **1.120**, respectively, to yield an α-oxo-dipyrrin and conversion to the thio derivative was completed with Lawesson's reagent. Formation of the sulphur bridged *B*,*C*,*D*-tricycle **1.122** was performed under base catalysis, which then underwent acid mediated sulfide contraction to yield a free-base *B*,*C*,*D*-tricycle. In the free base form this intermediate was found to be extremely unstable, and readily oxidized. This problem was overcome via the complexation of nickel, i.e., to yield **1.123**. Treatment of **1.123** with H_2/Pd-C removed the *B*-ring ester protecting group and enabled a classical pyrrole-aldehyde condensation to yield **1.124**, which upon zinc chelation, elimination of cyanide, ring closure and oxidation yielded racemic bonellin dimethyl ester with the **1.124 → (±)-1.109-Me$_2$** step occurring in 42% yield over two steps. The initial construction of each ring and appending one to another in a stepwise fashion yields a synthesis of multiple steps.

The elegance of Battersby's synthesis is derived from its simplicity, at least in contrast. Battersby's approach was starkly different, an East-West style [2+2] synthesis (Scheme 1.15).[193] Henry reaction of **1.125** followed by reduction yields **1.126**, which undergoes Michael addition with **1.127** under base catalysis to yield pyrrolo-nitrohexanone **1.128**. Under McMurry-Nef conditions, this yields the A,D-half, dipyrrin **1.129**. In an unprecedented step, the *D*-ring had been built onto the *A*-ring, as opposed to a mere combination of two pre-functionalized rings.

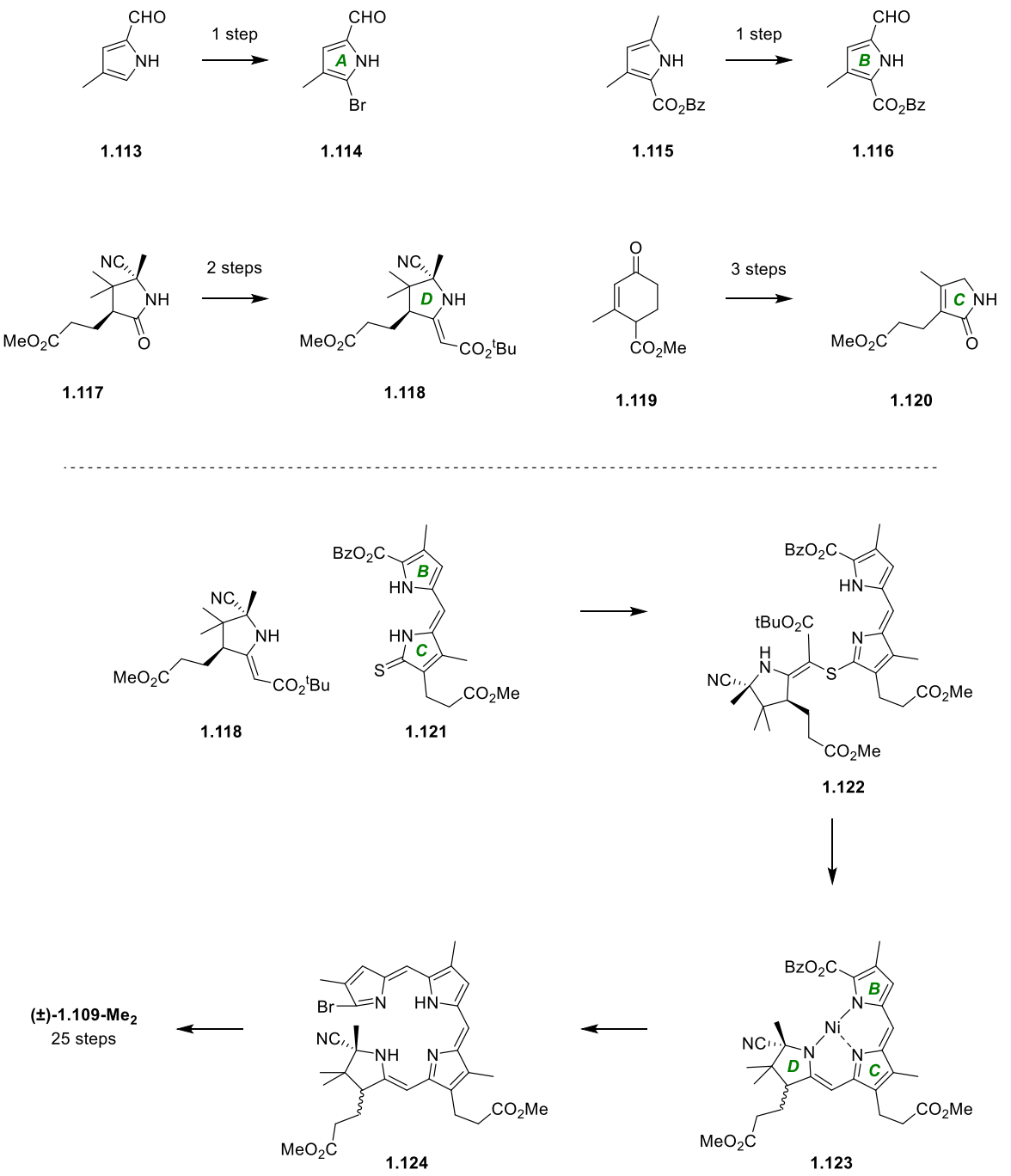

Scheme 1.14. A simplified representation of Montforts' [3+1] synthesis of (±)-bonellin dimethyl ester.[186]

Construction of the *B*-ring was simply a case of oxidation (**1.131**), whereas the *C*-ring required oxidation to the Δ^3-pyrrolin-2-one with *m*-CPBA, and removal of the *tert*-butyl ester with trifluoroacetic acid and hydroxyl removal with triethylsilane to yield **1.133**. Lastly, to form the *B*,*C*-half the *B*- and *C*-rings were condensed, the *tert*-butyl ester (**1.131**) transformed to a formyl group and the α-oxo moiety transformed

to a α-methoxy through the use of trimethyloxonium tetrafluoroborate, a Meerwein salt, yielding the dipyrrin **1.135** ready to condense.

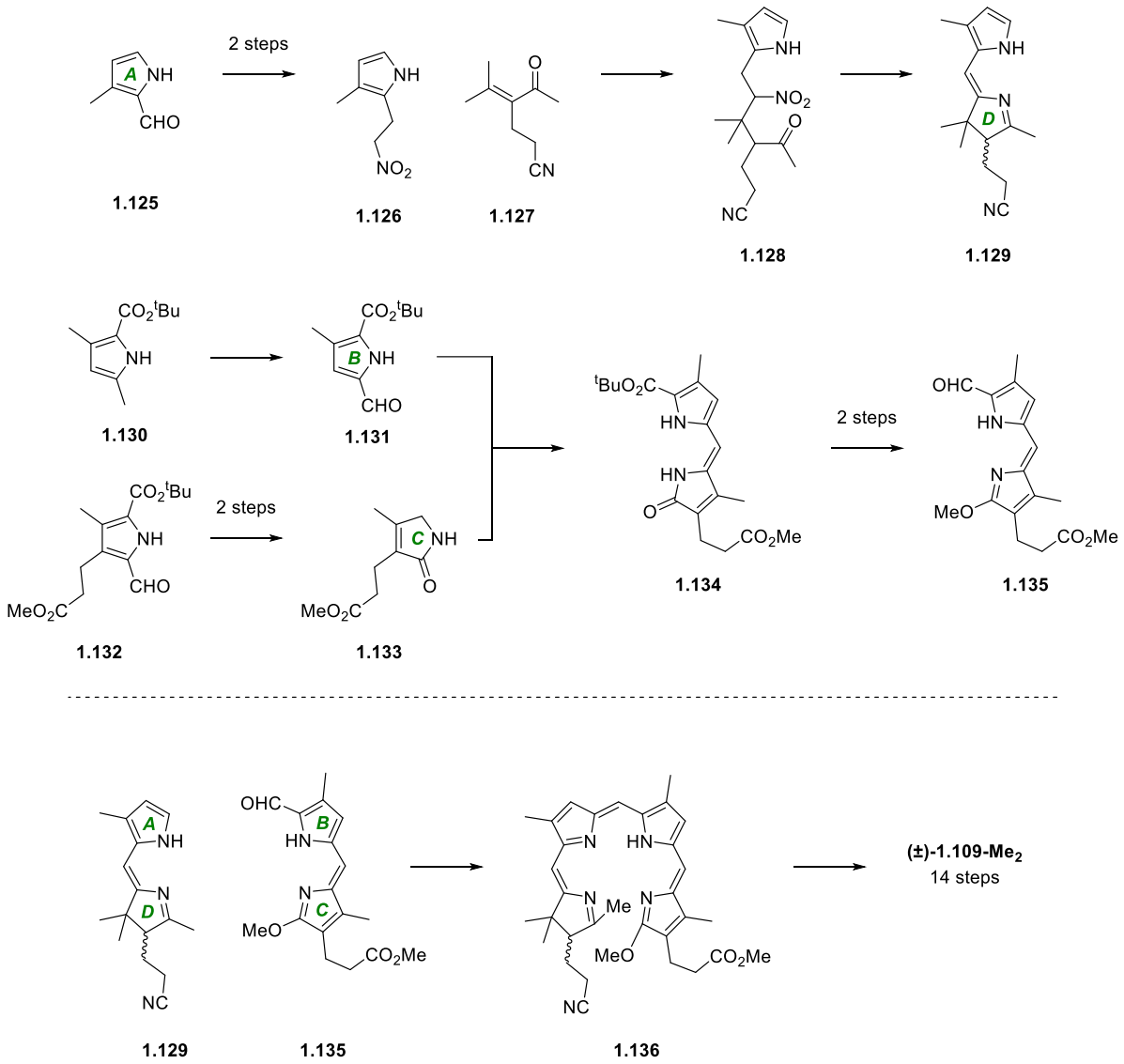

Scheme 1.15. A simplified representation of Battersby's [2+2] synthesis of (±)-bonellin dimethyl ester.[193]

Trifluoroacetic acid catalysis of **1.129** and **1.135** yielded the seco-chlorin system/dihydrobilatriene **1.136**. The ring-closure to yield **(±)-1.109-Me$_2$** was a photochemical one, as opposed to Montforts chemical closure. Irradiation of a tetrahydrofuran solution **1.136** in a sealed tube for 14 days with a tungsten lamp (1000 W) yielded the ring-closed system in only 36%. However, upon considering the amount of returned starting material, the yield of the photochemical ring closure step becomes 97%. The final stage of this synthesis was the conversion of the

cyano-group, carried through from **1.127**, to yield the methyl ester, which occurred in 88% yield.

The two syntheses vary drastically; A) Battersby's synthesis was of a [2+2] style opposed to Montforts' [3+1], B) and as a result contained far fewer steps (14 vs. 25) due to a more convergent synthesis (which was mainly a result of the symmetry used in the retrosynthetic analyses), C) a photochemical ring closure over the chemical method employed by Montforts.

Despite the differences exhibited here, it is evident to see that it is possible to generate biologically relevant chlorins utilizing a pyrroline ring, whether it is built onto another ring (as demonstrated by Battersby) or as a separate heterocycle and attached in a stepwise fashion (as demonstrated by Montforts). Particularly, utilizing the methodology of Montforts, we can hypothesize that given suitable time and vast quantity of reagents, it is possible to synthesize entirely asymmetric chlorins, e.g., Chl b_2.

1.2.4. Chlorins in PDT: What More Could We Want? Oxidation Resistance

Chlorins then have both been constructed elegantly by nature, and painstakingly by scientists. Some have even made their way into medical treatment. The most successful chlorin drug is surely BPDMA (**1.86**, Scheme 1.7), whilst food additives containing 'chlorophyllin' are widely used, the medical benefits remain unclear.[194,195] Whilst not used for oncology it is used to treat age related macular degeneration (ARMD) worldwide.

Other chlorins used in PDT include: *m*THPC (**1.40** Figure 1.10) and Laserphyrin™ (*a.k.a* Talaporfin Sodium or mono-L-aspartyl chlorin e_6, **1.139**, Figure 1.16). Laserphyrin™ was approved in Japan for the treatment of lung cancer,[196,197] with a strong absorption (log ε = 4.60) at 664 nm. Its rapid clearance from the body, and selective tumour localization make it a promising candidate for the treatment of future ailments.

However, two chlorins do not PDT fix. There is a continual stream of development towards new PSs, of all core structure types. A lot of work has already gone into

modification and bioconjugation of the rhodochlorin scaffold in order to enhance its efficacy as a PS.[198,199,200]

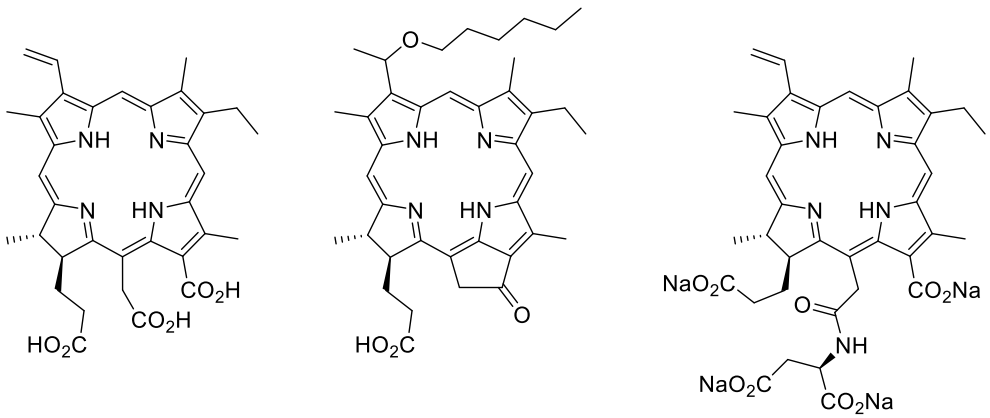

1.137 **1.138** **1.139**

Figure 1.16. Structures of chlorin PSs in PDT; **1.137** chlorin e_6, **1.138** HPPH or Photochlor®, and **1.139** Talaporfin Sodium or Laserphyrin™.

A compound already discussed for its synthetic methodology, tin(IV) ethyl etiopurpurin, otherwise known as Purlytin, or Rostaporfin,[174,176] (**1.90**, Scheme 1.8) has been in Phase II/III clinical trials for cutaneous cancer, metastatic breast cancer, AIDs-related Kaposi's sarcoma and ARMD.[201,202] Amazingly, in one Phase II/III clinical trial for breast cancer, treatment exhibited a complete response from >90% patients.[203] However, Rostaporfrin is itself not the solution to all of the problems; namely exhibiting dark toxicity and prolonged photosensitivity, and evidently from the structure water solubility (although this can be circumvented with formulations) is an issue.[204]

Another compound of note is **1.138**, known as Photochlor, or HPPH, it is a hexyl-ether derivative of phytochlorin.[205] Akin to Rostaporfin, it too is in a multitude of clinical trials.[206] Its most promising features, however, are low cutaneous phototoxicity and high absorption at 665 nm.[207]

However, there is a glaring issue here resolved by only a handful of the compounds discussed thus far; Bonellin, Rostaporfin and BPDMA. Even so, BPDMA is not used in an oncological PDT clinic and Bonellin has not yet been considered as a PS for PDT.

The issue lies in the oxidation state of the macrocycle, or should it be said: how easy it is or is not to change that oxidation state (Scheme 1.16). Inherently, porphyrins

are the fully oxidized examples here. Attempted oxidation of a porphyrin is likely to return the porphyrin, and some degradation products (ring-opened, meso-oxo, and any multitude of meso-β porphyrin linkages or multi-porphyrin arrays). The point of note, however, is that the electronic properties and symmetry of the macrocycle have not changed.

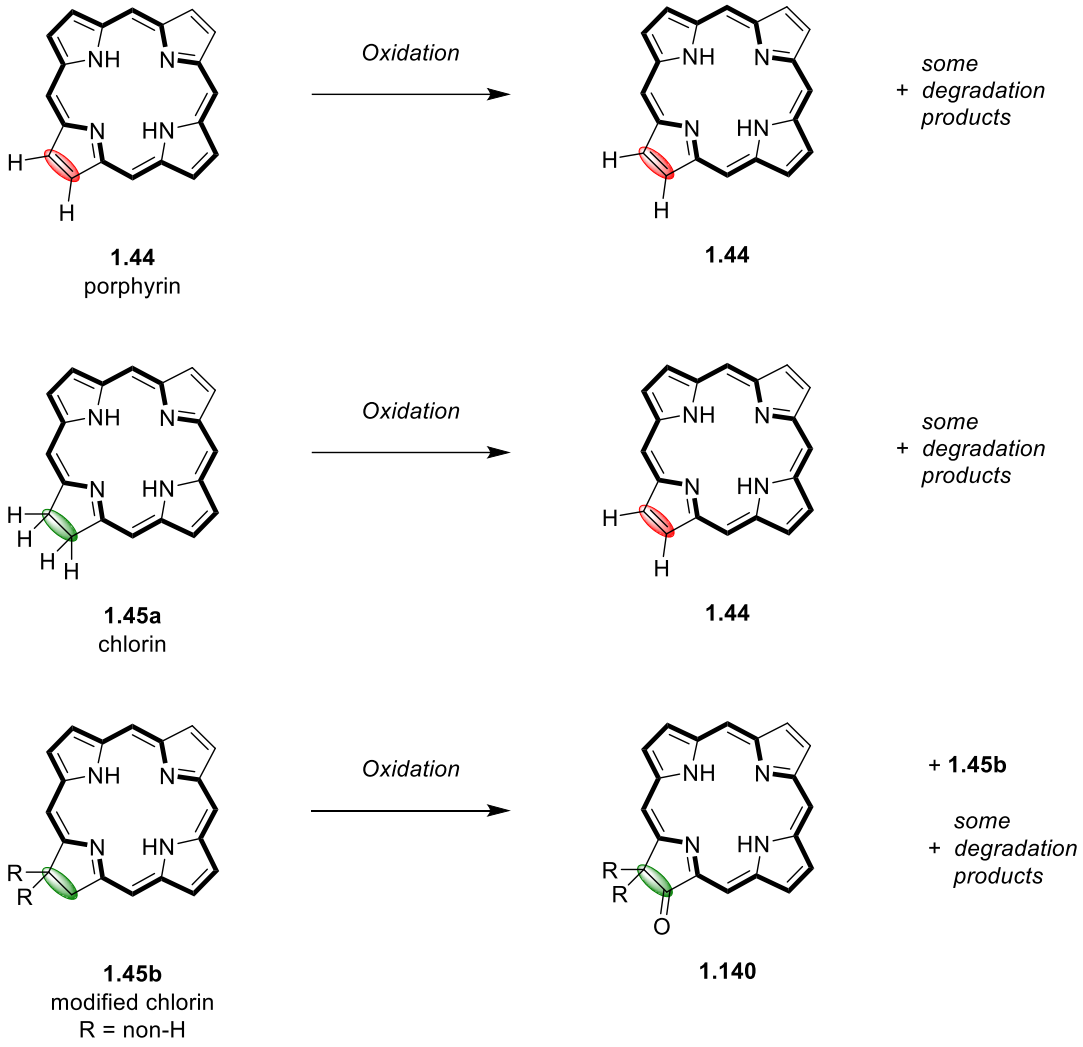

Scheme 1.16. Scheme depicting the oxidation products from typical mild oxidation of *top*: porphyrin, *middle*: chlorin and *bottom*: *gem*-disubstituted chlorin.

The oxidation of a chlorin prepared by a Whitlock Diimide reduction, however, will yield the porphyrin. Whilst it is easier to oxidize the bacteriochlorin to the chlorin and the chlorin to the porphyrin in the case of these reactions, it cannot be argued that the chlorin→porphyrin conversion does not occur. Herein lies the problem. If a PS has been designed to specifically exist as a chlorin, as a requirement for enhanced PDT (as exhibited by Figure 1.7), any oxidation or "adventitious dehydrogenation"[ii] will undo all of the work by the synthetic chemist who made the molecule.

Instead, the generation of a chlorin of type **1.45b** prevents this adventitious dehydrogenation, whilst the chlorin is oxidized to the oxochlorin, **1.140**, a transformation we have observed with *vicinal*-dihydroxyl chlorins and their transformation to octaalkyl oxochlorins (**1.68**, Scheme 1.4) which yields a minimal change in the spectroscopic properties of the tetrapyrrole.

1.3 – Photosensitizer Arrays

1.3.1 Multi-PS Systems: The Theory

Throughout this thesis thus far, the promise of successful PDT was dependent upon the three factors listed previously (Section 1.1.2). However, these discussions have assumed the nature of the PS to be a monomeric species, i.e., a single molecule PS (excluding the multiple components of Photofrin®.)

In the strive for ever more effective PDT, the concept of PS design is prevalent, aiming for success in the categories listed in Section 1.1.2. Whilst PS design is a lengthy process with many caveats, it begs the question: why not use multiple already approved/well understood PSs in one system? The concept being that within the same PS system there are multiple independent PSs and each would provide their own PDT affect. As has been highlighted previously (Section 1.1.3), differing PS cores have differing benefits and drawbacks. However, any PS system should be improved by the addition of other PS cores in the same system, in theory.

Whilst at first, this seems like an abstract concept, nature has once again beaten us to it. Multi-PS, or multi-chromophore, systems exist throughout nature ranging from light-harvesting pigment-protein complexes,[208] i.e., the special pair of chlorophylls in photosystem II,[209] to nucleic acids.

1.3.2 Multi-PS Systems: Spatially Arranged Chromophores – Don't Fret

Aside from natures endeavours, chemists have been trying to arrange chromophores spatially since the 1990s.[210] Multi-chromophoric arrays are a subject of immense current interest for multiple reasons. This field has enabled the study and application of many spacers used to separate chromophore units – fuelling developments in rigid hydrocarbon scaffolds,[35] given that the distance between the two chromophores in question is such a crucial factor. On the other hand, the photophysical consequences of such constructions are also of great interest. When two chromophores of suitable spectral overlap between emission spectra of a donor and absorption spectra of an acceptor motif, are placed within 1–10 nm of one another there is the possibility to observe Förster Resonance Energy Transfer (FRET).[211]

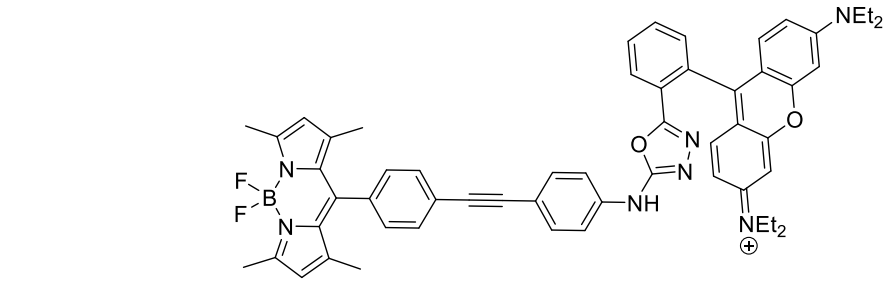

1.141

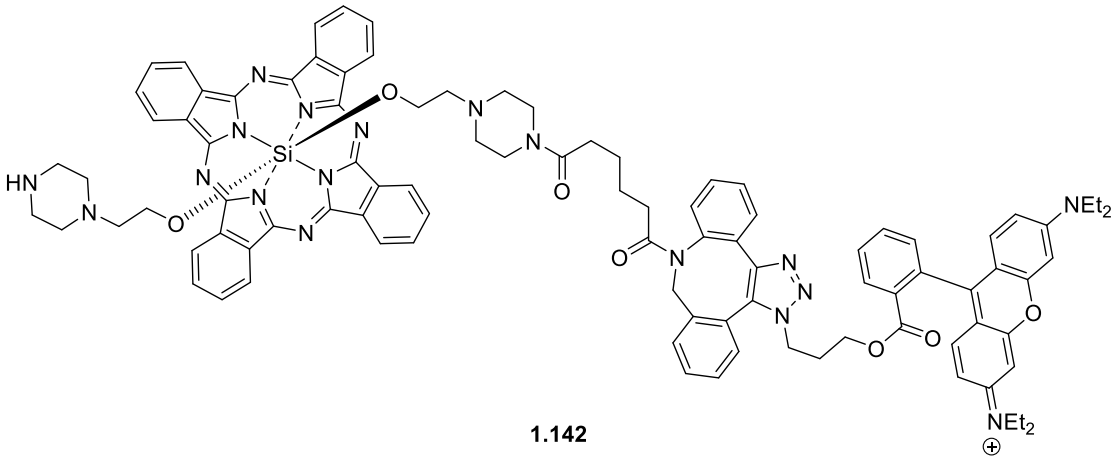

1.142

Figure 1.17. Structures of FRET systems based on pyrrolic fluorophores; BODIPY (**1.141**, *top*) and phthalocyanine (**1.142**, *bottom*).[212,213] Structures are displayed in "FRET on" mode.

FRET systems broadly encompassing pyrrolic fluorophores are vast in number, function, and structure type. Compound **1.141** was designed with the aim of Hg^{2+} sensing.[212] The toxicity of Hg is well understood, with it causing damage to central nervous and endocrine systems.[214] Originally, a thiourea linkage Is present between the phenylamine and the ring-closed form of the rhodamine dye, however upon sensing Hg^{2+}, the thio-motif is cleaved and a 1,3,4-oxadiazole ring is formed enabling the rhodamine fluorescence to be observed. A distinct change in the emission spectrum is observed with a decrease in the emission of the BODIPY emission at λ_{em} = 514 nm, and an increase in emission at λ_{em} = 589 nm, arising from the rhodamine. The calculated efficiency of FRET in this system was found to be 99%, and the R_0 value (distance at with energy transfer efficiency is 50%) was found to be 58.9 Å, further indicative of a highly efficient system. The response for Hg^{2+} was the highest of all M^{n+} ions surveyed, with Ag+ being the only other to provide a response.

Compound **1.142** instead was used for PDT. Whilst still containing a rhodamine motif, the authors utilize a Pc for their PS core. In prior works combining these two cores, the rhodamine was spaced form the silicon(IV) centre via PEG chains,[213] and FRET was observed (with the rhodamine being the donor and the Pc being the acceptor). In this instance, the authors propose PDT *via* FRET post in situ biorthogonal copper-free strain promoted alkyne-azide cycloaddition (SPAAC).[215] The authors were able to perform this SPAAC reaction in T-24 cells, as observed via diminishing fluorescence form the rhodamine motif. Whilst no R_0 or IC_{50} values were presented, the authors claim >90% phototoxicity at 0.5 μM, upon irradiation at λ_{ex} = 531 nm at E = 5.6 mW/cm^2 for 0.5 h.

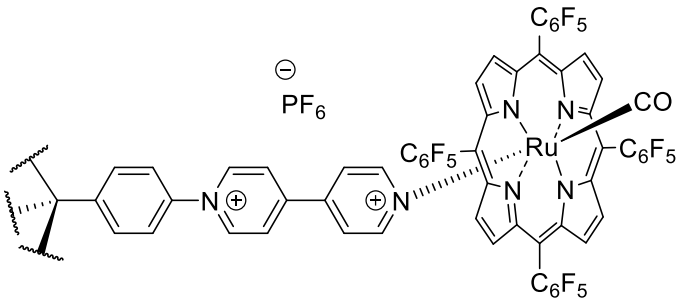

1.143

Figure 1.18. Structure of a rigid chromophore array based on tetraphenylmethane (TPM) and viologen building blocks.[216,217]

In one example of a rigid chromophore array, **1.143** comprises of the tetraphenylmethane (TPM) core. Appended to this is a viologen motif, which enables appending a ruthenium porphyrin.[217] The authors find that excitation of either the viologen motif or the ruthenium porphyrin yields quenching via photoinduced electron transfer, occurring at room temperature. The charge separated state was found to exist for 800 ps, over four times longer than observed for the monomeric adduct. This work highlights the ease in which mutlichromophoric systems can be formed, in highly predictable shape persistent architectures.

1.3.2 Multi-PS Systems: In Theory, But In PDT?

There are multi-PS systems that are continually used in PDT; namely hydrogels.[218] These, along with other 3D polymer scaffolds, aim to overcome to the solubility issues of traditional and successful PSs, but these are not PS arrays. In the same

vein, the use of nanoparticles (NPs) of Ag or Au is another strategy which has the same downfalls.[219]

In the application of PS arrays, there are, to our knowledge, currently no examples of rigid PS arrays being used as PSs for PDT. However, multi-PS systems have been utilized to great effect.

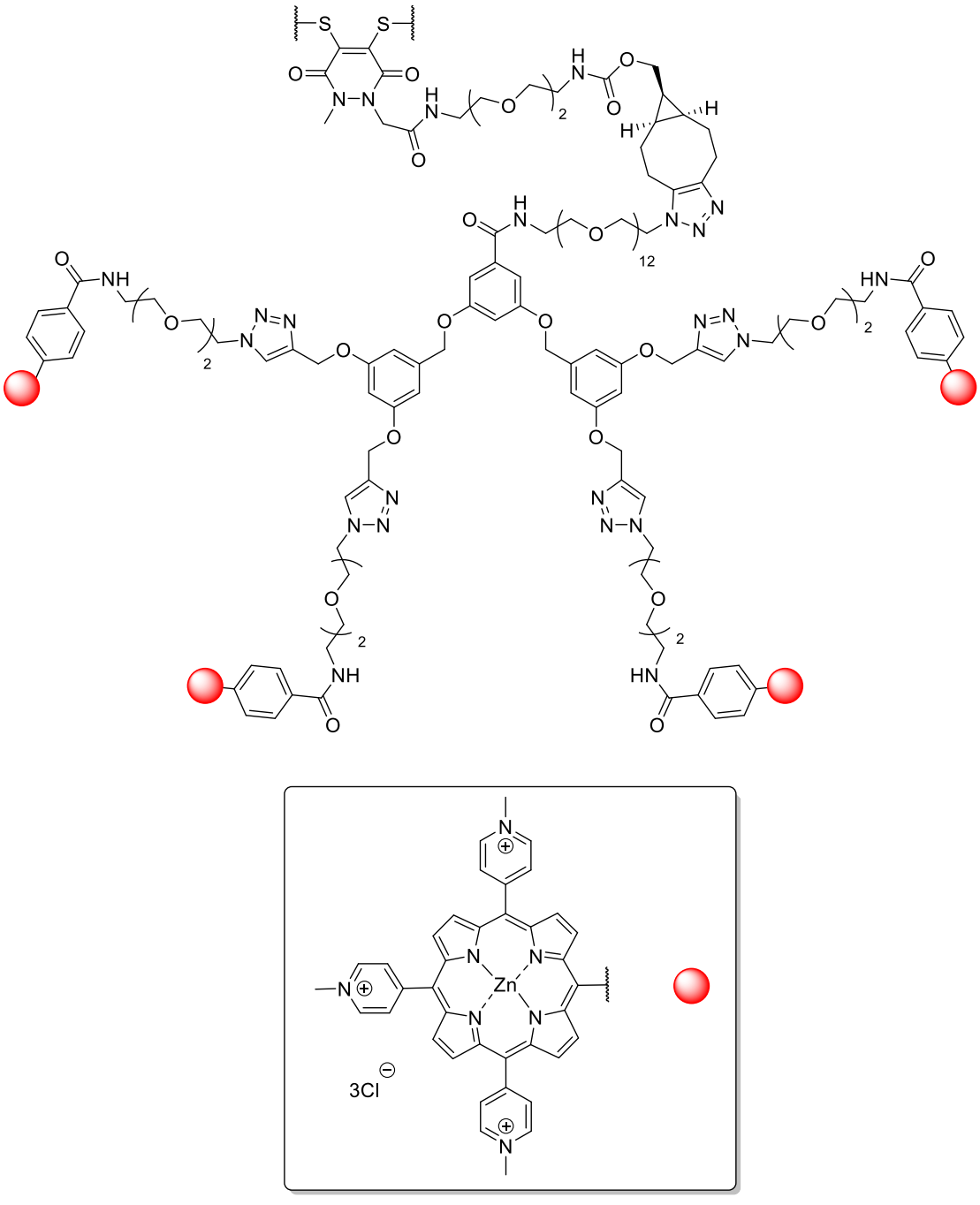

1.144

Figure 1.19. Structure of multi-PS system utilized by Bryden et al., in 2018.[220] Pyridazinedione is bonded across a disfulfide bridge in trastuzumab.

In 2018, Boyle *et al*. presented the synthesis and *in vitro* evaluation of antibody-porphyrin conjugate **1.144**.[220] Antibody drug conjugates have continually proven themselves to be highly effective in medicinal chemistry, despite their downfalls.[221a] However, the utilization of bridging disulfide bonds with motifs of interest has been shown to go some way to overcoming many of the issues with porphyrin-antibody drug conjugates.[221b]

Through the synthesis of a second generation dendron, bearing four alkyne motifs, the conjugation of four porphyrin motifs *via* traditional CuAAC chemistry is enabled. Successful SPAAC yielded a drug-to-antibody ratio of 15.4 porphyrins to one trastuzumab, a HER2 targeting antibody, as determined *via* UV-Visible spectroscopy, close to the theoretical maximum of 16. Further experimentation via SDS-PAGE highlighted the lack of partial re-bridging or unconjugated antibody fragments at lower molecular weights.

Conjugate **1.144** was analysed *in vitro* against BT-474 and MDA-MB-468 cell lines, with BT-474 cells those that overexpress native levels of HER2 receptor. Cells were irradiated at 20 J cm^{-2} of broad-spectrum illumination as opposed to a specific wavelength. Dark toxicity was not presented for conjugate **1.144** even at 1 μM across both cell lines, and **1.144** presented a LD_{90} of 37 nM, vastly lower than the typical values of monomeric porphyrinoid PSs for PDT. Across all experiments, no toxicity was observed for trastuzumab alone, indicating that the phototoxicity observed is as a direct result of porphyrin conjugation. The mid and facile synthetic procedures utilized highlight the utility of this kind of system in enabling higher efficacy of PDT.

2. Objectives

PDT has continually shown itself to be an effective modality in the destruction of diseased, or otherwise undesired tissues, viruses, and bacteria. There is an ongoing struggle to find a PS core that fulfils all the criteria set out to yield the perfect PS. Given this, whilst the aim of this thesis in general is to enhance the efficacy of PDT, the work can be broken down into two main aims.

The first of which is to understand the efficacy of oxidation resistant chlorins, i.e., of structure type **1.45b** as PSs for PDT. Given the importance of the wavelength of absorption of the PS – it is of paramount importance to retain a longer wavelength, through the prevention of adventitious dehydrogenation. Upon determination of the photophysical characteristics of this motif, it will then be appended with bioconjugatable handles. In doing this, there is the possibility in future to yield 3rd generation PSs. These compounds will undergo photophysical analyses to determine whether the structural changes necessary to yield bioconjugation will hinder the desirable photophysical characteristics. Lastly, these will undergo *in vitro* biological evaluations to fully understand their efficacy as PSs. Coupled with *in vitro* analyses of analogous porphyrins, this will give an indication of their utility in PDT.

The latter is taking another popular approach. Whilst one tack is to increase the efficacy of a PS core structure through either modulation of its photophysical properties, or implementing bioconjugatable handles to increase selectivity, and thus efficacy, another is merely to add more PSs to the same system. This work will surround the modulation of the 1,1,2,2-tetraphenylethylene (TPE) scaffold, a rigid D_{2h} symmetric core which can hold multiple PSs in one molecule. It is hypothesized that the generation of TPE-photosensitizer arrays will enable greater efficacy of the PS system. Further to this, assuming the TPE system retains its aggregation induced emission (AIE) properties could yield a theranostic PS system.

Chapter 3.

10-Aryl Chlorins – The Principal Elements

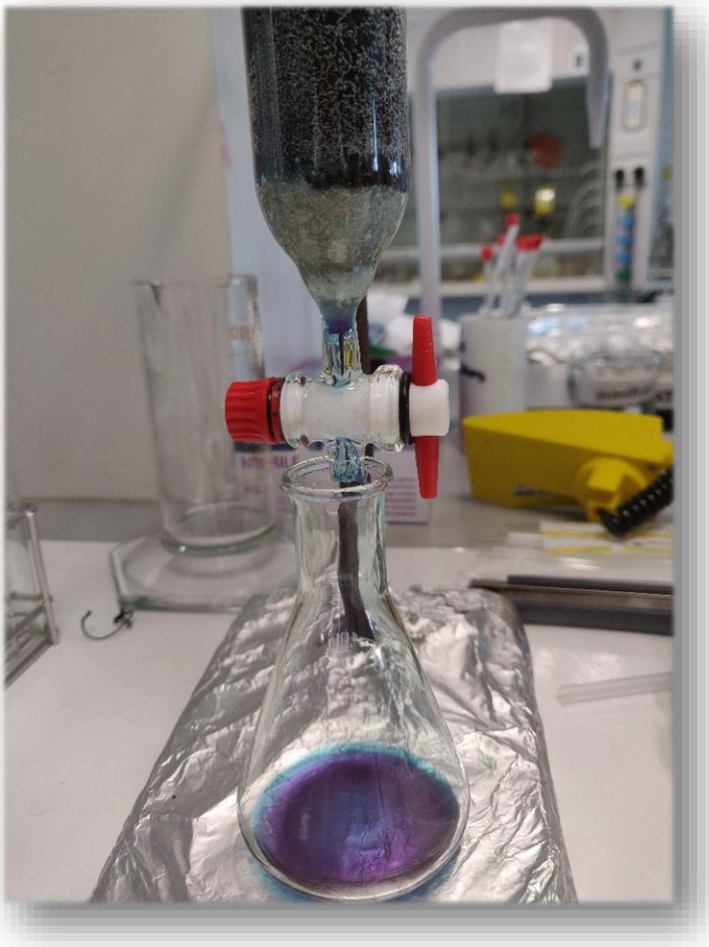

3. **10-Aryl Chlorins – The Principal Element**

3.1 Introduction

3.1.1 From Battersby to Lindsey

As detailed *vide supra* in Section 1.2.3, the generation of bonellin was performed by Battersby and Montforts.[186,193] Aside from Fischer's generation of oxo-chlorins,[158] these were the first examples of *geminal*-dimethyl chlorins conceived via *de novo* syntheses. Despite the prominence of bonellin in the synthetic literature surrounding the subject of *gem*-dialkyl tetrapyrroles (or those possessing C_β centred spirocyclic moieties), there are multiple other examples of this class of compound present in nature.

Heme *d* (**3.1**, Figure 3.1), termed "the green heme",[222] contains a spirolactone at one C_β and hydroxyl and methyl groups at the other, and is found in *Escherichia coli* grown at low pO_2.[223] Faktor I (**3.2**) is the result of handling precorrin I (an intermediate in the synthesis of vitamin B_{12} from uroporphyrinogen III),[224] in open air. It is a chlorin that also possesses a *gem*-dimethyl moiety. An analogous isobacteriochlorin, siroheme, contains the same groups in both *C*- and *D* rings.[225] Tolyporphins are glycosylated 7,17-dioxobacteriochlorins, with tolyporphin A (**3.3**) presented in Figure 3.1.[226] In all cases oxidation resistance is found on the respective rings.

However, excluding tetrapyrroles, nature is riddled with *gem*-dimethyl groups. Some well-known examples include: (-)-*trans*-Δ^9-tetrahydrocannabinol (**3.4**),[227,228] (1R)-(+)-α-pinene (**3.5**) and penicillin G (**3.7**).[229] Fasamycin A (**3.8**, Figure 3.1) is another antibiotic;[230] however, it exhibits activity against methicillin-resistant *Staphylococcus aureus* (MRSA) and vancomycin-resistant *Enterococcus faecalis*. Its synthesis has been visited on multiple occasions.[230] (-)-Spiromalbramide (**3.6**) is a fungal indole alkaloid which recently had its biosynthetic pathway elucidated.[231] All of this goes to show that in fact, that *gem*-dialkyl moieties are not as uncommon as may be perceived, given their existence in multiple vastly differing sections of the natural world.[232,233]

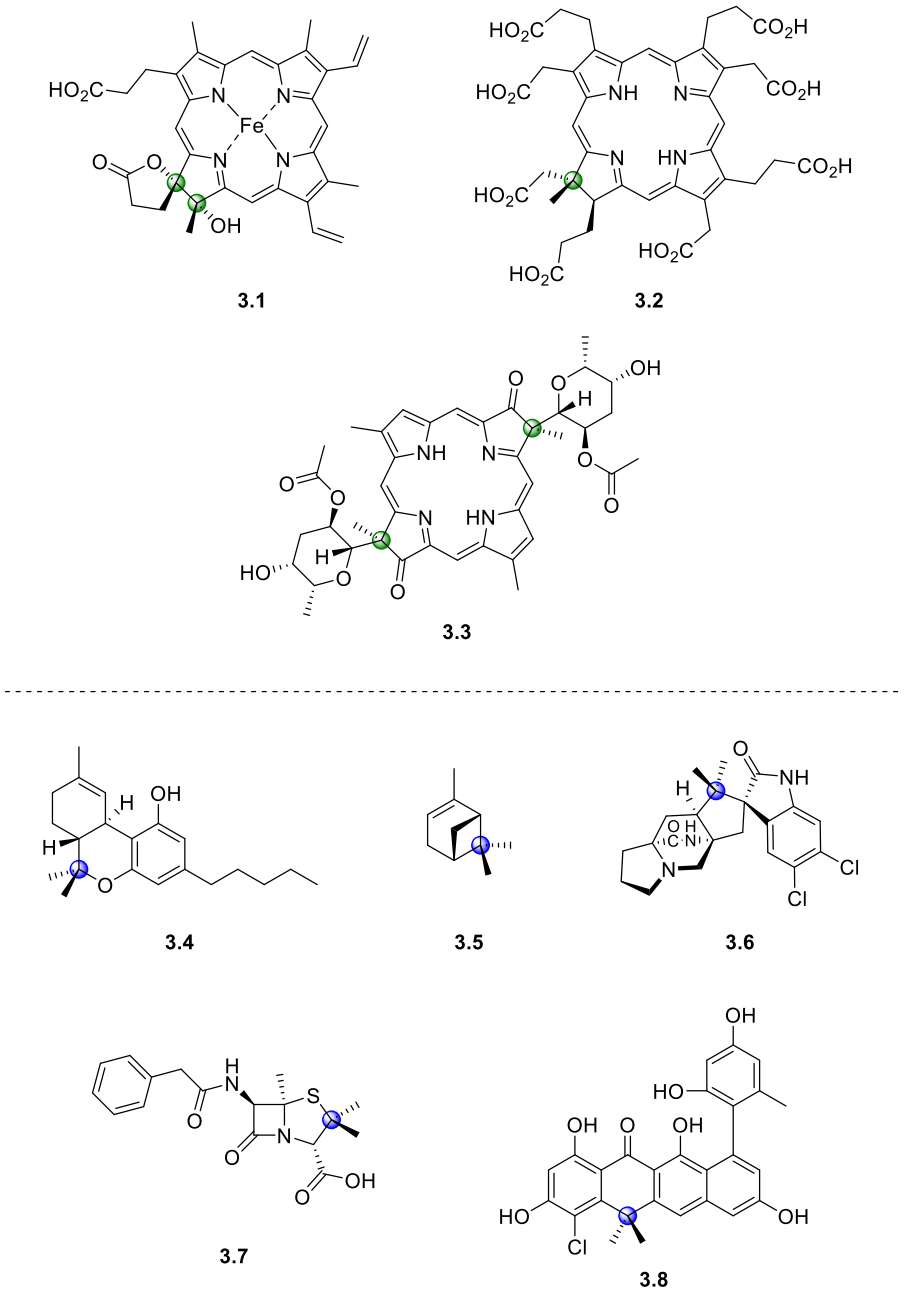

Figure 3.1. Structures of a variety of naturally occurring *gem*-dialkyl tetrapyrroles (*top*) with *gem*-dialkyl centres labelled in green and *gem*-dimethyl containing motifs from other parts of nature (*bottom*) with *gem*-dialkyl centres labelled in blue.[222,223,224,225,226,227,228,229,230,231]

At the turn of the millennium, the Lindsey group sought to construct oxidation resistant chlorins of their own. Through a survey of the literature, it became apparent to them that previous synthetic routes utilized by Battersby to chlorins and isobacteriochlorins "were particularly attractive".[234] These routes had been developed as a direct result of the initial synthesis of bonellin.[186] Two general approaches had been applied, both consisting of the linking of two dipyrrolic

species, i.e. a [2+2] style syntheses, with the difference residing in the final cyclization step being performed either photochemically or thermally (Scheme 3.1).

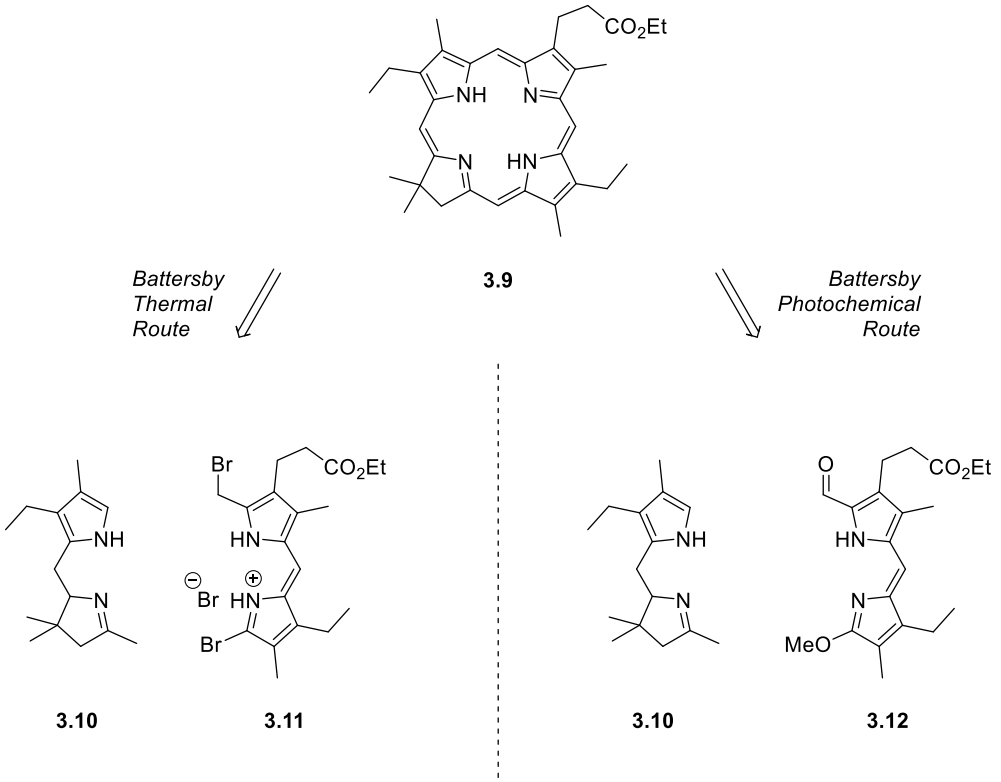

Scheme 3.1. Retrosynthetic analysis on one of Battersby's chlorins utilizing thermal routes (*left*) and photochemical routes (*right*).[235,236]

Whilst both methods successfully yielded chlorins, they both have downfalls. Thermal ring closure was performed in the presence of Cu(II) salts and gave copper chlorins in yields of no higher than 7%,[235] with subsequent demetallation performed with 1,3-propanedithiol in trifluoroacetic acid. In contrast, the photochemical route returned a significant amount of free base chlorin, i.e., up to 50%;[236] although, however these syntheses required extended irradiation of dilute solutions. Chlorins, using either method, were not generated in masses greater than 10 mg. Low yields aside, the functional group compatibility of the α-positions of all **3.10**–**3.12** yielded no regioisomeric products, in comparison to the mixed pyrrole-aldehyde condensations typically used today.

Given these findings, the Lindsey group set out to develop new halves using Battersby's thermal route as a template, despite the lower yields observed, given their initial hypothesis that this route would provide a greater substrate scope with evermore diverse substituents.[234]

Starting instead from pyrrole-2-carboxaldehyde (**3.13**, Scheme 3.2, with Battersby's synthesis in Scheme 1.15 for comparison), a Henry reaction with nitromethane to yield the (*E*)-2-(2-nitrovinyl)pyrrole (**3.14**) was employed. Subsequent reduction to the nitroethyl intermediate, followed by caesium fluoride catalysed Michael addition with mesityl oxide (**3.20**) to yield pyrrolo-nitrohexanone (**3.16**) which upon treatment with titanium(III) chloride under McMurry-Nef conditions yielded 2,3-dihydrodipyrrin **3.17**.[234] Issues arose with the preparation of **3.17**, and it was only a year later before the group changed their synthesis to use 2,3,4,5-tetrahydrodipyrrin **3.18**.[237] It was possible to generate the *N*-oxide **3.19**, and deoxygenate this to yield the desired tetrahydrodipyrrin. In 2005, Ptaszek's refinements yielded the single step cyclization and deoxygenation from **3.16**.[238] Yields for chlorins increased from 0–10% with **3.17** to 15–40% upon use of **3.18**.

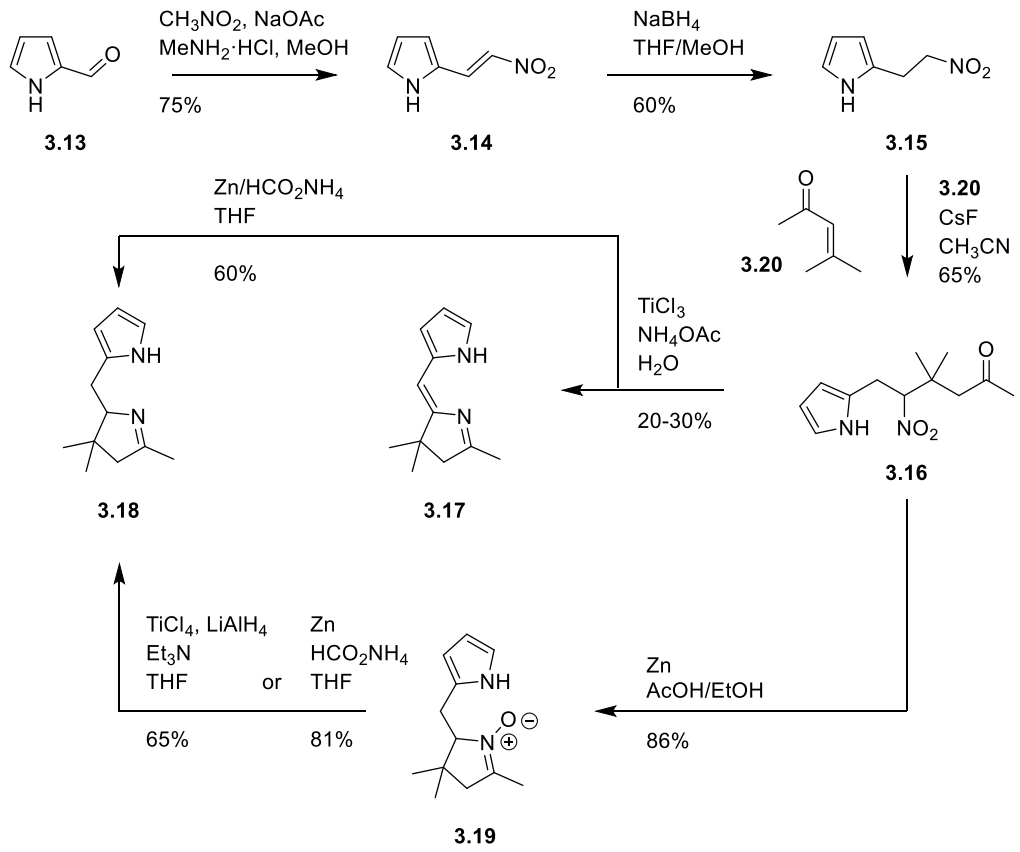

Scheme 3.2. Syntheses of 2,3-dihydrodipyrrin **3.17**, 2,3,4,5-tetrahydrodipyrrin **3.18** and intermediate *N*-Oxide **3.19**.[234,237,238]

Understandably, through repeated iterations of this synthesis and improvements, more and more has been learnt about it. Of note, two by-products: 2-(2-pyrrolyl)-1,3-dinitropropane results from the synthesis of **3.14**; however, it was described as

"ostensible".[238] Analogous by-products have been noted upon the utilization of β-aryl substituted pyrroles.[239] The other by-product is a tricyclic system, (**3.21,** Scheme 3.3) 1,9,9-trimethyl-5,11-diaza-tricyclo(6.2.1.$0^{2,6}$)undeca-2(6),3-diene, initially formed upon generation of **3.19** from **3.16**, it was obtained but not identified in the original 2000 manuscript.[234] The formation of this structure was explored further in 2001 via the treatment of **3.19** again with $TiCl_3$, along with the treatment of **3.18** with trifluoracetic acid in acetonitrile. Whilst no yield in either case was provided, the rate of reaction was described as "*very slow*"[237] upon the use of the latter procedure.

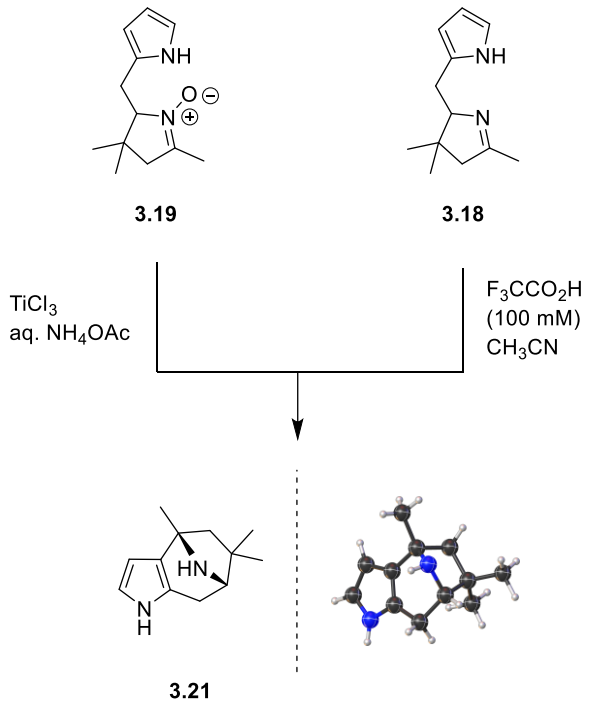

Scheme 3.3. Generation of tricyclic by-product **3.21** along with **3.21** in the crystal (CCDC No. 1119659).[237] Image generated in Olex2.[126] Thermal ellipsoids are at 50% probability.

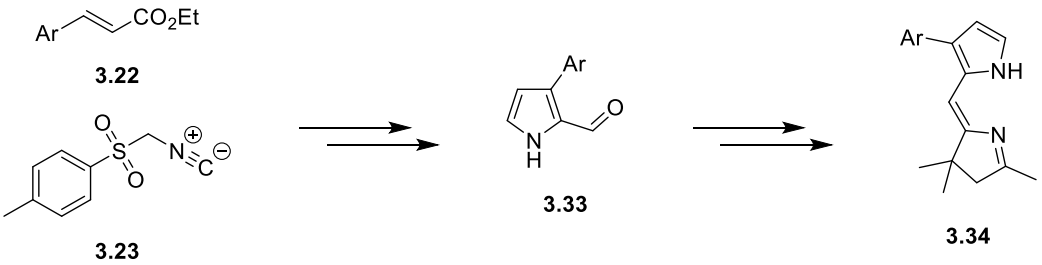

Scheme 3.4. Generation of 7-aryl substituted dihydrodipyrrins (**3.24**), through utilization of the van Leusen pyrrole synthesis, and analogous syntheses presented in Scheme 3.2.[239]

In the same journal issue as the initial synthesis of **3.17**, the same group presented the synthesis of β-aryl substituted analogues.[239] The generation of aryl pyrroles through the use of the van Leusen synthesis (**3.33**, Scheme 3.4),[240] followed by an analogous synthetic sequence yielded 7-aryl substituted dihydrodipyrrins (**3.34**).

Whilst specific developments in the synthesis of hydrodipyrrins were necessary to yield chlorins, the synthesis of porphyrins from dipyrrins had been continually undertaken for multiple years prior, particularly with Fischer's early syntheses of natural porphyrins.[241,242] However, these were meso-free dipyrromethanes (DPMs), as opposed to the meso-substituted DPMs desired by the Lindsey group. In 1994, it was noted by Lee and Lindsey that the chemistry of meso-substituted dipyrromethanes had "been rather undeveloped".[244] Prior to this, only one report exists from Ashley and co-workers, in which 5-(4-pyridyl)dipyrromethane was synthesized through the combination of pyrrole, pyridine-4-carboxaldehyde in methanol with HCl gas in a yield of "about 70%".[243]

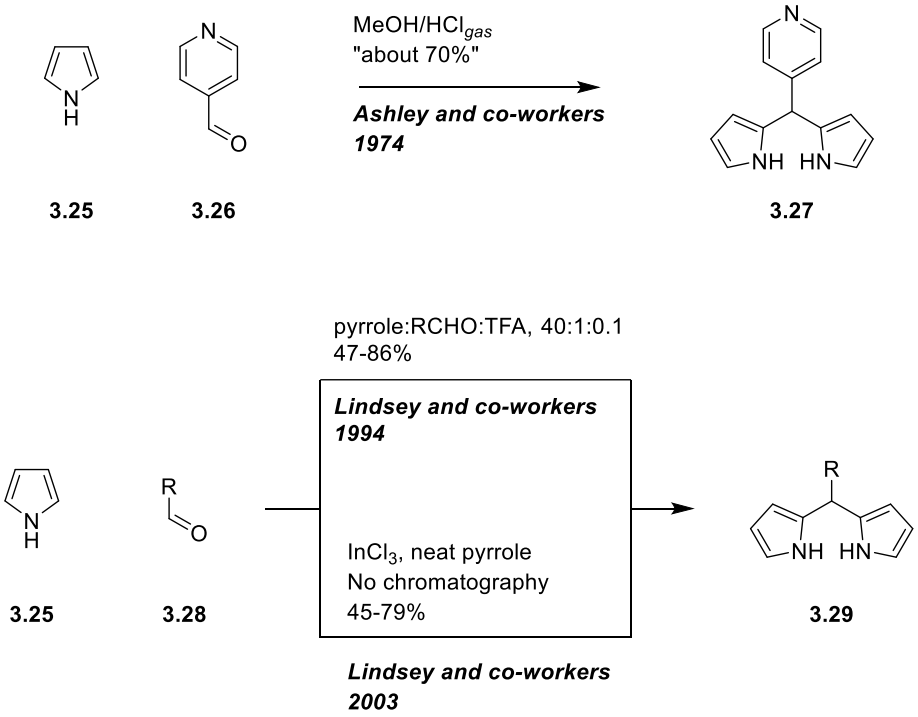

Scheme 3.5. Main iterations and refinements in the synthesis of meso-substituted DPMs by Ashley and co-workers,[243] and by Lindsey and co-workers.[245,246] R = alkyl, aryl.

In 1994, the initial method for generation of dipyrromethanes utilized a ratio of pyrrole:aldehyde:acid of 40:1:0.1 where the acids analysed were either trifluoroacetic acid or boron trifluoride diethyl etherate, with yields ranging from 47–

86%.[244] In 1999, further investigations were conducted with the aims of mitigating formation of *N*-confused DPMs and modifying the pyrrole:aldehyde ratio as to increase yield. The generation of *N*-confused DPMs “appears to be universal”.[245] It was also found that an increased pyrrole:aldehyde ratio increased the yield of the isolated DPM. The last refinement in DPM synthesis came in 2003, where the utilization of a Lewis acid, indium(III) chloride, as opposed to boron trifluoride diethyl etherate, or Brønsted acid, i.e., trifluoroacetic acid, was found to yield exclusively the dipyrromethane via recrystallization.[246] The solvent for the reaction, pyrrole, could be recovered in *ca.* 90% and therefore recycled. These dipyrromethanes were Vilsmeier-Haack formylated, and brominated following general procedures.[247]

With the two halves constructed, variations in the condensation conditions were also investigated. Whilst diverse hydrodipyrrin structures have been synthesized,[248] the synthesis of these chlorins typically occurs from a 2,3,4,5-tetrahydro-1,3,3-trimethyldipyrrin (**3.18**) and a 1-bromo-9-formyldipyrromethane (**3.30**). Whilst the first chlorins to be synthesized by the Lindsey group were 5,10-diaryl chlorins and the subsequent dipyrromethanes were 9-benzoyl as opposed to 9-formyl, a greater discussion on those methods utilized will be presented *vide infra*, and hence for this discussion the DPMs will be the formyl derivatives.

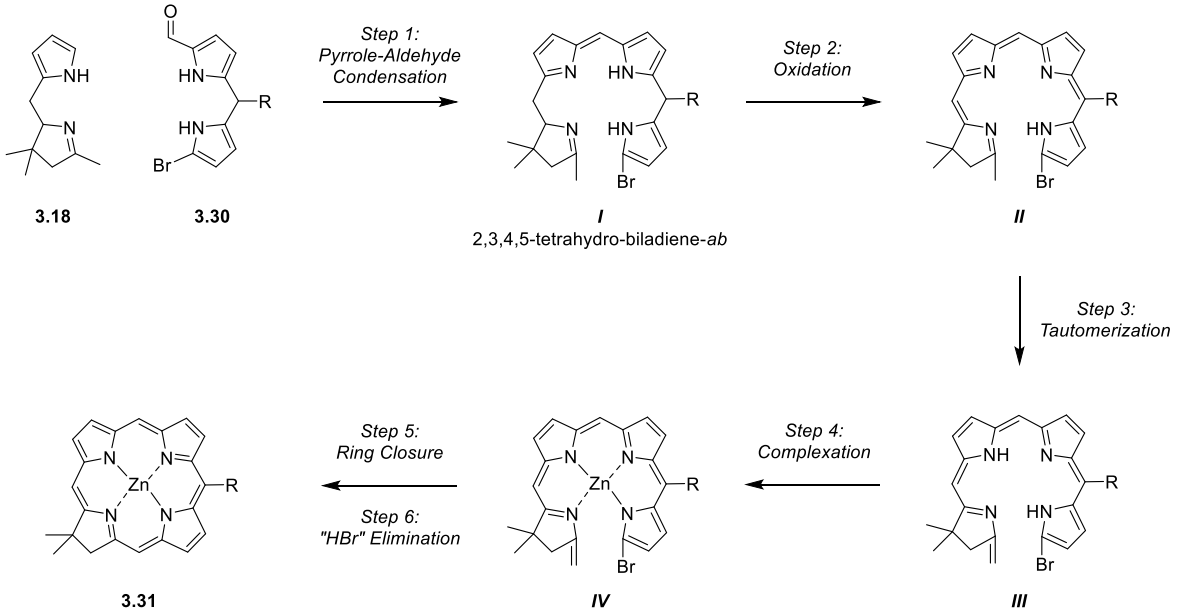

Scheme 3.6. Proposed intermediates in the Lindsey chlorin synthesis (***I*–*IV***), utilizing 2,3,4,5-tetrahydro-1,3,3-trimethyldipyrrin **3.18**, and 1-bromo-9-formyl-5-substituted dipyrromethane, **3.30**. R = alkyl, aryl.[234,249]

Akin to every constituent element of these chlorins, the final synthesis has been refined multiple times. In the first step, there is an acid catalysed pyrrole-aldehyde condensation linking the *A*- and *B*-rings in the generation of a 2,3,4,5-tetrahydrobiladiene-*ab* (*I*, Scheme 3.6). This intermediate is then oxidized, and subsequently tautomerizes to yield two-NH moieties in the core, as well as ene-imine tautomerization in the *D*-ring. This allows for the chelation of a zinc(II) centre which enables closure of the tetrapyrrole ring system *via* an [18π]-electrocyclization. Following this, HBr is eliminated, and the chlorin is yielded.

Subsequent publications have systematically investigated conditions for the pyrrole-aldehyde condensation, the oxidant (with $AgIO_3$, *p*-chloranil, benzoquinone, MnO_2, $MnO_2/AgIO_3$, and $K_4Fe(CN)_6{\cdot}3H_2O$ being examined) the base used ($NaHCO_3$, piperidine), and solvent (DMF, $C_6H_5CH_3$, 1,4-dioxane). Eventually, the conditions found to be most fruitful are those presented in Scheme 3.7.[250]

In 2007, the final refinements (for now) were made to the synthesis. Condensation of the two halves with *p*-toluenesulfonic acid monohydrate in a mixture of CH_2Cl_2 and CH_3OH at a concentration of 26 mM was found to produce the highest yield of product the biladiene-*ab* intermediate. Halting the reaction with 2,2,6,6,-tetramethylpiperidine, a sterically hindered non-nucleophilic base, and using it again for the subsequent metallation steps, it outperformed piperidine. Through multiple other investigations, the most suitable oxidant was found to be silver(I) triflate, acetonitrile as the solvent, and, because of the capability to form the initial complex and further synthetic utility, the use of anhydrous zinc(II) acetate was retained.[234,237,239,250]

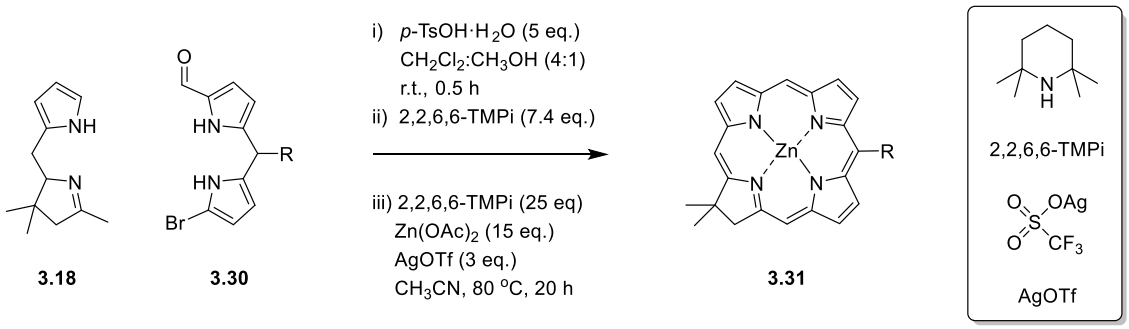

3.18 3.30 3.31

Scheme 3.7. Ideal refined conditions for the Lindsey chlorin synthesis, starting from the same starting materials as utilized in Scheme 3.6.[250]

As a result of building upon the years of work by Battersby, along with those who came before, and continual refinement of procedures therein,[238,246] the Lindsey chlorin synthesis has become ubiquitous today. Whilst the Montforts style synthesis does present the occasional application and use,[251] and the Jacobi style synthesis lead the way for the North-South bacteriochlorin synthesis,[182,252] the number of publications of those is dwarfed by those utilizing the Lindsey style synthesis.

3.1.2 Ground-breaking Uses of the Lindsey Chlorin Synthesis

Given then the synthetic advances between 1999 and the present day, what has the Lindsey chlorin synthesis given to the tetrapyrrole community of current? Displayed in Figure 3.2 are some prime examples of the achievements made using the Lindsey chlorin synthesis.

It has enabled the synthesis of non-natural purpurins, **3.32**, and other chlorin-imides. These compounds fill the "photophysical gap" between chlorins and bacteriochlorins with regard to their UV-Visible/spectroscopic properties[253]

Compound **3.33** is a chlorin bearing four distinct meso substituents.[116] An achievement already arduous on porphyrins,[254] the innate understanding of the selectivity of reactions on the chlorin periphery has enabled such achievements.

Compound **3.34** is a 12-acetyl substituted chlorin, generated through selective bromination of the eastern half. Molecules of this type have enabled the study of 12- *vs.* 13-substitution of these macrocycles, both positions of which lie on the a_{1u} style HOMO.[255]

Lastly, **3.35** was a compound yielded from an attempted synthesis of *N*-confused chlorins by the Borbas group.[256] *N*-confused porphyrins, in of themselves, present great interest to the synthetic chemist due to their vastly different reactivity, coordination chemistry and spectroscopy in comparison to regular porphyrins. Borbas and co-workers systematically flipped the *A*-ring, *C*-ring, and *B*-ring in their attempts. Eventually, **3.35**, a dihydro-trimethylcorrin was obtained in 4%, upon modification of the Lindsey conditions.

Whilst they were unable to yield their desired product, the results produced further understanding of this system, along with exposing evermore the utility of this synthesis.

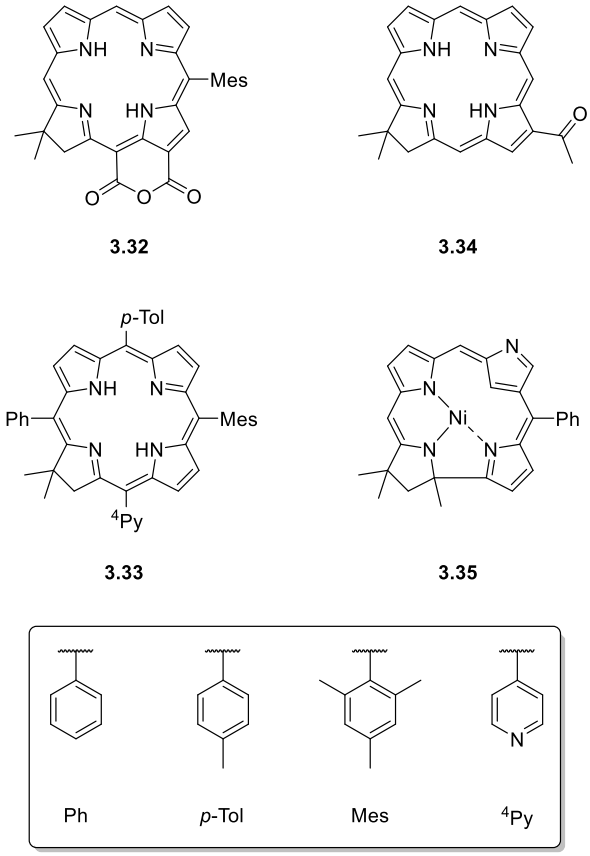

Figure 3.2. Structures of breakthroughs made whilst using the Lindsey chlorin synthesis.[116,253,255,256]

3.2 Results and Discussion

3.2.1 Aims and Objectives

The aim of this chapter is to evaluate the utility of the 10-aryl-17,18-dihydro-18,18-dimethylporphyrin core for photodynamic therapy (PDT). Whilst that core itself can be constructed; its sparsely substituted nature lends itself to other applications as opposed to that desired herein. We envisioned two additions to the core structure to facilitate such future endeavours utilizing this core in PDT.

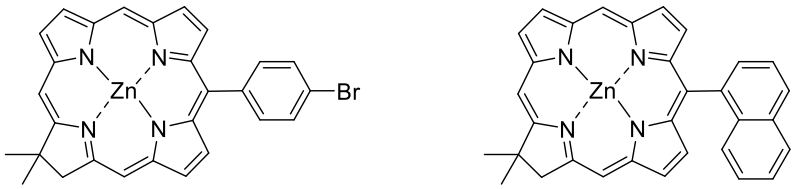

3.36a **3.36b**

Figure 3.3. Structures of targets in this chapter.

In generation of **3.36a**, we provide a synthetic handle which can be modified via Pd-catalysed cross-coupling reactions. These coupling reactions could yield porphyrin/tetrapyrrole arrays, or via coupling to a boronic acid/ester containing a group suitable for conjugation, yielding a third generation PS. Otherwise, the utility is endless given that from this position, the desired photophysical properties would not change drastically change upon conjugation.

In contrast, the aim of generation of **3.36b** was in order to be able to eventually generate fused hydroporphyrin systems. This modification would drastically extend the wavelength of absorption of the molecule, enabling it to perform as a better PS as to increase the wavelength of absorption of the compound, along with phototherapeutic window of the drug.

Upon the successful synthesis of **3.36a** and **3.36b**, detailed photophysical analyses of these cores will provide the necessary information to determine whether or not these compounds have the capability to be a suitable core for PSs in PDT.

3.2.2 Synthesis, Photophysical and Crystallographic Analyses of 10-Aryl Chlorins†

Given the nature of the chlorins desired, we proposed to utilize Lindsey's [2+2] chlorin synthesis which had been refined multiple times, as detailed *vide supra*.[234,238,250] Given the previous substrate scope presented for this synthesis, there was certainty in the formation of the desired products.[249]

To start with: the western half. Given its continual refinement it was possible to synthesize on suitable scale. The synthesis of this "deceptively simple precursor",[238] began from pyrrole-2-carboxaldehyde (**3.13**, Scheme 3.8).

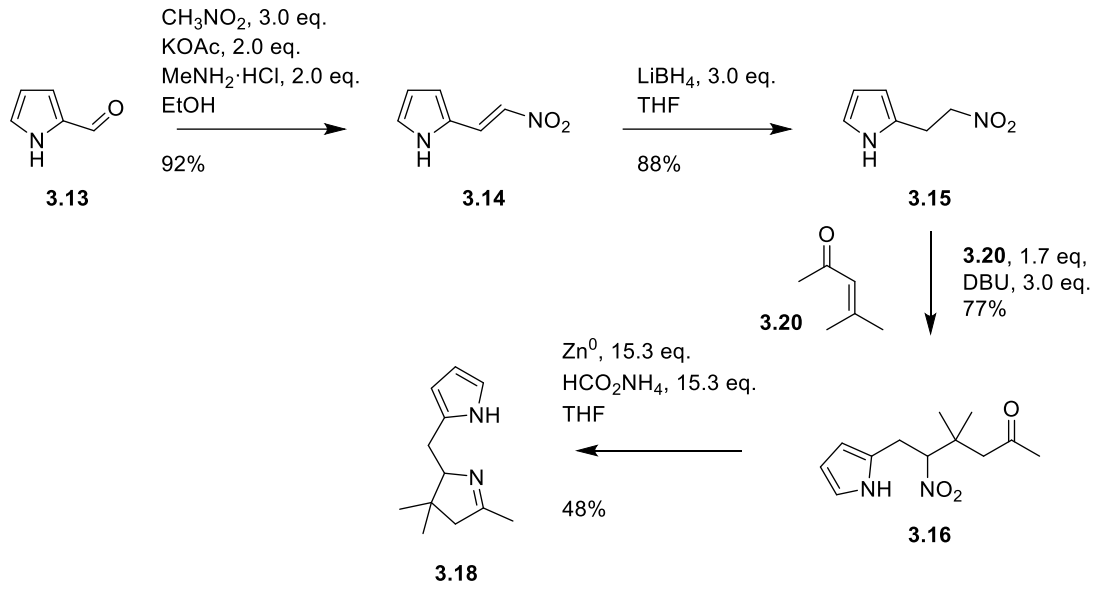

Scheme 3.8. Synthesis of 2,3,4,5-tetrahydro-1,3,3-trimethyldipyrrin (**3.18**) using refined procedures form pyrrole-2-carboxaldehyde (**3.13**) over four steps.[238]

Initially, a Henry reaction to yield (*E*)-2-(2-nitrovinyl)-*1H*-pyrrole (**3.14**), it was quickly found that older batches of **3.13** decreased the yield of this step. A suitable purification was found to be the utilization of a silica plug with diethyl ether as the eluent. Upon drying under high vacuum, this yielded a light-orange powder, typical

† *The detailed photophysical characterization of the compounds presented in this chapter, along with synthesis of dipyrromethanes **3.40a** and **3.40b** was performed by Z. Melissari. The crystallographic data presented in this chapter was collected, solved, and refined by Dr. B. Twamley.*

of **3.13**. Through utilization of refined procedures and purification of **3.13**, this intermediate was yielded cleanly in 92%.

Initially the use of $LiBH_4$ was chosen by the Lindsey group as to prevent the reduction of β-pyrrolic esters.[257] However, it was found that its utilization in the procedure with an unsubstituted pyrrole to be particularly fruitful. Treatment of **3.14** with three equivalents $LiBH_4$, for only 15 mins, yielded **3.15** in 88% as a yellow oil.

Compound **3.15** was found to be remarkably sensitive to a majority of factors; notably, upon light exposure the yellow oil quickly darkened to a black tar, storage at –20 ^oC did slow this process; however, between samples we saw little difference when storing **3.15** under an argon atmosphere or air. Thus, when isolated **3.15** was immediately carried forward upon confirmation of the products nature *via* thin layer chromatography (TLC) and ^1H NMR spectroscopy. The observation of triplets in the NMR spectrum *ca.* δ = 3.32 and 4.60 ppm ($CDCl_3$) were indicative of successful reduction.

Immediate addition of mesityl oxide (**3.20**) and 1,8-diazabicyclo[5.4.0]undec-7-ene (DBU) to **3.15** resulted in the generation of a viscous black oil. DBU is the base catalyst for the reaction, and it was also found to be suitable as the solvent by Ptaszek.[238] Whilst intermediates prior were suitable to be purified via silica plug (as to minimize time in contact with silica, i.e., to prevent acid catalysed degradation), **3.16** required column chromatography. Despite this necessity, on scales less than 10 mmol, **3.16** was routinely produced in yields of 70–77%. Starting from 10 g of **3.13** ,12 g, i.e., > 50 mmol of **3.16** was yielded, 46% over three steps.

The generation of **3.18** was initially far more troublesome. The purity, and structure, of **3.16** had been assigned to the best of our capability, even utilizing ^1H-^{15}N HSQC experiments to confirm the presence of two nitrogen environments. The first issue encountered was the quality of the Zn metal used. Over time, Zn will form an oxide coating if not properly stored under an inert atmosphere, and this will then prevent Zn^0 from being exposed to the reaction mixture, unable to perform the electron transfer steps necessary to complete the reaction. A procedure was devised by which Zn powder was stirred in dilute hydrochloric acid (1 M) for 18 h, followed by filtration and washing with: 1) H_2O as to remove excess acid, 2) EtOH to aid in the removal of water, and finally 3) Et_2O as to remove all prior solvent and aid in drying

of the solid. This new Zn^0 was then dried extensively under high vacuum to remove any residual solvent.

Upon surveying Ptaszek's experiments,[238] there was one set of conditions which solely produced **3.18** and returned no starting material, nor produced any **3.17**: 15 equivalents each of Zn^0 and HCO_2NH_4 in methanol heated to reflux. This experiment was carried out in order to discern a retention factor (R_f) for **3.18** in order to monitor future experiments *via* TLC. It was found that a new product was formed, and it presented an R_f = 0.24 (SiO_2, EtOAc) as a purple spot upon staining with *p*-anisaldehyde.

The Zn^0, along with the knowledge of the R_f was then applied to more fruitful conditions, as determined by Ptaszek, (those presented in Scheme 3.8) and upon stirring at elevated temperatures for substantially longer than reported (40 ^oC, 26 h instead of r.t., 2 h),[238] the desired **3.18** was eventually isolated as clear orange crystals. Thus, **3.18** had been yielded in 30% over 4 steps. Whilst it was possible to scale up the syntheses of **3.16** and other intermediates prior, we observed a drastic decrease in yield upon attempted up-scaling of this final step, and this was only performed on ca. 5 mmol scales.

The eastern half syntheses began from the respectively aryl aldehyde (**3.37a** or **3.37b**. Scheme 3.9) in an acid catalysed condensation. In these syntheses, trifluoracetic acid was utilized as the acid catalyst. Further to this, dichloromethane was utilized as a co-solvent to mitigate the use of pyrrole.

3.38a,**b** were then subsequently formylated with phosphorus(V) oxytrichloride in *N,N*-dimethylformamide, following reported procedures in good yield.[247] Lastly, bromination with *N*-bromosuccinimide in THF yielded the dipyrromethanes ready to condense in 70% and 55% respectively,[255] and both 13% over three steps. Whilst initially **3.37a**,**b** were produced on multigram scale, **3.40a**,**b** were typically isolated on ca. 300-400 mg scale, i.e., <1 mmol. This is partly due to the exceedingly arduous task of separating multiply brominated dipyrromethanes *via* column chromatography, but also because of the sensitivity of **3.40a**,**b** to myriad factors, in a manner similar to **3.15** presented previously.

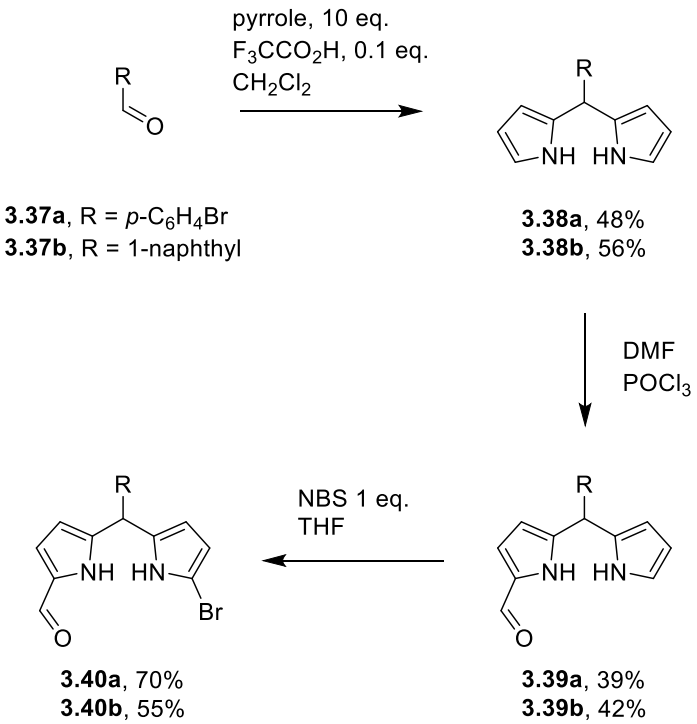

Scheme 3.9. Synthesis of 1-bromo-9-formyldipyrromethanes **3.41a** and **3.41b** for chlorin condensation, from aryl aldehydes **3.38a** and **3.38b** over three steps.[247,255] a = *p*-C_6H_4Br, b = 1-naphthyl.

Combination of western half **3.18** with the respective eastern half **3.40a**,**b** in the presence of *p*-TsOH·H_2O yielded the *A*-*B* ring linkage. Halting the condensation with TMPi and concentration of the reaction mixture yielded an orange solid, distinctive of dipyrrin chromophores, i.e., that presented in a 2,3,4,5-tetrahydrobiladiene-*ab* (Intermediate ***I***, Scheme 3.6). Further addition of $Zn(OAc)_2$, TMPi, AgOTf and heating at reflux in acetonitrile returned an almost black solution 20 h later. TLC analysis of the reaction mixture yielded a green spot which upon UV-illumination presented red fluorescence, a common characteristic of the basic tetrapyrrole cores. Column chromatography gave the desired chlorins as deep purple-green dichromatic solutions, which became violet solids upon removal of solvent in 37% (**3.36a**) and 36% (**3.36b**) respectively.

Treatment of these chlorins with excess TFA in dichloromethane resulted in a drastic colour change of the solution from purple to a deep green. Quenching the reaction with $NaHCO_3$, and subsequent aqueous work-up yielded the free base chlorins in rather moderate yields of 46 and 41%, respectively. Typically, demetallation of zinc tetrapyrroles occurs in no less than 90% yield, using the conditions described.

Initially, we assumed acidolysis of the chlorin, given the three free meso-positions, ideal sites for ring opened products to develop.

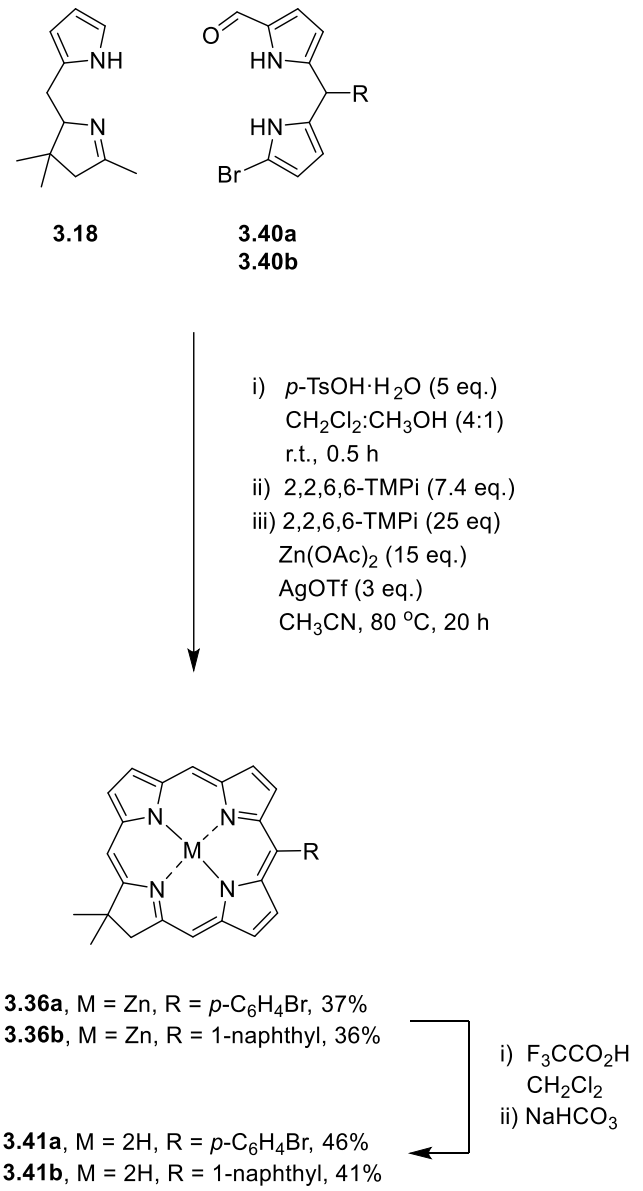

Scheme 3.10. Synthesis of target chlorins **3.36a**,**b** and their demetallation to yield free base chlorins **3.41a**,**b**.[250]

During our collation of these results, Borbas and co-workers presented a publication regarding the demetallation kinetics of 10-aryl chlorins.[258] The substrate scope encompassed **3.36a** amongst multiple other novel chlorins, and as opposed to quenching the reaction with $NaHCO_3$ (or any other inorganic salt solution) they utilized triethylamine. Using this method, it was found that the yield of the free base chlorin **3.41a** was 91%, a vast improvement on the procedure utilized herein.

Further to the demetallation of these chlorins, was their initial synthesis. A comparison of the two shows drastically different yields for the formation of **3.36a**, primarily due to Borbas and co-workers' utilization of the crude mixture of the respective brominated DPM, e.g., **3.40a**. Thus, whilst our yield of **3.36a** was 37% (97 mg), the yield of Borbas was 21% (12 mg). The results from their work indicated that chlorins with an electron rich 10-aryl group, e.g., *p*-$C_6H_4OCH_3$, demetallated with a rate constant of k = 3.7 x 10^3 min^{-1}, whereas a -C_6F_5 appended chlorin demetallated with a rate constant of k = 0.192 x 10^3 min^{-1}, a 19-fold decrease.[258]

The steady state photophysical analyses of **3.36a**, **3.36b**, **3.41a**, and **3.41b** are presented below. These chlorins were found to exhibit typical spectra as presented by the Lindsey group previously. The tabulated data is also presented in Table 3.1 below.

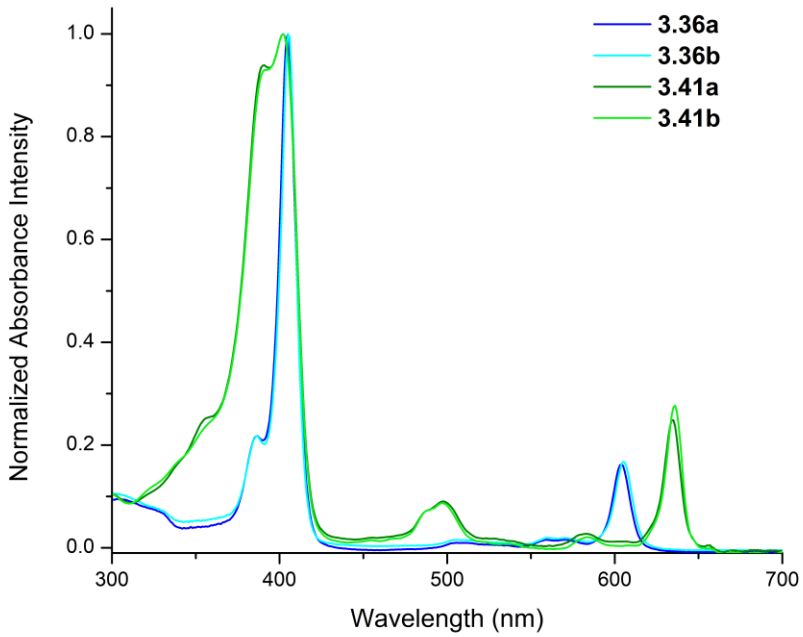

Figure 3.4. UV-Visible absorption spectra of **3.36a**, **3.36b**, **3.41a**, and **3.41b** in ethanol at room temperature. *These analyses were performed by Z. Melissari.*

All of the structures presented exhibit B-bands in the blue-violet region around 400 nm, (Figure 3.4) with minimal differences in wavelength of absorption (*ca.* 1–2 nm) at this band. For zinc chlorins **3.36a** and **3.36b**, there is little to no absorption prior

to the Q_y absorption, aside from the B bands, in contrast to the free-base derivatives which show distinct transitions in the region of 480–510 nm.

The Q_y absorptions differ minimally between **3.36a** and **3.36b**, and the same argument is applied for **3.41a** and **3.41b** – indicating a minimal electronic difference between the *p*-C_6H_4Br and 1-naphthyl groups. Instead, the difference is between the free base and zinc chlorins. In both cases, as noted *vide supra*, the lowering of the symmetry of the macrocyclic core (with respect to porphyrins) has produced an intense absorption at a longer wavelength of absorption. Instead, demetallation of the chlorins results in a ca. 30 nm red-shift, or bathochromic shift, in the Q_y band. This shift is indicative of a reduction in the energy gap between the frontier molecular orbitals. This is further evidenced given that the Zn(II) central ion has been shown to act as a Lewis acid, accepting electron density from the macrocycle core, and subsequently lowering the HOMO energy.[259,260]

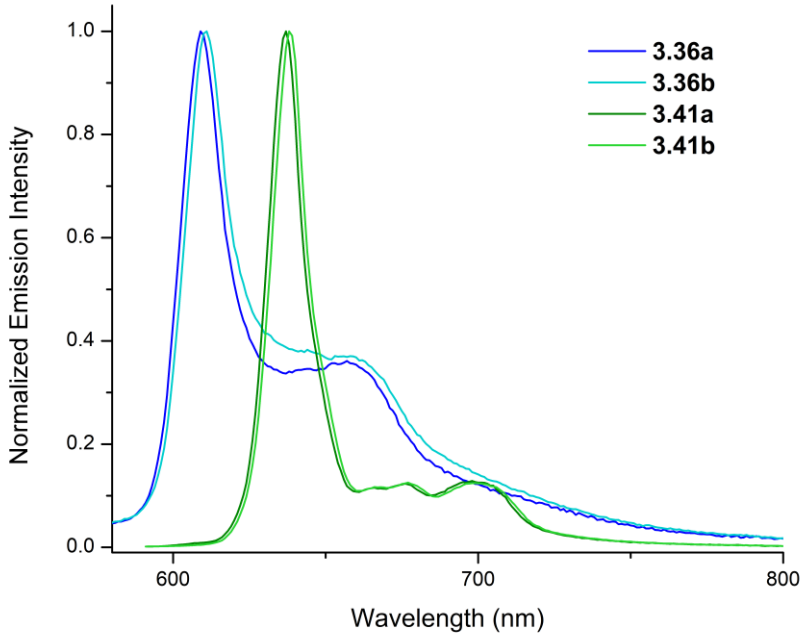

Figure 3.5. Emission spectra of **3.36a**, **3.36b**, **3.41a**, and **3.41b** in ethanol at room temperature. λ_{exc} = 558 nm (**3.36a**), 561 nm (**3.36b**), 500 nm (**3.41a**), 640 nm (**3.41b**). *These analyses were performed by Z. Melissari.*

The emission spectra of these chlorins are presented in Figure 3.5. The emission detected herein is the $S_1 \rightarrow S_0$ transition, as determined by Kasha, any decay of

$S_2(S_n) \rightarrow S_1$ is too fast to detect in this experiment. Both **3.36a** and **3.36b** show the $Q_y(0,0)$ around 610 nm, and a vibronic shoulder i.e., the $Q_y(1,0)$ band at ca. 660 nm. Likewise, The free base chlorins **3.41a** and **3.41b** exhibit their $Q_y(0,0)$ at *ca.* 638 nm and the $Q_y(1,0)$ shoulder at 700 nm, along with other vibronic satellites between 650–680 nm.

In combination with other dyes, it is possible to determine the quantum yields of fluorescence for these compounds; in the cases of **3.36a**,**b** and **3.41a**,**b** cresyl violet was used as a standard, with Φ_f = 0.56 (EtOH).[261] Through the application of equation 1, it is possible to determine fluorescence quantum yields for the chlorins presented.

$$\Phi_{f(x)} = \Phi_R \left[\frac{A_R(\lambda_R)}{A_x(\lambda_x)}\right]\left[\frac{D_x}{D_R}\right] \text{.....} \textit{Eq. 3.1}$$

Where $\Phi_{f(x)}$ is the quantum yield of fluorescence of the sample, Φ_R is the reference fluorescence quantum yield, A(λ) is the absorbance of each species at the wavelength of excitation and D is the integrated area under the corrected emission spectrum.

Table 3.1. Tabulated photophysical data for **3.36a**, **3.36b**, **3.41a**, **3.41b**. λ_{exc} = 558 nm (**3.36a**), 561 nm (**3.36b**), 500 nm (**3.41a**), 640 nm (**3.41b**) [*a*] – The Stokes shift was calculated from the corresponding UV-Visible absorption and emission spectra in EtOH. [*b*] For Φ_f , cresyl violet used as standard (Φ_f = 0.56, EtOH).[261] [*c*] For **3.36a**,**b**, rose bengal used as standard (Φ_Δ = 0.86, EtOH)[263] and for **3.41a**,**b**, *m*-THPC used as standard (Φ_Δ = 0.65, EtOH).[262] (Typical errors are Φ_f = ± 10%, and Φ_Δ = ± 10%. *These analyses were performed by Z. Melissari.*

	B & Q_y absorptions λ_{abs} (nm) ($\log_{10}\varepsilon$)		λ_{em} (nm)	Stokes Shift (cm^{-1})[a]	Φ_f [b]	Φ_Δ [c]
3.36a	405 (5.40)	604 (4.61)	609	163	0.04	0.90
3.36b	405 (5.54)	605 (4.76)	611	162	0.08	0.85
3.41a	407 (5.08)	638 (4.43)	637	74	0.08	0.70
3.41b	407 (5.24)	639 (4.64)	638	50	0.14	0.60

For the zinc chlorins, the fluorescence quantum yields are 0.04 (**3.36a**) and 0.08 (**3.36b**), respectively, whereas for free base chlorins they are 0.08 (**3.41a**) and 0.14 (**3.41b**), respectively. These results are comparable with those presented in the literature.[250]

Equation 1 can also be applied to determine the singlet oxygen quantum yield (SOQY, or Φ_Δ). For reference in this instance *m*-THPC was used for the free base chlorins with Φ_Δ = 0.65 in EtOH,[262] and Rose Bengal for the zinc chlorins with Φ_Δ = 0.86 in EtOH.[263] Whilst typically it is ideal to use the same probe for a range of compounds, this choice is dictated by the wavelengths of excitation. The method used to determine Φ_Δ herein is the direct method, i.e., direct detection of the luminescence produced by $^1O_2$ at *ca.* 1270 nm, as noted in Section 1.1.2, Figure 1.4. Once again, between **3.36a** and **3.36b** there is a minimal difference in this value, and the same argument applied for the **3.41a** and **3.41b**. The biggest difference is the change in SOQY between the two classes of chlorin. These tetrapyrroles will effectively undergo ISC to yield a T_1 state, which can then react with molecular oxygen ($^3O_2$) to yield $^1O_2$ via energy transfer. Enhancement of the $S_1 \rightarrow T_1$ transition can be executed through the addition of halogens, or transition metals. This is otherwise known as the heavy atom effect.[264,265,266] A higher population of the T_1 state means a higher probability of reaction with $^3O_2$ and thus generation of $^1O_2$. Hence, without the zinc there is less T_1 population, and lower Φ_Δ for **3.41a**,**b**. Whilst **3.36a** and **3.41a** both possess a heavy atom in the form of Br, the yields are not higher than those for **3.36b** and **3.41b** as it is not incorporated into the macrocyclic core, and thus the heavy atom effect is not present therein.

As noted in Section 1.1.2., there are certain criteria that will determine a PSs applicability in PDT. The compounds presented herein have exhibited a strong absorption in the red-region of the electromagnetic spectrum, along with a high SOQY. It has been shown that a single molecule is isolable, *vide infra*, from readily available reagents. Further to this, there have been options for further derivatization added to these molecules.

Lastly, during our synthesis of these chlorins, we were able to successfully generate crystals of both **3.36a** and **3.36b** which were suitable for analysis *via* single crystal X-ray diffraction experiments. Both sets of crystals were grown through slow evaporation of a mixture of dichloromethane and hexane at room temperature.

In the crystal of **3.36a** the asymmetric unit consists of three separate molecules of the desired compound, as well as dichloromethane and hexane solvates which were partially occupied (Figure 3.6). The asymmetric unit presents the three molecules in

a pseudo-trefoil arrangement which at first glance appear to be orchestrated by C-H···Br interactions. Analysis of the data, however, indicates that this is not the case, and the only interactions of note are between C^{7}-H^{7}…N^{23} (*C*-ring) of an adjacent chlorin with D…A distances of 2.63 Å. Across all three molecules, the Zn(II) centre was found to be ca. 0.315 Å displaced from the chlorin plane and all three molecules of **3.36a** show very minimal distortion between one another when overlayed.

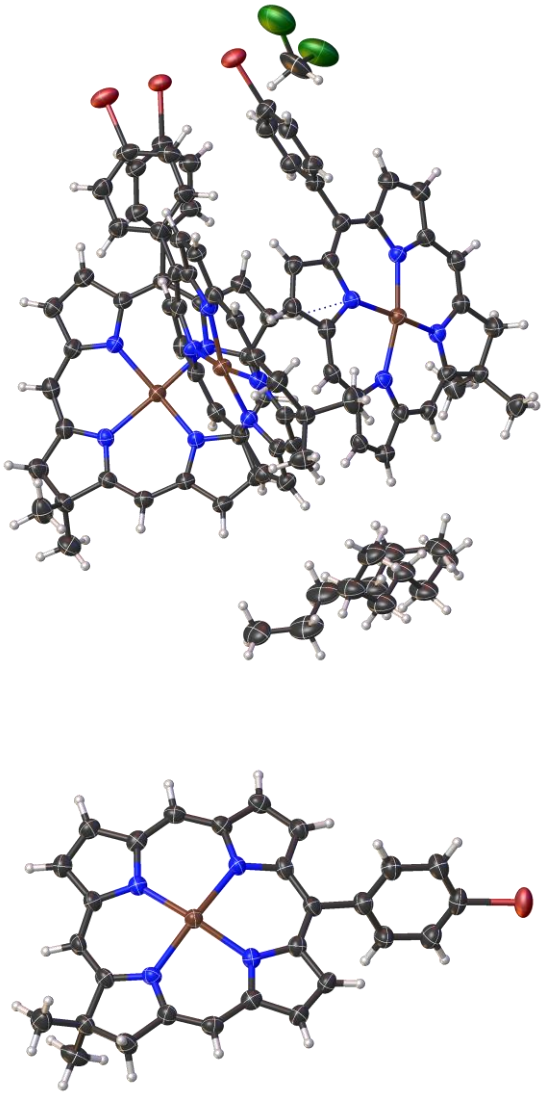

Figure 3.6. Single crystal X-Ray structure of **3.36a** with asymmetric unit (*top*) and one independent molecule (*bottom*). Image generated in Olex2.[126] Thermal ellipsoids indicate 50% probability. Data collected, solved, and refined by Dr. B. Twamley

The out of plane distortion of the zinc centre can be rationalized upon the examination of the interaction between two adjacent asymmetric units (or two adjacent trefoils) of **3.36a**. Distinct Zn…N interactions are observed between the Zn

centre of one chlorin and N^{22} (from the *B*-ring) of an adjacent chlorin molecule (Figure 3.7). These interactions exhibit D…A distances of 2.69 Å.

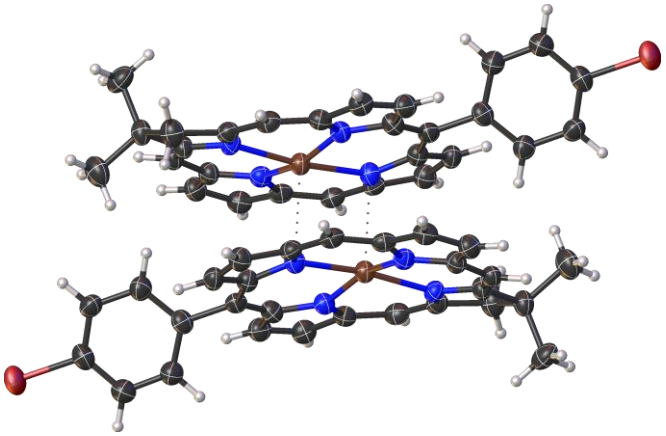

Figure 3.7. Zn…N interaction between two molecule of **3.36a** resulting in the out-of-plane distortion of the zinc centre. Image generated in Olex2.[126] Thermal ellipsoids indicate 50% probability. Data collected, solved, and refined by Dr. B. Twamley

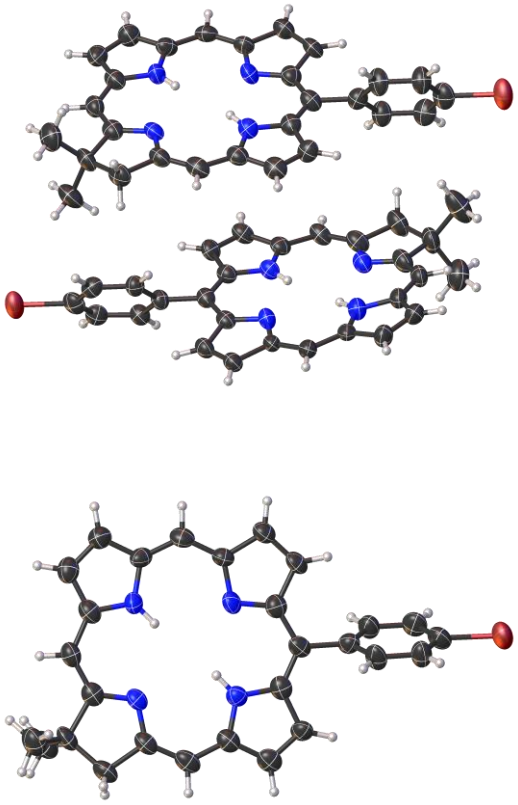

Figure 3.8. Single crystal X-Ray structure of **3.41a** with asymmetric unit (*top*) and one independent molecule (*bottom*). Image generated in Olex2.[126] Thermal ellipsoids indicate 50% probability. Data collected, solved, and refined by Dr. B. Twamley

In contrast, **3.36b** presents the asymmetric unit as an anti-parallel stacked dimer (Figure 3.8). No solvates were present in this crystal. No H-interactions were observed, nor any π-stacking between chlorin macrocycles. In contrast to **3.36a**, the two molecules in the asymmetric unit show differing distortions with one being almost entirely planar in the $C_{20}N_4$ core, whilst the other exhibits distortion in the *A*- and *B*-rings upon overlay. Interestingly, it was possible to identify the H-atoms in the core specifically at N^{21} and N^{23}.

3.3 Conclusions and Future Work

In this chapter, the synthesis of 10-aryl substituted chlorins **3.36a** and **3.36b** was presented, along with the generation of their free base counterparts, **3.41a** and **3.41b**. Both halves of the chlorin, prior to condensation, **3.18** and **3.40a** and **3.40b** were synthesized using multiply refined procedures but were still low yielding. In contrast, the yield of **3.36a** and **3.36b** were exemplary for a tetrapyrrole, indicating the vast efficacy of the condensation procedure used. Borbas' presentation of the use of triethylamine in the demetallation procedure, along with the kinetic analyses presented, enables refinement further of the procedure for the generation of free base chlorins. Crystallographic analysis of **3.36a** and **3.36b** indicated a highly planar structure in both cases, with a well-defined substitution pattern.

Photophysical analyses of these compounds provided key information towards the analysis of these structures as possible PSs for PDT. Namely, they possess large molar extinction coefficients, high SOQY in polar media, and have a long wavelength of absorption. All of these factors, as outlined in the Introduction, make them suitable candidates for preliminary investigations as PSs for PDT.†

† *[Pd] catalysed cross-coupling reactions performed on **3.36a**, along with the in vitro analyses of **3.36a**, **3.36b**, **3.41a**, and **3.41b** will be presented in the doctoral thesis of Z. Melissari.*

Chapter 4.

Bioconjugatable 5,10-Diaryl Chlorins – A Step Forward

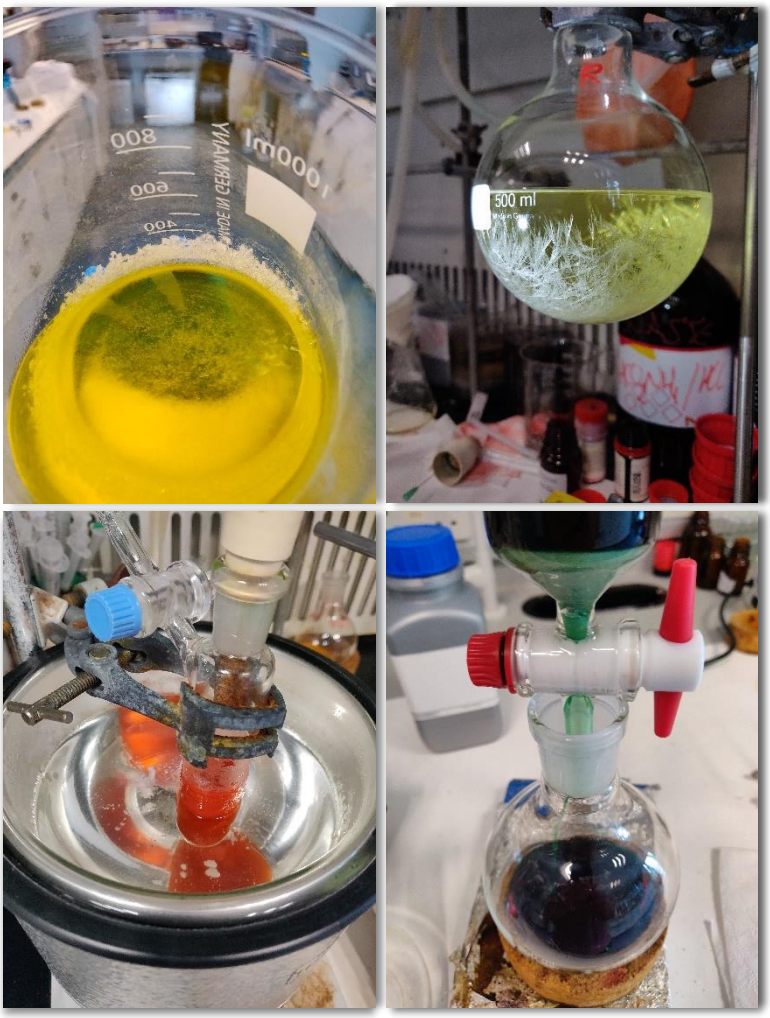

4. Synthesis, Photophysical, and *in vitro* Evaluation of Bioconjugatable 5,10-Diaryl Chlorins and Analogous *trans*-A_2B_2 Porphyrins

4.1 Introduction

4.1.1 Taking Steps Closer Towards Chlorophyll Mimicry

Further progress towards the generation of evermore substituted chlorins was not fueled by a specific natural product, instead a desire to generate macrocycles that "contain diverse substituents in specific patterns or that contain no substituents at all".[249]

A discussion on the generation of 2- and 3-aryl Western halves was presented *vide supra*, Scheme 3.4; however, this methodology is presented in Scheme 4.1 for completeness. Excluding brominations, discussion presented *vide infra*, the first novel substitution was at the 17- and 18-positions.[277] The 17-substutition was obtained upon the treatment of a solution of the chlorin in toluene with basic alumina (activity I), to yield racemic 17-hydroxy chlorins. Upon addition of DDQ, the 17-carbonyl chlorins were yielded. In the same publication, the 18-position was appended with a spiro-cyclohexyl moiety (*i.e.* X = $(CH_2)_4$, **4.12**, Scheme 4.1) as opposed to the typical *gem*-dimethyl unit.

The groundwork for C^{20}-subsituttion was initially laid in 1953 by Gairaud and Lappin,[278] and then by Yadav and co-workers in 2001.[279] The addition of electron deficient olefins to the 2-position of pyrroles was performed under $InCl_3$ catalysis, to yield substituted 2-(2-nitroethyl)pyrroles, and transformation into the respective 5-substituted dihydrodipyrrins (**4.10**, Scheme 4.1).

As noted in Section 3.1, there has been vast development in the synthesis of DPMs, and their formylation/acylation/aroylation.[237,247,280]

The utilization of differing bromination strategies has been paramount in fulfilling the objectives of the Lindsey group, and more generally furthering the field of *gem*-dimethyl chlorin synthesis. Selective bromination strategies have been generated for the; 2-positions,[281] 7- and 8-positions,[282] 12- and 13-positions,[255] 15-position

of chlorins and 20-positions of oxo-chlorins,[283] and the 15-position under acidic conditions.[284]

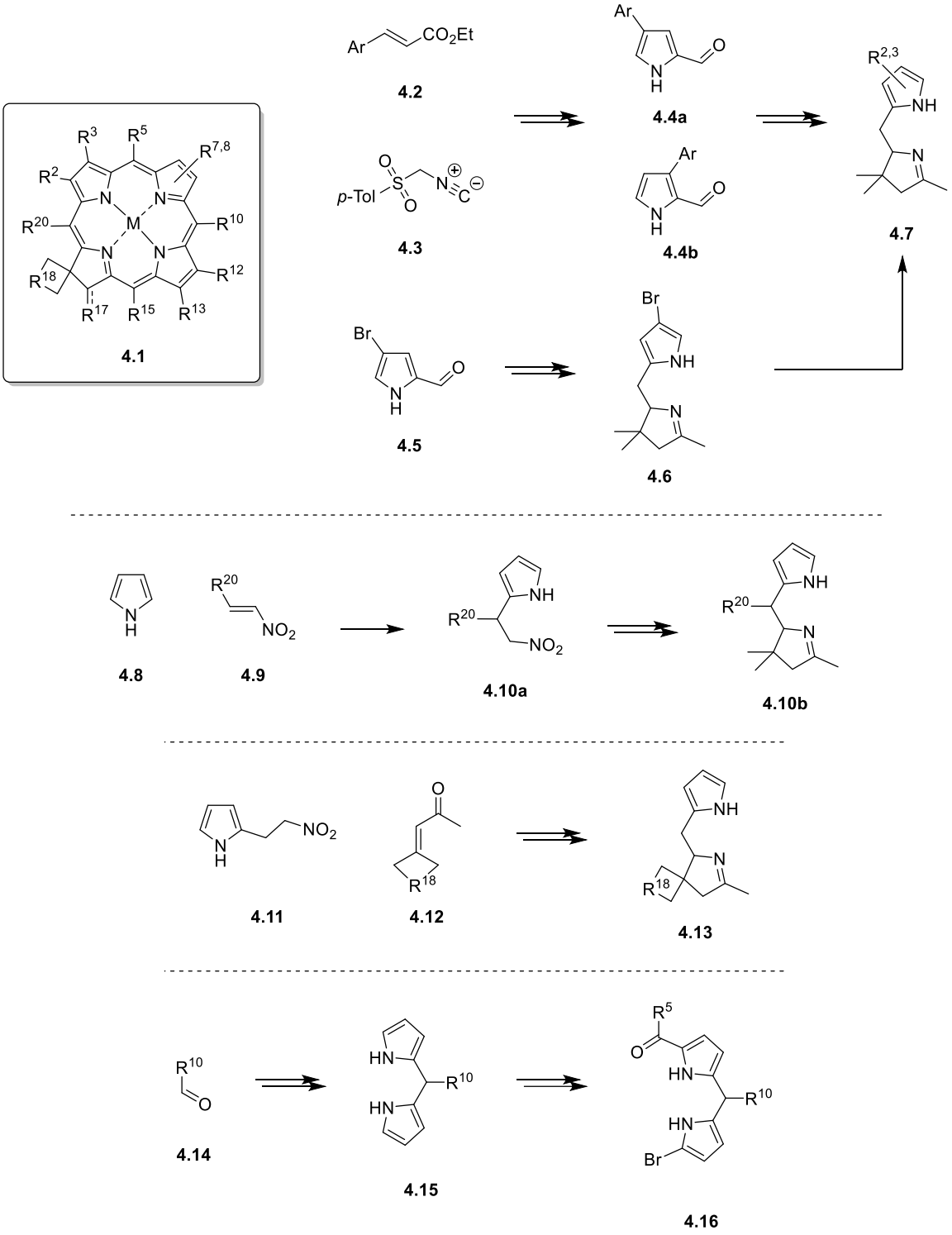

Scheme 4.1. Non-bromination strategies developed to substitute the chlorin periphery.[237,247,277,278,279,280]

4.1.2 New Halves, New Opportunities

All of this being said, however, no other functionalization has had such an impact as the bromination at the 3- and 13-positions.[285] The initial 2006 work from Laha et al. became the modern-day genesis to the chlorin bible, particularly in the field of generating chlorin arrays, as opposed to the chlorophyllin based arrays of Dougherty and Pandey.[286] Akin to the non-brominated variant which had been refined prior,[287] the novel 8-brominated western half (**4.6**, Scheme 4.1) was also refined by Krayer et al. in 2009.[288]

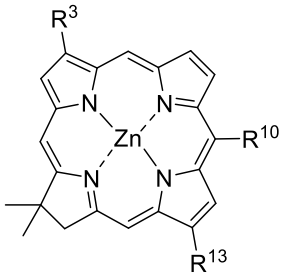

4.17-4.25

4.17, $R^3 = R^{13} = H$, $R^{10} = Mes$
4.18, $R^3 = CCTIPS$, $R^{13} = H$, $R^{10} = Mes$
4.19, $R^3 = H$, $R^{13} = CCTIPS$, $R^{10} = Mes$
4.20, $R^3 = R^{13} = CCTIPS$, $R^{10} = Mes$
4.21, $R^3 = H$, $R^{13} = COCH_3$, $R^{10} = Mes$
4.22, $R^3 = R^{13} = COCH_3$, $R^{10} = Mes$
4.23, $R^3 = R^{13} = R^{10} = H$
4.24, $R^3 = R^{13} = CCTIPS$, $R^{10} = H$
4.25, $R^3 = CCTIPS$, $R^{13} = COCH_3$, $R^{10} = H$

Figure 4.1. Structures for which photophysical data is presented below in Table 4.1.

Table 4.1. Selected photophysical data for multiple 3- and 13-subsituted chlorins. Data taken from Ref.[285] All data recorded in toluene at room temperature.

Compound	$\lambda_{abs}(Q_y)$ (fwhm) (nm)	$\log_\varepsilon(Qy)$
With 10-substitutent (R^{10} = mesityl)		
4.17	606 (12)	4.81
4.18	627 (12)	4.73
4.19	626 (11)	4.92
4.20	646 (12)	4.76
4.21	632 (14)	4.84
4.22	662 (18)	4.54
With no 10-substituent (R^{10} = H)		
4.23	606 (12)	4.81
4.24	645 (12)	4.93
4.25	655 (17)	4.75

This development, in particular, is so important due to both of these positions (3- and 13-) lying on the HOMO of the chlorin macrocycle. Such substitutions upon [Pd]-catalyzed cross-coupling reactions yield vast modifications to the UV-Visible

absorption spectra of these molecules; notably in extending their wavelength of absorption (**4.17**–**4.25**, Figure 4.1 and Table 4.1, *vide supra*).[285]

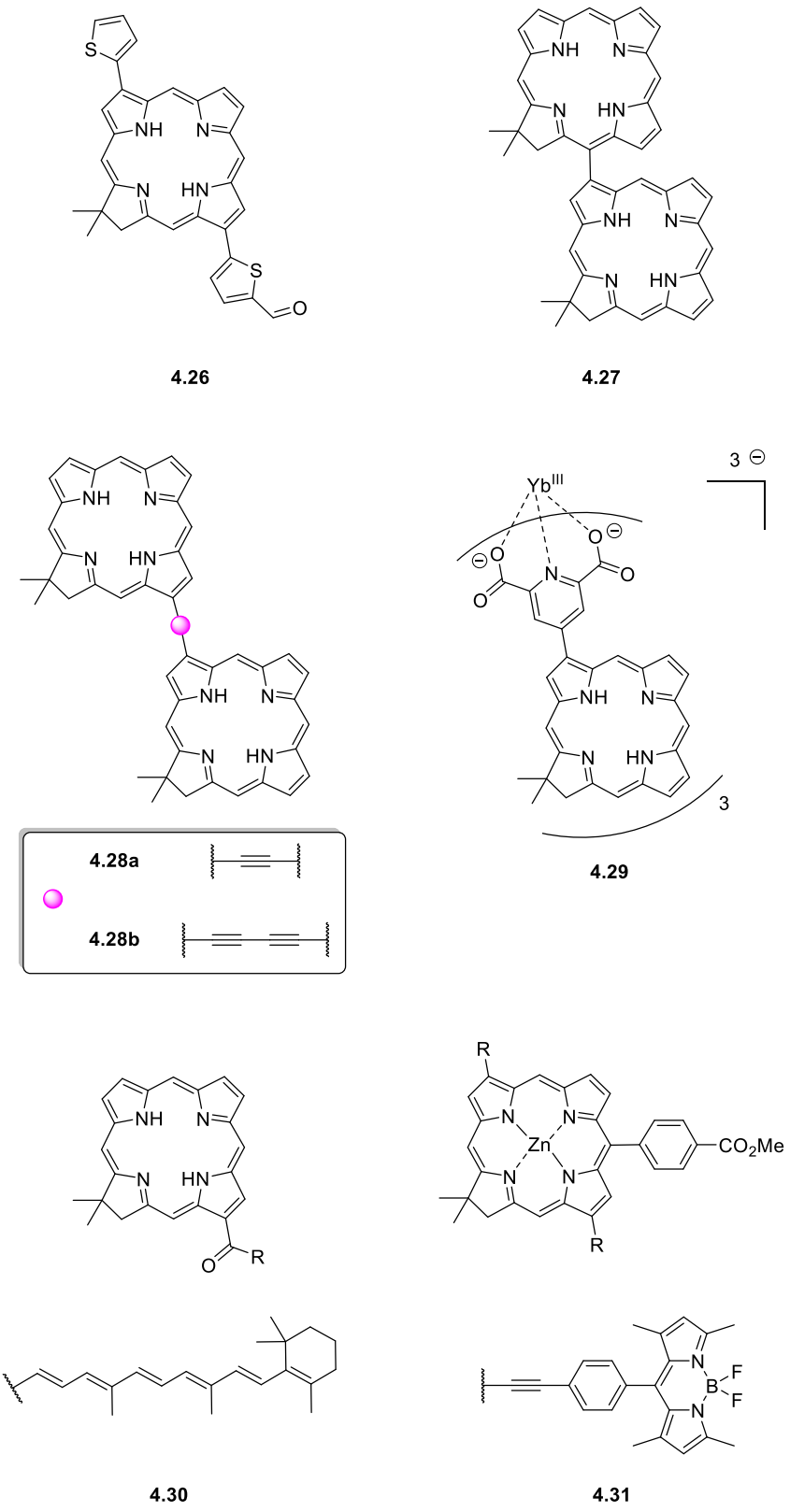

Figure 4.2. Novel chlorin architectures derived from the generation of 3- and 13-substituted chlorin macrocycles.[289,290,291,292,293,294,295,296,297]

These developments have yielded the generation of: 3,13-heterocycle substituted chlorins (**4.26**, Figure 4.2) ,[289], 15,3'-directly linked chlorin dimers (**4.27**),[290] "strongly conjugated hydroporphyrin dyads" (**4.28a**-**c**),[291] π-conjugated chlorin dimers,[292], chlorin lanthanide complexes (**4.29**),.[293], chlorin-chalcones (**4.30**),[294] 3-methoxy and 3-*N*,*N*-dimethylamino-chlorins,[295] and chlorin-BODIPY arrays (**4.31**).[296,297]

4.1.3 Applications to Bioconjugation and PDT

Whilst the leaps in chlorin chemistry, as presented *vide supra*, have been significant it quickly becomes apparent that the molecules **4.17**–**4.31** may be (at the very least) unsuitable for biological application, notably PDT. This poses a quandary: how does one utilize 3,13-substitution of chlorins to make them more suitable for PDT? Whilst the first *gem*-dimethyl tetrapyrrole to be observed intracellularly was **4.23** in the year 2009, it possessed no functionality.[298]

Bioconjugation is not a new trend, however, it is the defining distinction between second and third generation PSs. Bioconjugation strategies have been honed on porphyrins continually.[299,300,301,302,303,304,305,306]

In this thesis, bioconjugation is defined as the conjugation of a biologically active motif to a PS. The biologically active motif may be one of a wide range of molecules; biotin as a prime example, any number of peptides, or larger systems such as an antibody. In this regard, even easily accessible compounds such as 5-(4-aminophenyl)-10,15,20-triphenylporphyrin could be called "bioconjugatable", whereas 5,10,15,20-tetrakis(phenyl)porphyrin is not. Whilst it is well understood that the attachment of a triphenylphosphonium motif to a PS enables enhanced mitochondrial uptake, and possibly greater PDT efficacy, this is not a molecule of biological relevance and thus, this is not an example of bioconjugation.

A survey of the literature shows that the bioconjugation strategies (along with strategies utilized to enhance water solubility) involve the 5- and 10-positions of the macrocycle, which appears to be for three reasons; 1) these positions can be easily modified utilizing DPM chemistry, 2) there are no regioisomeric products (resulting from multiply brominated starting materials), and 3) incorporation of differing substituents at the meso-positions of the macrocycle leaves the β-positions (i.e. 3-

and 13-positions) free for functionalization as to modify the spectroscopic properties of the macrocycle.

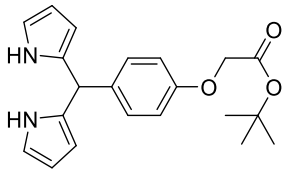

4.32

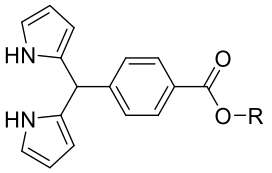

4.33a, R = CH_3
4.33b, R = CH_2CH_3

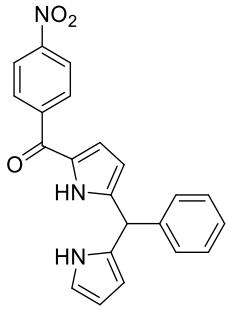

4.34

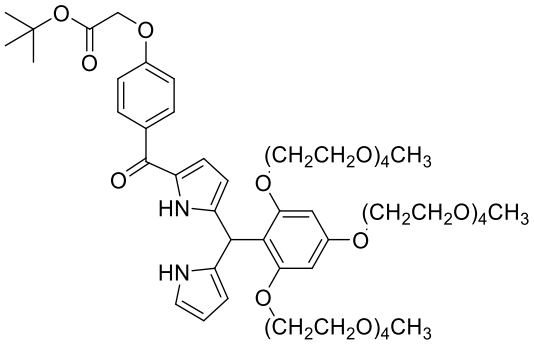

4.35

Figure 4.3. Eastern half synthons used in the synthesis of chlorins with pre-installed bioconjugation handles, and solubilization motifs in the case of **4.35**.[295,296,307,308]

In the first example of *gem*-dimethyl chlorin bioconjugation, Borbas and co-workers presented **4.32** and **4.34** in 2012 (Figure 4.3).[307] Complimentary synthetic routes were developed to yield two different linkages between the chlorin periphery and cyclen ligands: **4.32** was hydrolyzed to yield an aliphatic carboxylic acid whereas **4.34** was reduced to yield an aromatic amine. In contrast, the generation of **4.33a**,**b** is far simpler than either **4.32** or **4.34**. In 2015, Ptaszek utilized **4.33a** in the generation chlorin-BODIPY arrays.[296]

Compound **4.35** combines the bioconjugation strategy used by Borbas (**4.32**, Figure 4.3); however, shuffles this round to the 5-position of the macrocycle and utilizes PEG-chains at the 10-position to enhance solubility in polar media.[308] Other bioconjugation strategies have prevailed through [Pd]-catalyzed cross-coupling at the 15-positions, yielding **4.36**, through the utilization of the same motifs as presented in **4.32** and **4.35**, along with phosphonate solubilizing motifs (Figure 4.4).[295]

Aside from this already presented in Figures 4.3 and 4.4, little has been utilized to enhance the polarity of these chlorins. One publication utilizes the addition of *p*-$C_6H_4CO_2Et$ and *p*-C_5H_5N moieties to yield ABCD-chlorins, again through [Pd]-catalyzed cross coupling reactions, but no solubility studies nor any relevant biological experiments were performed.[116]

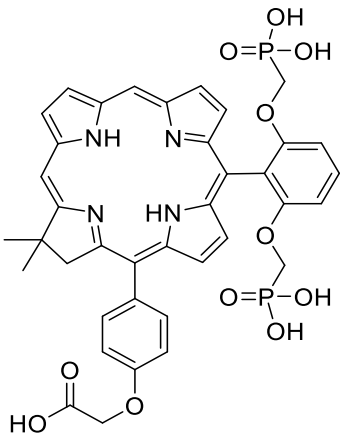

4.36

Figure 4.4. Bioconjugatable chlorin bearing its conjugation handle in the 15-position, installed via [Pd]-catalyzed cross-coupling, with a swallow-tail solubilizing moiety at the 10-position.[116,299]

At this point, it must be made clear that there are few, if any, examples of literature utilizing *gem*-dimethyl chlorins for PDT. There is, however, respective literature for tetramethyl bacteriochlorins, in the sea of literature regarding other bacteriochlorins for PDT.[309] In 2010, Bocian, Holten, Lindsey, Hamblin and co-workers presented the evaluation of a series of three “stable synthetic bacteriochlorins” in a work targeted at successfully utilizing PDT to overcome melanomas resistance to PDT, a phenomenon attributed to high melanin levels, by excavating the PS at wavelengths at which the pigments melanin and eumelanin have little to no absorption.[310]

The structures analyzed are presented in Figure 4.5. All three compounds were found to exhibit no dark toxicity after 24 h. The effectiveness of the compounds was found to be **4.38** > **4.37** > **4.39**, with **4.38** killing over 2 logs of C-mel cells at a [**4.37**] = 0.25 μM, and fluence of 5 J cm^{-2} (as measured by mitochondrial activity).[310] Shortly afterwards, the same authors published an *in vitro* study of broader scope – encompassing an extra nine bacteriochlorins and found a number of these new substrates exhibiting great promise as PSs, i.e., LD_{50} = 15 nM (HeLa), at “modest fluences” of 10 J cm^{-2} of NIR light.[311]

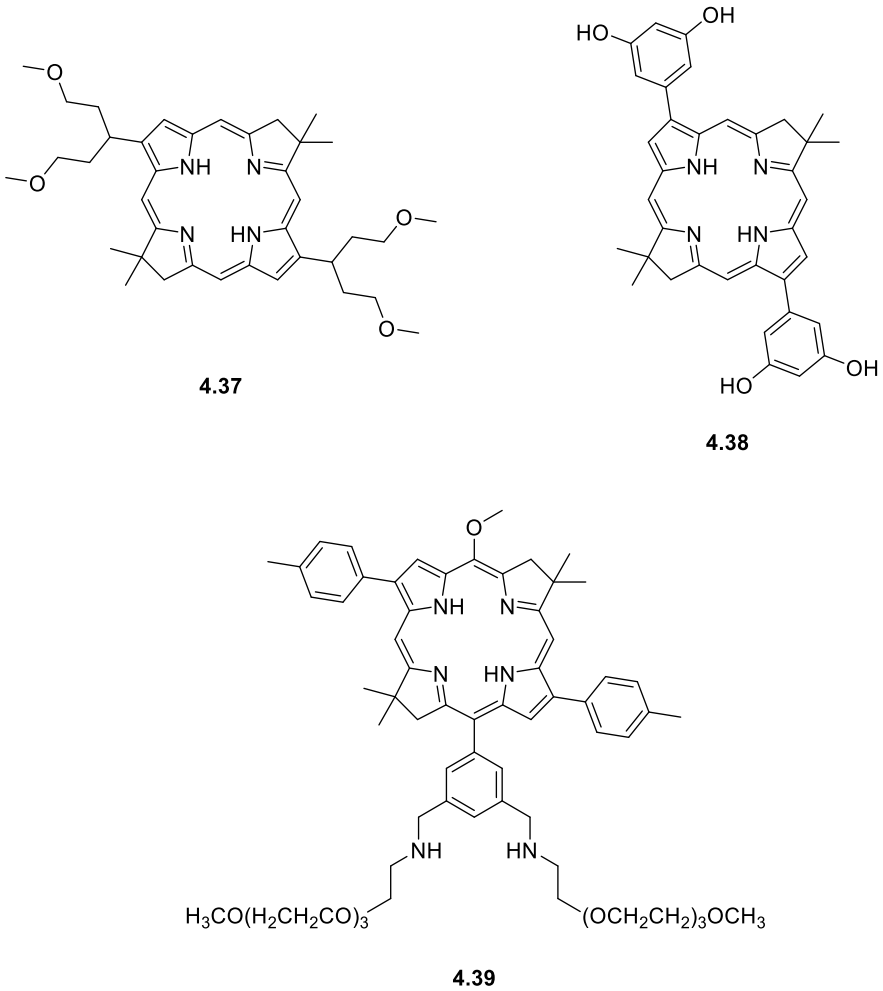

Figure 4.5. Synthetic bacteriochlorins analyzed for PDT efficacy against melanoma by Bocian, Holten, Lindsey, Hamblin, and co-workers.[310]

The closest that this class of chlorins has come to utilization in PDT is as their utilization in energy-transfer dyads. In 2008, the first synthetic chlorin-bacteriochlorin energy-transfer dyads were synthesized by Lee et al.[313], and it was noted that these systems exhibited energy transfer from the chlorin to the bacteriochlorin with a yield of >99% in all cases. Further to this, they exhibited exceptionally large Stokes shifts as a result, i.e., up to 110 nm.

Five years later, Yu & Ptaszek further investigated these systems in which the acceptor (bacteriochlorin core) was modified and found little to no difference in energy transfer yield.[314] It was noted that these systems, given their multiple narrow and tunable emissions in the NIR spectral window made them excellent candidates for *in vitro* imaging. In 2019, **4.40** (Figure 4.6) was presented, along with two bacteriochlorin-BODIPY dyad systems, and one other bacteriochlorin-chlorin

dyad.[312] The positioning of the PEG-chains (i.e., the 10-position of the chlorin) was a deliberate design tactic as to hinder any aggregation between tetrapyrrole cores. The *in vivo* studies performed exhibited the utility of this class of compounds for cancer detection, and possibly applications such as fluorescence guided surgery (FGS).[315]

Whilst it is enjoyable to see chlorins used in such applications, it is still not a *gem*-dimethyl chlorin in PDT. Instead, *gem*-dimethyl bacteriochlorins are used in their place, and there are two main reasons for this. The first being photophysical – bacteriochlorins have a longer wavelength of absorption than chlorins as a result of a much smaller HOMO-LUMO gap (see Figure 1.9). This trend is applicable regardless of whether the bacteriochlorin is of natural or synthetic origin. As displayed in Figure 1.7 the longer the wavelength of penetration, the greater the efficacy of treatment.

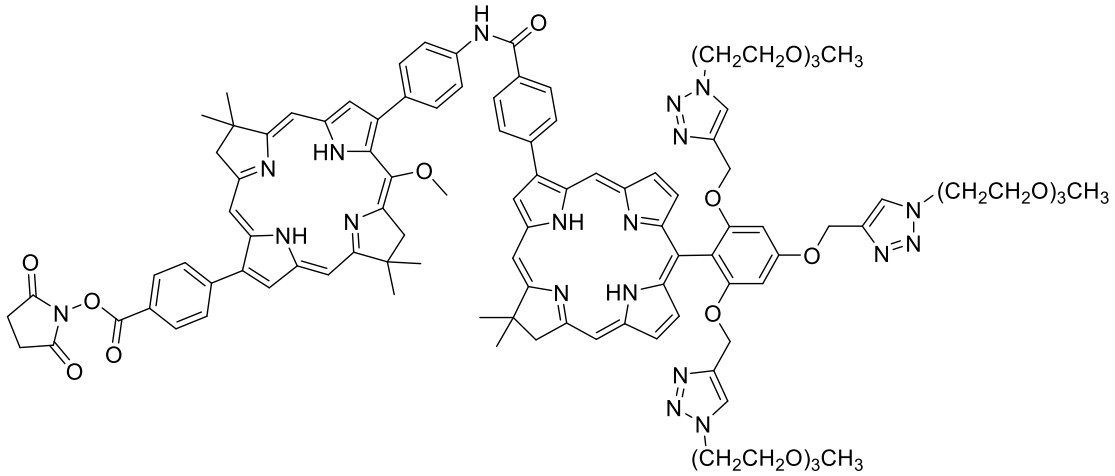

4.40

Figure 4.6. Chlorin-bacteriochlorin energy-transfer dyad designed for use as a NIR-fluorescence probe for cancer detection.[312]

The second reason is down to their synthesis. Regardless of whether the East-West or North-South synthetic route is utilized, their synthesis is the dimerization of a single dihydrodipyrrin. From there, bromination and [Pd]-catalyzed cross coupling reactions can be performed. In contrast to this, chlorins require the synthesis of two distinct different halves: a tetrahydrodipyrrin and a DPM (Scheme 4.2).[257,315,316]

Inherently then, dimerization (in the case of bacteriochlorins) yields identical substitution patterns occurring across the 2,3- and 12,13-positions with further

diversity enabled by selective bromination strategies and other such modifications thus forth. To our knowledge, no mixed condensation between two dihydrodipyrrins of differing substitution has been reported.

Whilst the synthesis of two halves is more arduous than the synthesis of just one, this apparent disadvantage yields far greater diversity in the resultant tetrapyrrole through pre-installation of desired handles/motifs. Dipyrromethane chemistry is dominated by modification of the 5-position (i.e., choice of aldehyde) and formylation/acylation/aroylation to modify another meso position, and bromination chemistry to yield β-substituents. The inclusion of a wider variety of motifs greatly enhances the ability to add moieties which increase the suitability of these molecules for PDT (be this via the addition of motifs to enhance solubility or enable radiolabeling, i.e., 3rd generation PSs). In every case, the research group(s) in question must way up the desired spectroscopic characteristics of the molecule being designed, versus the synthetic utility of the resultant tetrapyrrole.

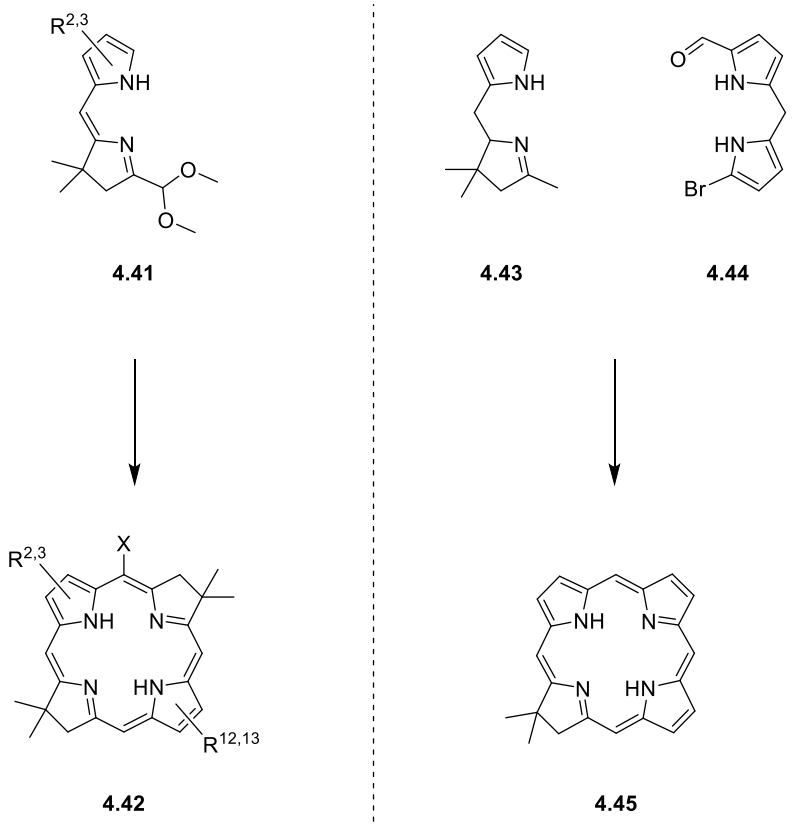

Scheme 4.2. Synthesis of bacteriochlorins and chlorins from hydrodipyrrin precursors, and dipyrromethanes. For **4.42**, X = H, OCH_3 dependent upon acid catalysis employed.[316] Substitution patterns have been kept as simple as possible for clarity, except $R^{2,3}$ and $R^{12,13}$ to highlight the dimerization of **4.41**.

4.2 Results and Discussion

4.2.1 Aims and Objectives

In Chapter 3, the syntheses of **3.36a**,**b** and **3.41a**,**b** were presented; oxidation resistant chlorins that could be used as 2nd Generation PSs for PDT. In the introduction to this chapter it has already been shown that despite the wealth of knowledge surrounding bioconjugation to porphyrins, there is little in the way of the same chemistry performed on the 17,18-dihydro-18,18-dimethylporphyrin scaffold. Further to that, there is little in the terms of strategies for solubilization of these motifs.

The aim of this chapter is to develop multifunctional chlorins that can easily be transformed into 3rd Generation PSs, through the application of the general structure **4.46**.

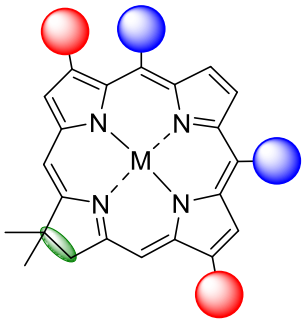

4.46

Figure 4.7. Core structure of the target products of this chapter.

These structures will contain orthogonal bioconjugation handles at the 5- and 10-positions of the macrocycle (blue circles), given their ease of introduction as shown in Figure 4.3.

Further to this, with the developments in generation of brominated halves for chlorin syntheses and the resultant changes in the UV-Visible absorption spectra, we aim to use this strategy to further increase the wavelength of absorption (red circles). Additionally, this strategy will also be applied in a manner such to increase the solubility of the resultant chlorin in polar, or even aqueous media.

These chlorins will be evaluated in a manner akin to those presented in Chapter 3, however focusing on the photophysical parameters necessary for PDT, along with *in vitro* analyses of the successful candidates.

4.2.2 On the Synthesis of 5,10-Diaryl Chlorins and Analogous *trans*-A_2B_2 Porphyrins‡

4.2.2.1 Eastern Half

Given the desire for orthogonal bioconjugation handles, it was necessary to choose a "*C*-terminus" and an "*N*-terminus". The *N*-terminus being of heightened importance given the ability to yield a myriad of functional groups for which to bioconjugate with, as opposed to a *C*-terminus in which options seem more limited.

We initially rationalized the generation of a 10-(*p*-nitrophenyl)chlorin as an early target; however, its synthesis is remarkably low yielding given its structure type, 3.8% as reported by Borbas in 2012.[307] Given previous work by the Boyle group,[89, 97,317] we then rationalized the utilization of an acetamido motif. The work of the Boyle group has continually utilized an A_3B-porphyrin with three 4-pyridyl motifs, and a *p*-acetamidophenyl on the remaining meso position (i.e., **1.42**, Figure 1.10). This acetamido group is then deprotected to yield the amine, and utilized in amide couplings, or further transformed into an azide for CuAAC reactions.

4-Acetamidobenzaldehyde (**4.47**, Scheme 4.3) was cleanly transformed into DPM **4.48** via a TFA catalyzed DPM synthesis, yielding the product in 85% as a white powder upon trituration with pentane. Upon repeated attempts following a reported procedure for DPM formylation,[314] **4.49** was not yielded as the desired product. Whilst a crude was obtained as a deep red oil, attempted purifications routinely yielded the same red oil, with minimal difference in the resultant ^{1}H-NMR spectrum post chromatographic purification. The only separable component of this red oil was unreacted **4.48**. Given the inability to fully characterize an intermediate, a new route had to be found.

At this point, Borbas' benzoylation of DPMs to yield appeared particularly attractive. As noted, the first synthesis of *gem*-dimethyl chlorins by the Lindsey group utilized chlorins of a 5,10-diaryl core.[234] Thus, whilst the question of where and how the

---

‡ *The crystallographic data presented in this chapter was collected, solved and refined by either Dr. B. Twamley or Dr. C. J. Kingsbury. The respective crystallographer is acknowledged in each figure caption.*

bioconjugation handle will be placed has been resolved a further question remains. What should be at the 10-position?

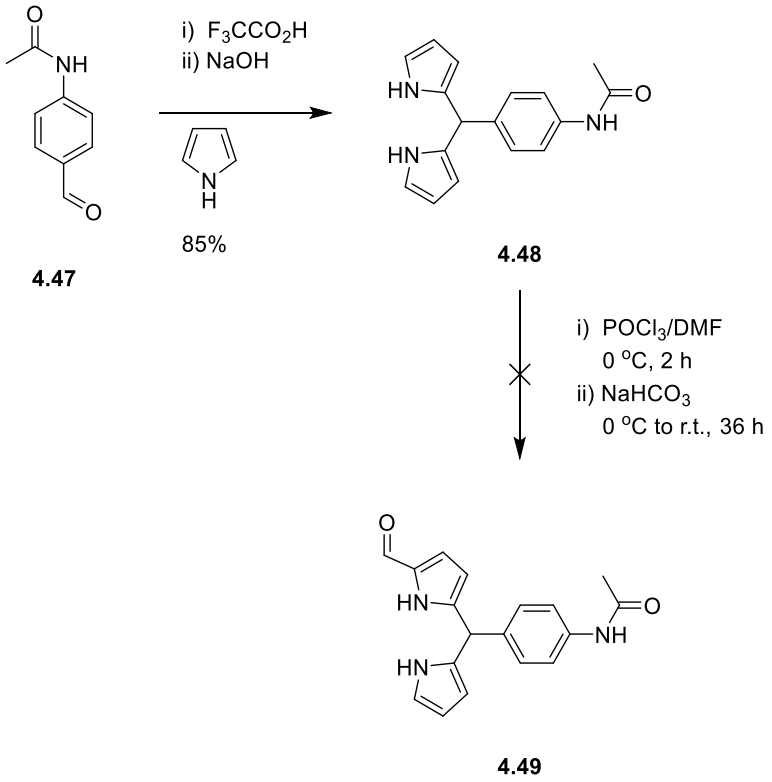

Scheme 4.3. Attempted synthesis of a Western half for chlorin condensation bearing an acetamido motif to introduce a bioconjugation handle.[314]

Ptaszek's generation of **4.33** initially seemed favorable;[296] however, our desire was to also expand the library of bioconjugation opportunities. The same reasoning applies to **4.32**.[307] The following two initial design criteria were implemented: the 10-substitutent could not contain any *ortho*-substituents, as this could later introduce atropisomerism into the structure, a factor which has only recently received a thorough evaluation with regards to PDT,[309] the 10-substituent must contain multiple anchor points for attachment of motifs, i.e., akin to the multiple PEG chains appended to **4.35**.[308] At this point, multiple substitution patterns are possible to yield *C*-termini. However, the motif chosen then was 3,4,5-trimethoxyphenyl.

A group that is common in pharmacophores,[318] antimitotic agents,[319] and polyphenol chemistry,[320] it has widespread use. Whilst unlikely to be used explicitly as the trimethoxylphenyl unit, i.e., fully protected, the applications must be noted. This group is particularly useful given the ability to selectively deprotect the *p*-methoxy unit with e.g., boron(III) trichloride or methanesulfonic acid,[321] or all three

with boron(III) tribromide.[322] This approach could yield highly functional 3,5-*X*-4-*Y*-substituted phenyls.

Thus, 5-(3',4',5'-trimethoxyphenyl)dipyrromethane (**4.51**, Scheme 4.4) was likewise synthesized in a TFA catalyzed DPM synthesis, utilizing dichloromethane as a co-solvent to mitigate the use of pyrrole in the reaction. Post-column chromatography **4.51** was yielded as a colorless crystalline solid in 30%.

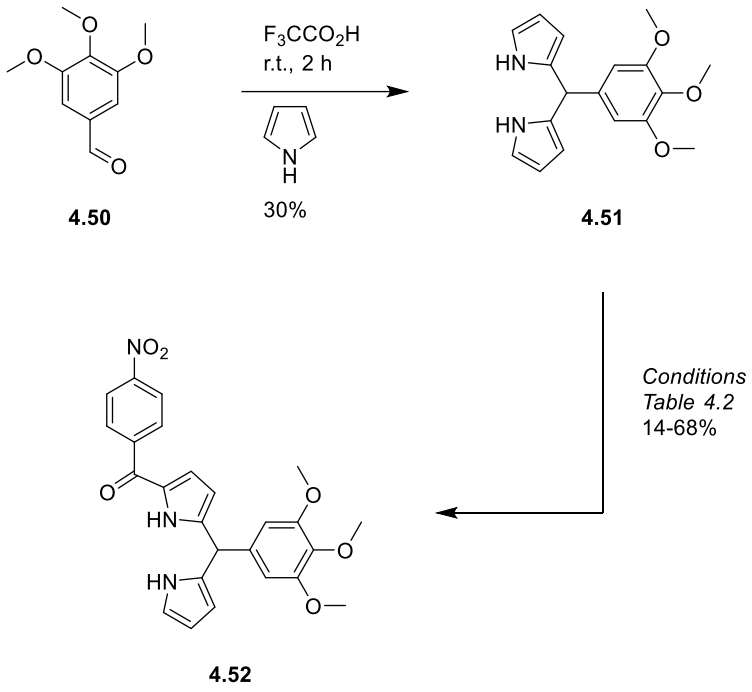

Scheme 4.4. Synthesis of eastern half **4.52** with preinstalled bioconjugation handles.

In stark contrast to the ease of synthesis of **4.51**, the synthesis of **4.52** is best described as either arduous, or at the very least non-facile. Initially, **4.51** was treated with ethyl magnesium bromide and *p*-nitrobenzoyl chloride (**4.53**) in toluene following the procedure reported by Borbas;[307] however, whereas they reported a yield of 58%, we observed yields of 26%. Initially, this low yield was put down to poor reagent quality, and as previously noted it is possible to purify **4.53** via hot recrystallization from benzene.[323] Instead, a hot recrystallization was performed in toluene, and upon cooling an amount of colorless white crystals ca. 2–3 mm in length were yielded in a yellow solution. These were filtered off and found to be remarkably offensive in odor, presumed to be *p*-nitrobenzoic acid. Concentration of the toluene solution initially yielded a yellow oil, which became an amorphous yellow solid upon extended drying under high vacuum. The benzoylation was then reported

utilizing Borbas' procedure on a greater scale – only to generate **4.52** in an almost identical yield.

In spite of the low yields, what also became apparent was the limited solubility of **4.52**, and it was found that an initial method of purification for **4.52** was precipitation from diethyl ether.

As well as the reaction with the neat benzoyl chloride, methods of acylation of dipyrromethanes consider the utilization of pyridyl thioesters. The methodology first reported by Masashi et al.,[324] utilizes the generation of *S*-(2-pyridyl)thioesters from the respective acyl chloride and 2-pyridinethiol (**4.54**). In their work, they found great success in generating a wide variety of benzophenones. This strategy was not applied to pyrrolic motifs however until 2000, by Lindsey and co-workers.[325]

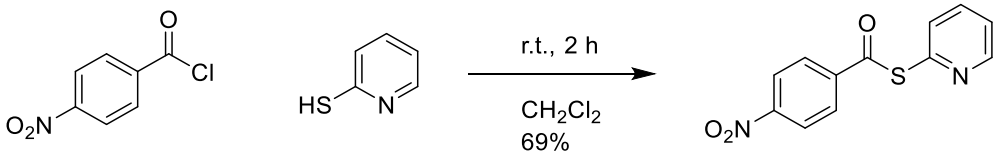

4.53 **4.54** **4.55**

Scheme 4.5. Synthesis of S-(2-pyridyl)thioester **4.55**.[324,325]

To this end, non-recrystallized **4.53** was combined with 1 eq. **4.54** in CH_2Cl_2, and **4.55** was yielded cleanly in 69%, a yield in line with those reported previously, e.g., 73% for *p*-tolyl and 72% for *p*-methoxyphenyl etc.[325] Whilst there is one report of **4.55** in the literature prior,[326] there is no synthesis of it reported, nor any characterization data.

Multiple attempts were made utilizing solvent mixtures listed for the precipitation of previously generated S-(2-pyridyl)thioesters; however, none were suitable. Eventually, hot recrystallization from ethyl acetate yielded the desired **4.55** as long colorless needles. These crystals were found to be suitable for X-ray diffraction analyses. Compound **4.55** was found to crystallize in the orthorhombic space group P*na2₁* (No. 33) with no solvate, and no major H-interactions worthy of note.

Upon successful synthesis and characterization of **4.55**, it was applied to the synthesis of **4.52**. Instead of toluene used previously, the choice was made to perform the reaction in THF as to increase the solubility of all the reactants. Initial attempts were made utilizing **4.55** as a suspension in THF; however, this diluted the

reaction mixture and as the reaction time remained constant – this reduced the yield (Entry 3, Table 4.2).

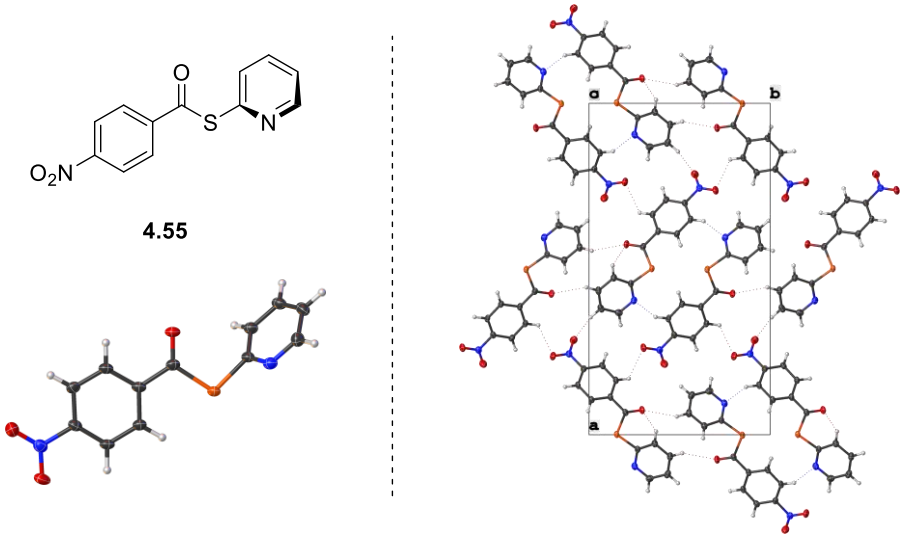

Figure 4.8. Single crystal X-Ray structure of thioester **4.55** with structure (*top left*), with asymmetric unit (*bottom left*) and view of packing along the (001) direction (*right*). Image generated in Olex2.[126] Thermal ellipsoids indicate 50% probability. Data collected, solved, and refined by Dr. B. Twamley.

Table 4.2. Experimental changes to increase the yield of **4.52**. * Yield decreased via improper purification.

Entry	*Acyl chloride (**4.53**) or Thioester (**4.55**)*	*Solvent*	*Method of Purification*	*Isolated Yield of **4.52***
1	**4.53** (Neat solid)	$C_6H_5CH_3$	Precipitation (Et_2O)	27%
2	**4.53** (Neat solid)	$C_6H_5CH_3$	Precipitation (Et_2O)	26%
*3**	**4.55** (suspension in THF)	THF	Column chromatography	14%
4	**4.55** (Neat solid)	THF	Precipitation (Et_2O)	25%
5	**4.55** (Neat solid)	THF	Wash with refluxing *i*PrOH	68%

In the next attempt, **4.55** was added as a neat solid, and in a return to precipitation as the method of purification, the yield was no higher than that for the use of the thioester (entries 1 & 2). In the last attempt, the crude material was combined with *i*PrOH post-work up and heated to reflux for 2 h before being passed through a glass frit (entry 5). This procedure yielded a vibrant yellow powder and black filtrate. The yellow powder was found to be analytically pure **4.52**, in excellent yield.

Lastly, bromination – a necessity in the synthesis utilized. Initially, we targeted mono-bromination as typically a myriad of differing bromination products is yielded, even if the equivalents of bromination reagent are carefully controlled. Initial treatment of **4.52** with non-recrystallized *N*-bromosuccinimide (NBS) (1 eq.) yielded two bands upon column chromatography. The first fire engine red band serendipitously yielded crystals upon standing at room temperature.

From the initial ϕ scan of the crystal obtained we are able to discern that the crystals were the structure **4.57**, which crystallized with no solvate, and in the monoclinic space group $P2_1/n$ (no. 14). Compound **4.57** was found to be a mixture of dipyrrins; non-brominated, mono- and di-brominated in percentages of 13.2%, 35.4%, 52.3%, respectively, as determined *via* analysis of residual electron density peaks in the SC-XRD data. The formation of these dipyrrins is an unsurprising result in hindsight, in the process of bromination, NBS had also oxidized any species in the vicinity.

Interestingly, the packing of **4.57** was not changed even when differing numbers of bromine atoms had been appended. Further to this, the hydrogen atom was placed as exhibited in Scheme 4.6, determined via the lesser C-N-C angle within the pyrrole versus pyrroline rings. Lastly, we could evidently observe π-π stacking between two molecules of **4.57** extending across the entire molecule excluding only the trimethoxyphenyl ring which was rotated 53.5° away from the dipyrrin plane.

The second band of this was a mixture of mono- and di-brominated dipyrromethanes as determined by electrospray ionization mass spectrometry (ESI-MS) with a ratio of roughly 3:1 for *m/z* = 617.9711 (n = 2), to *m/z* = 540.0595 (n = 1), and ^{1}H-NMR spectroscopy as determined by multiple resonances in the range of δ = 5.49–5.60 ppm, (amongst others) indicative of multiple meso-protons in respective DPMs.

Through the use of these conditions, we were unable to isolate an analytically pure sample of a mono-brominated mono-acylated DPM. Instead, the mixture **4.56** was yielded. Given this, it was decided that for future experiments it was more suitable to brominate **4.52** with much lesser equivalents of NBS and purify via silica plug as to remove ‘baseline contaminants’ prior to use in a chlorin condensation reaction. This procedure has been continually used by the Borbas group to suitable affect.[307]

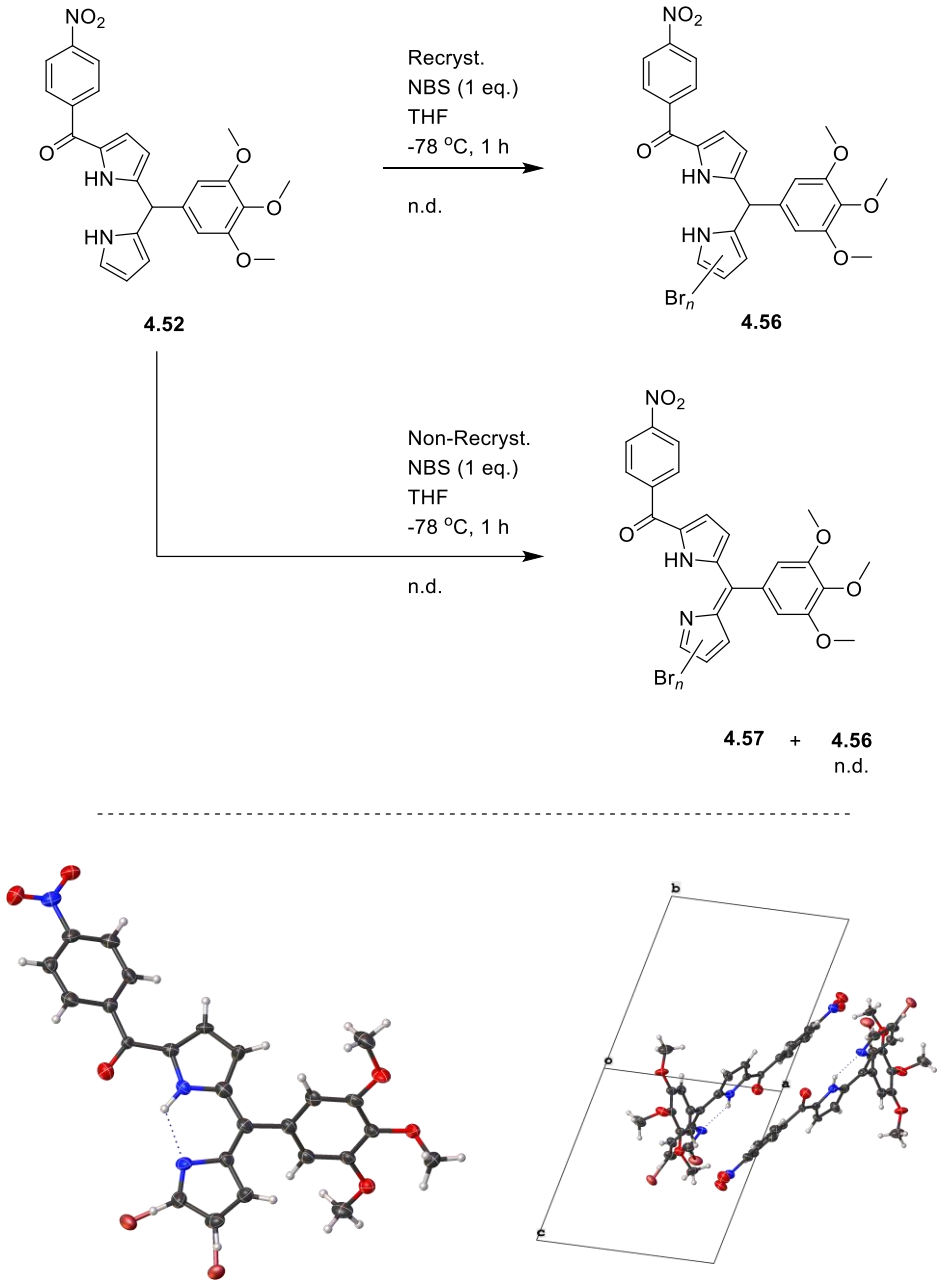

Scheme 4.6. Synthesis of bromo-dipyrromethane **4.56**, and generation of bromo-dipyrrin **4.57** upon the use of non-recrystallized NBS (*top*). Asymmetric unit of **4.57** with all parts shown (*bottom left*) and packing diagram of **4.57** showing the π-π stacking between two molecules, looking along the (011) direction (*bottom right*). Images generated in Olex2.[126] Thermal ellipsoids indicate 50% probability. Data collected, solved, and refined by Dr. C. J. Kingsbury.

4.2.2.2 The Western Half and Unexpected Diastereomeric Resolution

As noted, *vide supra*, the most well utilized elaboration to the *gem*-dimethyl hydroporphyrin core was that of the 3- and 13-positions (see Figure 4.2). It was noted at the time by Lindsey and co-workers that this would work provide "the foundation for tuning the spectral properties of chlorins in a systematic manner" to eventually yield chlorins suitable for application in artificial photosynthesis and photomedicine.[285]

The synthesis of **4.6** differs minimally from that of **4.43**. Obviously, there is a bromination step involved, but also there are the respective protection and de-protection steps. In the initial synthesis of **4.6**, no *N*-protection was utilized and as a result it was inadvertently found that the non-protected variant of **4.61** (Scheme 4.7) was explosive.[285] Upon the discovery of this, they decided on utilizing a *p*-Toluenesulfonyl protection strategy citing its ability to generate crystalline products,[327] as well as its ease of removal.

Again, akin to **4.43**, this synthesis has been refined. In 2009, Krayer published refinements with the aims of; lessening consumption of reagents and solvents, limiting use of chlorinated solvents, limiting chromatography, and improving yields.[328]

Both sets of synthesis, i.e., **4.43** and **4.6**, start from pyrrole-2-carboxaldehyde. Initial investigations on this step in particular by Anderson and Lee indicated that with NBS the 4-isomer was found to be the major product when low temperatures were used along with short reaction times. Increasing the temperature to r.t or higher will promote the generation of the 4,5-dibrominated product, albeit in 1.4%.[329] Other procedures implementing Br_2, or other bromination agents, did not yield such a favorable product distribution.[291] Thus, application of their findings yielded **4.5** via recrystallization in 87% yield.

Treatment of **4.5** with NaH, and subsequently *p*-TsCl yielded the protected analogue via recrystallization in 76% yield. Interestingly, in the original 2006 publication, there is no isolation of **4.60**, and instead it is only isolated in Krayer's 2009 refinements.[328] The Henry reaction was performed simply utilizing **4.59** and Krayer's refined conditions, which yielded the **4.60** as a vibrant yellow solid in 92%.

Multiple refined procedures for the transformation of **4.60** into **4.61** have utilized silica in the reaction mixture, or Montmorillonite K10, with $NaBH_4$ as the reducing agent,[287,330] with the aim of facilitating the purification *in situ*. In our experience this reduced the yields significantly. Coupled with this, as we found in Chapter 3, $LiBH_4$ out-performed $NaBH_4$. Thus, application of these conditions *typically* yielded the desired 2-(2-nitroethyl)pyrrole **4.61** in 69%.

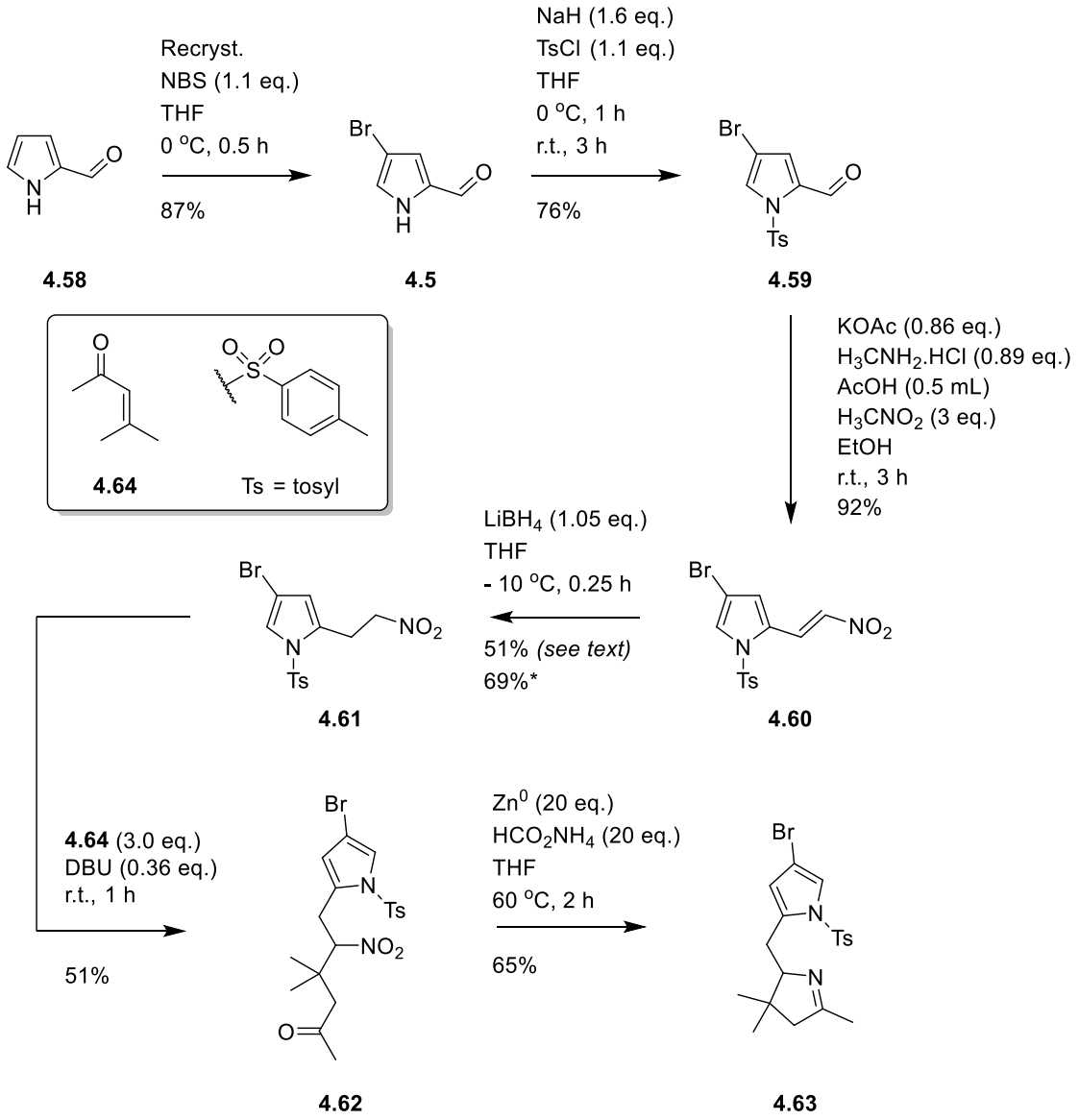

Scheme 4.7. Synthesis of protected western half synthon **4.63** over 6 steps from pyrrole-2-carboxaldehyde (**4.58**).[285,328]

One of the benefits of Krayer's refinements is the scales at which they can be performed on. The utility of the refinements were fully displayed when the synthetic

sequence began with 38 g of **4.58**, i.e., 400 mmol. In the work presented herein, the scale presented was half that of Krayer, with representative yields at every step.

As noted, *vide supra*, yields for the reduction step with $LiBH_4$ were continually achieved in the range of 65–69% on scales less than 50 mmol in the work surmounting this thesis. Upon scaling up from 50 mmol for 125 mmol, we observed a significant decrease in yield along with a large amount of white powder filtered off during the recrystallization step (entry 5, Table 4.3).

Analysis of the powder via ^{1}H-NMR spectroscopy indicated it was the dimeric by-product (Figure 4.9), as detailed briefly by Krayer, but not mentioned in the original manuscript.[285] Whilst the number of resonances increasing was something immediately evident, another key feature was the observation of separate tosyl moieties being in different environments, as presented by two tosyl-CH_3 resonances at δ = 2.44 and 2.45 ppm.

Likewise, this continued throughout the spectrum with every individual environment. Immediately noticeable are the 3-pyrrolyl protons at δ = 5.99 and 6.17 ppm, amongst others. Through ^{1}H-^{13}C HSQC, ^{1}H-^{15}N HMBC, ^{1}H-^{13}C HMBC, selective TOCSY DIPSI and selective NOESY experiments, we were able to provide a complete assignment of the sample presented.

Table 4.3. Tabulated data for the production of dimer **4.65**.[285,328] † = this work.

Entry	*Solvent, [**4.60**]*	*Time*	*Temp*	*Reducing agent (Equiv.)*	*Scale*	*Yield **4.61***	*Yield **4.65***
1[271]	$CHCl_3$/iPrOH (3:1), [0.088 M]	1.5 h	r.t.	$NaBH_4$ (2 eq.)	22.8 mmol	58%	n.d.
2[313]	THF/MeOH (unknown), [0.15 M]	Unknown	0 °C	$NaBH_4$ (2 eq.)	Unknown	50%	n.d.
3[313]	THF, [0.200 M]	0.25 h	- 10 °C	$LiBH_4$ (1 eq.)	234 mmol	77%	n.d.
4[313]	THF, [1 M]	Unknown	- 10 °C	$LiBH_4$ (1 eq)	Unknown	40%	n.d.
5† *This work*	THF, [0.208 M]	0.25 h	- 10 °C	$LiBH_4$ (1.05 eq.)	125 mmol	51%	10%

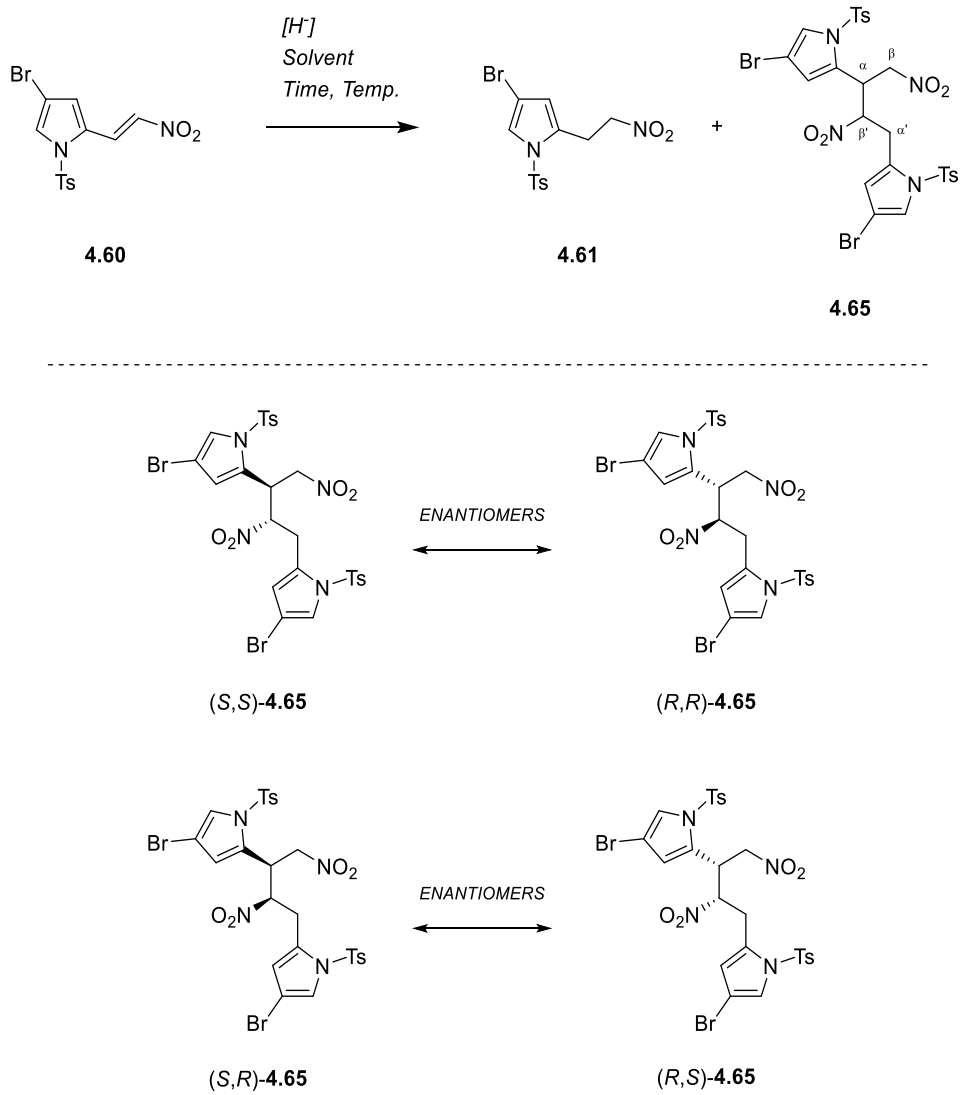

Scheme 4.8. *Top*: General scheme for the reduction of **4.60**, and generation of desired **4.61** along with undesired dimer **4.65**, α and β labels have been added to illustrate the dissymmetry of **4.65**. *Bottom*: All the diastereomers of **4.65** are presented, excluding chirality induced by the Ts motif, and the enantiomeric relationships within the set.

Upon confirmation of the nature of this product, we attempted to rationalize its formation in such a yield. Whilst it is evident that **4.65** is the result of the respective nitronate of **4.61** attacking another molecule of **4.60**, it should not have been produced in such scale. In examinations prior, no yields of **4.65** have been presented by other authors. For multiple entries in table 4.3, the amount of **4.65** was described as ‘substantial’, whilst no actual yield was provided for any of the refinement attempts undertaken.

The sample of **4.60** used was stored at 0 °C whilst protected from light and under an Ar atmosphere albeit for 27 weeks prior to use as a result of obvious world

events. We observed no physical changes in the appearance of this sample of **4.60** between the time of its preparation and the time of its use. No comments have been made regarding the stability of **4.60**, and whilst we cannot confirm its degradation, we cannot exclude it either.

Post-NMR analyses, crystals of **4.65** serendipitously formed in the NMR tube. In our SC-XRD experiments, **4.65** returned a space group of P*bca* (No. 61) with no solvate. Analysis of the asymmetric unit revealed (*R*,*R*) stereochemistry for that molecule of **4.65**.

Given the inversion center present in the cell, inherently the (*S*,*S*)-diastereomer also exists for **4.65**. This is therefore implying that both (*R*,*R*) as seen in the asymmetric unit, and (*S*,*S*) are present. In our ^{1}H-NMR spectroscopic analyses (along with the respective 2D-NMR spectroscopic analyses undertaken) we observe only one set of resonances for the aliphatic nitro-butane system, indicative of a single species in solution or a pair of enantiomers.

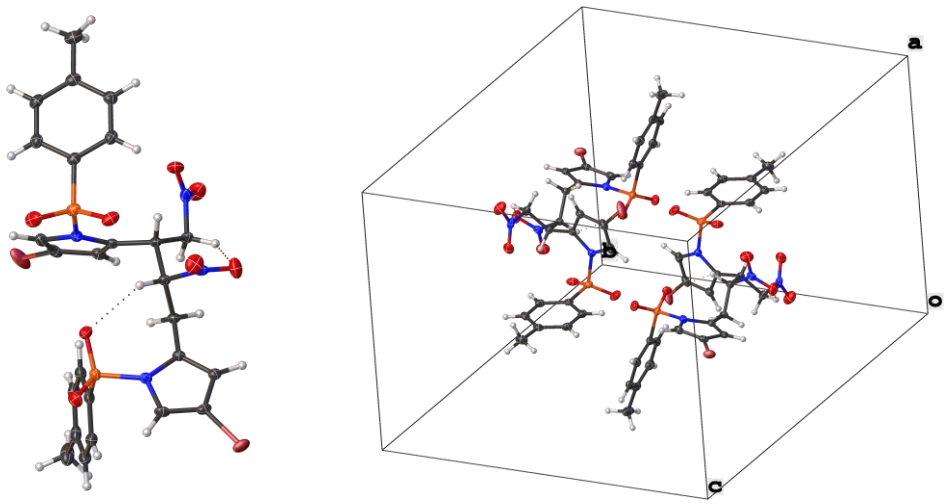

Figure 4.10. Single crystal structure of **4.65** with (*R*,*R*)-**4.65** (asymmetric unit) shown (*left*) and packing diagram (*right*). Images generated in Olex2.[126] Thermal ellipsoids indicate 50% probability. Data collected, solved, and refined by Dr. B. Twamley.

In the SC-XRD structure of **4.65** we observe two separate intramolecular hydrogen bonds; with S=O…H exhibiting D…A of 3.071(3) Å, and N(O)=O…H exhibiting D…A of 3.038(3) Å (Figure 4.10, *left*) These interactions exist in both (*R*,*R*) and (*S*,*S*) enantiomers, however in (*R*,*S*) or (*S*,*R*) enantiomers, the distances between these donors and acceptors are too great to facilitate these contacts.

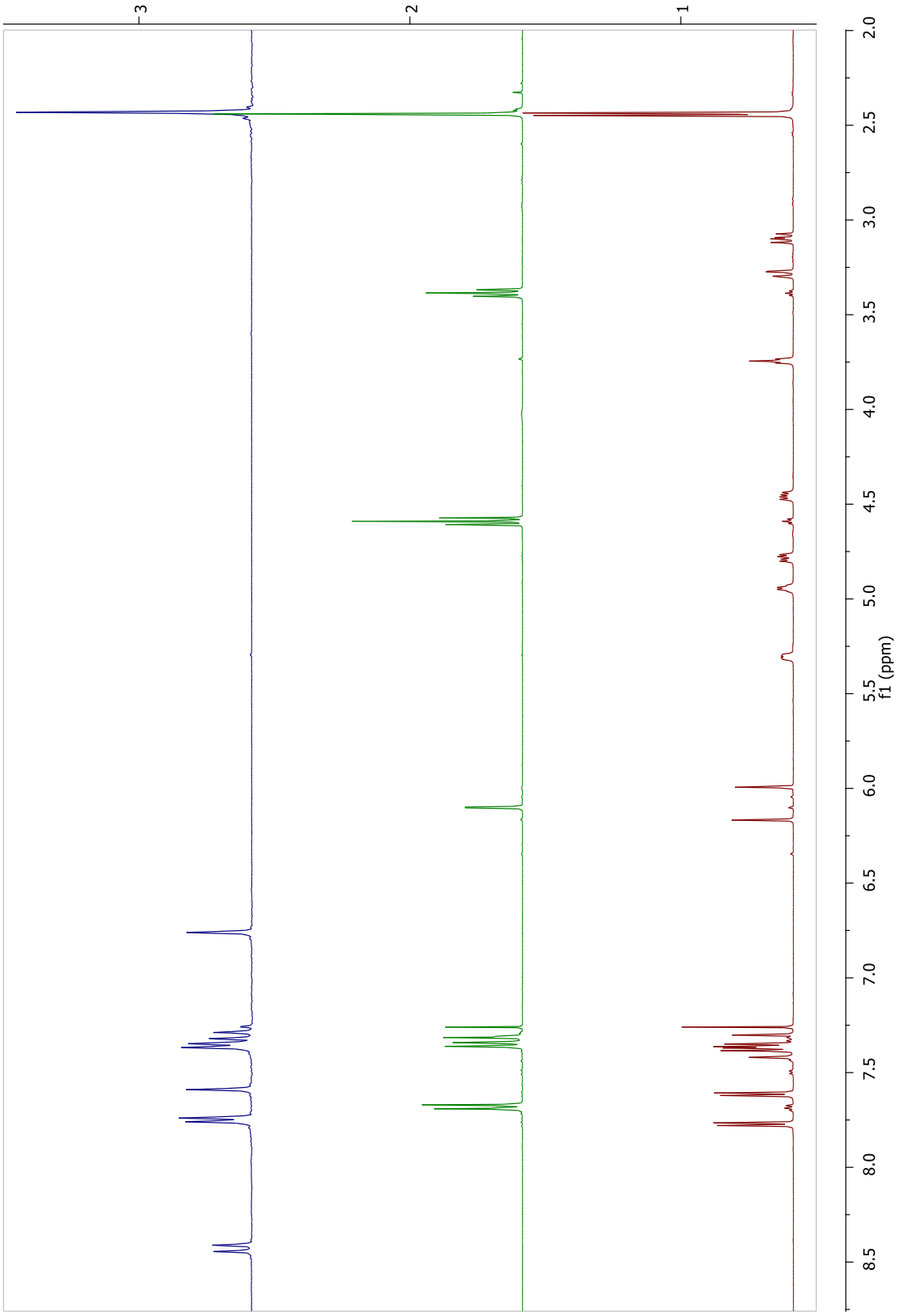

Figure 4.9. Stacked ^{1}H-NMR spectra of **4.60** (*blue, left*), **4.61** (*green, middle*) and crude **4.65** (*red, right*), all in $CDCl_3$, conducted at room temperature.

It could be argued that this C-H…O interaction involving the sulfonyl moiety is just an artifact in the solid state. To investigate if this was present in the solution state, ^{1}H-NMR analyses of the non-tosylated motif would be necessary. Unfortunately however, given the explosive nature of the non-tosylated monomer i.e., non-tosylated **4.61**, this is not an experiment we desired to undertake until all other experimental options had been thoroughly exhausted. Given the interactions presented *vide supra*, however, this seems unlikely.

Considering that the purification of **4.61** is *via* hot recrystallization in *i*PrOH (*c.a.* 100 °C), i.e., a polar protic solvent, there is a large thermodynamic driving force enabling the adoption of the most stable conformation for any particular molecule. Hence, it is plausible that there could be a mechanism selectively driving the thermodynamically favorable formation, and kinetic precipitation, of (*R*,*R*) and (*S*,*S*) diastereomers of **4.65** (Scheme 4.9).

Further evidence for the strength of these intramolecular H-bonds was observed upon analyzing the melting points of the three compounds involved, for **4.61** M.p. 127–130 °C (dec.), lit.[271] 125–127 °C, for **4.60** M.p. 162–168 °C (dec.), lit.[271] 164–170 °C whereas for **4.65** (bulk) 220–223 °C (dec.), lit.[271] 115–117 °C.

Until this point, we have assumed the formation of all four diastereomers and from there, selective mechanisms occur in solution to yield exclusively (*R*,*R*)-**4.65** and (*S*,*S*)-**4.65**. The other option would be for (*R*,S)-**4.65** and (*S*,*R*)-**4.65** to not form at all. Looking at Scheme 4.8, *bottom*, we observe vast steric crowding between nitro- and 2-(*N*-tosyl)-pyrrolyl motifs. Assuming retro-addition of the nitronate of **4.61**, this reaction step will cycle until there is a transition state of low enough energy to form a diastereomer of **4.65** in which the molecule is stable. To ascertain this, experimentation via density functional theory (DFT) calculations would be necessary.

Whilst the structure of **4.65** has been unanimously assigned, we cannot rationalize exactly why it formed in such a yield. To date thus, it is a joyous, anomalous, and serendipitous result.

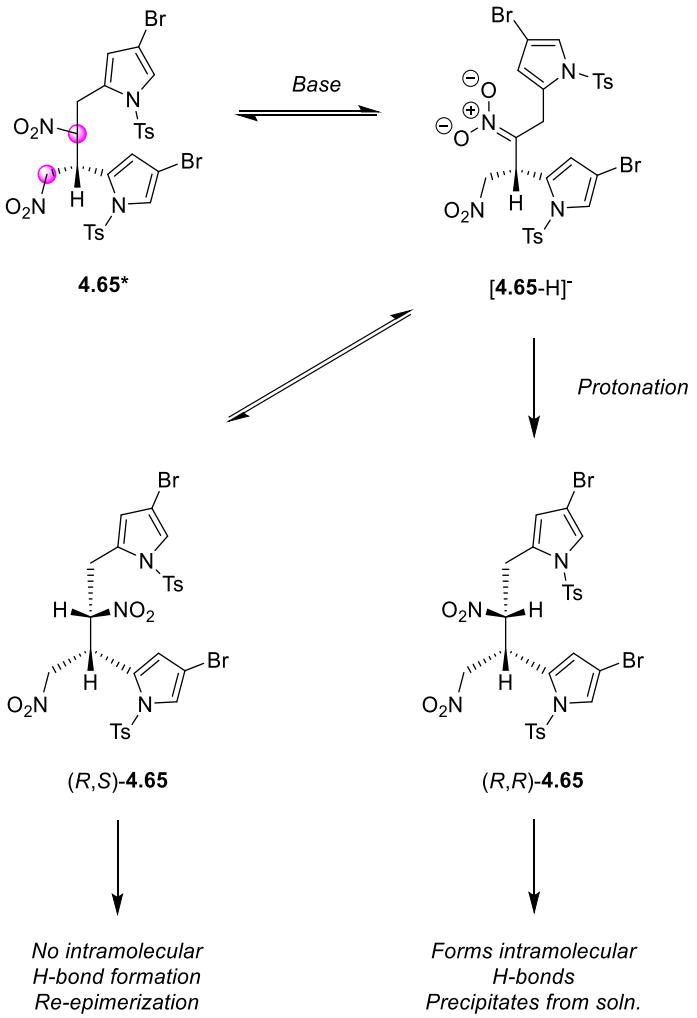

Scheme 4.9. Proposed generation of diastereomerically resolved **4.56** *via* acid catalyzed epimerization of the racemic bulk sample. Possible borane-based stabilization of [**4.65**-H]$^-$ has been omitted.

Michael addition to **4.61** in DBU occurred cleanly, with minimized DBU and increased equivalents of mesityl oxide (**4.64**) as per Krayer's refinements.[328] The final cyclization step again required elevated temperatures and greater equivalents of Zn^0 and HCO_2NH_4; however, a much shorter reaction time. These two intermediates, **4.62** and **4.63**, were the only two in the entire sequence which required column chromatography. As a result of this, **4.62** was limited to production on a much lesser scale than intermediates prior. With regards to **4.63**, the inability to utilize magnetic stirring for such a suspension of Zn^0 limited the scale more so than the necessity for column chromatography. Regardless, the protected brominated western half **4.63** was yielded over 6 steps in 13.9%, with limited chromatography, a true testament to the work of Krayer.[328]

Concomitant with our serendipitous crystallographic endeavors of **4.65**, we were able to analyze a variety of the intermediates present in Scheme 4.7 via single crystal X-ray diffraction; **4.59**, **4.60**, **4.62** and **4.63**.

In all cases, the pyrrolic fragments present approximately consistent internal bond distances throughout the series. Further to this the tosyl groups adopt consistent structures with N-S and N-C bond torsion angles at c.a. 90^{o}. Each asymmetric unit presented contains one molecule of the title compound, and no solvates were observed in any structure. Full crystallographic data will be presented in the Appendix section.

Compound **4.59** was found to crystal in the chiral space group P$2_12_12_1$ (No. 19), whilst itself not possessing a chiral center. Given the Flack parameter of -0.016(2), it is apparent that the crystal analyzed contains a structure as presented below, with the tosyl group pointing backwards ‘under’ the pyrrole.

Compound **4.60** comparably shows larger thermal ellipsoids than the other data presented herein, but within the datasets shows excellent agreement.

Typically, the synthesis of bacteriochlorins requiring the bis(methoxy)methyl imine in the reduced ring is more prevalent in the literature. As a result of this – hydrodipyrrin structures typically contain this motif, and as a result of this preference, the structures for intermediates we have present structures for herein have remained untouched (for bis(methoxy)methyl structures see. CCDC 730192 and 730193,[328] 2125374,[331] and 2083662.[332]). At current, no structure exists for **4.61**; however, the structure of its constitutional isomer was presented in 2014.[333]

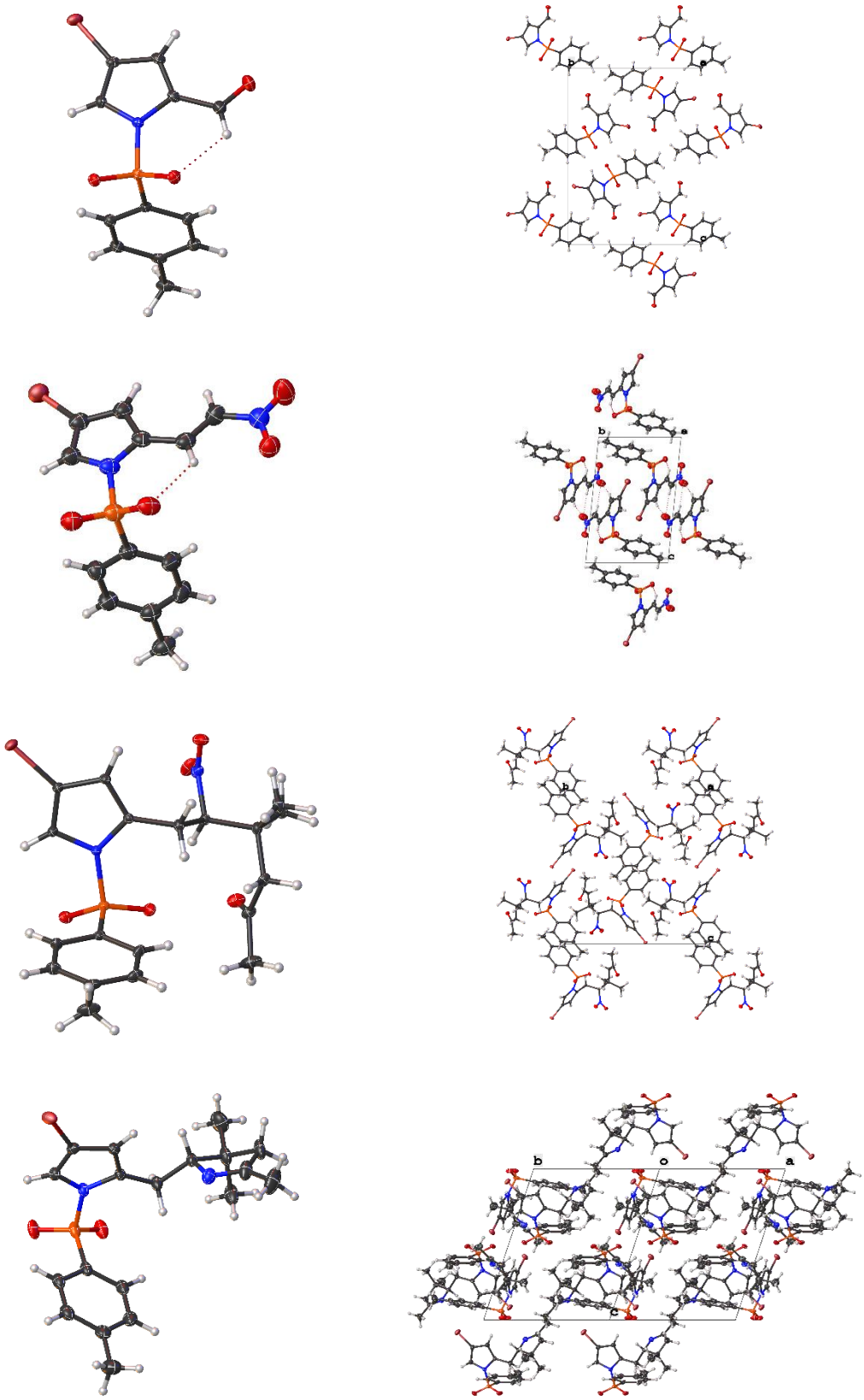

Figure 4.11. Single crystal structures of **4.59**, **4.60**, **4.62** and **4.63** (*top to bottom*) with the asymmetric unit shown (*left*) and a packing diagram (*right*) along the (100) direction for **4.59**, **4.60** and **4.62**, and along the (110) direction for **4.63**. Images generated in Olex2.[126] Thermal ellipsoids indicate 50% probability. Data collected, solved, and refined by Dr. C. J. Kingsbury.

4.2.2.3 A Solubilizing β-Substituent

Substitution at the 3- and 13-positions of the chlorin macrocycle presents stark differences to the UV-Visible absorption spectra of the chlorin, more so than meso-modifications. This is as a result of the extension of the π-conjugation throughout the system, hence why in Table 4.1 the considerations only include CC-TIPS or -$COCH_3$ substitutions. For an analogous set of chlorins, if $R^{3,13}$ = H, $\lambda(Q_y)$ = 606 nm, if $R^{3,13}$ = Ph, $\lambda(Q_y)$ = 623 nm and if $R^{3,13}$ = CC-TIPS, $\lambda(Q_y)$ = 646 nm.[334]

Very few 3,13-di(ethynylaryl)substituted chlorins have been described in the literature,[292,295,296,313,334,335] and the majority utilize phenylethynyl as the substituent in question. Further to motifs that would not aid solubility in aqueous media include 9-phenanthryl- and 4-(phenylethynyl)phenyl along with the BODIPY-chlorin arrays presented in Figure 4.2. This leaves us with few substituents mentioned in the literature; (4-formylpheny)ethynyl, (4-*N*,*N*-dimethylaminophenyl)ethynyl, and (4-methoxycarboxyphenyl)ethynyl.

The design of this motif presents major differences to the discussion for Eastern half **4.52**: i.e., the motif designed will be a phenylethylene, and thus will not have the opportunity to introduce atropisomerism, nor will it be utilized for bioconjugation, and thus the groups appended should remain constant regardless of external factors. At first thought, perhaps 4-ethynylpyridine, however pyridyl substituents in the presence of zinc-tetrapyrroles can form coordination oligomers.[336]

A survey of the literature indicates that scientists struggle not only with the solubilization of tetrapyrroles in aqueous media, but also organic solvents. In 2001, Screen et al.[337] detailed their inability to solubilize a porphyrin polymer in organic solvents, even with added base, which “precluded spectroscopic characterization”.[337] Their solution was to append tetra-alkyl isophthalamides with long alkyl chains in order to enhance the solubility – which it did. We rationalize that replacing these long alkyl chains with something much shorter, e.g., ethyl, would yield a final tetrapyrrole better suited for later *in vitro* analyses.

Whilst the syntheses presented herein and those of Screen et al.[337] have similar products, differing routes are taken to yield them. Screen started from 5-bromoisophthalic acid, aminated and then coupled with TMS-acetylene. Instead, treating isophthaloyl dichloride (**4.66**, Scheme 4.10) with diethylamine in the

presence of catalytic pyridine yielded N^1,N^1,N^3,N^3-tetraethylisophthalamide (**4.67**) quantitatively.

Bromination was performed using a method described by Balasubramanian and co-workers.[338] As noted by the authors, the importance of bromoarenes in paramount in the current chemical landscape. In spite of this, the majority of bromination procedures utilize moisture sensitive Lewis acids, lengthy reaction times, and/or poor yields. Initially, Lambert reported bromination of nitrobenzene with NBS in aqueous H_2SO_4.[339] Later, Dolbier reported a new method utilizing NBS in TFA as the solvent with H_2SO_4 as the catalyst.[340] Balasubramanian demonstrated their modified method to be *meta*- selective for deactivated aromatics, notably demonstrated on 3-nitrobenzamide.

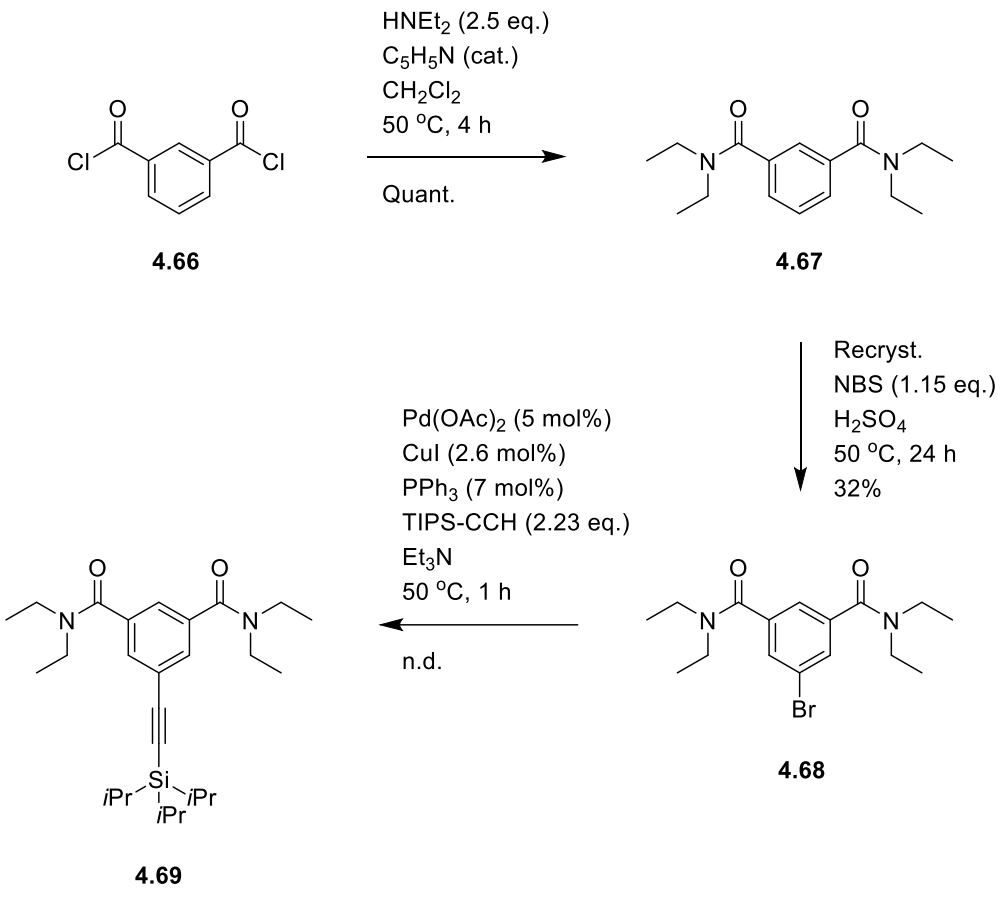

Scheme 4.10. Synthesis of a protected phenylethylene for coupling to the chlorin core to enhance solubility.[337]

Treatment of **4.67** with non-recrystallized NBS in concentrated H_2SO_4 yielded the desired **4.68** in 32% yield, as well as returning the starting material in 30% yield. Column chromatography was performed, however was initially unsuccessful.

Repeated attempts at column chromatography separated the majority of the desired product, however. Fractions containing both **4.67** and **4.68** were combined and again treated with 1.15 eq. NBS in concentrated. H_2SO_4, to yield further **4.68**.

Both **4.67** and **4.68** could be recrystallized from diethyl ether and formed opaque colorless crystals. Compound **4.67** (Figure 4.12) was found to differ minimally in bond-lengths with respect to the analogous N^1,N^1,N^3,N^3,N^5,N^5-hexaethylbenzene-1,3,5-tricarboxamide.[341] The amide motifs were found to be pointing in anti-parallel directions and rotated away from the phenyl plane by 73.5° and 96.0°, respectively. Whilst a multitude of C-H…O interactions can be observed between amide oxygens and the ethyl groups of adjacent amides, the major interaction of note is between C^5-H…O with D…A = 3.44 Å, indicating the propensity of this position for electrophilic aromatic substitution and thus exemplifying the selectivity of this position for bromination.

Compound **4.68** presented again a structure with amides pointing in opposite directions, rotated away from the phenyl plane by 91.9° and 107.4° respectively (Figure 4.12). As a result of substitution of the C^5, C-H…O interactions are instead formed from $C^{4/6}$ to an adjacent amide, with D…A = 3.34 Å and 3.38 Å. Subsequently the structure forms an infinite polymeric chain along the crystallographic *a*-axis (Figure 4.13).

In initial attempts to yield a phenylethylene, trimethylsilyl acetylene (TMS-acetylene) was used in the Sonogashira coupling. Whilst the coupling progressed steadily as observed by TLC, upon ^{1}H-NMR analyses it was indicated from the multitude of resonances in the aromatic region that there were multiple differing products, and observation of the aliphatic regions indicated that the CC-TMS moiety was self-cleaving.

Given the heightened stability of tri(isopropyl)silyl (TIPS) motifs, the conditions of Screen et al.[337] were applied with TIPS-acetylene (Scheme 4.10). In this instance, no cleavage was observed and the desired phenylethylene was yielded as a brown oil. Attempted deprotection of the TIPS-motif with either tetra(*n*-butyl)ammonium fluoride (TBAF) or K_2CO_3/CH_3OH yielded differing mixtures of products; however, there was a constant blue emission upon irradiation with UV-light (365 nm), indicative of 1,3-butadiyne formation.[342]

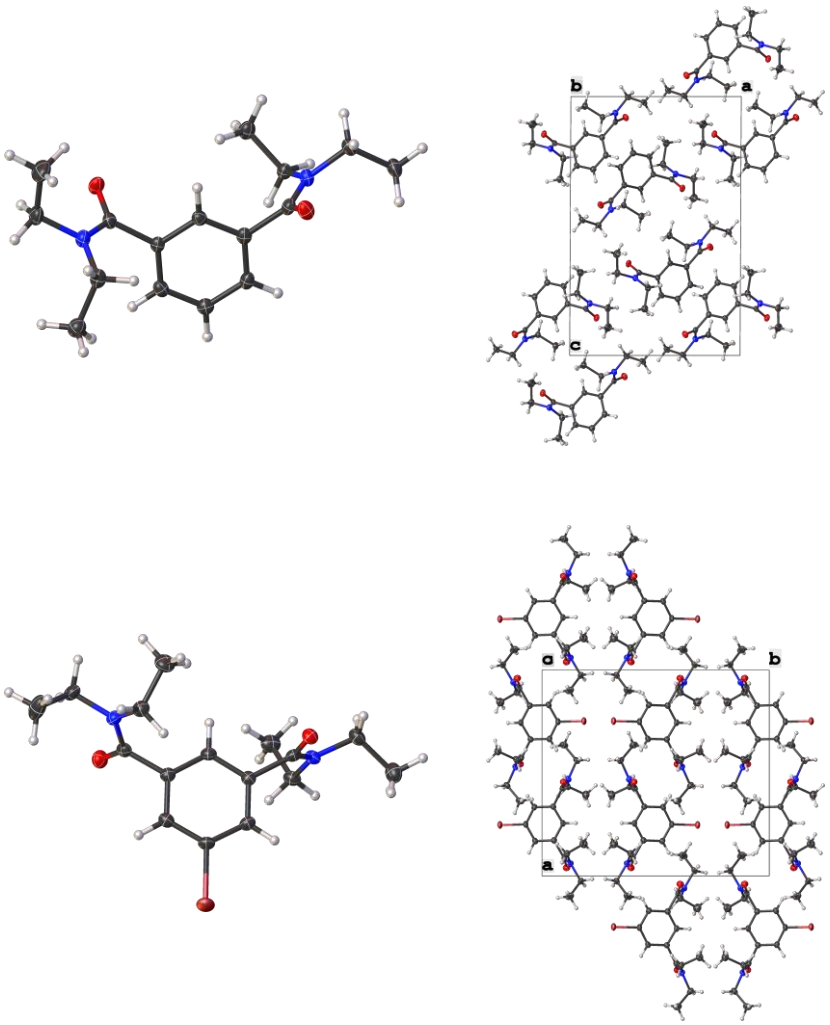

Figure 4.12. Single crystal structures of **4.67** (*top*) and **4.68** (*bottom*) with the asymmetric unit shown (*left*) and a packing diagram (*right*) along the (010) direction for **4.67**, and along the (001) direction for **4.68**. Images generated in Olex2.[126] Thermal ellipsoids indicate 50% probability. Data collected, solved, and refined by Dr. C. J. Kingsbury.

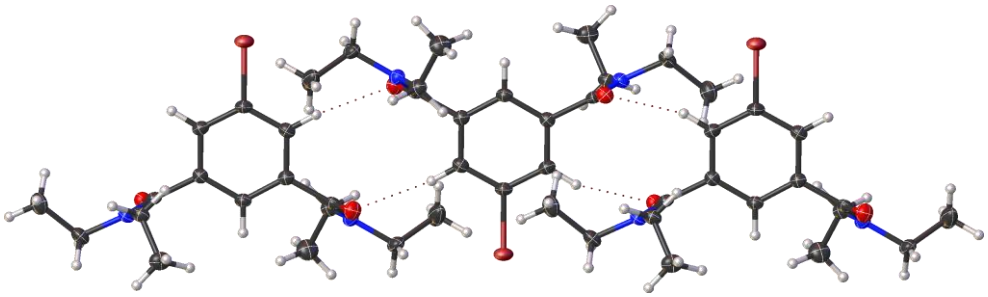

Figure 4.13. C-H…O chain formed by **4.68** along the *a*-axis. Images generated in Olex2.[126] Thermal ellipsoids indicate 50% probability. Data collected, solved, and refined by Dr. C. J. Kingsbury.

To further examine the utility of **4.68**, an exploratory Suzuki coupling reaction was performed with 4-formylphenylboronic acid, in the hope of later generating photoactive arrays with heightened solubility in organic media. Analysis of the

product **4.69** (Scheme 4.11) indicated the incorporation of triphenylphosphine oxide in a ratio of roughly **4.69**:Ph_3PO of 3:1. There are multitude reports of removal of Ph_3PO from such mixtures, and the procedure of Batesky et al.[343] appeared fruitful given their substrate scope for examination; containing multitude polar motifs upon aromatic scaffolds.

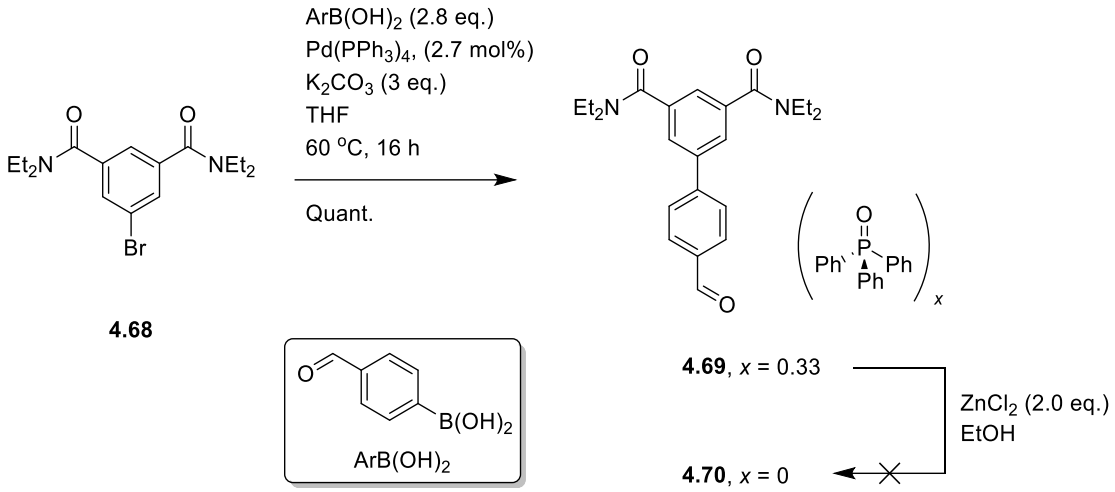

Scheme 4.11. Attempted synthesis of biphenyl 4**.70** via Suzuki coupling from **4.68**, and attempted Ph_3PO removal.[343]

This technique did not remove Ph_3PO to any discernible degree, as determined by ^{1}H-NMR analyses. Whilst a suitable strategy at first glance, given the result observed by ^{1}H-NMR spectroscopy and diminished yield, it is likely that the 1,3-bisamide structure presented in the desired product formed a coordination complex preferentially with zinc ions in solution, as opposed to the desired $ZnCl_2(OPPh_3)_2$ complex.

Given the failures observed in the deprotection of **4.69**, coupled with laboratory restrictions as a result of the COVID-19 pandemic, this approach not used and thus not applied to future chlorins in this thesis. We have however presented the utility of a novel solubilizing motif – with proven capabilities in [Pd]-catalyzed cross coupling reactions.

4.2.2.4 On the synthesis of bioconjugatable 5,10-diaryl chlorins

Respective eastern (**4.52**) and western halves (**4.63**) both required treatment prior to their condensation. As noted in Section 4.2.2.1, the bromination of **4.52** exhibited an inseparable distribution of products. Further compounded by the instability of brominated-formylated dipyrromethanes it was decided bromination immediately prior to condensation was the most suitable method. Treatment of **4.52** with recrystallized NBS in THF, followed by immediate purification via silica plug (as to remove baseline impurities) yielded **4.71** ready to condense. It is from this **4.71** that equivalents for the subsequent steps were calculated.

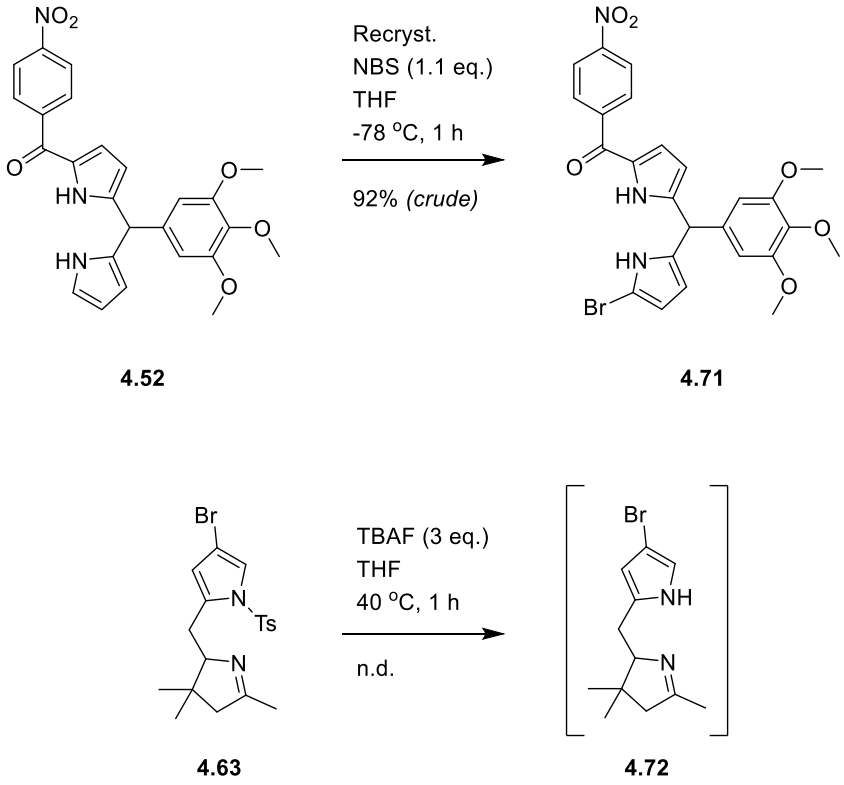

Scheme 4.12. Preparation of eastern (**4.71**) and brominated western (**4.72**) halves for chlorin condensation.[328]

Compound **4.72** was prepared via deprotection using tetra(*n*-butyl)ammonium fluoride in THF. Initial attempts at this procedure via literature reports required heating the solution to reflux.[288] Whilst this, presumably, successfully cleaved the tosyl group from **4.63**, ^{1}H-NMR spectroscopy evidenced apparent decomposition of all species of interest. Instead, it was found that maintaining the reaction at 40 °C was suitable to facilitate this protection. **4.72** was generated within 24 h of use as to mitigate decomposition.

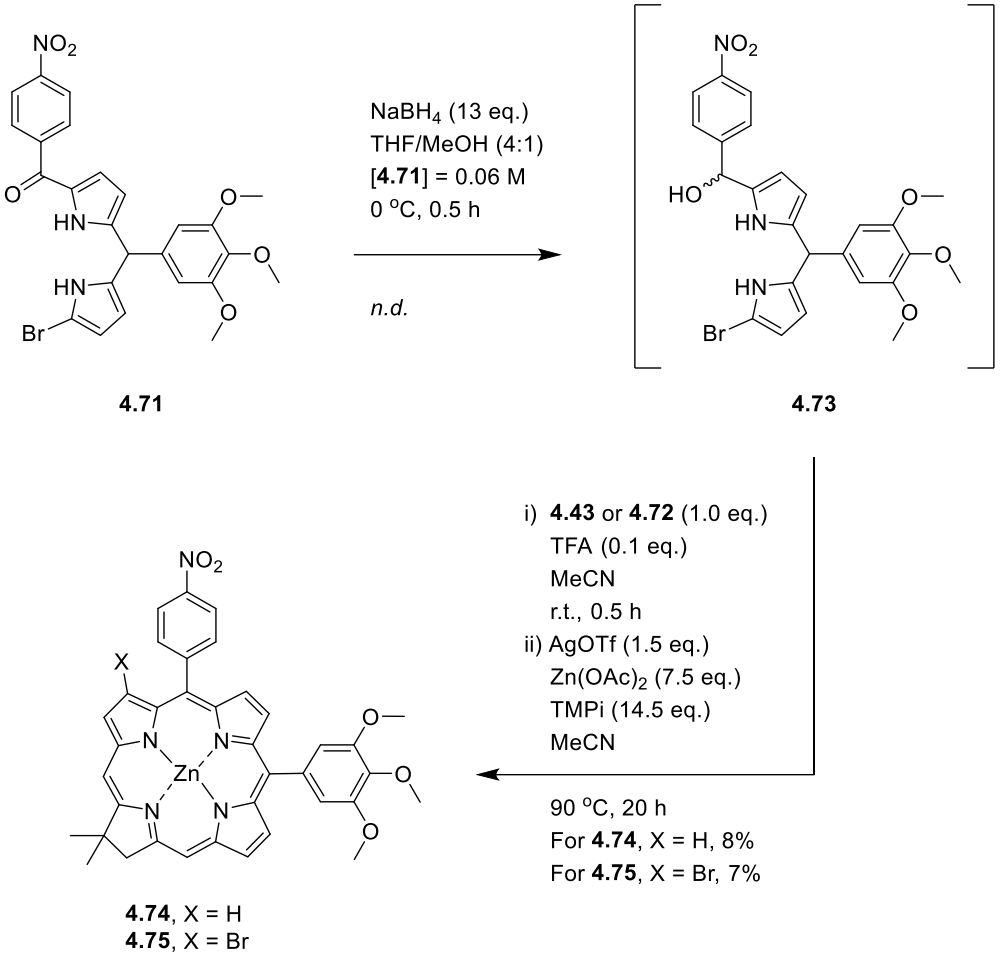

Scheme 4.13. Reduction of **4.71** and condensation with western halves, **4.43** or **4.72** to yield chlorins **4.74** and **4.75**.[307,325]

Reduction of **4.71** with $NaBH_4$ yielded **4.73** cleanly in 0.5 h, as determined via TLC, transforming it from a mustard yellow solid to a light-yellow vicious oil (Scheme 4.13). The procedure used for condensation herein is different to that presented previously (Section 3.2.2). Combination of **4.73** with either **4.43** or **4.72** in the presence of TFA for 0.5 h initially formed the respective 2,3,4,5-tetrahydrobilene-*a*. Immediate quenching of the acid-catalyzed condensation with TMPi, along with the addition of oxidizing agent AgOTf and a source of zinc, $Zn(OAc)_2$, yielded chlorins **4.74** and **4.75** in 8 and 7%, respectively, post column chromatography as green and deep blue solids, respectively.

Initially upon the synthesis of **4.74**, ^{1}H-NMR spectroscopy revealed a series of extra resonances in the regions which we had observed the methoxy-protons, as well as the protons present on the *p*-nitrophenyl moiety. Repeated column chromatography of the sample in a less polar eluent revealed a brown band at a lower R_f than **4.74**,

and through UV-Visible spectroscopy initially it was confirmed as a zinc porphyrin, *vide infra*. This result was indicative of insufficient **4.43** in the reaction mixture, and subsequently, **4.73** had dimerized. This issue did not prevail in the synthesis of **4.75**, however. Whilst only a modest drop in yield between **4.75** and **4.74**, it is in line with the changes in yield presented previously for an analogous comparison of 5,10-diaryl substituted chlorins.[285]

In contrast to **4.74**, synthesis of **4.75** produced a separable amount of the 3,13-dibrominated chlorin **4.75b** , in 0.3% yield. The chlorins presented $\Delta R_F = 0.02$ (silica, EtOAc:C_6H_{14}, 1:1), with the bis-brominated **4.75b** exhibiting the higher R_F. The UV-Visible absorption spectra of **4.75** and **4.75b** are presented in Figure 4.15. Despite the more favorable wavelength of absorption presented by **4.75b**, given the minimal amount of **4.75b** isolated, it was not considered for *in vitro* analyses.

4.2.2.5 On the Synthesis of Analogous *trans*-A_2B_2 Porphyrins

Whilst the generation of **4.74** and **4.75** was a success, yielding oxidation resistant bioconjugatable chlorins which can be evaluated with regards to their efficacy as PSs for PDT, the substrate scope for the study would be small.

We sought to broaden our study utilizing compounds that had a more familiar structure to the majority in the PDT community, in particular something far more accessible. By enhancing the accessibility of these 'competitors' it also sought to answer the question as to whether the development of **4.74** and **4.75** was a worthwhile endeavor in the synthesis of new PSs for PDT. Initial inspiration for which came from the by-product formed in the synthesis of **4.74**. Porphyrins take up the largest class of agents evaluated with regards to PDT, as noted in Section 1.1.3. Further to this, as a result of the COVID-19 pandemic, and subsequent restrictions in research laboratories institution-wide, a simple one step synthesis seemed more practical.

As noted, the dimerization in our prior case was yielded serendipitously. Instead, Rao *et al*. had previously published a route for the generation of free base *trans*-A_2B_2 porphyrins from mono-acylated dipyrromethanes which showed excellent scalability.[325] Thus, utilizing the conditions outlined by Rao *et al*.[325] free base porphyrin **4.76** was yielded cleanly over a single step in 25% yield, which yielded a suitable crop of porphyrin (422 mg) with ease (Scheme 4.14).

Analysis of **4.76** by ^{1}H-NMR spectroscopy serendipitously led to the formation of crystal suitable for analysis via SC-XRD (Figure 4.14). The asymmetric unit was found to consist of two halves of porphyrins, bisected through the C^{20}-C^1 and C^{10}-C^{11} bonds, related to one another through an inversion center at the porphyrin core. The main difference between the two 'half porphyrins' (Figure 4.14, *bottom right*) was the H-bonding motifs present between the methoxy units and the present $CDCl_3$.

The porphyrin core was found to be planar, within 0.04 Å across the $C_{20}N_4$ core, and exhibited π-stacking at 3.65 Å. As a result of the *trans*-A_2B_2 substitution pattern consisting of both electron-donating and electron-withdrawing groups, a 5,15-stretch was noted. Further to this, there is distortion of the E_g mode, in which a

rotation of the pyrrole rings (NH containing) away from the porphyrin core by 5.85° from the meso-C_4-plane is observed.[344,345,346]

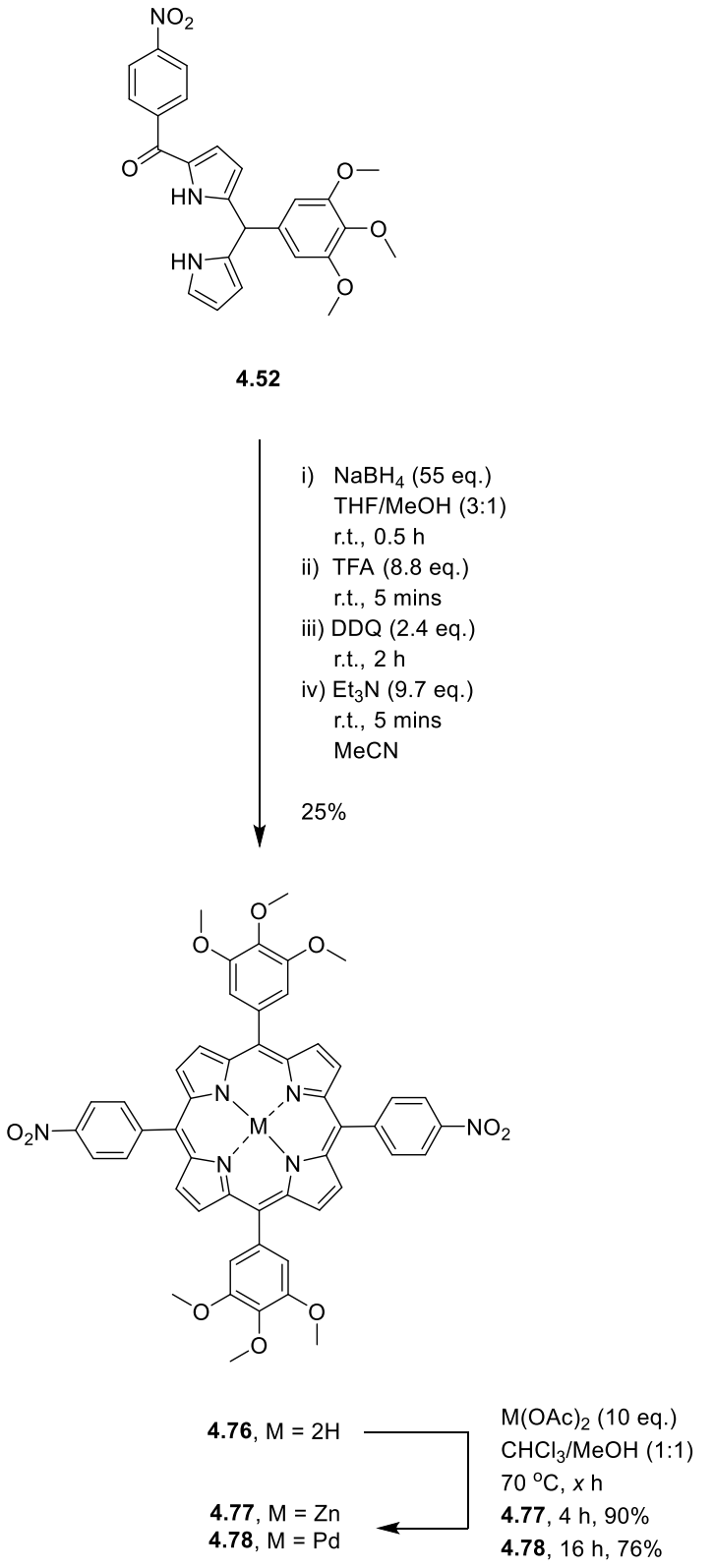

Scheme 4.14. Synthesis of porphyrins **4.76**–**4.78** from **4.52** utilizing the procedure of Rao *et al*.[325]

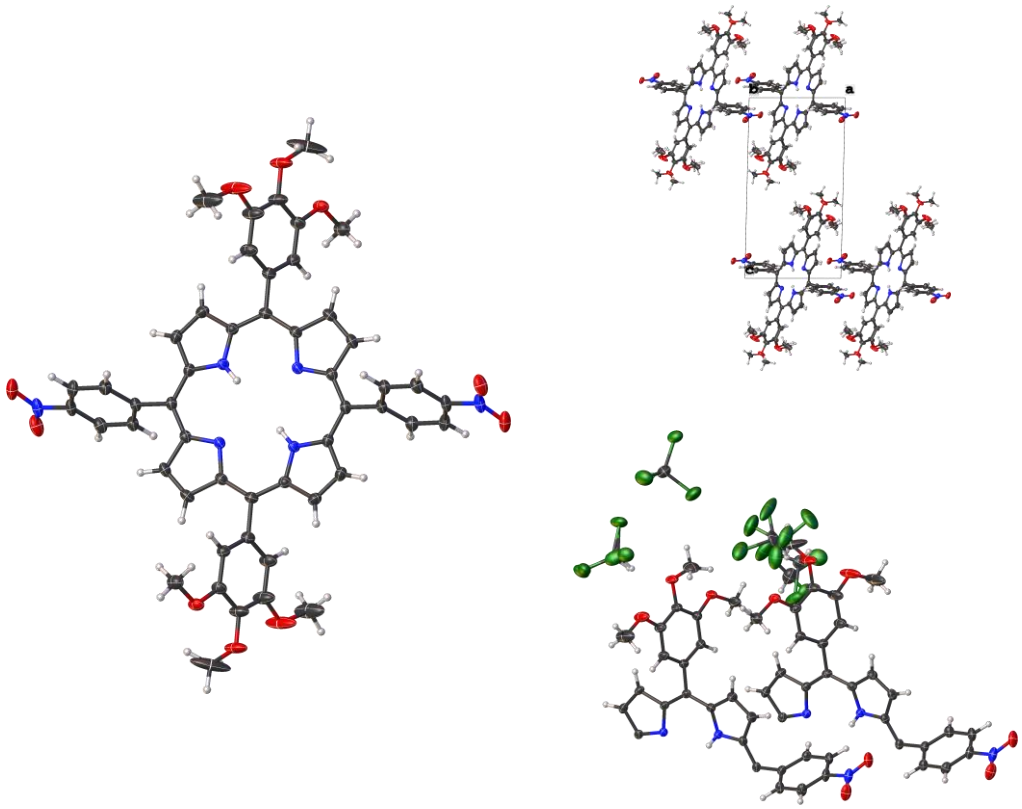

Figure 4.14. Single crystal X-ray structure of **4.76** with; one independent molecule of **4.76** shown (*left*), packing diagram along the (010) plane (*top right*) and the asymmetric unit containing residual $CDCl_3$ (*bottom right*). Images generated in Olex2.[126] Thermal ellipsoids indicate 50% probability. Data collected, solved, and refined by Dr. C. J. Kingsbury.

Again, we sought to further the amount of **4.77** we had generated from the chlorin synthesis and thus metallation of **4.76** with zinc occurred cleanly in 90%.

In the last broadening of the substrate scope, we sought another metalloporphyrin. The use of metals in medicine has recently seen an explosion in drug development,[347] however aside from this we have already discussed the utilization of $[Ru(bipy)_3]^{2+}$ type PSs, and Sn(IV) ethyl etiopurpurin (Rostaporfin) (Section 1.2.3, Scheme 1.8). We drew our inspiration from padeliporfin. Padeliporfin (WST-11) is a semi-synthetic palladium(II) bacteriochlorophyll arising from modifications to BChl *a* (see Figure 1.6, **1.39**) that has been approved for the treatment of adenocarcinoma of the prostate in the EU,[348,349] giving hope to heavy metal containing PSs. Thus, utilizing the same procedure as for **4.77**, **4.78** was yielded in 76% albeit after a longer reaction time (Scheme 4.14).

Whilst the numbers **4.74**–**4.78** have been used throughout to refer to the PS candidates in question, to make the differences in structures more easily evident a

change in nomenclature is necessary. Thus; **4.74** becomes **ZnC^1**, **4.75** becomes **ZnC^2**, **4.75b** becomes **ZnC^2-Br**, **4.76** becomes **H$_2$P**, **4.77** becomes **ZnP** and **4.78** becomes **PdP**.

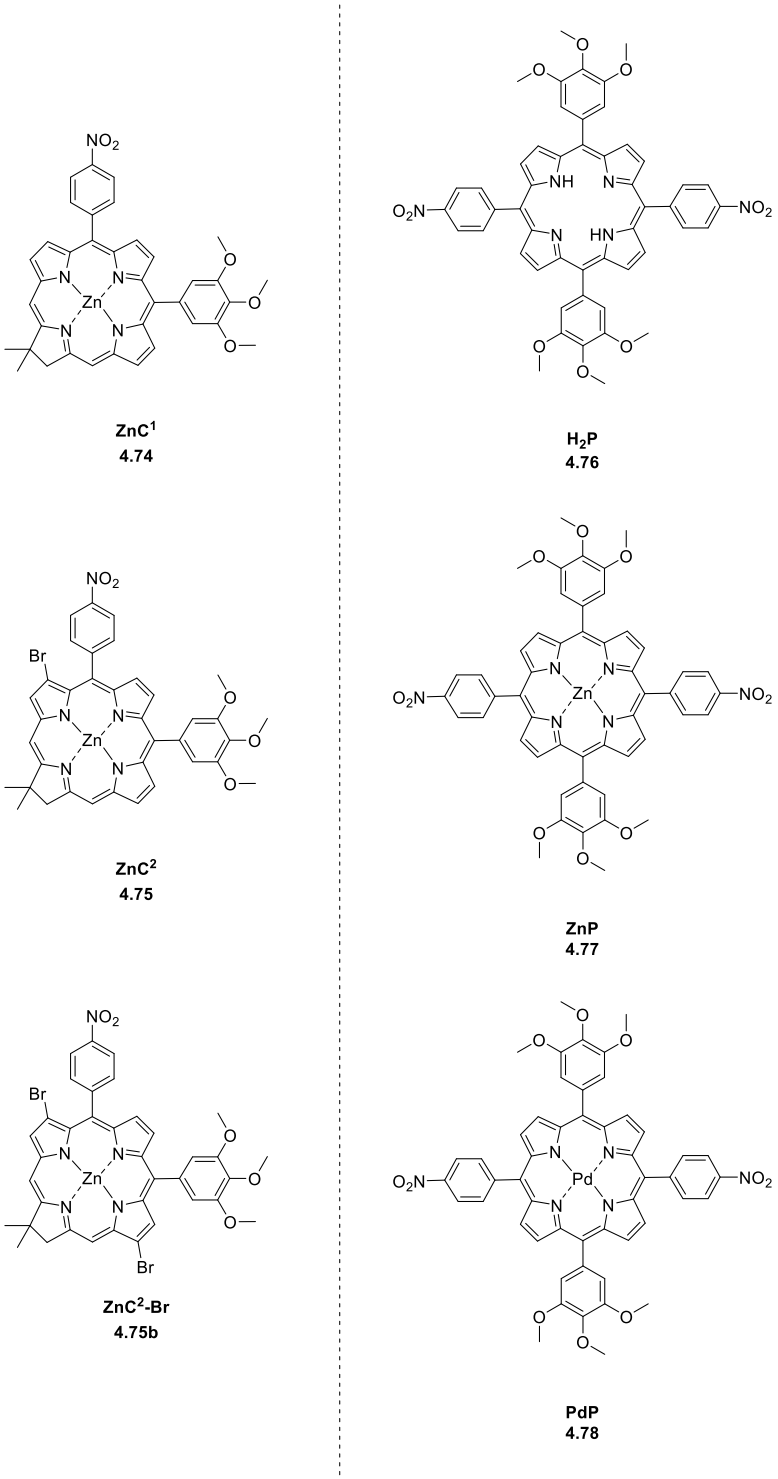

Figure 4.15. Structures of the compounds (chlorins *left* and porphyrins *right*) analyzed throughout the rest of the chapter, with both compound numbers (**4.74**–**4.78**) and abbreviation (**ZnC^1**, **H$_2$P**, etc.) presented for clarity.

4.2.3 Photophysical Analyses of PS Candidates

As noted in Section 1.2.1 (Figures 1.12, 1.13) the differing symmetries present in chlorins and porphyrins (approximate C_{2v} for chlorins verses D_{nh} type for porphyrins) yields vastly different spectral features.

ZnC^1 and **ZnC^2** and **ZnC^2-Br** present typical spectra for the class of tetrapyrrole, when compared with previous examples,[234] however the propensity of 3-bromo and 3,13-dibromochlorins to be used exclusively as intermediates in the synthesis of 3-ethynyl- or other 3-aryl-chlorin type products from [Pd^0]-catalyzed cross coupling reactions, there is significantly less data present in the literature.

Chlorins **ZnC^1**, **ZnC^2** and **ZnC^2-Br** present B-bands of 415 ($\log_{10}\varepsilon$ = 5.30), 418 ($\log_{10}\varepsilon$ = 5.37) and 421 nm ($\log_{10}\varepsilon$ = *n.d.*) with increasing degrees of bromination yielding increasing wavelengths of absorption. Further to this, bands of *c.a.* 10^2 x lower intensity in the range of 500–600 nm, and an intense Q_y absorption at 616 ($\log_{10}\varepsilon$ = 4.70), 618 ($\log_{10}\varepsilon$ = 4.73) and 624 ($\log_{10}\varepsilon$ = *n.d.*) nm respectively (THF) (Figure 4.16). For **ZnC^1** and **ZnC^2**, whilst **ZnC^2** presents the largest extinction coefficient for the Q_y band, it is of a lower intensity when compared with the respective B-bands (0.229 *vs.* 0.251). Whilst the differences are minimal, they do exist. The biggest difference across the spectra evidently being the extension (i.e., a red shift) of the Q_y absorption by 6 nm in the case of **ZnC^2-Br**. **ZnC^2** instead shows a greater fwhm when compared to **ZnC^1**, akin to the properties observed for Ac-appended chlorins (see Table 4.1). Data for the compounds presented herein is presented in Table 4.4, *vide infra*.

ZnC^1 and **ZnC^2** exhibit typical fluorescence spectra (Figure 4.17). In each case, there is a strong $Q_y(0,0)$ fluorescence emission around 620 nm, with a feature that is of a distinctly lower emission intensity present at around 680 nm ($Q_y(1,0)$).

The porphyrins presented herein exhibit vastly different spectra within their own series for a multitude of different reasons. Initially and most obviously there is a comparison between free base and metalloporphyrins. **H$_2$P** exhibits D_{2h} symmetry, and as a result of asymmetry along *x*- and *y*-axes along with vibronic overtones, four Q-bands are yielded. In the cases of **ZnP** and **PdP**, the symmetry of the core is heightened to D_{4h}, i.e., the *x*- and *y*-axes are now equivalent. This yields one Q-band, with the vibronic overtone yielding the second.

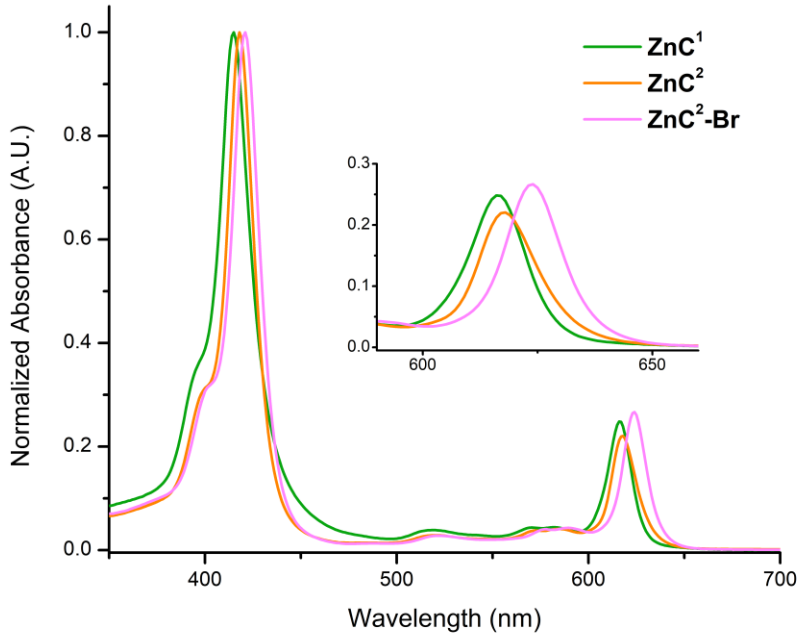

Figure 4.16. Normalized UV-Visible absorption spectra of **ZnC^1**, **ZnC^2** and **ZnC^2-Br** in THF at room temperature.

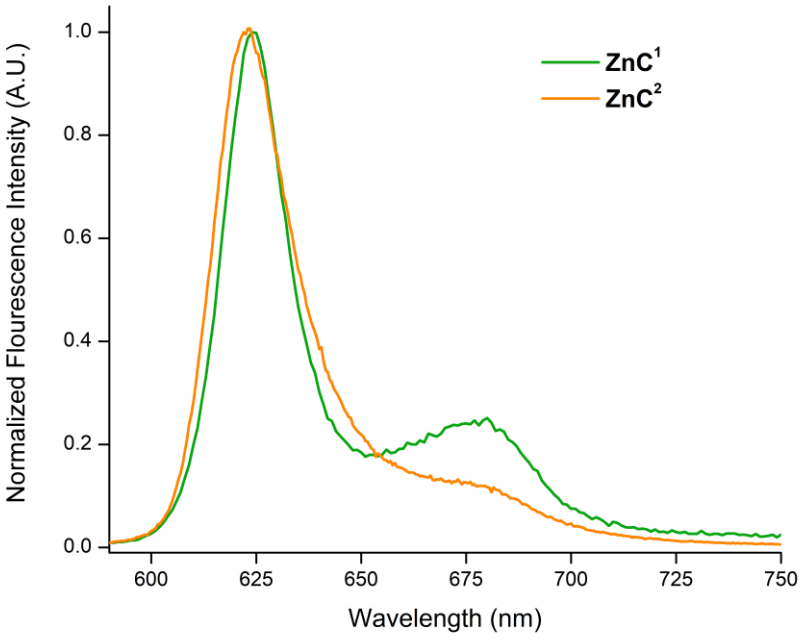

Figure 4.17. Normalized Emission spectra of **ZnC^1** and **ZnC^2** in THF at room temperature. λ_{exc} = 418 nm.

All three porphyrins present typical Soret bands (B_x + B_y) in the 420–430 nm range with expected shifts between the three presented (Figure 4.18). **H_2P** (red, Figure 4.18 exhibits four Q-bands of decreasing intensity in the manner IV > III > II > I, i.e. an *etio*-type spectra. In the cases of **ZnP** and **PdP**, the Q(1,0) band is of greater intensity than the Q(0,0) band. This difference is greatest in **PdP**, where the Q(0,0) is only c.a. 0.18 of the intensity of the Q(1,0) (Inset, Figure 4.18).

In stark contrast to **ZnC^1** and **ZnC^2**, the absorption of longest wavelengths in all three cases (**H_2P**, **ZnP** and **PdP**) is 50–100 times smaller than that of the Soret band. Out of all five PS candidates, **H_2P** presents the longest wavelength of absorption (648 nm).

The fluorescence peaks of these porphyrins are, in general, far broader than those of **ZnC^1** and **ZnC^2** presented in Figure 4.17. For **H_2P**, the features of the emission are far better resolved than in the cases of **ZnP**, with **H_2P** exhibiting two distinct features, one around 650 nm and the other around 720 nm, whereas **ZnP** presents a distinct feature at 620 and a second around 650 nm (Figure 4.19).

Across the series, a variety of Stokes shifts are present from 78 cm^{-1} for **ZnC^2** to 2718 cm^{-1} for **PdP**. All photophysical data is presented in Table 4.4.

The fluorescence quantum yields of the PS candidates were calculated using H_2TPP (**1.46**) as a reference using the following equation:

$$\frac{\emptyset_x}{\emptyset_R} = \frac{(1-10^{-A_R})}{(1-10^{-A_x})} \cdot \left(\frac{{n_x}^2}{{n_R}^2}\right) \cdot \left(\frac{\int I_{PL}(X)}{\int I_{PL}(R)}\right) \ldots\ldots\ldots\ldots \boldsymbol{Eq.\,4.1}$$

where ϕ_x is the quantum yield of the sample, and ϕ_R being the quantum yield of the reference. A_R represents the absorption of the reference compound at the wavelength of excitation, (with the utilization of $1 - 10^{-AR}$ a recommendation made by Würth *et al*.[352]), *n* is the refractive index of the sample, and I_{PL} is the intensity of the photoluminescence. This general form of the equation can be applied to both singlet oxygen quantum yields, and fluorescence quantum yields.

H_2P, **ZnP** both presented definitive fluorescence quantum yields of 0.09 and 0.06 respectively. As a result of the chelation of Zn, in **ZnP**, there is a greater T_1 population, and subsequently lesser S_1 population, resulting in a lessened fluorescence response i.e., lesser $S_0 \leftarrow S_1$ decay, with respect to **H_2P**.

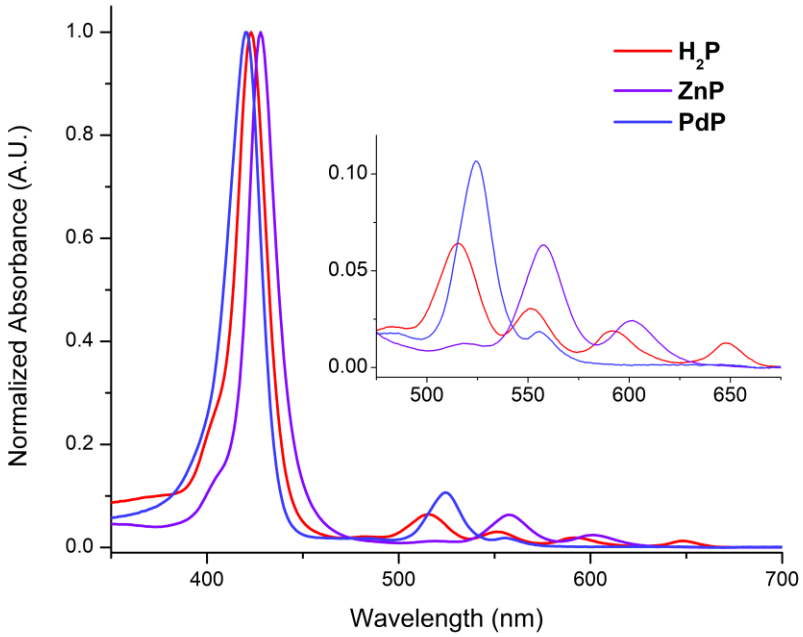

Figure 4.18. Normalized UV-Visible absorption spectra of **H_2P**, **ZnP**, and **PdP** in THF at room temperature.

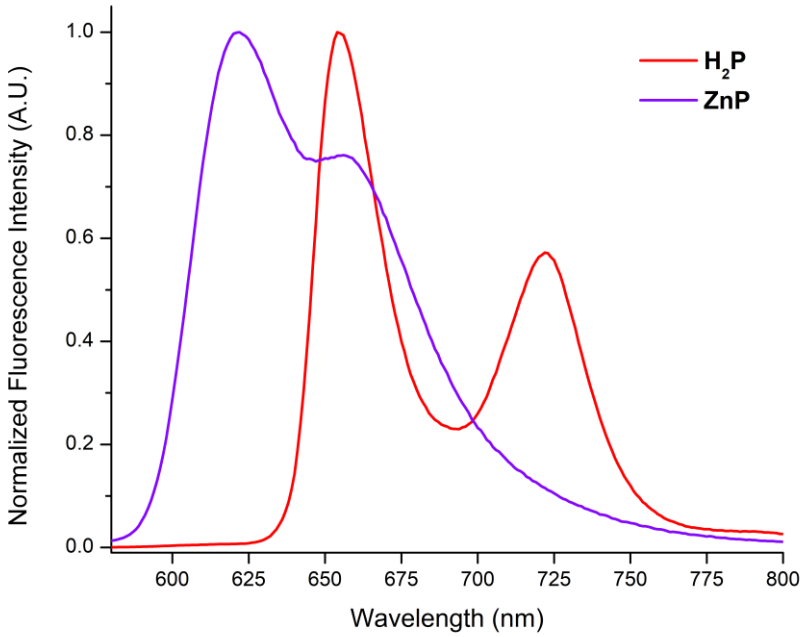

Figure 4.19. Normalized emission spectra of **H_2P** and **ZnP** in THF at room temperature, λ_{exc} = 418 nm. Regarding the omission of **PdP**, see text.

Table 4.4. Tabulated photophysical data for PS candidates; **H_2P**, **ZnP**, **PdP**, **ZnC^1** and **ZnC^2**. [*a*] The intensity of the longest wavelength Q-band divided by the intensity of the Soret band; [*b*] The Stokes shift was calculated from the corresponding UV/Vis absorption and emission spectra in THF; [*c*] Measurements were performed by exciting the tetrapyrrole at λ_{exc} = 424 nm with H_2TPP in toluene (Φ_F = 0.07) used as a reference;[335] [*d*] Measurements were performed by exciting the compounds at λ_{exc} = 418 nm with phenalenone in DMSO used as reference.[336] [*e*] **ZnC^1** and **ZnC^2** were excited at λ_{exc} = 418 nm in THF. Typical errors for the presented values are: (percentage of value) Φ_F ± 10%, Φ_Δ ± 10%.

Tetrapyrrole	*λ_B (nm) [$log_{10}(\varepsilon_B)$]*	*λ_Q (nm) [$log_{10}(\varepsilon_Q)$]*				*I_Q/I_B[a]*	*λ_{EM} (nm)[e]*	*Stokes Shift (cm^{-1})[b]*	*Φ_f[c]*	*Φ_Δ/Φ_R [d]*	*Correction Factor See text*
4.74 / ZnC^1	415 [5.30]	518 [3.89]	571 [3.94]	582 [3.95]	616 [4.70]	0.25	624, 680	208	*n.d.*	0.005	0.74
4.75 / ZnC^2	418 [5.37]	520 [3.84]	574 [3.98]	585 [4.02]	618 [4.73]	0.22	622, 676	78	*n.d.*	*n.d.*	0.70
4.75b / ZnC^2-Br	421 [*n.d.*]	522 [*n.d.*]	578 [*n.d.*]	589 [*n.d.*]	624 [*n.d.*]	0.27	*n.d.*	*n.d.*	*n.d.*	*n.d.*	*n.d.*
4.76 / H_2P	423 [5.75]	515 [4.56]	551 [4.23]	592 [4.03]	648 [3.85]	0.01	655, 722	165	0.09	0.85	0.58
4.77 / ZnP	428 [5.81]	558 [4.61]		602 [4.19]		0.02	620, 656	482	0.06	0.16	0.38
4.78 / PdP	420 [5.59]	524 [4.61]		556 [3.86]		0.02	655, 721	2718	0.00	*See text*	0.70

Whilst **PdP** was found to produce a numerical fluorescence quantum yield of <0.0005 (repeated in triplicate) in this instance, given that the emission is of such a low intensity it is not a surprise that most publications refer to Pd-porphyrins as non-fluorescent.[353] The utilization of metals (or other heavy atoms) does enhance intersystem crossing, enabling greater T_1 population, but this method does also enhance recombination to the singlet state via Spin-Orbit Coupling (SOC).[354,355,356] To *et al.* propose that relaxation of a photogenerated S_1 state to the S_0 in Pd-porphyrins *via* radiative decay may be fast enough to compete with intersystem crossing, thus yielding fluorescence.[357]

Initial attempts at measuring singlet oxygen quantum yields using direct luminescence of $^1O_2$ were performed in THF, akin to simple absorption and emission measurements, with phenalenone (**4.79**) used as a reference.[351] Phenalenone has previously been described as a "universal reference compound" and thus seemed the ideal candidate, with ϕ_Δ = 0.96 ± 0.02.[351] Initial values of SOQY typically exceeded 1, which is not possible. Upon comparison of the absorption spectra of the solutions of phenalenone in THF pre- and post-irradiation there were drastic changes in the spectra.

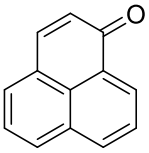

4.79

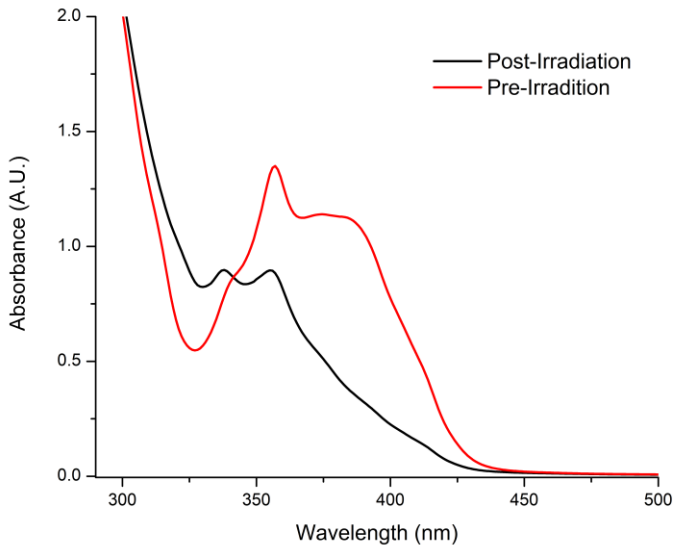

Figure 4.20. Structure of phenalenone (**4.79**, *left*) and spectra of the solution of **4.79** in THF used to determine singlet oxygen quantum yields both pre- and post-irradiation (*right*).

Figure 4.20 displays the differing spectra pre- and post-irradiation. In red, the expected spectrum of phenalenone, defined by $S_0 \rightarrow S_3$, $\pi \rightarrow \pi^*$ transition at *ca.* 355 nm, along with the broad band of the $S_0 \rightarrow S_2$, $\pi \rightarrow \pi^*$ transition present at 350–400 nm.[358,359,360] In stark contrast, the black trace shows two absorption bands of equal intensity, an entirely different spectrum to that presented initially. Evidently, there is an incompatibility in this system, i.e., utilizing phenalenone in THF for the determination of SOQY.

Following on from this, we considered other options. Given the knowledge of the solubility of all PS candidates in DMSO, we pondered as to whether this would be a suitable system.

The measurement of $^1O_2$ falls into two separate categories: direct and indirect. Direct methods utilize the luminescence of $^1O_2$ at *c.a.* 1270 nm to measure quantum yields. The latter requires a chemical trap, i.e., something that reacts with $^1O_2$ which results in a spectrophotometric change, or a change in another measurable variable.

In 2019, Lutkus et al.,[361] measured the pressure change in a sealed system to calculate the singlet oxygen quantum yields of certain singlet sensitizers in DMSO. They were able to do this because DMSO can be oxidized by $^1O_2$ to dimethyl sulfone, and through oxygen consumption a decrease in pressure was observed. This thus makes DMSO the $^1O_2$ trap. This is the only example of $^1O_2$ measurements utilizing a method of this kind, and it appears not to have influenced the utilization of DMSO in SOQY measurements across the literature.

Despite this, we proceeded to generate values of SOQY in DMSO. Given that DMSO consumes some of the $^1O_2$, according to Lutkus,[361] the values presented herein therefore underrepresent the capacity of the PS candidates to generate $^1O_2$.

Interestingly, **ZnC^1** was found to produce minimal $^1O_2$, to almost a negligible amount. The *gem*-dimethyl chlorin system has rarely been characterized with regards to it SOQY, however in Chapter 3, it was illustrated that 10-aryl substituted Zn-chlorins **3.36a** and **3.36b** both exhibited $\phi_\Delta > 0.80$ in EtOH. **ZnC^1** and **ZnC^2** however both possess a 5-aryl group as well, and in both cases, there are far more rotational and vibrational means of decay plausible than in **3.36a** and **3.36b** (NO_2 and OCH_3 rotations).

The SOQY values obtained for **H_2P** and **ZnP** were typical for the compound class presented and can be rationalized in the same manner to that performed for the discussion of fluorescence quantum yield.

In stark contrast to the simplistic evaluation of **H_2P** and **ZnP**, **PdP** presented a wholly unexpected result. Irradiation at a dilute solution of **PdP** in DMSO ($A(\lambda_{EXC}) \approx 0.3$, with $\lambda_{EXC} = 424$ nm), two peaks were presented the range being examined of 1240–1340 nm., the raw data for which is presented in Figure 4.21. The traces have been normalized to enhance visualization of this new peak.

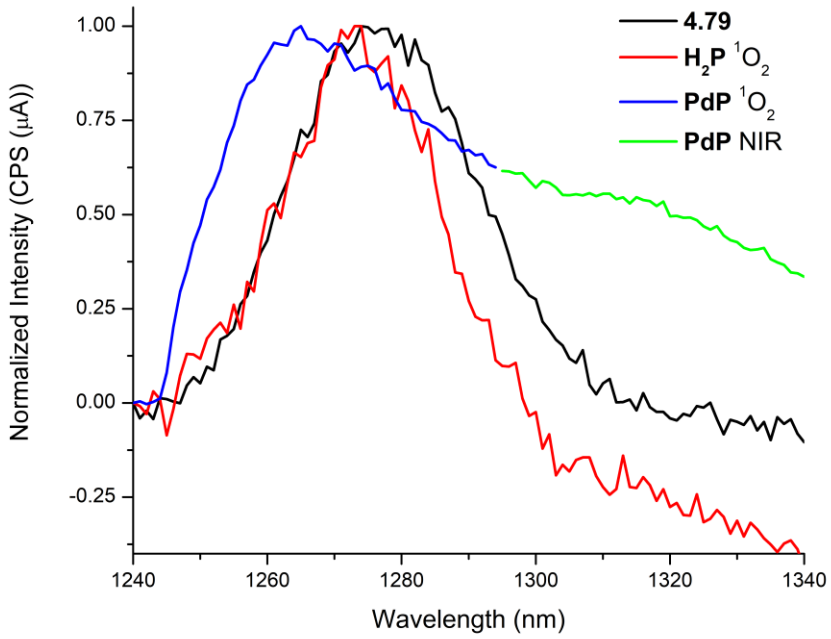

Figure 4.21. Trace of $^1O_2$ luminescence as produced by **4.79** (*black*), **H_2P** (*red*), and separated traces for $^1O_2$ evolution by **PdP** (*blue*) and unidentifiable NIR emission (*green*). Data was normalized against the peak of highest intensity, and the datapoint at 1240 nm was taken to be a baseline in every case.

The trace in black represents the $^1O_2$ luminescence, as produced by **4.79**, with an intense peak centered around *c.a.* 1274 nm, i.e., an expected spectrum. The trace in red represents the $^1O_2$ luminescence as produced by **H_2P**, again a typical peak albeit narrower, but once again centered around *c.a.* 1274 nm. The traces in blue and green are those from experimentation on **PdP**. In blue, i.e., from 1240–1298 nm, we have a trace that could be attributed to $^1O_2$, albeit exhibiting a distinct hypsochromic shift of 9 nm. The latter half of this trace, in green, appears

reminiscent of a shoulder or a second lesser intense peak which appears to have a maxima at *c.a.* 1310 nm.

The NIR emission observed is peculiar given that as noted previously, Pd-porphyrins are deemed non-fluorescent. The field of NIR emission has grown extensively in recent years with a wide variety of compounds being studied for this particular property.[362] Both tetrapyrrole based pigments,[363] and metal complexes have been studied in particular.[364] However, the emission present at *c.a.* 1310 nm in Figure 4.21 appears to coincide with little else. It appears that the system applied herein thus presents an incompatibility in the SOQY evaluation of **PdP**. Otherwise, given the length of this wavelength of emission, it is highly unlikely that a singular intramolecular fusion would yield such a response.

Whilst we were able to generate data for some of the PS candidates, we are actively seeking a system for the direct detection of $^1O_2$ which works for all PS candidates presented.

4.2.4 In Vitro Analyses of PS Candidates

In vitro analyses of the five PS candidates were carried out on the 4T1 cell line. The 4T1 cells are epithelial, i.e., lining outer surfaces of organs and blood vessels throughout the body. The growth and metastatic spread of this cell line in BALB/c mice replicates stage IV human breast cancer.[365] In particular, the 4T1 cell line represents a triple negative cancer type, i.e., a cancer that is estrogen receptor-negative, progesterone receptor-negative, and HER2-negative.[366,367,368] Further to this, this cell line is also resistant to 6-thioguanine,[369] a common leukemia chemotherapeutic. All of this suffice to say it is difficult to treat.

Given the lack of water solubility present in the PS candidates presented herein, stock solutions were made in DMSO. All stocks were generated using biological grade DMSO and passed through 0.22 μm filters for two reasons: to ensure the stocks remained sterile, but also to ensure no large aggregates were present in these stocks. Prior to administration of the PS to cells, the concentration of the stocks was accurately determined via UV-Visible spectroscopy. Despite the differing solvents, in the cases presented herein the minimal DMSO content was assumed to have no effect on the absorption coefficients nor presented any solvatochromism, i.e., *v*(DMSO) ≈ 1/300 *v*(DMSO/THF).

Throughout the series, a vast range of concentrations were observed: **ZnC^{1}** and **ZnC^{2}** both yielded stock solutions of suitable concentrations of 12.93 and 3.28 mM, respectively, along with **ZnP** which yielded a concentration of 3.33 mM. **H$_2$P** and **PdP** both yielded lower concentrations of 0.14 and 0.22 mM respectively, i.e., a 10^2 range over the series. Whilst otherwise a nuanced observation, the concentrations of the stocks presented determine the maximum concentration of PS that can be analyzed before DMSO mediated cytotoxicity is present in the *in vitro* experiments. Thus, **H$_2$P** could only be tested until [**H$_2$P**] = 2.8 μM, whereas **ZnC^{1}** could be tested until [**ZnC^{1}**] = 258 μM.

Presented in Figure 4.22 are the results from the dark toxicity assays undertaken. **ZnP** (Figure 4.22, *top*) presents the best dark toxicity profile from those presented in the top panel, with minimal cytotoxicity even at 50 μM. In contrast, both **ZnC^{1}** and **ZnC^{2}** both exhibit stark dark toxicity after 3 μM, with less than 20% cell viability for **ZnC^{1}** at 50 μM, and c.a. 30% cell viability for **ZnC^{2}** at the same concentration. Whilst

alarming at first glance, these values are well outside the ideal phototherapeutic range and subsequently present minimal concern.

Given the lower concentration of stocks for **H_2P** and **PdP**, these PSs were analyzed over a much smaller window of concentrations, more akin to a phototherapeutic concentration. Both **H_2P** and **PdP** exhibit minimal dark toxicity, even at the highest concentration analyzed [**H_2P**,**PdP**] = 2.5 μM.

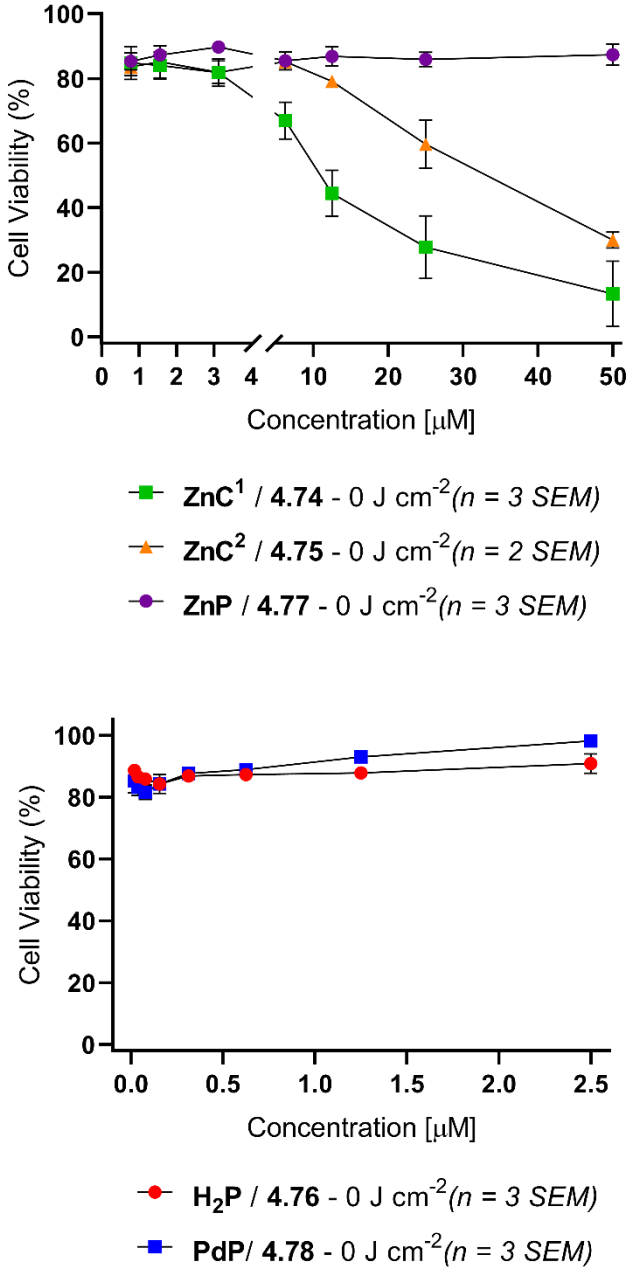

Figure 4.22. Dark toxicity assays performed on the 4T1 cell line using the five PS candidates presented herein **ZnC^1**, **ZnC^2**, **H_2P**, **ZnP**, and **PdP**. Data is presented as the mean ± SEM of three independent experiments. Incubation time across all experiments was 24 h.

No PS analyzed yielded a cell viability of 100% when normalized against non-treated cells. This is due to the experiment requiring the minimal light exposure possible throughout the experiment.

Interestingly, all porphyrins analyzed were non-toxic in the concentration ranges analyzed, whereas the chlorins analyzed were cytotoxic at elevated concentrations. Both chlorins **ZnC^{1}** and **ZnC^{2}** are more polar molecules than the porphyrins presented, except perhaps **ZnP**, as evidenced by the concentrations of stock solutions generated. However, given the differing responses between **ZnP** and **ZnC$^{1/2}$** we can rationalize this difference in terms of photophysical properties of the PSs. Whilst the cells were exposed to the minimum amount of light necessary, **ZnC$^{1/2}$** have a strong absorption at > 615 nm, at a longer wavelength and significantly more intense than the absorption of **ZnP**. It is likely that that minimal amount of light the experiment was exposed to activate enough PS at high concentrations to yield the exhibited phototoxicity, in the dark toxicity experiment.

Given that minimal cytotoxicity was observed until ca. 3.125 μM, a suitable concentration range for analysis of phototoxicity was determined to be 0 – 2 μM. All cells were irradiated at 415 nm. Whilst the goal of the thesis herein is to utilize the *gem*-dimethyl-chlorin scaffold for PDT (thus, absorption at a longer wavelength, deeper penetration of light and more successful treatment), for the sake of *in vitro* analyses, in which the depth of tumor is much smaller than in the real world, irradiation at the B-bands is the most viable option given that the PS is still becoming activated. This being said, the B and Soret bands of the PS candidates presented are not all the same. To rationalize this issue, and give all PSs the same light dose, correction factors were applied to each of the PSs.[370]

The key point in the utilization of correction factors is that it is more appropriate to utilize the number of photons absorbed to assess the actual light dose given to the system, and that this can only be truly understood when the spectral overlap between the light source and PS candidate is considered, a principal which was only recently been highlighted by F. Schaberle.[370]

As noted by Beer-Lambert, the intensity of absorbed light by a homogenous solution capable of absorbing light can be described through Equation 4.2, where the intensity of light absorbed (I_{abs}) at a wavenumber of v cm^{-1} is equal to the product of

the initial light intensity (I_0) at the same wavenumber and $1\text{-}10^{-A(\nu)}$, all of which are dependent on the frequency of the light.

$$I_{abs}(\nu) = I_o(\nu)\left(1 - 10^{-A(\nu)}\right) \ldots\ldots\ldots\ldots\ldots \boldsymbol{Eq.4.2}$$

In an experimental setting, when light sources are used their outputs are typically measured in energy type units; be it Watts (W) or Joules per second (J s^{-1}). It is possible to relate the initial intensity of the light using equation 4.3.

$$I_o(\nu) = \frac{P(\nu)}{h\nu} \ldots\ldots\ldots\ldots \boldsymbol{Eq.4.3}$$

In which h is Planck's constant, and P(ν) is the power of the light source at a given wavenumber. Thus then, the number of photons (N_{ph}) is the summation of wavelengths over a given time period and can be generated through the combination of Equations 4.2 and 4.3 and is given in Equation 4.4.

$$N_{ph} = \Delta t \sum \frac{P(\upsilon)}{h\upsilon}(1 - 10^{-A(\upsilon)}) \ldots\ldots\ldots\ldots \boldsymbol{Eq.4.4}$$

The ideal number of photons absorbed are considered by assuming all light power (P_r) is emitted at a single wavenumber ν_r at the maximum absorption of the PS candidate (A_r). Thus then, the light dose correction factor (LDC) is defined as the ration of photons absorbed to the ideal number of photons (Equation 4.5):

$$LDC = \frac{N_{ph}}{N_{ph}^{r}} = \frac{\Delta t \sum \frac{P(\tilde{\upsilon})}{\tilde{\upsilon} hc}(1 - 10^{-A(\tilde{\upsilon})})}{\Delta t \frac{P_r}{\tilde{\upsilon_r} hc}(1 - 10^{-A_r})} \ldots\ldots\ldots\ldots \boldsymbol{Eq.4.5}$$

Whilst Equation 4.4 describes the calculation for the number of photons, it is not considering the absorption of the PS candidate. Figure 4.23 shows emission spectra of the 415 nm LED used, and the absorption of **H_2P**. The region in which that LED emits light that **H_2P** can absorb is the overlap between the two graphs (*hatched, dark grey, middle*). Integration of this area yields the correction factor for **H_2P**. This process was applied to all PS candidates and LDCs were observed from 0.38 for **ZnP** to 0.74 for **ZnC^1**, through the shifting of the Soret and B-bands of the respective PSs.

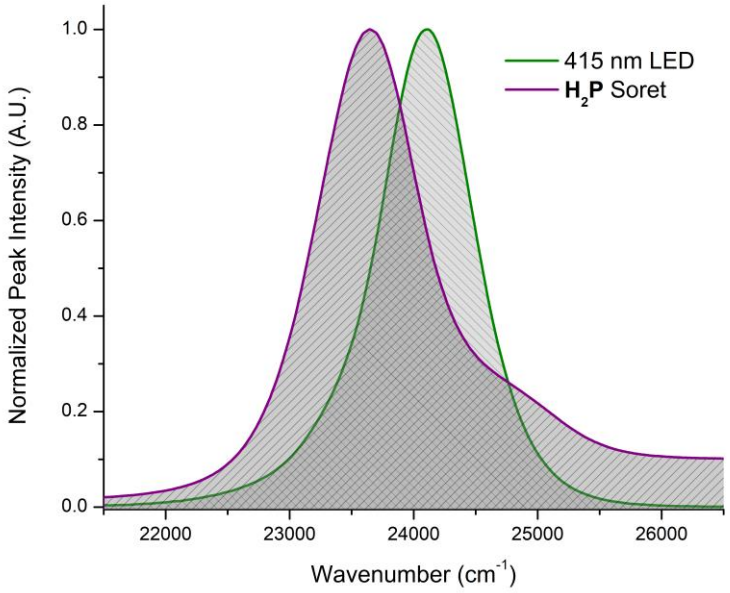

Figure 4.23. Spectral overlap between the light source used for phototoxicity assays and **H_2P**. Determination of correction factor has been represented with **H_2P** as an example.

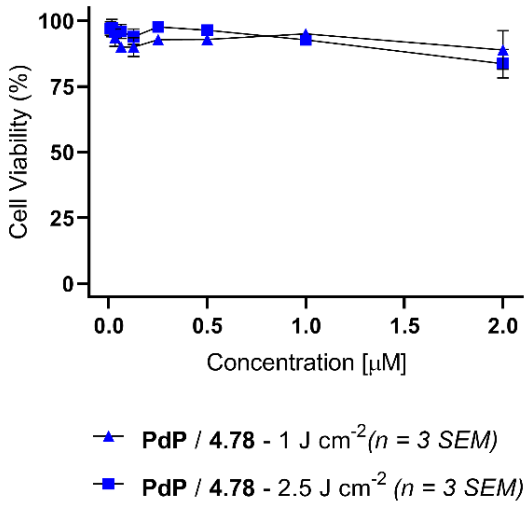

Figure 4.24. Phototoxicity assays performed on **PdP** at 1 and 2.5 J cm^{-2}. Experiments were performed in triplicates. Data is presented as the mean ± SEM of three independent experiments. Incubation time across all experiments was 24 h.

For the phototoxicity assays, initial experiments were performed at a light dose of 1 J cm^{-2}, followed by experiments conducted at 2.5 J cm^{-2}, i.e., relatively low light doses.

Interestingly, **PdP** exhibited a phototoxicity profile akin to its dark toxicity profile, i.e., it exhibited little to no toxicity. Even more peculiar still, there was no significant difference between the 1 J cm^{-2} and 2.5 J cm^{-2} experiments (Figure 4.24). Whilst

the minimal dark toxicity of **PdP** was promising, albeit over a minimal concentration range, the marked absence of phototoxicity at either light dose warrants the ceasing of investigation into the use of **PdP** as PS for PDT. This phototoxicity profile may be indicative of a lack of internalization of the PS. However, given the lack of fluorescence of **PdP** this could not be investigated either via flow cytometry (*vide infra*) or by measuring PS-associated fluorescence on cell lysates.

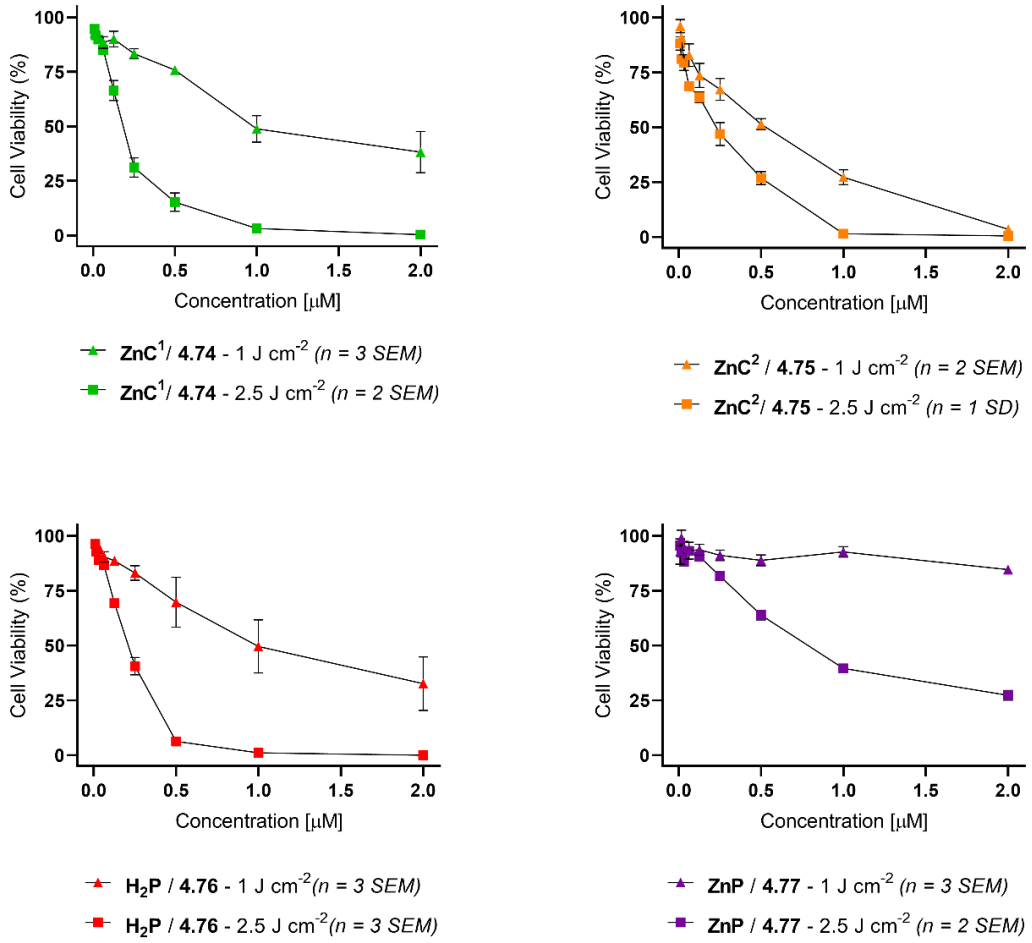

Figure 4.25. Phototoxicity assays performed on 4T1 cells using **ZnC^1**, **ZnC^2**, **H$_2$P** and **ZnP** at 1 and 2.5 J cm^{-2}. Experiments were performed in triplicates. Data is presented as the mean ± SEM of three (or less where applicable) independent experiments. Incubation time across all experiments was 24 h.

Of the remaining four PS candidates, three are successful in achieving near complete cell death (Figure 4.25). **ZnP** was found to only yield c.a. 27% cell viability at 2 μM and 2.5 J cm^{-2}. In contrast, all other PS candidates yielded < 1% cell viability at the same concentration and light dose.

From the phototoxicity assays presented, we are only able to calculate IC_{50} values for **H_2P**, **ZnC[1]** and **ZnC[2]** at 2.5 J cm^{-2}. To be able to calculate an accurate IC_{50} value, there must be a data point exhibiting complete cell death. Given that at no light dose examined did **ZnP** exhibit complete cell death, no IC_{50} can be calculated. Likewise for all other PS candidates at 1 J cm^{-2}, complete cell death was not present at any concentration analyzed. IC_{50} values were calculated from a graph of $\log_{10}$[**PS**] vs. normalized response, with a variable gradient least squares fit. **ZnC[1]** exhibited the lowest IC_{50} of all with 185 nM, followed in close second by **H_2P** with an IC_{50} = 197 nM. From the limited data currently present, **ZnC[2]** yielded an IC_{50} of 231 nM.

These results were unexpected considering that **ZnP** display the highest ϕ_Δ while **ZnC[1]** was very inefficient in producing singlet oxygen. We investigated whether this poor activity was due to a lack of internalization of the PS. For this we utilized flow cytometry. Cells were incubated with [**PS**] = 2 μM, a concentration at which no PS presented dark toxicity, and incubated for 24 h prior to fixing with paraformaldehyde and monitoring the flow cytometric response. We rationalized that given the structural similarity between **ZnC[1]** and **ZnC[2]**, a differing uptake profile was highly unlikely and whilst uptake may be found to differ, any difference found would be insignificant and within the realms of experimental error.

All PS candidates analyzed produced a typical profile of a maximum uptake at 24 h. Of the three analyzed, **H_2P** presented the best uptake, whereas **ZnP** produced the worst, which correlated with the presented phototoxicity profiles. Whereas of the three, **ZnP** had the better solubility in DMSO, **H_2P** presents the better uptake than **ZnP**. Further to this, **H_2P** has a larger uptake than **ZnC[1]**. Whilst **H_2P** does present a higher fluorescence quantum yield (ϕ_f (**H_2P**) = 0.09 as opposed to ϕ_f (**ZnP**) = 0.06) it alone does not rationalize a 10-fold decrease in uptake.

Noted in the syntheses of **H_2P** and **ZnP** was a distinct drop in polarity upon metallation of **H_2P**, as noted by TLC. Despite this, both **H_2P** and **ZnP** have the ability to form solvating hydrogen-bonds i.e., through the methoxy and nitro-aryl motifs. However, the difference between the two lies in the core of these porphyrins – with **H_2P** being able to form H-bonds through the rotated *A* and *C* rings as noted in **Figure 4.14**, whereas **ZnP** is able to form Zn…OR'R''/OH_2 type interactions which can aid in solvation.

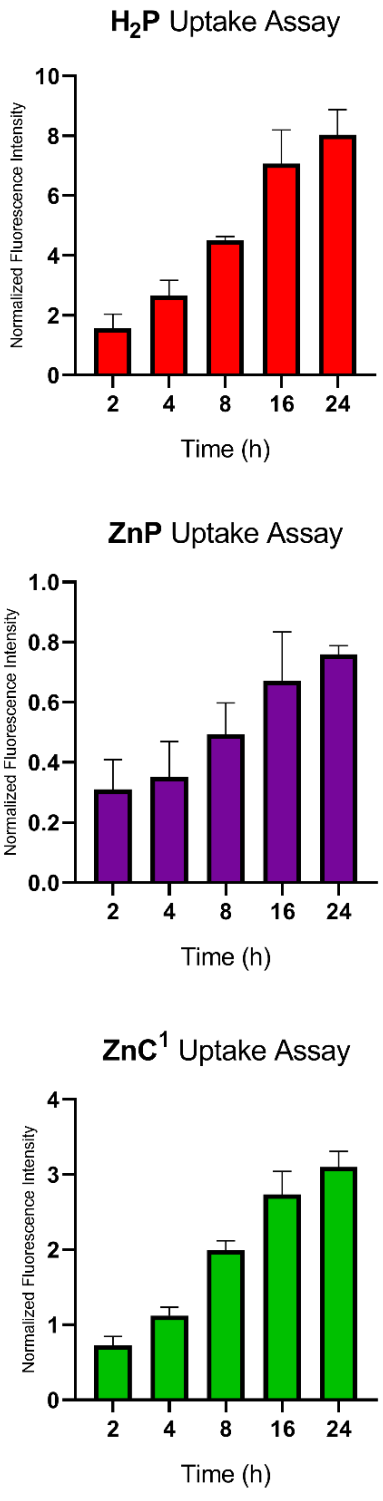

Figure 4.26. Uptake assays performed on **H_2P** (*top, red*), **ZnP** (*middle, purple*), and **ZnC^1** (*green, bottom*). Fluorescence data was measured *via* flow cytometry. [**PS**] = 2 μM in all cases. Fluorescence measurements were normalized against the auto-fluorescence in the control cells and each individual time point. In all cases, PS candidates were excited at 405 nm. For **ZnC^1**, detection was using the VL4 filter (615/24 nm). For **H_2P** and **ZnP**, detection was using the VL5 filter (675/30 nm). For ZnP Data is presented as the mean ± SEM of three independent experiments.

These core interactions may be of some importance, particularly upon the comparison of **ZnP** and **ZnC^1**. Whilst looking at Figure 4.26, it appears plausible to suggest that **ZnC^1** shows an uptake four-fold that of **ZnP**, the differing quantum yields for the compounds render this comparison ineffective. For a truer comparison of uptake, further experiments would be required in the form of cell lysis. Generation of a calibration curve would be a more suitable approach to be able to directly compare the uptake of these PS candidates.

Whilst these two PSs exhibit highly similar cores, the peripheral substitution differs drastically. **ZnC^1** and analogous structures have been shown to exhibit hydrogen-deuterium exchange at the meso-positions, indicating protons ideally suited to forming hydrogen-bonds through distinct electron deficiency. This is a process that **ZnP** evidently cannot exploit.[371]

Following on from this, we wanted to further understand the photochemical processes these PSs were undergoing upon irradiation. This is possible through the use of certain photo-responsive probes. The two we chose to utilize were APF (**4.79**, aminophenyl fluorescein, Scheme 4.15, *top*) and DHE (**4.81**, dihydroethidium, Scheme 4.15, *bottom*).

Whilst we are aware of the limited production of $^1O_2$ by **ZnC^1**, and much greater production of $^1O_2$ by **H$_2$P**, we had no evidence of any Type I photochemistry. It is precisely because of this lack of $^1O_2$ generation from **ZnC^1** we rationalized that it may exhibit a greater Type I photochemical response.

Upon exposure of the non-fluorescent **4.79** to hydroxyl radicals, the amino-phenyl residue is cleaved to yield a fluorescein (**4.80**) whose fluorescence is easily detected. Dihydroethidium **4.81** is instead oxidized by superoxide radical anions to yield the specific oxidation product, **4.82**.[372] Likewise, this also has a distinct, and measurable fluorescence. We analyzed the two most cytotoxic candidates, **H$_2$P** and **ZnC^1** at a series of concentration 0.125 – 1.00 μM at a range of light doses, from 0 – 2.5 J cm^{-2}.

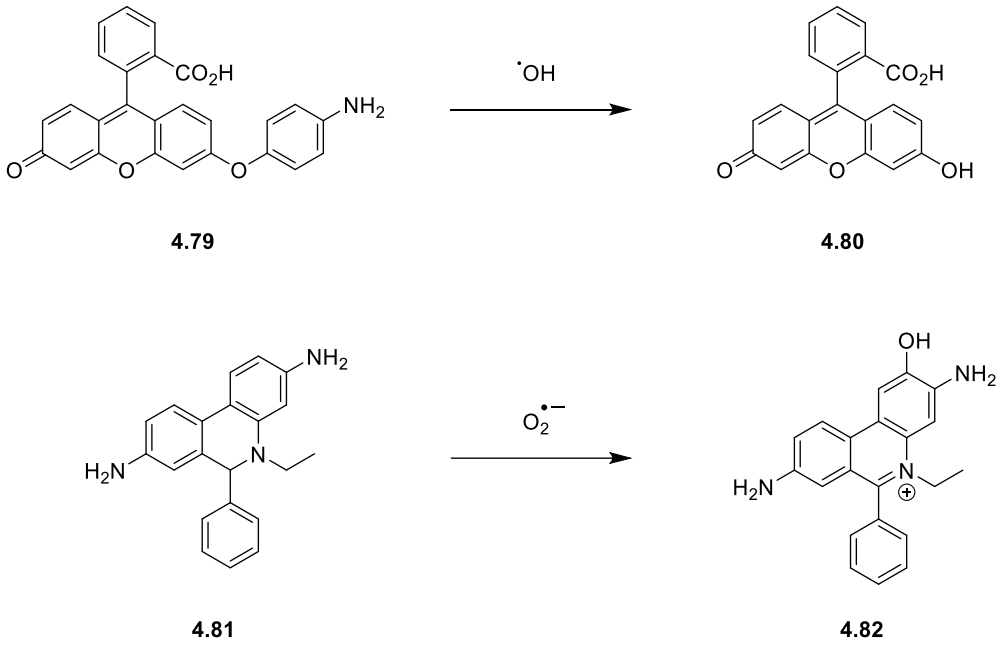

Scheme 4.15. Transformation of probes APF (**4.79**, *top*) and DHE (**4.81**, *bottom*) upon interaction with either hydroxyl radicals, or superoxide radical anions, respectively.

H_2P shows an APF response that increases with both light dose, and concentration of **H_2P**. In contrast, **ZnC[1]** appears to show no APF response with increase in light dose, and instead only a response with a decrease in concentration. The detection of the fluorescence of **4.80** was done at 530 nm, which is only just exceeding an absorption band of **ZnC[1]** at 518 nm (THF). Thus, it is proposed that the emission from **4.80** is being absorbed by **ZnC[1]**, and most likely emitted as fluorescence at a wavelength that was not being detected. This would explain the apparent increase in emission intensity, i.e., if less **ZnC[1]** is present, less of the fluorescence form **4.80** can be absorbed, and subsequently more can be detected. Whilst this exhibits a distinct incompatibility between **ZnC[1]** (and more generally chlorins) with fluorescin based sensors, it provides an excellent case for chlorin-fluorescin energy transfer dyads.

Both **H_2P** and **ZnC[1]** exhibited suitable DHE responses. **H_2P** showed an excellent response with easily visible increases in response with increased concentration of **H_2P** and light dose. Such was the response of DHE to **H_2P** at 1 μM that from 1 J cm^{-2} onwards that **4.82** was self-quenching. This self-quenching is observed as a loss of linearity (Figure 4.27, *top left, trace with up-right triangles*)

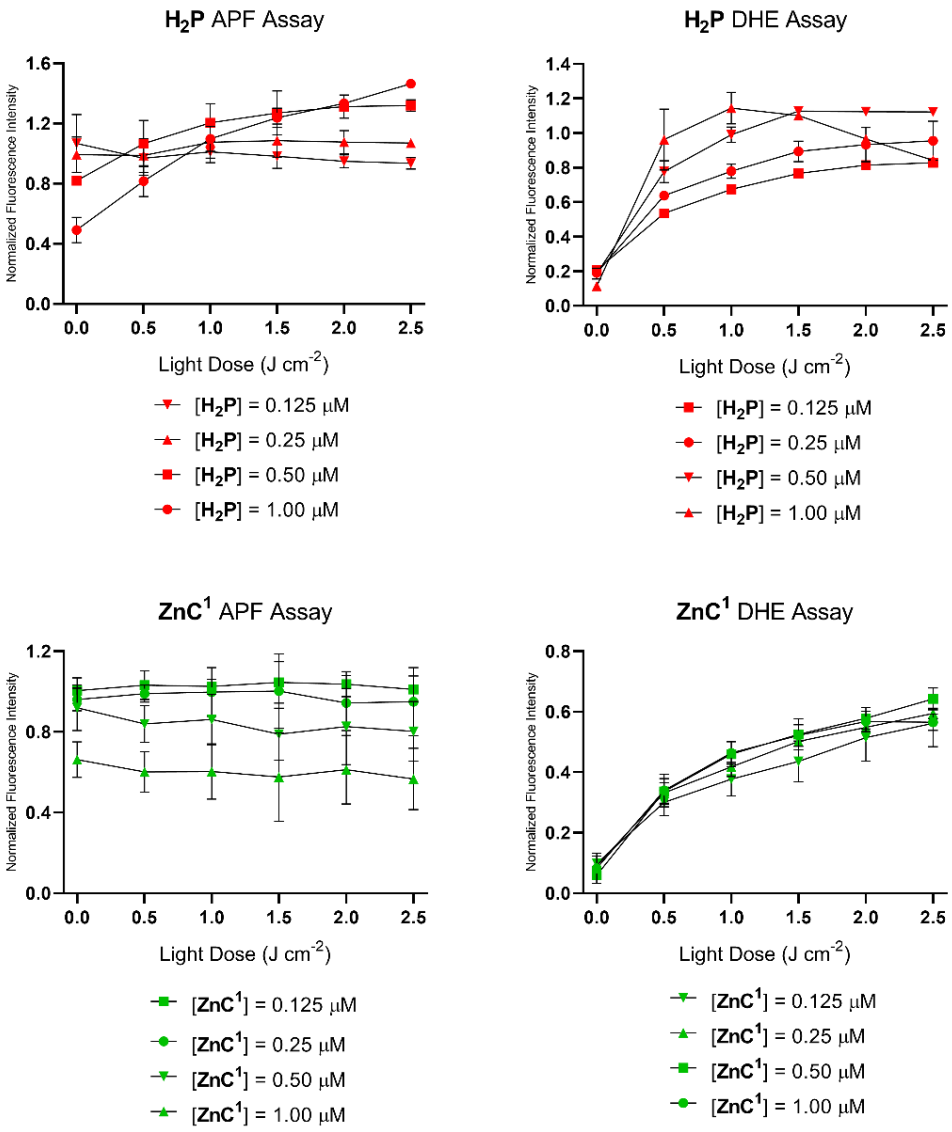

Figure 4.27. Analysis of ROS generation via the use of APF and DHE probes. Data is presented as the mean ± SEM of two independent experiments.

The fluorescence response from **4.82** is detected at 590 nm, just between two absorption bands of **ZnC^1**. Thus, positive responses were observed between response from **4.82** vs. concentration of **ZnC^1** and vs. light dose. Interestingly there was minimal difference in response between concentration. This is indicative of highly efficient production of $O_2^{\bullet-}$ by **ZnC^1**.

We attempted to utilize SOSG (singlet oxygen sensor green); however, upon analysis of the raw data it became evident that the probe had degraded, and the subsequent data was redundant. Further to this, as noted for APF, as a fluorescein-based sensor, the data generated for **ZnC^1** would've been redundant.

4.3 Are any of these PS candidates viable?

The discussion of viability of these PS candidates will discussed by subject in the order they were initially presented.

The syntheses of **ZnC^1** and **ZnC^2** are realistically far too lengthy for these molecules to be utilized outside of academic research. We are continually striving to make PDT a mainstream cancer therapy, and this is not a possibility with **ZnC^1** and **ZnC^2**. They require the synthesis of two halves: **4.52** (the last isolable and stable eastern half intermediate) and **4.63** (the penultimate intermediate in the western half, that is the most suitable for long term storage).

Eastern half **4.52** required the synthesis of thioester **4.55** to be isolated in a suitable yield. Even with the minimal chromatographic purifications utilized in the synthesis of **4.52**, there is substantial chromatography required in the synthesis of **4.63**. Whilst the procedures for the synthesis of **4.43** and **4.76** have been continually refined, both require chromatographic purifications. Aside from this these intermediates have been synthesized on suitable scale.[288] Whilst that is the case, to date there has not been an example of a truly scalable *gem*-dimethyl chlorin synthesis. Literature reports typically and continually do not exceed 40 mg of chlorin.

The other issue in the synthesis of these chlorins is perbromination. As noted throughout this thesis there is a distinct lack of data for β-bromo-*gem*-dimethyl chlorins. In reality, it is entirely plausible to suggest that this is because obtaining these in high purity is exceedingly tiresome. Instead, we observe chlorins that are products of Stille, Suzuki, and Sonogashira cross-coupling reactions. This is because it is typically much easier to separate the coupled product from residual starting material and/or proto-debrominated starting material. It could be argued that the utilization of wavelength extended chlorins presents better candidates for PDT, but then this begs the question: where is the basic science presented in this field? The answer is, simply: it has not yet been presented.

The synthesis of **H$_2$P**, **ZnP** and **PdP** by contrast is far more facile and easily scalable, assuming the successful synthesis of **4.52**. Whilst chlorins may only be isolated on 40 mg scale, **H$_2$P** was initially synthesized in a yield of 422 mg, 25%. Upon the synthesis of **4.52**, **H$_2$P** is only one step, and **ZnP** and **PdP** is only two.

Whilst these both require chromatographic purification; the purification is of much greater ease requiring only a silica plug with careful selection of solvents.

Photophysically, however, the chlorins are far superior. With the long wavelength of absorption presented i.e., $\lambda(Q_y)$ = 616–624 nm (THF), there should be more successful treatment of tumors *in vivo*. All of this being said, **H_2P** presents a longer wavelength of absorption, albeit at a much lower intensity (c.a. 15%). Despite the lack of $^1O_2$ produced by **ZnC[1]**, we have still shown it is capable of generating ROS. Further to this, **H_2P** was also shown to exhibit a large ϕ_Δ.

PdP poses an interesting quandary, as to what was occurring under illumination, and what was yielding the NIR emission upon our attempts to discern ϕ_Δ. Whilst the insertion of palladium into tetrapyrroles to yield PSs is a desirable endeavor, we have had to present an honest and cautionary tale of our exploits. In the case of WST-11, the utilization of palladium is only successful because 1) the bacteriochlorophyll periphery contains multiple motifs suitable for its solubilization in aqueous media and 2) being a bacteriochlorin at its core, the wavelength of absorption is suitably long enough prior to the insertion of palladium. The differing symmetries and spectra therefore do not hamper WST-11 photophysically in the same manner to our comparison between **H_2P** and **PdP**.

Lastly, as PS candidates in an *in vitro* setting:

PdP cannot be considered a successful PS candidate in any form. Its' very poor solubility, coupled with no differing profile between dark and photo-toxicities, coupled with no suitable way to monitor internalization of **PdP**, it is wholly unsuitable.

ZnP is more suitable, in the sense that it had good solubility, and with minimal dark toxicity in the concentration range examined (i.e., up to [**ZnP**] = 50 μM). Unfortunately, it presents an uptake profile that is less than ideal, and again a less than ideal phototoxicity profile. It is arguable that upon increasing the light dose to c.a. 10 J cm^{-2}, full cell death could be observed at 1 μM, but that is an exceptionally high light dose for an initial *in vitro* study.

Of the porphyrins, **H_2P** presents the most suitable biological data *in vitro*. Unfortunately, it is hampered by solubility – particularly in terms of analyzing the dark toxicity profile. However, this is an issue that can be circumnavigated with

formulations akin to those seen for Temoporfin,[373] or the utilization of differing solvents for administration.[374]. Its phototoxicity profile is excellent (within the data presented herein) and yields an IC_{50} in 10^2 nM range.

Chlorin **ZnC^2** was proposed in order to examine the effect of enhanced Type II reactivity via incorporation of the 3-Br substituent. Unfortunately, we are still at a loss as to how to determine ϕ_Δ for all PS candidates, and until this is performed, we will not know if this strategy was a success. Regardless, it has presented suitable phototoxicity data, on par with **ZnC^1**. To be able to draw realistic conclusions of the efficacy of **ZnC^2** as a PS, further experimentation is needed, excluding its synthetic pitfall.

Lastly, **ZnC^1**. Of all five PS candidates analyzed, **ZnC^1** presented the highest dark toxicity, albeit with cell death only occurring outside the phototherapeutic range. It presented excellent phototoxicity profiles, with an IC_{50} value, again, in the 10^2 nM range, at a suitably low light dose. We were able to quantify its phototoxicity through the generation of superoxide radical anions, however any utilization of fluorescin based sensors is impossible given the spectral overlap between **ZnC^1** absorption and fluorescin emission.

4.4 Conclusion and Future Work

In conclusion, we have presented the successful synthesis of novel Eastern Half **4.52**, containing orthogonal bioconjugation handles at the (eventual) 5- and 10-positions of the chlorin macrocycle. Further to this, the generation of analogous porphyrins therefrom highlights not only the synthetic versatility of **4.52** but the suitability and synthetic ease to which certain porphyrins can be synthesized.

We have also exhibited our serendipitous generation of **4.65**, and crystallographically explored the intermediates in the synthesis of Western half **4.63**. This research highlights a great amount of knowledge missing surrounding the synthesis of key intermediates in modern day chlorin syntheses.

The scalable synthesis of **4.68** and compounds therefrom, whilst not implemented in this thesis, shows promise in the generation of tetrapyrroles (or other carbon-heavy arrays) which are soluble in more polar, or even aqueous, media.

The synthesis of **ZnC^1** highlights one of the few examples of bioconjugatable, polar chlorins. The synthesis of **ZnC^2**, and isolation of **ZnC^2-Br**, add data into a sparse chemical landscape when it comes to the differences between differing levels of bromination upon the chlorin core: utilized for their heavy atoms and not just as coupling partners.

Photophysical analyses of these PS candidates remain incomplete, however highlights the incompatibility of phenalenone in THF systems, and highlights how determinations of SOQY utilizing DMSO may not yield results of great accuracy.

This research presents the first analyses of *gem*-dimethyl chlorins as PDT agents. Excluding their synthetic downfall, the compounds presented herein (**ZnC^1** and **ZnC^2**) present themselves as suitable candidates for further analyses.

The porphyrins presented herein also highlight how commonly used strategies in PS generation are not always successful, namely **PdP** as the prime example. **H$_2$P** was found to be nearly as phototoxic as **ZnC^1**, for instance. To our knowledge, this is the first example of a series of analogous 2H, Zn, and Pd-porphyrins analyzed concomitantly.

The utilization of chlorins in PDT is a flourishing field. As shown Chapter 1, there are many ways to generate chlorins, both *via de novo* synthesis and from

porphyrins. The incorporation of oxidation resistance however is a feat achieved my far fewer synthetic methods. Battersby's initial generation of Bonellin dimethyl ester (**1.109**) paved the way to some of the PSs presented in this chapter. It begs the question as to whether, for PDT, the synthetic arduousity outweighs the PDT effect. In this instance, the answer is no.

There are other common strategies to generate oxidation resistant chlorins, namely that of Cavalerio and co-workers (Scheme 1.6). *N*-methyl pyrrolidine fused chlorins have shown exemplary PDT efficacy, and they are also facile in their synthesis. To our knowledge, they have not been shown to oxidize to the porphyrin. Likewise, the cycloaddition to yield **1.86** (Scheme 1.7) Despite the lack of oxidation resistance, natural chlorins (Chl *a* and *b*, chlorin e_6) present excellent scaffolds to yield PSs for PDT.

So where do *gem*-dimethyl chlorins belong? Where is their place in chemistry? Throughout, these molecules have been utilized in dyad type systems, as simple analogues to natures chlorins. With no phytyl esters, or β-formyl, -vinyl, or -alkyl motifs, *gem*-dimethyl chlorins have continually enabled us to study in great detail fundamental photophysical processes.

Within the research presented herein, further experiments are required to fully discern the suitability of the compounds presented herein, i.e., **ZnC^2** requires a great deal of experimentation, even despite its initial success. Further to this, determination of logP values may go some way into understanding the uptake profiles observed across the series.

This research goes a great deal into understanding the use of *gem*-dimethyl chlorins as PSs for PDT, and alone on a synthetic argument there is no point considering them. But instead it does raise further questions: i.e., what phototoxicity profile would an analogous 5,10-porphyrin yield?

Chapter 5.

Tetraphenylethylene-BODIPY Arrays: A Valiant Endeavour for a Brighter Future

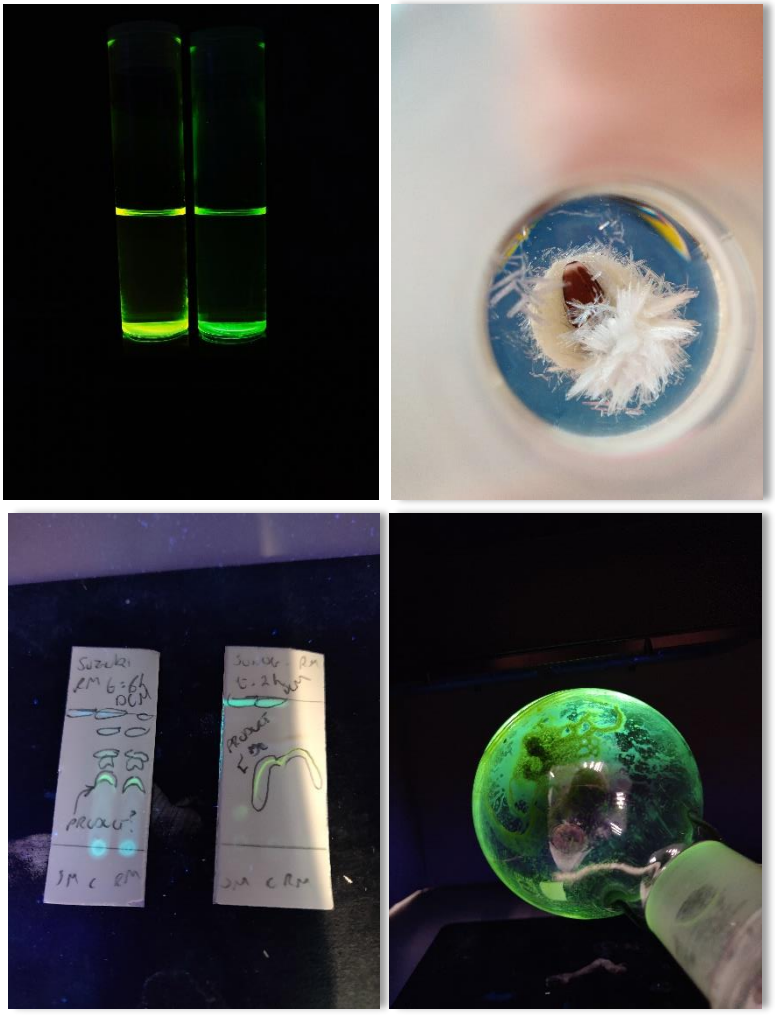

5. On The Synthesis of Tetraphenylethylene (TPE) Based Photoactive Arrays

5.1 Introduction

5.1.1 Tetraphenylethylenes (TPE) and Aggregation Induced Emission (AIE)

1,1,2,2-Tetraphenylethylene (TPE, **5.1**) has a long history, however when it was first synthesized appears a subject still up for debate. Bhosale and co-workers,[375] attribute the first synthesis of TPE to Boissieu in 1888.[376] However, in the abstract entitled 'New Method for the Preparation of Tetraphenylethylene' no references are made to other methods for comparison.[377] Others, instead, attribute this feat to Schmidlin.[378]

A survey of the literature indicates a myriad of differing routes to **5.1**. In the case of **5.2** (X = S), on three separate occasions from 1872–1904 the reported method was distillation,[379,380,381] in 1907, Cone and Robinson reported the phosphorus(V) chloride mediated rearrangement of **5.5** to yield TPE (Scheme 5.1).[382] In the case of **5.3**, treatment with acetyl chloride was found to yield TPE,[383] akin to **5.6** which was also found to yield TPE upon treatment with acetyl chloride.[384] Other generations of TPE from **5.6** merely use 'acid'.[385] Schlenk and Bergmann in particular investigated the formation of TPE from **5.4** utilizing a wide variety of reagents.[386] Treatment of **5.7** with silver(0) was also found to yield TPE.[387]

The reactions carried out in the modern day vary in the desire and necessity to generate multiply substituted TPEs. For example, the double arylation of bis(phenyl)acetylene is an effective strategy to generate multiply substituted TPEs, with excellent scope.[388] Other methods simply improve on the generation of TPE: treatment of **5.11** with copper chloride in DMSO cleanly yields TPE.[389] Treatment of diphenylmethane **5.13** with *n*BuLi, followed by benzophenone **5.14** yields **5.6**.[390] Interestingly, bromination of **5.13** leads directly into Boissieu's initial method.[376]

However, the most commonly used synthesis for the generation of the TPE core is the McMurry synthesis. Interestingly, this type of Ti-mediated coupling was first reported by Mukaiyama et al.,[391], then Tyrlik et al.,[392] and lastly McMurry in 1974.[393] However, it is the pitfalls of initial procedures (namely the lack of scope on

aryl and alkyl motifs in refs.[391,392]) that lead to the 1978 work, and the reasoning behind this reaction taking the McMurry name.[394]

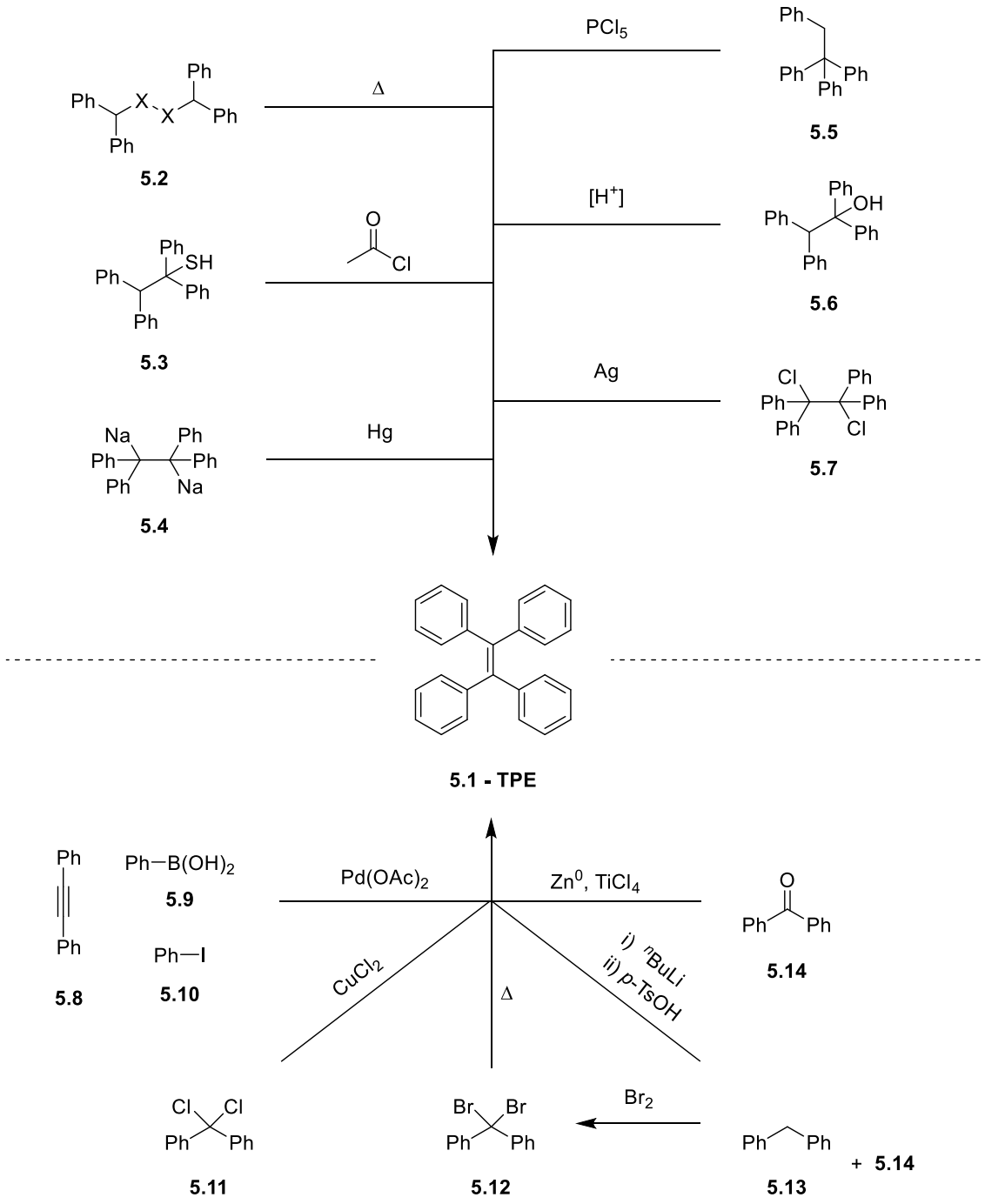

Scheme 5.1. Differing methods to synthesize TPE (5.1) with historic methods (*top*, from **5.2**–**5.7**) and more modern methods (*bottom*, from **5.8**–**5.14**). For **5.2**, X = O, S. [375,376,377,378,379,380,381,382,383,384,385,386,387,388,389,390]

Whilst the story of the synthesis of TPE is thus long and illustrious, at current TPE is just another organic molecule. The first utilization of a TPE in a system for its exhibition of AIE was not reported until 2006.[395]

In 2001, the Tang group were in search of “highly emissive linear and hyperbranched polymers”,[396] which attracted them to siloles. They noticed that during the purification of 1-methyl-1,2,3,4,5-pentaphenylsilole (**5.15**, Figure 5.1) when spotting their TLC plate, the wet spot could barely be visualized with a UV lamp but upon evaporation of the solvent the spot was clearly visible.[397] Further experimentation showed that **5.15** in pure EtOH had ϕ_F = 0.63 x 10^{-3}, however in H_2O:EtOH at 9:1 *v/v*, ϕ_F = 0.21, an increase 333-fold. After H_2O:EtOH *v/v* = 1:1, the increase in emission was observed, and the authors noted ‘nanoscopic aggregates’.[397] This publication then was the beginning of aggregation induced emission science.

This phenomenon goes against what we already know, rather counter-intuitive. Typically, organic lumiphores tend to exhibit the phenomenon ‘aggregation caused quenching’ (ACQ), which is typically a result of π-π stacking. There are multiple examples of this, one typical example is perylene (**5.16**, Figure 5.2). Entirely flat, it is very easy to see how non-emissive aggregates could form. Förster and Kasper were the first to report the effect in 1954,[398] and to date it is generally recognized that aromatic lumiphores exhibit ACQ, a belief cemented upon the publication of Birks’ “*Photophysics of Aromatic Molecules*”.[399]

Whilst the π-stacking of **5.16**,[400] pyrene, and multiple other systems explains why they do not exhibit AIE, this does not explain why AIE arises. Initially we must consider **5.1** and **5.15** in dilute solution and the solid state. Whilst drawn flat on paper, these molecules are not flat in 3D space. In the case of **5.1** every phenyl ring is rotated by *c.a.* 45–58°,[401] and even if the phenyl rings were co-planar in the C^2-C^5 silole backbone of **5.15** – the tetrahedral Si center would mean the molecule is not flat.[402] So, there is no propensity for π-stacking in either molecule.

In dilute solution then all of these phenyl rings, that mean the molecule is not flat, will rotate. They will continue to rotate until the solution becomes too concentrated, at which point adjacent molecules of **5.1**, or **5.15**, interact with each other and hinder (or restrict) their intramolecular rotation (RIR). As a result of this RIR, highly emissive aggregates are formed. Analogous processes occur with ‘locked variants’ of TPE, e.g. **5.17** (Figure 5.2), which instead of RIR exhibits restricted intramolecular vibration (RIV), as a result of the phenyl rings being locked by ethylene bridges. It

has been noted that some of the differences between molecules that exhibit AIE vs. ACQ can be as small as two methyl groups, as in the difference between **5.18** and **5.19** (Figure 5.3).[403]

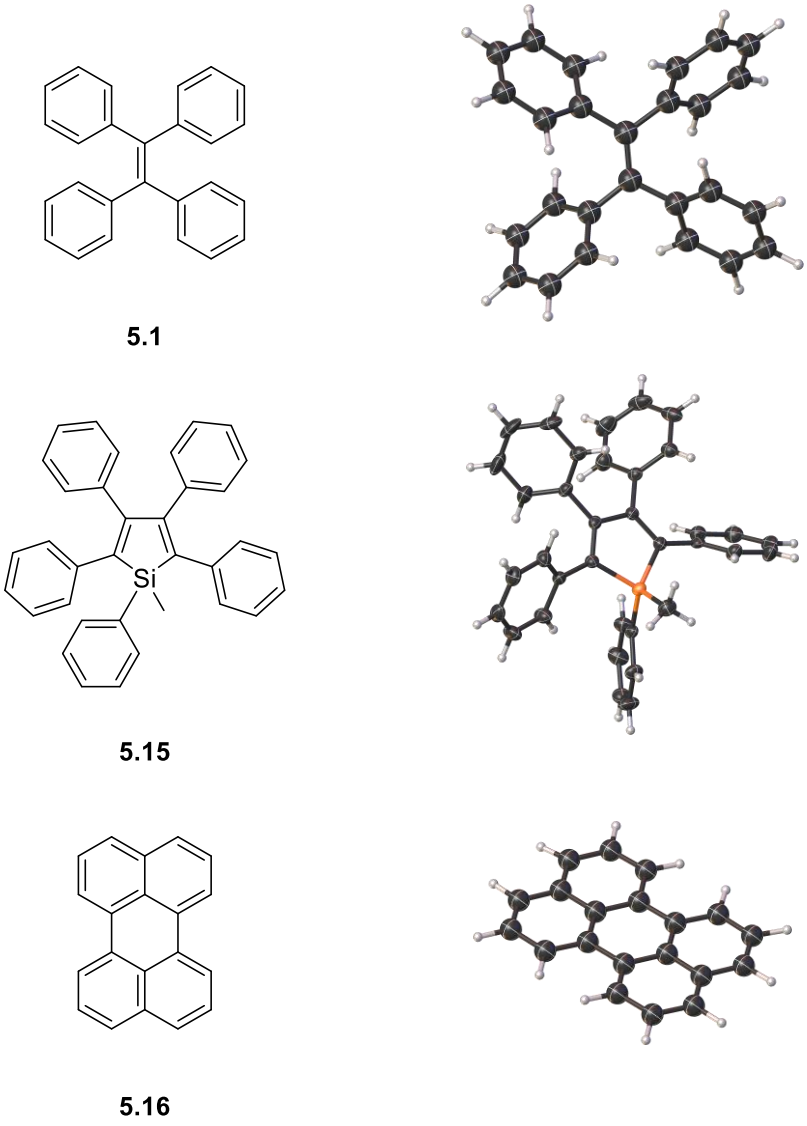

Figure 5.1. Structure (*left*) and Single crystal X-ray structure (*right*) of **5.1** (*top*), **5.15** (*middle*) and **5.16** (*bottom*). For **5.1**, image generated from CCDC No. 1275289.[401] For **5.15**, image generated from CCDC 273482.[402] For **5.16**, image generated from CCDC 1231185.[403] Images generated in Olex2.[126] Thermal ellipsoids indicate 50% probability.

Given that siloles were the class of compound for which the term AIE was coined, it seems fitting they have their own section in the literature.[404] In one particular example, the photoluminescence (PL) of hexaphenylsilole (HPS) in dipropylamine was utilized to evaluate CO_2 evolution. The formation of the carbamate ionic liquid decreased the solubility of HPS and subsequently PL intensity increased.[405]

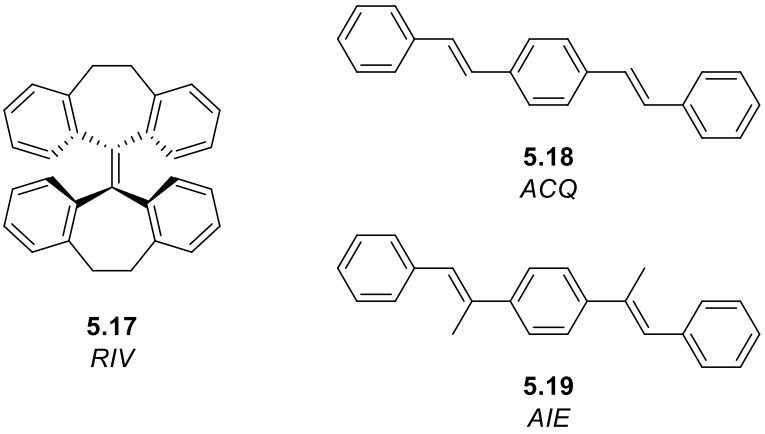

Figure 5.2. Structure of a molecule that exhibits RIV as its AIE mechanism, **5.17** (*left*), and similar molecules that differ in their exhibition of ACQ or AIE, **5.18** and **5.19** (*right*).[403]

5.1.2 Tetraphenylethylenes (TPE) as Organic Scaffolds

The TPE scaffold has many applications, all of which have been catalogued elegantly elsewhere.[406,407,408] However, given its structure i.e., D_{2h} symmetric, what efforts have gone into using TPE as a core scaffold?

Other rigid scaffolds include adamantane, [2.2.2]bicyclooctane, and [1.1.1]bicylopentane, the functionalization chemistry of which was recently covered by Grover and Senge.[409] Whilst the generation of spatially defined arrays is of interest, for the implementation of AIE, a moiety such as **5.1** must be present.

The TPE motif is commonly incorporated into metal organic frameworks (MOFs) and covalent organic frameworks (COFs), particularly for its emission in the solid state. In 2012, Shustova *et al.*,[410] synthesized a MOF from TPE **5.21** and zinc nitrate (Figure 5.3). Their design enabled the studying of strain energy of the TPE core and generation of an understanding of the relationship between that and the luminescence and stability of the resultant MOF. Through the utilization of an ethynyl spacer between the TPE core and the MOF-anchoring 3,5-bis(carboxyl)phenyl motifs they were able to generate principles which can be used to generate luminescent MOFs with a near dark 'off' state, and revealed that ligands could be locked in high energy confrontations via topological design.

In 2018, Ding et al., combined the tetraphenylmethane (TPM) moiety with TPE in order to generate a 3D COF for white light emitting diodes (LEDs).[411] Through a

[4+4] imine condensation, the produced COF was found to emit yellow PL upon excitation, and upon coating a blue LED with the COF the resultant LED exhibited white emission, with CIE coordinates of (0.30, 0.35). Furthermore, it exhibited high stability over 1200 h upon constant use.

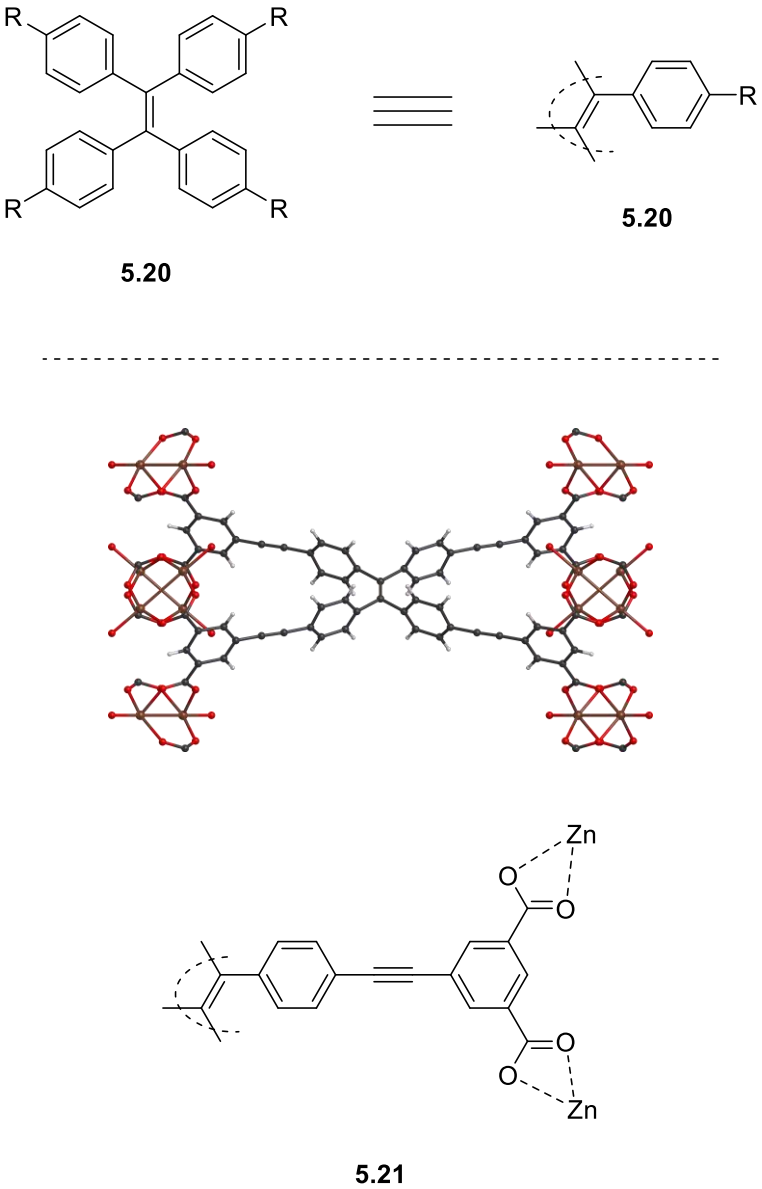

Figure 5.3. Minimized representations of TPE structures (**5.20**, *top*) and structure of TPE based MOF made by Shustova et al.[410] in the crystal (**5.21**, *middle*) and minimized structural representation (**5.21**, *bottom*) For **5.21**, Image generated from CCDC No. 893293.[410] Image generated in Olex2.[126] Atoms represented as spheres for clarity.

Excluding metals however, TPEs have been incorporated into myriad macrocycles and nanocages,[412] with applications ranging from explosives detection,[413] to chemotherapeutic encapsulation.[414]

In 2014, Feng et al., synthesized TPE-based macrocycles **5.22a**-**c** with the aim of examining the AIE response upon administration of nitrated aromatics, akin to compounds found in explosives (Figure 5.4).[413] The differing linkages present in **5.22a**-**c** were utilized as to analyze the importance of CH_3-π interactions between adjacent TPE molecules for the AIE mechanism. It was found that the nitro-aromatic compounds analyzed disrupted these interactions and 'switched-off' the AIE response. Monitoring this result via fluorescence (95:5, *v/v*, H_2O:THF) it was possible to observe a distinct decrease of fluorescence emission intensity with increase concentration of TNT (2,4,6-trinitrotoluene). Transferring this to a paper test, it was found that **5.22a** was able to detect TNT at a concentration of [TNT] = 10^{-13} M. Across the entire series of nitro-aromatics, **5.22a** was found to yield the greatest photoluminescence response.

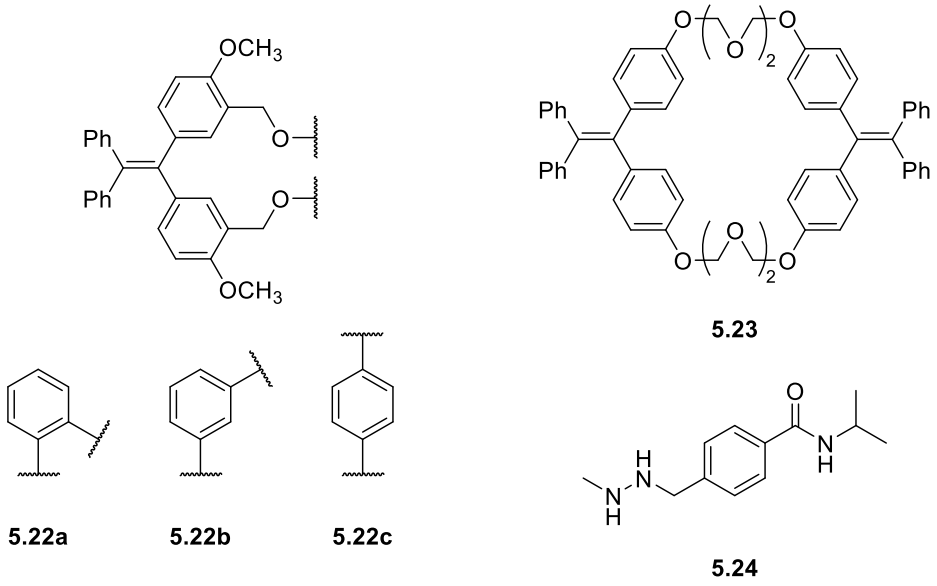

Figure 5.4. Structures of TPE-macrocycles used to detect nitro-aromatics used as explosives (**5.22a**-**c**, *left*),[413] and bis-TPE macrocycles (**5.23**, *top right*) utilized to encapsulate chemotherapeutics (**5.24**, procarbazine, *bottom right*).[414]

In 2013, Song et al.,[414] utilized bis-TPE macrocycle **5.23** to encapsulate the chemotherapeutic procarbazine (**5.24**, Figure 5.4). Through examination of prior single crystal X-ray diffraction results the authors rationalized that the absence of π–π stacking enabled them to exhibit 'extrinsic void space in solid state'.[414] Upon addition of water to a THF solution of **5.23**, strong emission was observed, and as the water fraction increased the λ_{MAX} did also from 448 → 473 nm. The resulting aggregates were found to be stable over at least 72 h in 95:5 H_2O:THF solution.

Administration of the picrate salt of **5.24** along with sonication yielded a decomposition of the spherical aggregates observed which yielded 'birds nests' composed of nano-rods to which picrate-procarbazine salt could be loaded (upon standing at r.t.). It was found *via* UV-Visible spectroscopy that the loading of the salt was 5.3 mg per 100 mg of **5.23**. Sonication of this again showed a 92% release of the salt in 3 h. No experiments were performed to analyze the reproducibility of this system i.e., how many cycles can this system undergo prior to decomposition?

5.1.3 TPE-Dye Conjugates

However, thus far, we have not seen the synthesis of dye-TPE conjugates. The utilization of a dye in the system can yield a second photometric response, i.e., AIE is yielded from the TPE motif, but there is also an absorption/emission profile that is distinctive to the dye used which can be monitored. Unfortunately, there a few examples (*vide infra*).

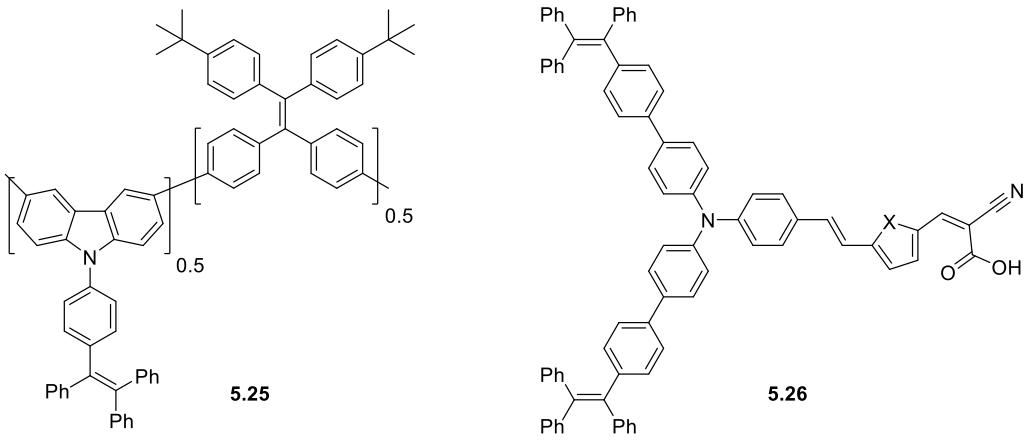

Figure 5.5. Structures of TPE-Dye conjugates, with Dong's TPE-Carbazole co-polymer,[415] (**5.25**, *left*) and the TPE-TPA conjugate of Shi et al.[416] (**5.26**, *right*). For **5.26**, X = O, S.

Dong et al.[415] synthesized a TPE-carbazole co-polymer (**5.25**, Figure 5.5, *left*) in which the TPE motif was incorporated into both the backbone of the polymer, and the side chain. Instead of monitoring any response from the carbazole however, the only photometric response observed was the PL of the TPE moiety. The greatest response achieved was obtained in H_2O:THF and 9:1, *v/v*. Upon addition of TNT, PL was observed to decrease almost 10-fold as [TNT] = 74 μM. No other nitro-aromats were analyzed in the communication.

Shi et al.,[416] generated D-A chromophores for use in dye sensitized solar cells (DSSCs). They utilized the TPE motifs as the donor part of the system, with the cyanoacetic acid motif acting as the acceptor and anchoring groups with either thiophene or furan as the conjugated bridge. In comparison with previously synthesized analogues omitting the TPE motif,[417] the addition of TPE red shifted λ_{MAX} by 4 nm (to 480 nm) and decreased the extinction coefficient by *c.a.* 2500 $M^{-1}cm^{-1}$. The inclusion of the TPE moieties showed no change in efficiency in comparison with prior non-TPE containing analogues, however the authors propose that the inclusion of TPE may block charge recombination.

5.1.4 TPE said to BODIPY "Have we met before?"

The combination of TPE and other pyrrolic dyes has been reported with Aza-BODIPYs,[418] and aluminum porphyrins.[419] Aside from these, the most prominent area of TPE-Pyrrolic dye combination is with the BODIPY core.[421,422] Previously, studies haves analyzed differing linkages of TPE-BODIPY systems, and differing placement of the TPE on the BODIPY periphery.

Zhao et al.,[422] synthesized a series of BODIPYs with a meso-TPE with varying methyl groups around the BODIPY periphery, one of the most common functionalization strategies for BODIPYs (Figure 5.6). The photophysical properties of **5.27a**-**c** were analyzed in both film and solution state. The methyl substituted BODIPYs presented a typical response, however when analyzing these compounds regarding AIE only **5.27a** yielded an AIE response, whereas all others yielded an ACQ response as water-faction increased. Their results lead them to conclude that the prescence of methyl groups on the BODIPY periphery can inhibit intramolecular charge transfer behavior.

Gomez-Duran et al.,[423] also examined α-substitution in their generation of TPE-styryl BODIPYs (**5.28**). From their experiments they concluded that a direct meso-TPE linkage was indifferent to a meso-Ph motif, but instead generation of a vinyl linkage between the α-position of the BODIPY and the TPE yielded large bathochromic shifts in both absorption, and emission. However, upon generation of this sizeable, conjugated network the AIE activity was found to be diminished.

Compound **5.29** was presented along with a series of other meso-acetylene BODIPYs in which the TPE motif was exchanged for 2,3,3-triphenylacrylonitrile.[424]

In comparison with the meso-(phenylacetylene) analogue, it presented an analogous λ_{MAX}, and slight reduced HOMO-LUMO gap. However, **5.29** was found to be AIE inactive. No emission was observed for compound **5.29**, and thus the authors propose that the fluorescence is quenched due to charge transfer from the TPE moiety to the BODIPY, which acts as the acceptor.

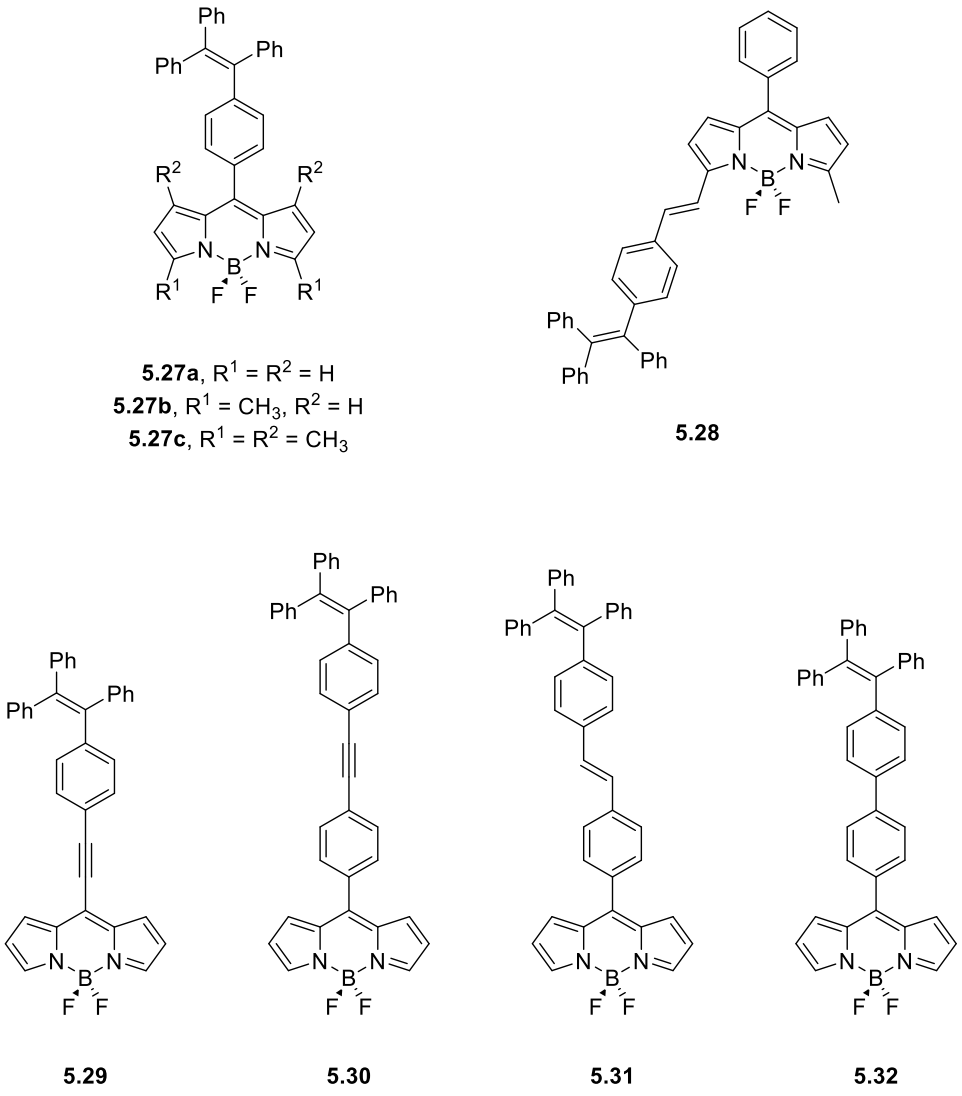

Figure 5.6. Structures of previously investigated TPE-BODIPY conjugates.[420,421,422,423,424,425]

In 2012, Hu et al.,[425] presented the synthesis of compounds **5.30**–**5.32**, in which the BODIPY-meso-phenyl group and TPE motif were separated by acetylene and vinylene linkers. In the case of **5.32** there was no separation. They found that PL on **5.32** was found to be quenched upon increasing water fraction, whereas **5.31** exhibited a more typical AIE profile of increased PL with increased water fraction. **5.30** exhibited both the locally excited (LE) state of the BODIPY throughout, as well

as AIE-type twisted intramolecular charge transfer (TICT) band. The authors propose that **5.32** could be utilized as a fluorescent dye for intracellular imaging.

5.2 Results and Discussion

5.2.1 Aims and Objectives

As exhibited *vide supra*, the AIE phenomenon can be extraordinarily useful, as exhibited by the number of applications the TPE motif has lent itself to. However, there is little in the scope of TPE-Dye conjugates, in comparison to the mountain of literature regarding TPE. It is also interesting to observe that within **5.27**–**5.32**, despite the continual incorporation of the TPE motif, there is not the continual exhibition of AIE.

The utilization of the BODIPY core is omnipotent within PDT,[426,427] and not just as a well-studied ACQ motif. Further to this, we have continual interests in novel BODIPY photonics applications.[38,428,429,430,431]

The aim of this chapter is to develop the first tetra-BODIPY TPE systems. We rationalize that by differing the linkage between the TPE and BODIPY cores, we will observe differing photophysical properties in all; solid, solution and aggregated states. Given the propensity for the BODIPY motif to be used within PDT, the resulting arrays will be analyzed with regards to their $^1O_2$ production, and we will present a discussion regarding their suitability as PSs for PDT.

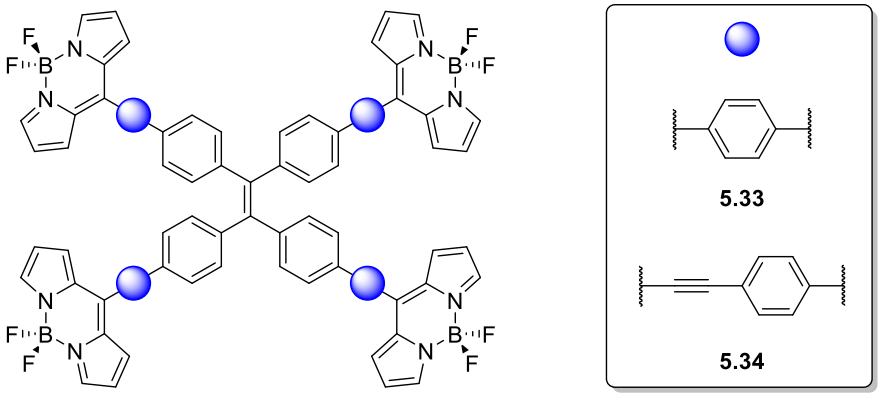

Figure 5.7. Core structure of the target products of this chapter.

5.2.2 On the Synthesis of TPE-BODIPY Arrays[2]

As discussed *vide supra*, there are a multitude of methods for synthesis of the TPE core (Scheme 5.1), however given its simplicity we utilized the McMurry synthesis. Given the linker motifs that had been decided (phenyl, **5.33** and 4-ethynylphenyl, **5.44**) we rationalized that [Pd]-catalyzed cross couplings were a suitable method to install aldehydes, as to build the DPMs necessary.

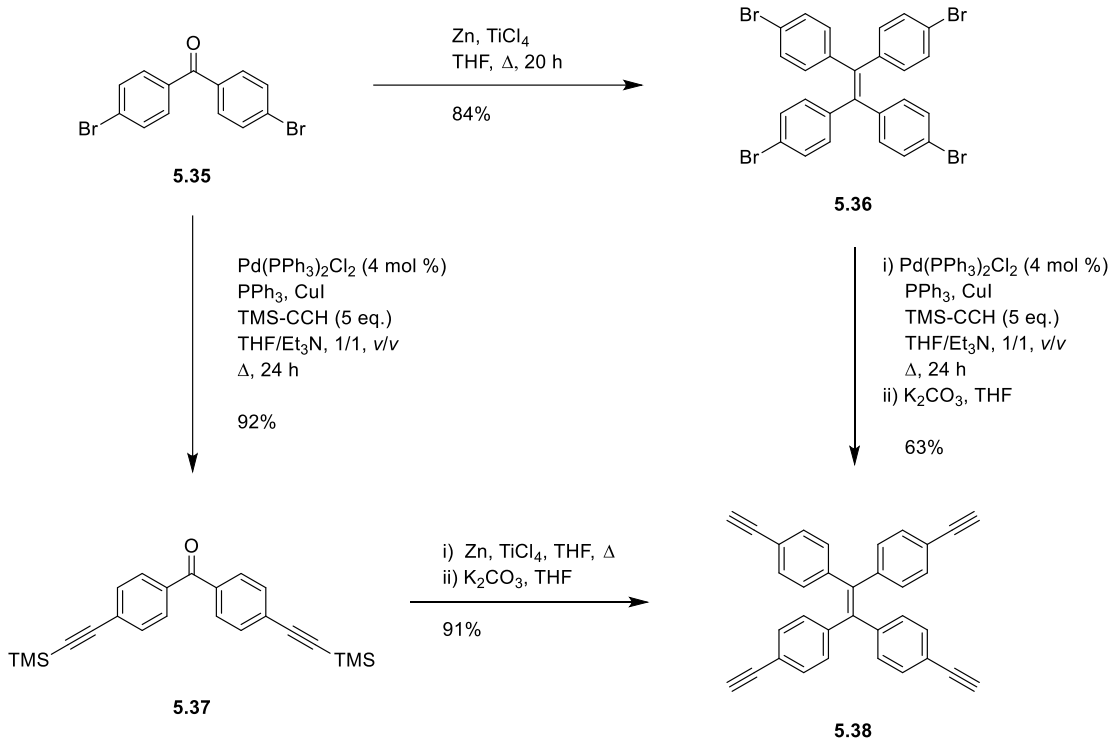

Scheme 5.2. Synthesis of simple TPE-starting materials **5.36**, and **5.38** via two differing methods.[432,433,434]

The syntheses of the simple TPE precursors began from 4,4'-dibromobenzophenone (**5.35**, Scheme 5.2). McMurry coupling of **5.35** cleanly yielded 1,1,2,2-tetrakis(4-bromophenyl)ethylene **5.36** in 84% yield. Subsequent Sonogashira coupling with TMS-acetylene followed by K_2CO_3 mediated

[2] *The singlet oxygen quantum yield determinations of the **5.33** and **5.34** were performed by B. Khurana. The aggregation induced emission studies (AIE) of **5.33** and **5.34** were performed by Dr. G. Emandi. The crystallographic data presented in this chapter was collected, solved, and refined by Dr. B. Twamley.*

deprotection yielded 1,1,2,2-tetra(4-ethynylphenyl)ethylene **5.38** in 63%, or 52% from **5.35** over two steps.

We sought to increase our yield of **5.38**, and thus reversed the order of the procedures. Initial Sonogashira coupling of TMS-acetylene and **5.35** yielded the bis(trimethylsilyl)benzophenone **5.37** cleanly in 92% yield, which was then followed by McMurry coupling and K_2CO_3 mediated deprotection to yield **5.38** in 91% over three steps.

Compound **5.37** was found to crystallize from a saturated solution in methanol, and crystallized in the orthorhombic space group P*ccn* (No.56) with no solvate. This structure completes the series of standard 4,4'-di(*X*)benzophenone structures where X = F, Cl, Br, I.[435,436,437,438] Minimal differences were observed throughout the series, namely, with minor changes in the C-C(O)-C angle and differing degrees of puckering of the phenyl rings.[435,436,437,438]

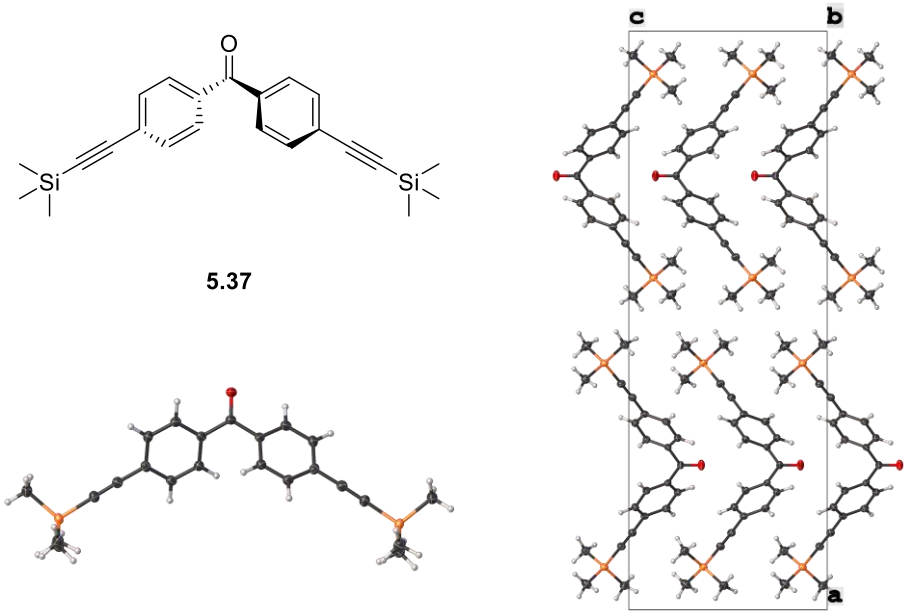

Figure 5.8. Single crystal X-Ray structure of **5.37** with one independent molecule of **5.37** (*bottom left*) and a packing diagram along the 010 plane. Image generated in Olex2.[126] Thermal ellipsoids indicate 50% probability. Data was solved, collected and refined by Dr. B. Twamley.

Treatment of **5.36** with 4-formylphenylboronic acid under Suzuki conditions yielded TPE-tetraaldehyde **5.39** in 56% as a green solid, *vide supra*. Typically, in the syntheses of DPMs there are two main routes of choice: trifluoroacetic acid catalyzed, or indium(III) chloride catalyzed.[230,231,232] Whilst TFA catalysis is more widespread (given the ease of access to TFA, coupled with the cost difference in

reagents), we rationalized that a minimal production of tripyrrane was more pivotal here than in a typical DPM synthesis (Scheme 5.3). For this reason, we opted for $InCl_3$ catalysis. Following reported procedures,[232] we yielded TPE-tetra-DPM **5.40** in 56% yield, surprisingly high given this is a 4-fold DPM synthesis. Oxidation of the DPM, followed by BF_2-insertion yielded **5.33** in 32%.

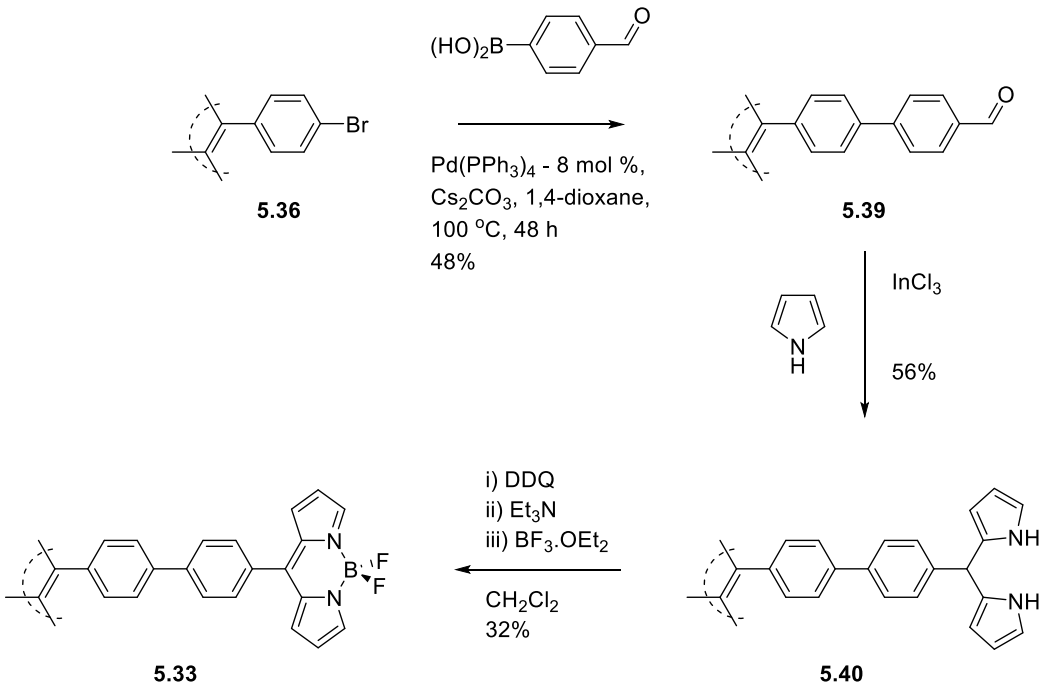

Scheme 5.3. Synthesis of phenyl spaced TPE-BODIPY conjugate **5.33** via Suzuki coupling, followed by DPM formation and BF_2-insertion.

Attempts were made to grow X-ray suitable crystals of **5.39** as to understand better its structure in array type settings. Prior structural studies consisted only of powder X-ray diffraction experiments of derivates of **5.39** in COFs.[439,440] Multiple attempts were made to crystallize **5.39** form common laboratory solvents (CH_2Cl_2, THF, CH_3OH and *i*PrOH amongst others) and in all cases **5.39** was found to precipitate out. The best result from those common solvents was *i*PrOH, however none of the crystals were found to be suitable for diffraction. Eventually, slow evaporation of a CH_2Cl_2/TFA solution of **5.39** yielded crystals suitable for diffraction (Figure 5.9).

Compound **5.39** was found to crystallize in the monoclinic space group *C*2/*c* (No. 15). Its structure was found to be quite similar to that of **5.36.**[441] Unsurprisingly there was a distinct lack of Br…Br interactions as a result of the lack of Br in **5.39**, in comparison with **5.36**. However, **5.39** did exhibit typical host-guest nature of **5.36**,[442] but in this instance we were unable to identify the exact composition of

these voids, subsequently the diffuse diffraction component was omitted from the data.

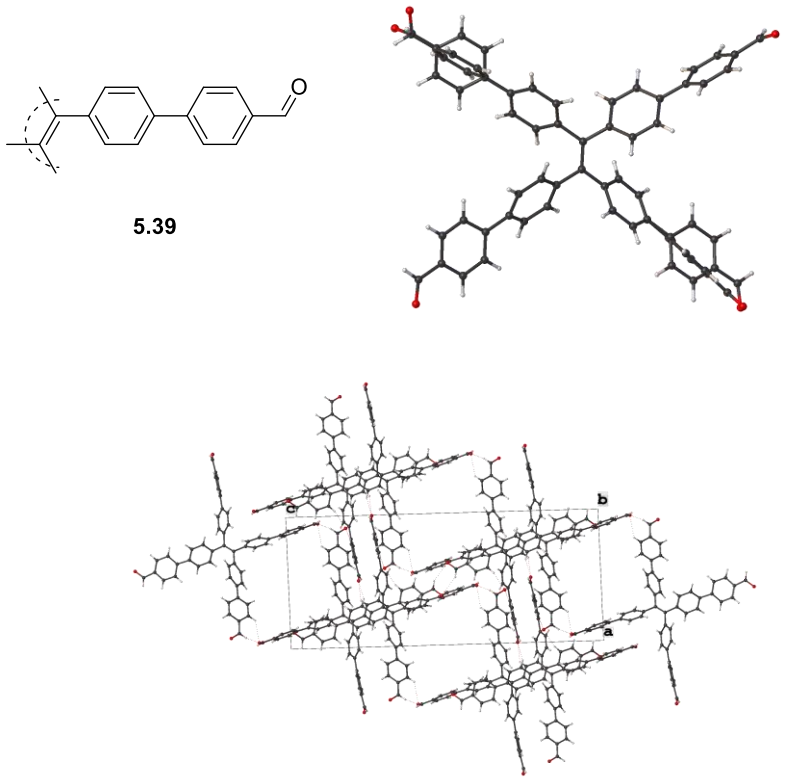

Figure 5.9. Single crystal X-Ray structure of **5.39** with one independent molecule of **5.39** (*top right*) with phenyl-ring rotational disorder shown, and a packing diagram along the 010 plane (*bottom*). Image generated in Olex2.[126] Atoms represented as spheres for clarity. Data was solved, collected and refined by Dr. B. Twamley.

Compound **5.38** was treated with 4-iodobenzaldehyde under Sonogashira conditions to yield the tetra-aldehyde **5.41** in 40% yield (Scheme 5.4). Once again, an $InCl_3$-mediated DPM synthesis yielded the tetra-DPM **5.42** in 25% yield, and from this the tetra-BODIPY was yielded in 19%. Interestingly, the yields for the ethynyl-phenyl spaced system were lower at every step, in comparison to the phenyl spaced system. Given these low yields, we attempted Suzuki and Sonogashira couplings with **5.36** and **5.38** with the respective BODIPY (i.e. for **5.36** the coupling partner would be 5-(4-ethynylphenyl)BODIPY), and in both cases we were unable to yield any product. Thus, the yield of **5.33** from **5.36** is 8% over three steps, and for **5.34** from **5.38** the yield is 3%.

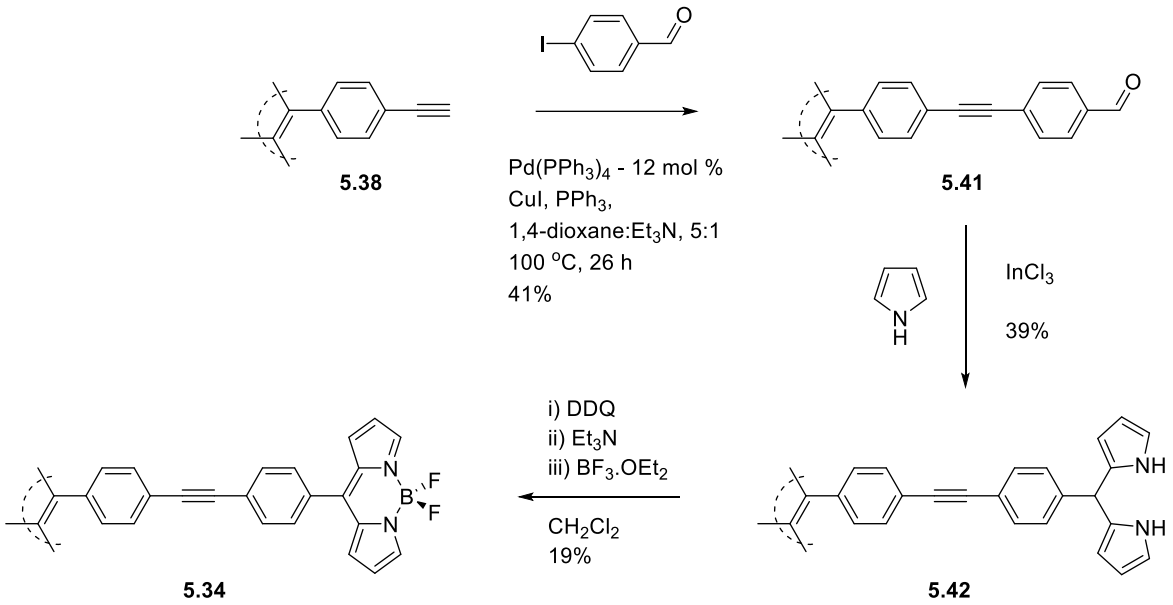

Scheme 5.4. Synthesis of ethynyl-phenyl spaced TPE-BODIPY conjugate **5.34** via Sonogashira coupling, followed by DPM formation and BF_2-insertion.

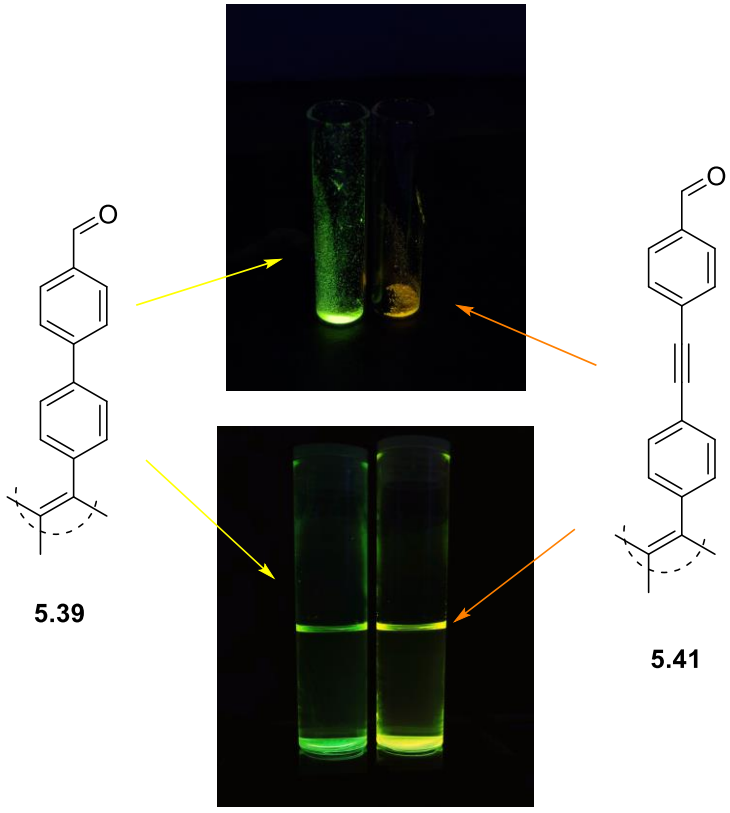

Figure 5.10. Structures and photographs of aldehydes **5.39** and **5.41** being illuminated under UV-light (360 nm) in the solid state (*top*) and in THF solution (*bottom*).

Interestingly, upon the syntheses of aldehydes **5.39** and **5.41**, we noticed distinct differences in their physical appearances. Whereas **5.39** was a vibrant yellow

powder, **5.41** was distinctly orange. The differing colors also presented in the solution state. The differing responses under UV illumination (360 nm) as presented below (Figure 5.10).

5.2.3 On the Aggregation Induced Emission Properties of TPE-BODIPY Arrays

Given the proposed evaluation of tetra-BODIPY TPE arrays as PSs for PDT, **5.33** and **5.34** were the only compounds considered for evaluation regarding AIE. Structurally, these two systems differ only in the ethynyl spacer utilized in **5.34**, but are otherwise identical.

Following from the majority of prior literature reports regarding AIE, we were confident in the use of THF/H_2O mixtures in order to analyze any possible AIE response, where THF is our solvent and H_2O is our anti-solvent. For all measurements, [**5.33**, **5.34**] = 10 μM, and between each measurement the water fraction changed by 0.1 (or 10%).

Typically, BODIPYs absorb in the region of λ_{MAX} = 495–515 nm, dependent upon; the solvent used for measurement, the electronic nature of substituents upon the BODIPY core, and the position of the substituents around the BODIPY core. As noted *vide supra*, Gomez-Duran et al.,[423] noted the indifference between a meso-phenyl and meso-TPE BODIPY, in comparison their generation of α-styryl BODIPYs yielded large bathochromic shifts in both absorption and emission maxima. The same three points can be argued for the emission maxima of BODIPYs, which typically emit around λ_{em} > 530 nm.[443]

Presented below in Figure 5.11 are the absorption (*top*) and emission spectra (*bottom*) for **5.33**, and in Figure 5.12 the analogous spectra are presented for **5.34**. Given what has been discussed previously, we can see that **5.33** exhibits a typical absorption profile for a BODIPY (Figure 5.11, *top*, 0%, *black plot*). Upon addition of H_2O, there are minor incremental decreases in intensity until a water fraction of 70% is achieved. Between 70% and 80% H_2O fraction, there is a large drop in intensity. Regardless, λ_{MAX} remains constant at all water fractions analyzed.

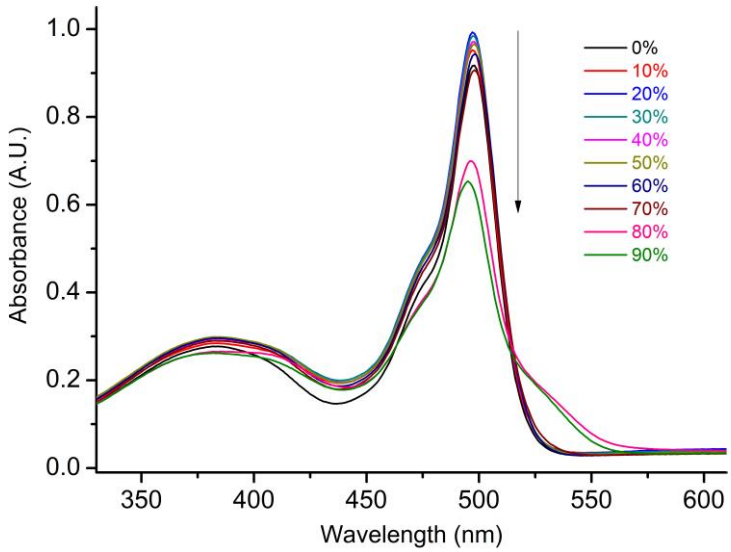

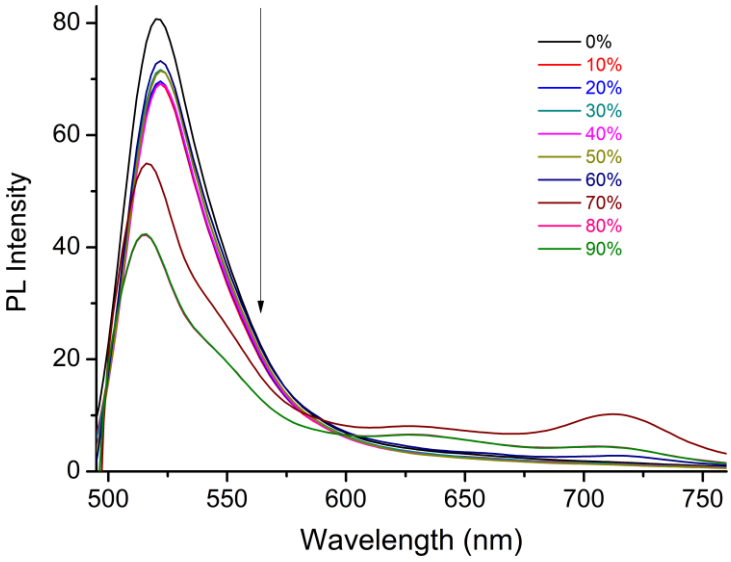

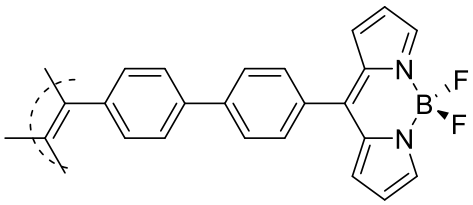

5.33

Figure 5.11. Absorption and emission spectra of tetra-BODIPY TPE array **5.33** in THF/H_2O mixtures. Legend refers to water content in sample being analyzed.

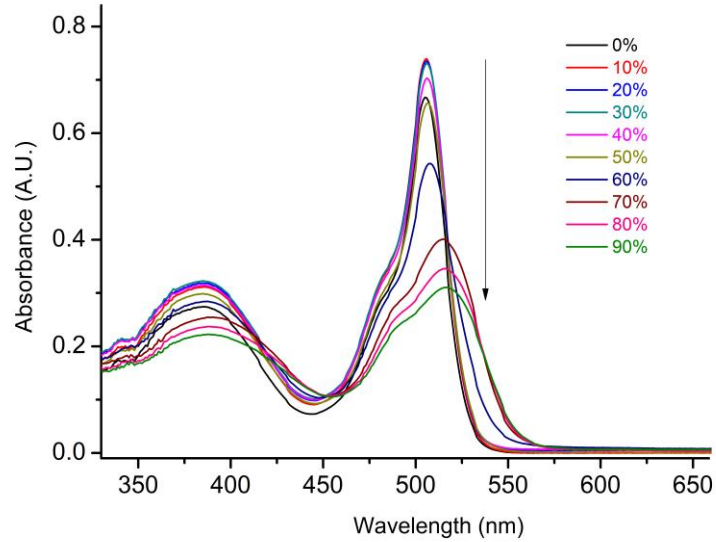

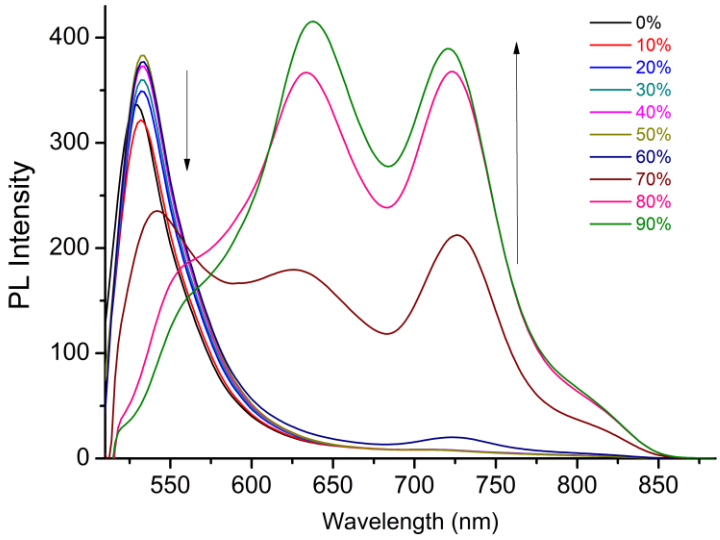

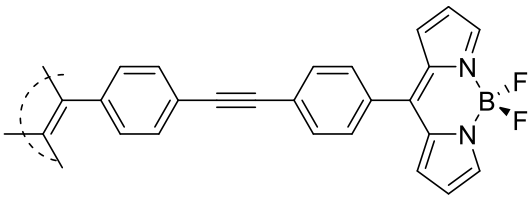

5.34

Figure 5.12. Absorption and emission spectra of tetra-BODIPY TPE array **5.34** in THF/H_2O mixtures. Legend refers to water content in sample being analyzed.

Akin to **5.33**, **5.34** exhibits a typical BODIPY absorption profile (Figure 5.12, *top*, 0%, *black plot*). In contrast to **5.33**, there is a drastic change at a H_2O fraction of 60%, and a decrease of intensity by approximately 50% when a water fraction of 90% is reached. Throughout this increase in water fraction however, there have been a distinct bathochromic shift of the typical BODIPY absorption peak.

Upon excitation of **5.33** (Figure 5.11, *bottom*) there is a decrease in PL intensity with an increase in H_2O fraction, with no change in λ_{EM}. Despite a small broad peak appearing around 725 nm at H_2O fraction of 70%, **5.33** can be said to exhibit non-emissive aggregates.

In contrast, **5.34** exhibits a vastly differing emission profile upon increasing water fraction. Between 0–60 % H_2O fraction, little changes in emission intensity, with minor incremental decrease in intensity. At H_2O = 70%, one peak becomes three. The locally excited (LE) state of the BODIPY is still present, albeit red shifted at *c.a.* λ_{EM} = 540 nm, and two new peaks appear at *c.a.* λ_{EM} = 645, 730 nm. Upon increasing the water fraction further, the LE excited BODIPY state becomes again red-shifted to *c.a.* λ_{EM} = 560 nm, however it eventually becomes a shoulder as the intensity of the two peaks surpass it. These solutions are pictured in Figure 5.13.

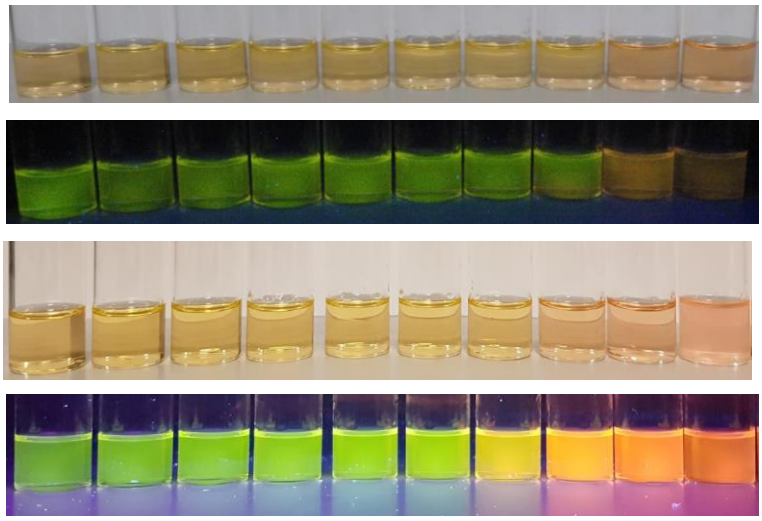

Figure 5.13. Solutions of **5.33** and **5.34** in THF:H_2O mixtures with increasing water fraction (*left, 0% → right, 90%*), and both under ambient lighting (*top*) and UV illumination (365 nm, *bottom*).

For the series of compounds **5.30**–**5.32**, similar trends are observed herein.[425] Given the similarity in structures, their results would suggest that the emission observed herein at λ_{EM} = 645 nm is a twisted intramolecular charge transfer (TICT)

band. Given the markedly similar intensities of the emission at λ_{EM} = 730 nm, we must consider this as an aggregation induced dual emission, a phenomenon previously examined on the diarylethene scaffold.[444]

Given that any intermolecular vibration and rotation are both hindered due to dense packing in the solution state, the dual emission presented is likely the result of differing π-π stacking modes in solution. Given this density, we propose that this packing is unlikely to be end-to-face i.e., BF_2…TPE interactions, but instead differing interactions between TPE cores. Proposed structures for these differing π-stacking modes are presented in Figure 5.14.

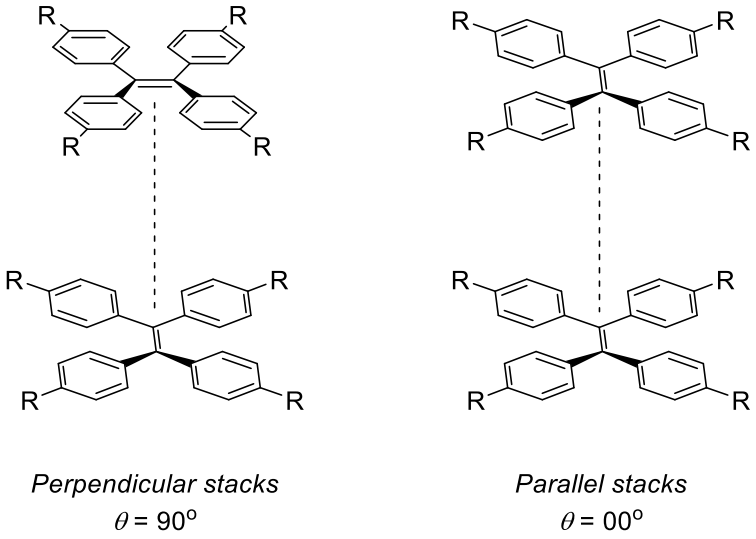

Figure 5.14. Proposed differing π-stacking modes present in molecular aggregates of **5.34** in THF:H_2O mixtures were H_2O > 70%.

5.2.3 On the $^1O_2$ Production of TPE-BODIPY Arrays

Given we have previously extensively investigated BODIPYs with regards to their singlet oxygen generation,[428] we have also investigated arrays **5.33** and **5.34**. As noted in Chapter 4, $^1O_2$ is a key modality for the evaluation of the potential cytotoxicity of PS candidates. Also noted in Chapter 4 was the possibility to detect $^1O_2$ via direct or indirect methods. Herein we have utilized 1,3-diphenylbenzoisofuran (DPBF), a probe that has been well studied and continually utilized for SOQY determinations.[445] For our reference, we used H_2TPP, **1.46**.[446]

Upon exposure to $^1O_2$, DPBF (**5.43**) undergoes a [4+2] cycloaddition to form the endoperoxide which eventually decomposes to *ortho*-dibenzoylbenzene (**5.45**) (Scheme 5.5). Upon monitoring the change in absorption of DPBF with respect to time, it is possible to determine the rate of consumption of DPBF, and subsequently SOQY for the desired species.

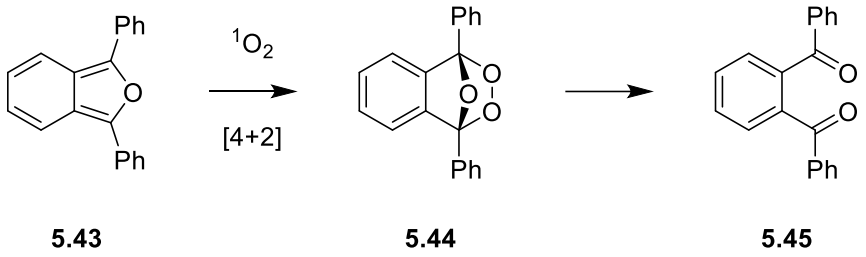

5.43 **5.44** **5.45**

Scheme 5.6. [4+2] Cycloaddition reaction of DPBF (**5.43**) with $^1O_2$.

Initially, the absorbance of **5.43** was adjusted to the range of *c.a.* 0.85–0.95 at 417 nm in air saturated solvent, at which point **5.33** or **5.34** were added to the cuvette. A plot of absorbance of **5.43** vs. time (s) is presented below for **5.33** and **5.34**.

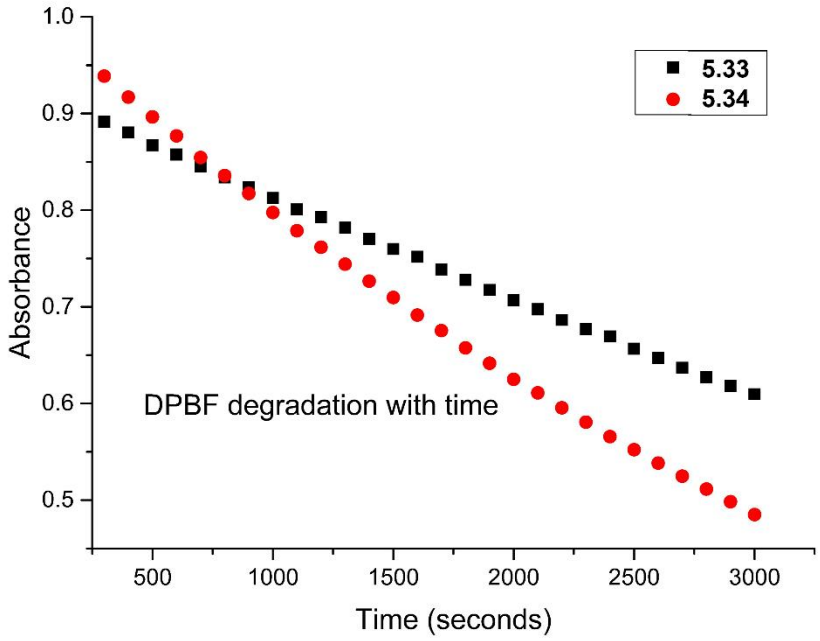

Figure 5.15. DPBF (**5.43**) degradation plots for TPE-arrays **5.33** and **5.34** in air saturated CH_2Cl_2:CH_3OH, 1:1, *v/v*. System irradiated at 532 nm with an average intensity of 10 mW cm^{-2}. [**5.43**] = 0.15 M.

Through a comparison of the gradients for the plots presented (in duplicate, within standard deviation) it was determined that the SOQY for **5.33** is ϕ_Δ = 0.09, whereas

for **5.34** ϕ_Δ = 0.15. The higher SOQY observed for **5.34** can be rationalized as a result of enhanced, and increased conjugation throughout the molecule. To our knowledge, this is the first SOQY determination for a TPE-BODIPY conjugate of any kind.

Whilst both produce $^1O_2$, only **5.34** exhibits AIE. This begs the question as to what would occur upon $^1O_2$ evolution in the aggregated state. From the offset, the SOQY would be significantly lower than in the solution state. It is highly likely that the molecules closer to the edges of these aggregates (regardless of shape) would become excited and that closer to the center would not. Because of this apparent shielding, it is unlikely that these aggregates would be able to generate $^1O_2$ effectively. It is more likely, instead, that irradiation of these aggregates in order to generate $^1O_2$ would instead merely reveal the PL of the aggregate system.

The incorporation of multiple PSs onto a single system is not a novel idea in of itself,[220] however as we have stated herein the decoration of a TPE with four PS molecules is. Logic dictates that the greater the number of PS molecules, the greater the SOQY, or therapeutic response. However this can only be true if each PS acts as an individual PS. A key criterion then, in these systems, is the retention of the properties of the singular PS (in this case, BODIPY), and thus it is hopeful to observe a multiplication of the effects.

We have shown that both **5.33** and **5.34** can produce $^1O_2$, which is a very positive finding in our eventual aim of utilizing these conjugates as multi-PS arrays. The results presented dictate that for **5.33** the properties of the BODIPY are retained only, but in the case of **5.34** the properties of the BODIPY are enhanced via TPE conjugation. In both cases then, **5.33** and **5.34** could be suitable as multi-PS arrays upon overcoming synthetic shortfalls.

5.3 Conclusions and Future Work

Herein we have presented the first tetra-BODIPY TPE arrays **5.33** and **5.34**, in which we have differed the linking group between the TPE and BODIPY cores (phenyl in **5.33**, and phenylethynyl in **5.34**). Whilst the yields for the synthesis of these arrays were low (8% for **5.33** and 3% for **5.34**), some positives can be drawn; namely the generation of tetra-aldehyde **5.41** presents itself as a molecular tecton in materials science applications.

The structural difference between these linkages has been clearly exhibited in the photophysical analyses undertaken; notably the addition of an ethynyl spacer in **5.34** yielding a vastly heightened AIE response in a mixed solvent system (THF:H_2O). The dual emission observed is not the first of its kind, and is rationalized through the generation of differing π-π stacked dimers in the aggregated state.

Despite synthetic shortfalls, *vide supra*, **5.34** presents itself as an ideal candidate for intracellular imaging with distinct emission bands across the visible spectrum. Further to this, both **5.33** and **5.34** present themselves as suitable PS candidates given their photophysical profile, along with their $^1O_2$ production.

This initial investigation indicates the possibility of further uses of TPE (or more broadly, phenylethylene) cores in the generation of spatially defined PS arrays for a handful of applications; namely light-emitting systems and theranostics.

6. Outlook

Chapter 3

10-Aryl chlorins **3.36a,b** and their freebase counterparts **3.41a,b** were synthesized in order to determine the photophysical suitability of the 17,18-dihydro-18,18-dimethylporphyrin scaffold for application as a PS in PDT. Their singlet oxygen generation in polar media, coupled with a long wavelength of absorption made them suitable candidates which warranted further investigation of this structure type.

Chapter 4

The generation of **ZnC^1** highlights possibilities for the generation of bioconjugatable 17,18-dihydro-18,18-dimethylporphyrins for PDT. The photophysical data presented puts it on par with these presented in Chapter 3 in terms of wavelength of absorption. Despite vastly differing singlet oxygen quantum yields, their biological efficacy has been shown to be suitable, albeit by different means. In the same vein, the syntheses of **H_2P** indicates that synthetic arduousity does not always lead to enhanced PDT efficacy. **H_2P** was derived from the same precursor as **ZnC^1** and yielded in good yield in one step. Questions are then raised regarding the suitability of sparsely substituted tetrapyrroles for PDT, for example a 5,10-diarylporphyirn.

Whilst there is a desire to build the PS with highest efficacy possible, eventually there is a ‘cost ceiling’. Although some experiments remain in order to fully ascertain the true PDT efficacy of the chlorins presented herein, enough data has been gathered to suggest that the chlorins presented herein will go no further (in terms of PDT) than academic research.

The ability to generate such sparsely substituted systems lends these systems to other applications, namely those of photophysical origin enabling the study of fundamental processes in dyads of a wide variety structure types.

Chapter 5

The synthesis of arrays **5.33** and **5.34** is the first example of tetra-BODIPY TPE-based systems. Their synthesis, *via* stepwise coupling and BODIPY construction, enables for the generation of modified systems, *via* using sterically hindered coupling partners or using substituted pyrroles of differing substitution patterns. For both arrays, the yields were low despite the synthesis being only three steps from the initial TPE-precursor. **5.34** exhibited a dual AIE response, enabling its utilization in myriad applications surrounding the topics of light emitting systems, and theranostic applications. **5.33** however did not exhibit AIE, and thus the ACQ implemented by the BODIPY remains the dominant effect.

TPE-BODIPY systems of this type require further study regarding at what point the ACQ effect from the BODIPY outweighs the AIE presented by the TPE. Further to this, other synthetic routes must become available for these arrays to maintain viability in any application.

7. Experimental

7.1 General

7.1.1 Chemistry General

Analytical thin-layer chromatography (TLC) was performed using silica gel 60 (fluorescence indicator F254, pre-coated sheets, 0.2 mm thick, 20 cm × 20 cm; Merck) plates and visualized by UV irradiation (λ = 254 nm or 365 nm) or another method specified. Melting points are uncorrected and were measured using a Stuart SMP10 melting point apparatus. NMR spectra were recorded using Bruker AV 600 (600 MHz for ^{1}H NMR, 151 MHz for ^{13}C NMR) and Bruker AV 400 (400 MHz for ^{1}H NMR, 101 MHz for ^{13}C NMR) instruments. Chemical shifts are given in ppm and referenced to the residual peak of the deuterated NMR solvent ($CDCl_3$, δ_H = 7.26 ppm, δ_C = 77.160 ppm and DMSO-D_6, δ_H = 2.50 ppm, δ_C = 39.520 ppm). The assignment of the signals was confirmed by 2D spectra (COSY, HMBC, HSQC). Signal multiplicities are abbreviated as follows: singlet = s, doublet = d, triplet = t, quartet = q, multiplet = m. ESI mass spectra were acquired using a Bruker micrOTOF-Q III spectrometer interfaced to a Dionex UltiMate 3000 LC in positive and negative modes as required. The instrument was calibrated using a tune mix solution, (Agilent Technologies ESI-l Low concentration tuning mix) this was also used as an internal lock mass. Masses were recorded over the range 100-1400 m/z. Operating conditions were as follows: end-plate offset 500V capillary 4500V, nebulizer 2.0 Bar, dry gas 8.0 L min^{-1}, and dry temperature 180 ^{o}C. MicroTof control 3.2 and HyStar 3.2 software were used to carry out the analysis. Due to intermittently functioning MALDI apparatus at Trinity College Dublin, we were unable to obtain molecular ion peaks for **PdP**, **ZnC^2**, and **ZnC^2-Br**. Multiple attempts were made via ESI-MS to obtain said molecular ion peaks, however none of these were successful.

To protect air and moisture sensitive compounds, the corresponding reactions were carried out under ‘Schlenk’ conditions using argon as inert gas. Air and residual moisture were removed from the instruments by a hot air gun under high vacuum and the flasks were purged with argon subsequently. This cycle was repeated up to three times as necessary.

Most commercially available reagents were used as received unless otherwise noted. For example, THF, Et_2O, $C_6H_5CH_3$, and CH_2Cl_2 were obtained by passing

the degassed solvents through an activated alumina column. Alternatively, anhydrous DCM was obtained via drying over phosphorus pentoxide and distillation. However, some reagents were purified prior to use;. Zn^0, NBS, *p*-nitrobenzoyl chloride. Pyrrole was passed through a small amount of silica prior to use, and NaH was washed with hexane prior to use.

Preparation of Zn^0

To a beaker was added powdered crude zinc metal (c.a. 200 g), and on top of this was added $HCl_{aq.}$ (500 mL, 1 M). The solution was stirred rapidly for c.a. 18 h to yield a silver suspension. The suspension was filtered through a glass frit, and washed extensively with distilled water. The filter cake was then washed with EtOH, and finally Et_2O. The filter cake was then dried to the greatest extent possible under vacuum, before being carefully transferred to a round bottom flask. The solid was dried extensively under high vacuum, with a heat gun being utilized to drive off residual solvent. The flask is back-filled with Argon, and capped with a septa to yield homogenous activated Zn^0. *NOTE*: Two traps are necessary in this instance, as microparticulate Zn^0 can enter the Schlenk line. *NOTE*: Zn^0 is pyrophoric, storage under inert gas is a necessity.

Preparation of NBS

To an amount of boiling distilled water (c.a. 250–750 mL) is added crude NBS. The solution is continually heated to c.a. 95 ^oC, and stirred rapidly. NBS is added until it no longer dissolves, at which point extra water was added to yield a homogenous solution once again. The solution was filtered through a glass frit and allowed to cool to room temperature before being placed into a fridge to cool for *c.a.* 18 h. The subsequent yellow solution and white crystals are filtered, and crystals dried under high vacuum. *NOTE*: Cooling the solution below 0 ^oC will freeze the solution, rendering it impossible to filter.

Preparation of *p*-nitrobenzoyl chloride

To a round bottom flask was added *p*-nitrobenzoyl chloride (pale yellow solid, c.a. 5.7 g, 20 mmol), and toluene (50 mL). The mixture was heated to 90 ^{o}C and stirred until no solid remained. The solution was added to cool to R.T. before being chilled to –20 ^{o}C for 1 h. The solution was filtered, and white needles were collected. The filtrate was concentrated and yielded a vibrant yellow oil (50 ^{o}C, 50 mbar). Upon exposing the oil to high vacuum (*c.a.* < 2 mbar), the residual toluene was liberated, and yellow crystals appeared. Other methods were trialed (use of either $SOCl_2$ or an acid wash) however both of these returned less of the desired material.

Where precursors and targets have been prepared following the literature, the individual references were cited in the corresponding chapters. The synthesis of **4.55** has been reported previously but full characterization was unavailable.[326]

In several cases, the preparation of chlorins presented in Chapter 3 has been performed in collaboration with Z. Melissari. Further, compounds were previously unknown or incompletely characterized and have been prepared by Z. Melissari, with full experimental details available elsewhere.[447]

7.1.2 Photophysical General

The photophysical analyses presented in Chapter 3 were performed by Z. Melissari, and the procedures and results can be found elsewhere.[447]

The absorption spectra were recorded in THF at room temperature and molecular extinction coefficients were calculated from Beer Lambert‘s law A = ε.c.l, where A the absorbance of the molecule at specific wavelength; ε the molar extinction coefficient; c the concentration of the sample in the cuvette; l the length of the light path (the width of the cuvette 1 cm).

The corresponding tetrapyrroles were dissolved in THF, or DMSO, and their absorbance in the UV-Vis spectrum was adjusted to ca. 0.10 at the wavelength of excitation. Steady-state fluorescence emission spectra were obtained upon excitation at 424 nm for all tetrapyrroles. Fluorescence quantum yields (Φ_f) were calculated with H_2TPP in toluene as standard,[335] (Φ_f = 0.07) and determined by equation 1.

$$\frac{\emptyset_x}{\emptyset_R} = \frac{(1-10^{-A_R})}{(1-10^{-A_x})} \cdot \left(\frac{{n_x}^2}{{n_R}^2}\right) \cdot \left(\frac{\int I_{PL}(X)}{\int I_{PL}(R)}\right) \ldots\ldots\ldots\ldots \boldsymbol{Eq.\,4.1}$$

where Φ is the quantum yield; A_R is the absorbance of the species at the exciting wavelength λ, n is the refractive index of the solutions, and I_{PL} is the integrated area under the corrected emission spectrum.

The same equations were applied to the SOQY determinations.

The corresponding chlorins were dissolved in DMSO and their absorbance in the UV-Vis spectrum was adjusted to ca. 0.10 at the wavelength of excitation. Direct detection of the luminescence emission of $^1O_2$ at 1275 nm was achieved upon excitation at 418 nm. Singlet oxygen quantum yields (Φ_Δ) were calculated by equation 4.1 with phenalenone used as a reference (Φ_Δ = 0.96 ±0.02).[336] The wavelength range of the emission was recorded from 1150 nm to 1350 nm; 15 s integration time; 14 nm excitation slit; 40 nm emission slit. Subscripts X and R refer to the unknown and reference solutions, respectively.

7.1.3 Biology General

Cell culture and preparation of PS Candidate stock solutions

The mouse 4T1 breast cancer cell line was purchased from American Type Culture Collection (AATC). Cells were maintained in Dulbescco's Modified Eagle's Medium, DMEM (Sigma) supplemented with 10% inactivated fetal bovine serum and 1% penicillin/streptomycin and kept at 37 °C in a humidified incubator with 5% CO_2. Cells were detached using trypsin-EDTA (Sigma), counted using a Neubauer chamber, and seeded at the desired intensity in cell culture plates.

Stock solutions of each PS Candidate were prepared in DMSO (Sigma) and passed through sterile 0.22 μm filters. These were stored at –18 °C, and were thawed completely (37 °C) prior to use. Concentration was confirmed by measuring the absorbance of diluted samples in THF (Lambert-Beer law). Before each experiment, the stock solution of each PS candidate was diluted in culture medium at the indicated concentration and added to the cells.

Cellular viability by Alamar blue

4T1 (7,000 cells/well) cells were seeded in 96-well plates. After 24 h, PS Candidates were added to the cells in a concentration ranges specified. All concentrations were tested in triplicate. After an incubation period of 24 h, the cells were washed 3 × with 200 µL of PBS. For dark toxicity assays, these cells were incubated for a further 24 h.

In phototoxicity assays, the cells were pre-incubated with the PS candidates for 24 h. Then, they were washed with 3× with 200 µL of PBS, then the medium was changed to RPMI (Roswell Park Memorial Institute Medium) as to mitigate phenol red absorption. The cells were then irradiated with a 415 nm LED at the light dose of either 1 or 2.5 J cm^{-2}. The light dose was corrected considering the overlap between the LED and the PS Candidate spectra.[350] After irradiation, the medium was then swapped back to DMEM.

In both experiments, after the additional incubation of 24 h, cell viability was determined using the Alamar blue (resazurin) assay. Briefly, the cells were incubated for 2 h with resazurin (Sigma) and the fluorescence of its metabolic product was determined using a Synergy HT Multi-mode microplate reader (Biotek) (528/20 nm excitation and 590/35 nm emission filters). The mean of each triplicate was normalized as a function of untreated cells, which were assumed to metabolize 100% of resazurin.

Cellular internalization by flow cytometry

4T1 (40,000 cells/well) were seeded in 24-well plates and left to adhere for 24 h. Afterwards, the cells were incubated with **H_2P**, **ZnP** and **ZnC^1** at a concentration of 2 µM. After different incubation times (from 2 h to 24 h), the cells were washed with 2× with 200 µL of PBS, detached using trypsin-EDTA, and centrifuged. The obtained pellet was resuspended in PBS, the PBS was then aspirated, and the cells were fixed with paraformaldehyde (4% PFA in PBS). The cells were left for 0.5 h in the dark, and then washed with PBS. Fixed cells were not kept for longer than 48 h. The cells were resuspended in PBS and analyzed on a Novocyte 3000 cytometer (ACEA). The fluorescence of the tetrapyrrole was measured upon excitation with a

405 nm laser and detection using the VL4 (615/24 nm) or VL5 (675/30 nm) filters, dependent upon the fluorescence spectra of the tetrapyrrole. Data is presented as mean fluorescence normalized to the mean fluorescence of untreated cells at each time point.

Evaluation of ROS Production by APF and DHE

Stock solution of the PS candidates (**H_2P**, **ZnC^1**) were made to a concentration of 2 μM in PBS. Both probes were diluted from stock solutions (MeOH) to a working concentration of 5 μM in PBS. The concentration of the PS candidate was varied whilst that of the probe was not. Wells were added which contained only the probe, and only the PS candidate. All wells were in triplicates.

The plate used was analyzed with Synergy HT Multi-mode microplate reader (Biotek) to discern any autofluorescence prior to irradiation. The plate was irradiated for 0.5 J cm^{-2} at a time (time dependent on measured homogenous power output of 415 nm LED prior to beginning the experiment), and then the fluorescence was analyzed (485/20 nm exc. and 530/20 nm detection for APF, 485/20, 590/35 for DHE). This was repeated until a total light dose of 2.5 J cm^{-2} had been administered.

The fluorescence data was normalized (in all cases) by subtraction of autofluorescence from the reading before normalizing against the fluorescence response of the probe. Results shown are from two independent experiments.

7.2 Synthesis and Characterization

[17,18-dihydyo-18-18-dimethyl-10-(4-bromophenyl)porphyrinato]zinc(II) – 3.36a

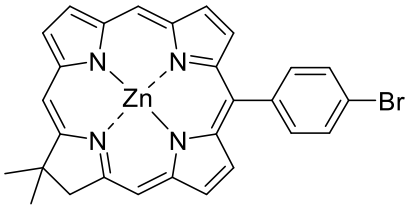

3.36a

To one flask was added 2,3,4,5-tetrahydro-1,3,3-trimethyldipyrrin **3.18** (90 mg, 0.473 mmol), 1-bromo-9-formyl-5-(4-bromophenyl)dipyrromethene **3.40a** (206 mg, 0.505 mmol) and anhydrous CH_2Cl_2 (10.8 mL). In another flask, *p*-TsOH.H_2O (472 mg, 2.48 mmol, ≈ 5 eq.) was dissolved in anhydrous MeOH (6.25 mL). The two solutions were combined and stirred at 20 °C for 0.5 h, at which point 2,2,6,6-tetramethylpiperidine (0.63 mL, 3.71 mmol, 7.5 eq.) was added and the mixture was concentrated. The resulting yellow solid was suspended in anhydrous MeCN (50 mL), and further 2,2,6,6-tetramethylpiperidne (2.10 mL, 12.40 mmol, 25 eq.) was added along with anhydrous zinc acetate (1.370 g, 7.50 mmol, 25 eq.), and silver triflate (0.387 g, 1.508 mmol, 3 eq.). The resulting mixture was stirred at 90 °C for 21 h. Excess solvent was removed under reduced pressure, and the crude reaction mixture was purified via flash column chromatography (silica, CH_2Cl_2:C_6H_{14}, 1:1). The product eluted in the second fraction, which was blue in colour. Excess solvent was removed under reduced pressure to yield the product as a dark green-purple powder (97 mg, 173.6 µmol, 36.7 %).

^{1}H NMR ($CDCl_3$, 400 MHz): δ = 9.65 (s, 1H), 9.11 (d, *J* = 4.4 Hz, 1H), 8.89 (d, *J* = 4 Hz, 1H), 8.80 (d, *J* = 4.4 Hz, 1H), 8.73 (s, 1H), 8.66 (s, 1H), 8.65 (s, 1H), 8.50 (d, *J* = 4.4 Hz, 1H), 7.96 (d, *J* = 8.4 Hz, 2H), 7.83 (d, *J* = 8 Hz, 2H), 4.55 (s, 2H), 2.04 (s, 6H). ^{13}C{^{1}H} NMR ($CDCl_3$, 101 MHz): δ = 174.4, 159.6, 154.3, 153.3, 146.7, 146.3, 145.7, 141.5, 135.2, 133.3, 132.9, 129.9, 128.9, 128.4, 127.7, 127.1, 122.1, 109.6, 97.2, 94.5, 50.4, 45.5, 31.7, 31.1. MALDI-TOF HRMS: calcd. for $C_{28}H_{21}N_4ZnBr$ 556.0241, found: 556.0256 [M^+]. R_F = 0.78 (silica, CH_2Cl_2:C_6H_{14}, 1:1). UV-Vis (CH_2Cl_2): λ_{abs} (log ε) = 384 (5.22), 404 (5.80), 608 (5.00). M.P.: >220 °C.

[17,18-dihydyo-18-18-dimethyl-10-(naphthalen-1-yl)porphyrinato]zinc(II) – 3.36b

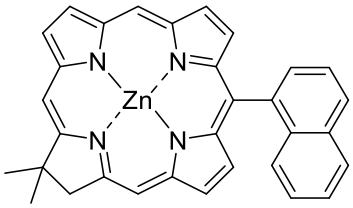

3.36b

To one flask was added 2,3,4,5-tetrahydro-1,3,3-trimethyldipyrrin **3.18** (33.6 mg, 176.6 µmol), 1-formyl-9-bromo-5-(naphthalen-1-yl)dipyrromethene **3.40b** (57.8 mg, 152.4 µmol), and anhydrous CH_2Cl_2 (4 mL). In a separate flask, *p*-TsOH.H_2O (111 mg, 0.583 mmol) and anhydrous MeOH (1 mL) were added. The two solutions were mixed and stirred at 20 °C for 0.5 h whilst protected from light. After which time, 2,2,6,6-tetramethylpiperidine (0.16 mL, 0.948 mmol) was added and the solution concentrated. The resulting solid was suspended in anhydrous MeCN (20 mL). Further 2,2,6,6-tetramethylpiperidine (0.55 mL, 3.26 mmol) was added along with anhydrous zinc acetate (358 mg, 1.95 mmol) and silver triflate (100 mg, 0.390 mmol). The solution was then heated at 90 °C for 20 h whilst protected from light. Excess solvent was removed under reduced pressure, and the residue was purified via flash column chromatography (silica, CH_2Cl_2:C_6H_{14}, 1:1). The product eluted in the second fraction, which was blue in colour. Excess solvent was removed under reduced pressure to yield the product as a dark green-blue solid (29.0 mg, 54.7 µmol, 35.9 %).

^{1}H NMR ($CDCl_3$, 400 MHz): δ = 9.64 (s, 1H), 9.11 (d, *J* = 4 Hz, 1H), 8.80 (d, *J* = 4.4 Hz, 1H), 8.78 (d, *J* = 4 Hz, 1H), 8.72 (s, 1H), 8.66 (s, 1H), 8.56 (d, 1H, *J* = 4.4 Hz), 8.44 (d, *J* = 4.4 Hz, 1H), 8.26–8.22 (m, 2H), 8.16 (dd, *J* = 2 x 1.2, 6.8 Hz, 1H), 8.10 (d, *J* = 8 Hz, 1H), 7.84–7.80 (m, 1H), 7.48–7.44 (m, 1H), 7.19–7.16 (m, 1H), 7.08–7.04 (m, 1H), 4.56 (s, 2H), 2.07 (s, 3H), 2.05 (s, 3H). ^{13}C{^{1}H} NMR ($CDCl_3$, 101 MHz): δ = 171.1, 159.5, 154.1, 153.3, 148.1, 146.1, 139.8, 136.4, 133.2, 133.1, 133.0, 131.6, 129.2, 128.5, 128.3, 127.9, 127.4, 127.1, 126.0, 125.6, 124.4, 109.7, 97.1, 50.5, 31.1(7), 31.1(0). MALDI-TOF HRMS: calcd. for $C_{32}H_{24}N_4Zn$ 528.1292 found. 528.1301 [M^+]. R_F = 0.46 (silica, CH_2Cl_2:C_6H_{14}, 1:1). UV-Vis (CH_2Cl_2): λ_{abs} (log ε) = 386 (5.07), 404 (5.80), 609 (5.03). M.P.: >250 °C.

17,18-dihydro-18-18-dimethyl-10-(4-bromophenyl)porphyrin – 3.41a

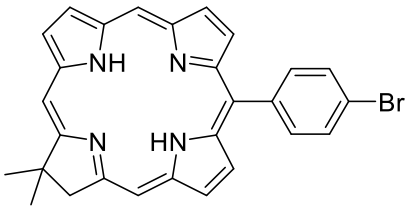

3.41a

To a round bottom flask was added **3.36a** (54.0 mg, 96.6 µmol), and CH_2Cl_2 (10 mL). To the resulting solution was added trifluoroacetic acid (0.25 mL, 3.27 mmol), and the mixture was stirred at 20 ºC for 1 h. A further aliquot of trifluoroacetic acid (0.25 mL, 3.27 mmol) was added and the solution stirred for a further 1 h at 20 ºC. The reaction mixture was quenched with the addition of sat. $NaHCO_3$ soln. The layers were separated, and the organic phase was washed with sat. $NaHCO_3$ soln. (1 x 25 mL), water (1 x 25 mL), brine (1 x 25 mL) and dried ($MgSO_4$). The resulting solution was passed through a pad of silica (CH_2Cl_2) and excess solvent was removed under reduced pressure to yield the product as a dark green solid (22.0 mg, 44.4 µmol, 46 %).

^{1}H NMR (600 MHz, $CDCl_3$): δ = 9.88 (s, 1H), 9.25 (d, *J* = 4.4 Hz, 1H), 9.03 (s, 1H), 9.01 (d, *J* = 4.2 Hz, 1H), 8.98 (d, *J* = 4.4 Hz, 1H), 8.96 (s, 1H), 8.84 (d, *J* = 4.6 Hz, 1H), 8.81 (d, *J* = 4.6 Hz, 1H), 8.66 (d, *J* = 4.2 Hz, 1H), 8.05 (d, *J* = 8.1 Hz, 2H), 7.90 (d, *J* = 8.0 Hz, 2H). 4.62 (s, 2H), 2.08 (s, 6H), -1.94 (s, 1H), -2.31 (s, 1H) ppm. ^{13}C{^{1}H} NMR (151 MHz, $CDCl_3$): δ = 175.6, 163.1, 152.2, 151.1, 141.1, 140.9, 139.6, 135.6, 135.0, 134.4, 132.7, 131.9, 130.1, 128.5, 128.0, 123.9, 122.4, 119.9, 107.4, 97.1, 94.5, 52.1, 46.6, 31.3 ppm. ^{15}N/^{1}H-HSQC ($CDCl_3$): 134.06 (N^{21}), 134.12 (N^{23}) ppm. HRMS (APCI) Calcd.: 495.1179 for $C_{28}H_{24}N_4Br$, Found.: 495.1181 $[M+H]^+$. R_F = 0.71 (silica, CH_2Cl_2:C_6H_{14}, 1:1). UV–Vis (CH_2Cl_2) λ_{abs} (log ε) = 395 (5.00), 407 (5.08), 491 (3.90), 503 (4.00), 586 (3.56), 638 (4.43) nm. M.P.: 248–250 °C.

17,18-dihydro-18,18-dimethyl-10-(naphthalen-1-yl)porphyrin – 3.41b

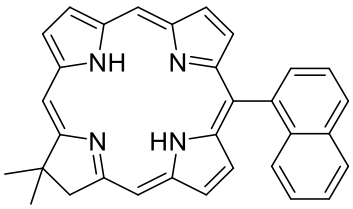

3.41b

To a round bottom flask was added **3.36b** (36.0 mg, 67.9 µmol) and CH_2Cl_2 (7 mL). To the resulting solution was added trifluoroacetic acid (0.20 mL, 2.62 mmol), and the mixture was stirred at 20 ºC for 1 h. TLC indicated the completion of the reaction and thus the reaction mixture was quenched with sat. $NaHCO_3$ soln. The layers were separated, and the organic phase was washed with sat. $NaHCO_3$ soln. (1 x 25 mL), water (1 x 25 mL), brine (1 x 25 mL) and dried ($MgSO_4$). The resulting solution was passed through a pad of silica (CH_2Cl_2) and excess solvent was removed under reduced pressure to yield the product as a dark green solid (13.0 mg, 27.9 µmol, 41 %).

^{1}H NMR (600 MHz, $CDCl_3$): δ = 9.87 (s, 1H), 9.26 (d, *J* = 4.3 Hz, 1H), 9.03 (s, 1H), 8.99 (d, *J* = 4.3 Hz, 1H), 8.96 (s, 1H), 8.89 (d, *J* = 4.2 Hz, 1H), 8.75 (d, *J* = 4.5 Hz, 1H), 8.58 (d, *J* = 4.5 Hz, 1H), 8.38 (d, *J* = 4.2 Hz, 1H), 8.27 (d, *J* = 8.4 Hz, 1H), 8.24 (d, *J* = 6.7 Hz, 1H), 8.14 (d, *J* = 8.4 Hz, 1H), 7.87–7.84 (m, 1H), 7.51– 7.48 (m, 1H), 7.24 (d, *J* = 8.7 Hz, 1H), 7.10–7.08 (m, 1H). 4.66 (s, 4H), 2.10 (s, 3H), 2.09 (s, 3H), -1.81 (s, 2H), -2.19 (s, 2H) ppm. ^{13}C{^{1}H} NMR (151 MHz, $CDCl_3$): δ = 175.3, 163.2, 153.5, 151.1, 140.9, 139.7, 139.1, 136.6, 136.0, 134.4, 133.1, 132.7, 132.2, 132.1, 128.6, 128.5, 128.4, 128.3, 128.0, 126.1, 125.8, 124.4, 123.8, 123.3, 118.9, 107.4(6), 107.4(5), 97.0, 94.6, 52.2, 46.6, 31.4, 31.3 ppm. ^{15}N/^{1}H-HSQC ($CDCl_3$): 134.5 (N^{21}), 133.5 (N^{23}) ppm. HRMS (APCI) Calcd.: 467.2230 for $C_{32}H_{27}N_4$, Found.: 467.2234 $[M+H]^+$. R_F = 0.66 (silica, CH_2Cl_2:C_6H_{14}, 1:1). UV–Vis (CH_2Cl_2) λ_{abs} (log ε) = 394 (5.15), 407 (5.24), 494 (4.11), 501 (4.17), 587 (3.70), 639 (4.64) nm. M.P.: > 300 °C.

1-(4-nitrophenyl)-5-(3,4,5-trimethoxyphenyl)dipyrromethane – 4.52

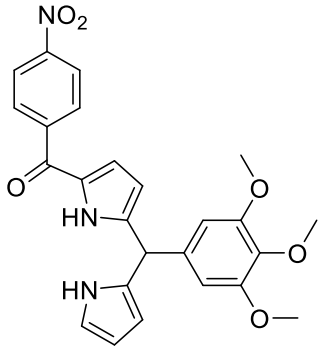

4.52

To an oven and flame dried round bottom flask was added 5-(3,4,5-trimethoxyphenyl)dipyrromethane **4.51** (1.974 g, 6.32 mmol) and anhydrous THF (12 mL). Added to the solution was EtMgBr (1M in THF, 16 mL, 16 mmol), and the resulting solution was stirred at r.t. for 10 mins, before being cooled to – 78 °C. Added in one portion was *S*-2-pyridyl 4-nitrobenzothioate **4.55** (1.630 g, 6.34 mmol), and the solution was stirred at – 78 °C for 10 mins, before being allowed to warm to r.t., and subsequently stirred at r.t. for 0.5 h. To the reaction mixture was added CH_2Cl_2 (200 mL), and sat. $NaHCO_3$ soln. (200 mL). The solution was then taken to pH 7 with sat. NH_4Cl soln. The layers were separated, and the aqueous layer was extracted with CH_2Cl_2 until it ran clear. The organic extracts were combined, washed with brine (1 × 100 mL) and dried ($MgSO_4$). Excess solvent was removed at reduced pressure. To the residual solid was added *i*PrOH (*c.a.* 250 mL) and the mixture heated at 130 °C for 2 h, and immediately filtered through a sintered glass frit. The yellow solid was washed with *i*PrOH until it ran clear. The solid was then washed through with CH_2Cl_2 until it became yellow, and discarding the initial filtrate (10 mL or so, black). Excess solvent was removed under reduced pressure to yield the desired **4.52** as a vibrant yellow solid (1.997 g, 4.33 mmol, 68%).

^{1}H NMR (400 MHz, DMSO-D_6): δ = 12.17 (br s, 1H), 10.67 (br s, 1H), 8.33 (d, *J* = 8.8 Hz, 2H), 7.99 (d, *J* = 8.8 Hz, 2H), 6.74 (m, 1H), 6.67 (m, 1H), 6.56 (s, 2H), 6.14 (m, 1H), 5.94 (m, 1H), 5.80 (m, 1H), 5.51 (s, 1H), 3.71 (s, 6H), 3.63 (s, 3H) ppm. ^{13}C{^{1}H} NMR (101 MHz, DMSO-D_6): δ = 181.2, 152.7, 148.9, 144.3, 144.2, 137.9, 136.2, 131.2, 129.7, 129.2, 123.6, 121.2, 117.5, 109.9, 107.0, 106.5, 105.7, 59.9,

55.9, 43.4 ppm. HRMS (ESI): calcd. for $C_{25}H_{22}N_3O_6$ 460.1503, found: 460.1497 $[M]^{+\cdot}$. R_F = 0.51 (silica, EtOAc:C_6H_{14} 1:1, visualization with Br_2). M.P.: 232 – 233 °C (dec.)

***S*-2-pyridyl 4-nitrobenzoate – 4.55**

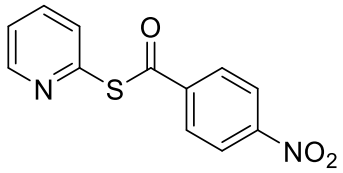

4.55

To a round bottom flask was added 2-mercaptopyridine **4.54** (5.68 g, 51.12 mmol), and CH_2Cl_2 (250 mL). Added dropwise over 0.5 h was a solution of *p*-nitrobenzoyl chloride **4.53** (9.99 g, 53.89 mmol) in CH_2Cl_2 (100 mL). The solution was stirred at r.t. for 1 h. Upon mixing of the solutions a color change of yellow to orange was observed, followed by the formation of an orange precipitate approximately 0.5 h after complete addition of the solution. A minor exotherm was also noted throughout the addition process. The solution was diluted with CH_2Cl_2 to 600 mL, and subsequently washed with $NaOH_{(aq)}$ (2M, 1 × 200 mL), H_2O (1 × 300 mL) and brine (1 × 300 mL). The organic phase was dried ($MgSO_4$) and excess solvent was removed at reduced pressure. The crude solid was dried under vacuum for 1 h. The crude product was purified via hot recrystallization from EtOAc (c.a. 400 mL). The product was filtered and dried under high vacuum to yield the product as colorless needles (9.295 g, 35.71 mmol, 69%).

^{1}H NMR ($CDCl_3$, 400 MHz): δ = 8.71 (m, 1H), 8.35 (d, *J* = 8.9 Hz, 2H), 8.18 (d, *J* = 8.9 Hz, 2H), 7.83 (m, 1H), 7.73 (m, 1H), 7.39 (m, 1H) ppm. ^{13}C{^{1}H} NMR ($CDCl_3$, 101 MHz): δ = 188.3, 150.9, 150.3, 141.3, 137.7, 130.9, 128.7, 124.3, 124.2 ppm. R_F = 0.58 (silica, EtOAc:C_6H_{14} 1:1, UV). M.P. = 154–156 °C.

1-bromo-9-(4-nitrobenzoyl)-5-(3,4,5-trimethoxylphenyl)dipyrromethane – 4.56

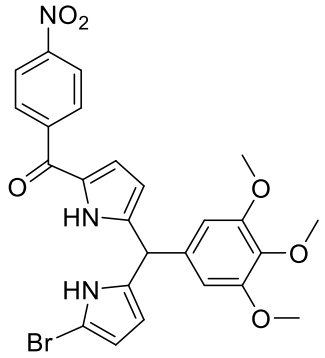

4.56

To a round bottom flask was added **4.52** (785 mg, 1.70 mmol), and anhydrous THF (15 mL). The resulting solution was cooled to -78 °C and added was recrystallized *N*-bromosuccinimide (313 mg, 1.76 mmol, 1.03 eq.) The mixture was stirred at -78 °C for 1 h, at which point H_2O and EtOAc (30 mL, each) were added. The solution was allowed to warm to room temperature. The layers were separated, and the organic phase was washed with H_2O (2 × 100 mL), brine (1 × 100 mL) and dried ($MgSO_4$). Excess solvent was removed at reduced pressure. TLC analysis of the crude product indicated c.a. less than 5% **4.52** and less than 5% again of the di-brominated species and thus this was directly carried forward.

^{1}H NMR (400 MHz, $CDCl_3$) δ = 9.44 (s, 1H), 8.33 (d, *J* = 8.8 Hz, 2H), 7.98 (d, *J* = 8.8 Hz, 2H), 6.80 (m, 1H), 6.41 (s, 2H), 6.18–6.16 (m, 1H), 6.12 (m, 1H), 5.93 (m, 1H), 5.42 (s, 1H), 3.87 (s, 3H), 3.80 (s, 6H). HRMS (APCI): $C_{25}H_{22}N_3O_6Br$, Obsvd. 538.0614 $[M]^-$. HRMS (APCI): $C_{25}H_{21}N_3O_6Br_2$ Obsvd. 617.9711 $[M]^-$. R_F = 0.67 (silica, EtOAc/C_6H_{14}, 1/1,visualization with Br_2 stain).

4-bromo-2-((2*R*,3*R*)-4-(4-bromo-1-tosyl-1*H*-pyrrol-2-yl)-1,3-dinitrobutan-2-yl)-1-tosyl-1*H*-pyrrole & 4-bromo-2-((2*S*,3*S*)-4-(4-bromo-1-tosyl-1*H*-pyrrol-2-yl)-1,3-dinitrobutan-2-yl)-1-tosyl-1*H*-pyrrole – 4.65

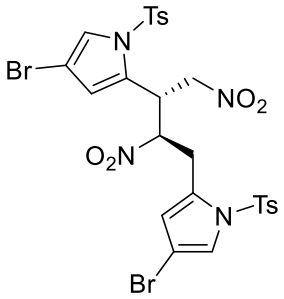

(*R*,*R*)-**4.65**

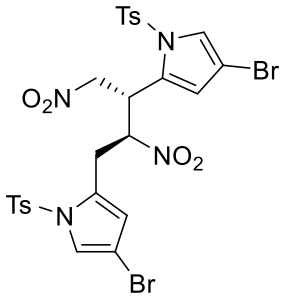

(*S*,*S*)-**4.65**

To **4.60** (46.410 g, 125.0 mmol) was added THF (600 mL). The resulting solution was stirred and purged with Ar for 0.5 h whilst being cooled to –10 °C (ice/NaCl/acetone bath). Added portion wise was $LiBH_4$ (2.859 g, 131.2 mmol). The solution was stirred for 0.25 h, then sat. aq. NH_4Cl was added (250 mL) and the solution was stirred for 5 mins. The layers were separated, and the aqueous layer was extracted with EtOAc (1 × 300 mL). The organic extracts were combined, washed with brine (1 × 200 mL) and dried ($MgSO_4$). Excess solvent was removed under reduced pressure and the residue was dried under high vacuum for 2 h to yield a light brown solid. Added to the solid was *i*PrOH (600 mL), and the solution was heated to 100 °C for c.a. 15 mins. The solution was immediately filtered (sintered glass frit) to yield (*R*,*R*)-**4.65,** (*S*,*S*)-**4.65** as an off-white powder (5.040 g, 6.8 mmol, 10.9%). The filtrate was allowed to cool to room temperature and stored at – 10 °C overnight to yield **4.61** as light brown crystals (23.890 g, 64.3 mmol. 51%).

Data for **4.65**: ^{1}H NMR ($CDCl_3$, 600 MHz): δ = 7.77 (d, *J* = 8.3 Hz, 2H), 7.61 (d, *J* = 8.3 Hz, 2H), 7.42 (s, 1H), 7.38 (d, *J* = 8.3 Hz, 2H), 7.36 (d, *J* = 8.2 Hz, 2H), 7.30 (d, *J* = 1.6 Hz, 1H), 6.17 (d, *J* = 1.0 Hz, 1H), 5.99 (s, 1H), 5.31 (dd, *J* = 11.0, 3.3 Hz, 1H), 4.94 (dd, *J* = 12.6, 6.4 Hz, 1H), 4.78 (dd, *J* = 14.6, 6.4 Hz, 1H), 4.46 (dd, *J* = 14.5, 7.6 Hz, 1H), 3.29 (dd, *J* = 15.6, 1.9 Hz, 1H), 3.10 (dd, *J* = 15.7, 11.3 Hz, 1H), 2.45 (s, 3H), 2.44 (s, 3H) ppm. ^{13}C NMR (151 MHz, $CDCl_3$): δ = 146.8, 146.2, 135.2, 134.6, 130.7(2), 130.7(0) 130.6, 128.0, 127.4, 127.0, 123.9, 122.8, 118.5, 117.2, 100.9(5), 100.9(3), 87.8, 74.2, 37.8, 27.9, 21.9, 21.8. HRMS (ESI-) *m/z* calcd. for

$[C_{26}H_{24}N_4O_8S_2Br_2+Cl]^-$, $[M+Cl]^-$: 776.9096, found: 776.9075. R_F = 0.70 (silica, CH_2Cl_2:C_6H_{14}, 3:1). M.P.: 220–223 °C (dec.), lit.[1] 115–117 °C.

5-bromo-N^1,N^1,N^3,N^3-tetraethylisophthalamide – 4.68

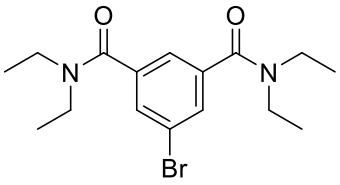

4.68

To a round bottom flask was added N^1,N^1,N^3,N^3-tetraethylisophthalamide **4.67** (14.25 g, 50 mmol) and conc. H_2SO_4 (35 mL, 12 M). The mixture was stirred at 50 °C for 0.5 h, at which point in one portion *N*-bromosuccinimide (10.23 g, 57.5 mmol) was added. The resulting mixture was heated at 50 °C and stirred for 24 h. The reaction mixture was then poured onto ice (500 g) and allowed to warm to room temperature. The solution was neutralized ($NaHCO_3$). The layers were separated, and the aqueous layer was extracted with EtOAc (5 × 400 mL). The organic extracts were combined, dried ($MgSO_4$), and excess solvent was removed at reduced pressure. The residue was adsorbed onto silica (THF) and purified via column chromatography (silica, EtOAc). Column chromatography yielded **4.67** (5.05 g, 18.3 mmol) and a mixture of both **4.67** and **4.68**. This mixture was exposed to the same reaction conditions and purified accordingly to eventually yield the desired product as the second colorless fraction. The crude **4.68** was recrystallized from diethyl ether to yield colorless needles (5.720 g, 16.1 mmol, 32%).

^{1}H NMR (400 MHz, $CDCl_3$): δ = 7.51 (d, *J* = 1.2 Hz, 2H), 7.25 (m, 1H), 3.50 (s, 4H), 3.22 (s, 4H), 1.20 (s, 6H), 1.08 ppm (s, 6H). $^{13}C\{^1H\}$ NMR (100 MHz, $CDCl_3$): δ = 168.8, 139.4, 130.0, 122.8, 122.8, 43.5, 39.5, 14.3, 12.9 ppm. HRMS (ESI): m/z Calcd. 377.0835. Found: 377.0839 $[C_{16}H_{23}N_2O_2Br+Na]^+$. R_F = 0.38 (silica, EtOAc, UV). M.P. = 91–93 °C.

N^1,N^1,N^3,N^3-tetraethyl-5-((triisopropylsilyl)ethynyl)isophthalamide – 4.69

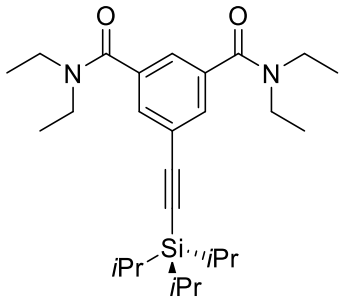

4.69

To an oven and flame dried Schlenk tube was added; $Pd(OAc)_2$ (22.0 mg, 98 µmol), CuI (10.0 mg, 52.5 µmol), PPh_3 (35 mg, 133.4 µmol), and 5-bromo-N^1,N^1,N^3,N^3-tetraethylisophthalamide **4.68** (711 mg, 2.00 mmol). All solids were dried under high vacuum (< 0.1 mbar) at r.t. for 1 h. The flask was backfilled with Ar and added to it was anhydrous Et_3N (8 mL), the mixture subsequently underwent three freeze-pump-thaw cycles. To the stirring solution was added TIPS-acetylene (1.0 mL, 4.46 mmol) and the solution was heated to 50 °C for 1 h. Excess solvent was removed at reduced pressure, and the residue was passed through a silica pad (THF:C_6H_{14}, 1:1). Excess solvent was removed at reduced pressure to yield a brown oil which was directly carried forward.

^{1}H NMR (400 MHz, $CDCl_3$): δ = 7.49 (d, *J* = 1.5 Hz, 2H), 7.27 (t, *J* = 1.5 Hz, 1H), 3.53 (s, 4H), 3.25 (s, 4H), 1.24 (s, 6H), 1.12 ppm (m, 27H). ^{13}C{^{1}H} NMR (100 MHz, $CDCl_3$): δ = 169.8, 137.8, 130.5, 124.6, 123.8, 105.5, 93.0, 43.54, 39.53, 18.8, 14.4, 13.0, 11.4 ppm. HRMS (APCI): m/z Calcd. for $C_{27}H_{45}N_2O_2Si$ 457.324636. Found: 457.324482 $[M+H]^+$. R_F = 0.55 (silica, THF:C_6H_{14} 1:1, UV).

5-(4-formylphenyl)-*N*^{1},*N*^{1},*N*^{3},*N*^{3}-tetraethylisophthalamide – 4.70b

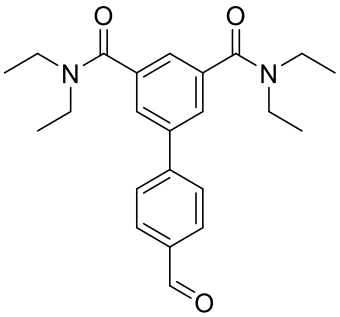

4.70b

To a flame and oven dried Schlenk tube was added 5-bromo-*N*^{1},*N*^{1},*N*^{3},*N*^{3}-tetraethylisophthalamide **4.68** (351 mg, 0.988 mmol), 4-formylphenylboronic acid (414 mg, 2.76 mmol, 2.8 eq.), K_2CO_3 (400 mg, 2.89 mmol), and $Pd(PPh3)_4$ (31 mg, 26.8 µmol, 2.7 mol%). All solids were dried under high vacuum (< 0.1 mbar) at r.t. for 1 h. The flask was backfilled with Ar and added to it was anhydrous THF (10 mL) and the mixture subsequently underwent three freeze-pump-thaw cycles. The solution was then stirred for 18h at 60 °C. The RM was then passed through a silica pad (THF). This crude was then purified *via* column chromatography (silica, THF:C_6H_{14}, 1:1). ^{1}H NMR analyses of the assumed product showed contamination with Ph_3PO in a ratio of **4.70b**:Ph_3PO at roughly 3:1.

To this was then added *i*PrOH (50 mL) and $ZnCl_2$ (411 mg, 3 mmol, > 3 eq.), and the solution was stirred at r.t. for 18 h. The solution was filtered. EtOAc and H_2O were both added. The layers were separated, and the aqueous layer was extracted with EtOAc (4 × 50 mL). The organic extracts were combined, washed with brine (1 × 100 mL), dried ($MgSO_4$) and excess solvent was removed at reduced pressure.

The desired product was not isolated.

^{1}H NMR (400 MHz, $CDCl_3$) δ = 10.06 (s, 1H), 7.97 (d, *J* = 8.3 Hz, 2H), 7.75 (d, J = 8.2 Hz, 2H), 7.67–7.62 (m, 4H), 7.54 (m 1H), 7.45 (m 2H), 7.38 (t, *J* = 1.3 Hz, 1H), 3.57 (d, *J* = 6.1 Hz, 4H), 3.29 (d, *J* = 6.2 Hz, 4H), 1.26 (s, 6H), 1.18 – 1.01 (s, 6H) ppm.

[17,18-dihydro-18,18-dimethyl-5-(4-nitrophenyl)-10-(3,4,5-trimethoxyphenyl)porphyrinato]zinc(II) – 4.74/ZnC[1]

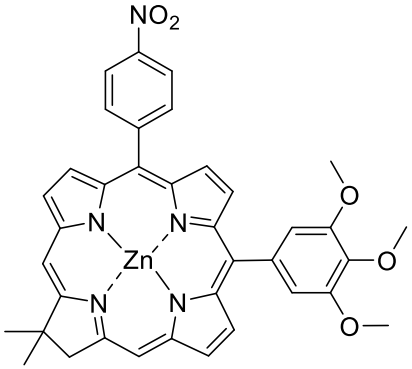

4.74 / **ZnC[1]**

To a round bottom flask was added **4.56** (1.200 g, 2.220 mmol), anhydrous THF (35 mL) and anhydrous MeOH (9 mL). The solution was cooled to 0 °C, and added portion wise over 5 mins was $NaBH_4$ (1.100 g, 29.08 mmol). At t = 0.5 h, TLC analysis (silica, EtOAc:C_6H_{14}, 1:1) indicated complete consumption of **4.56**, at which point, EtOAc (100 mL) and H_2O (50 mL) were both added. The layers were separated, and the aqueous layer was further extracted with EtOAc (3 × 50 mL). The organic extracts were combined, washed with brine (1 × 100 mL), dried ($MgSO_4$), and excess solvent was removed under reduced pressure.

To the residual oil was added anhydrous MeCN (22 mL), and **4.43** (420 mg, 2.207 mmol) and TFA (0.15 mL). The mixture was stirred at r.t. for 0.5 h, before being diluted with anhydrous MeCN (135 mL). Added to the solution was: AgOTf (846 mg, 3.29 mmol), $Zn(OAc)_2$ (3.06 g, 16.67 mmol) and 2,2,6,6-TMPi (5.50 mL). The solution was brought up to 90 °C and stirred for 20 h. Excess solvent was removed at reduced pressure, and the residue was taken up in CH_2Cl_2 and the major green band was eluted on a silica plug (EtOAc:CH_2Cl_2, 1:9). The crude product was further purified via column chromatography (silica, $CHCl_3$:EtOAc, 5:95), and precipitated from $CHCl_3$:C_6H_{14} to yield the desired **4.74** as a green powder (122 mg, 176.5 μmol, 8%).

^{1}H NMR (DMSO-D_6, 400 MHz): δ = 8.80 (d, *J* = 4.5 Hz, 1H), 8.74 (s, 1H), 8.73 (s, 1H), 8.69 (s, 1H), 8.63 (s, 1H), 8.58 (d, *J* = 8.6 Hz, 2H), 8.45 (d, *J* = 4.4 Hz, 1H), 8.37 (d, *J* = 4.4 Hz, 1H), 8.26 (d, *J* = 8.6 Hz, 2H), 8.18 (d, *J* = 4.4 Hz, 1H), 7.28 (s,

2H), 4.55 (s, 2H), 3.95 (s, 3H), 3.87 (s, 6H), 2.00 (s, 6H) ppm. $^{13}C\{^{1}H\}$ NMR (DMSO-D_6, 101 MHz): δ = 171.7, 159.8, 153.9, 151.1, 149.5, 148.0, 147.0, 146.4, 146.0, 145.1, 143.0, 137.4, 137.2, 134.3, 132.0, 129.2, 128.9, 127.8, 123.1, 121.8, 120.2, 115.1, 111.6, 95.3, 93.6, 60.4, 56.1, 49.9, 45.1, 30.6 ppm. Calcd for $C_{37}H_{31}N_5O_5Zn$ $[M]^+$ 689.1617, found, 689.1885. R_F = 0.70 (silica, EtOAc/C_6H_{14}, 1:1). UV–Vis (THF) λ_{abs} (log ε) = 415 (5.30), 518 (3.89), 571 (3.94), 582 (3.95), 616 (4.70) nm. λ_{em} (THF): 624, 680 nm. M.P. = 241–242 °C (dec.)

[17,18-dihydro-18,18-dimethyl-3-bromo-5-(4-nitrophenyl)-10-(3,4,5-trimethoxyphenyl)porphyrinato]zinc(II) – 4.75/ZnC^2

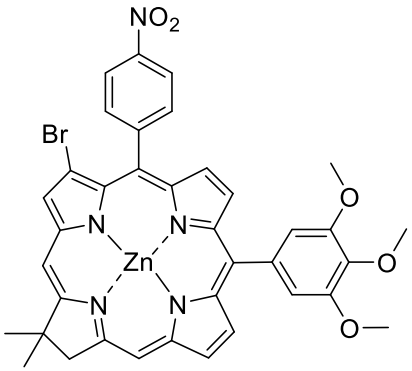

4.75 / ZnC^2

To a round bottom flask was added **4.63** (1.799 g, 4.24 mmol), and anhydrous THF (10 mL). Added in one portion was TBAF in THF (12 mL, 1 M, 12 mmol, 2.83 eq.). The solution was stirred at 40 °C for 1 h, at which point TLC (silica, EtOAc) confirmed the completion of the reaction. The solution was quenched with the addition of sat. NaHCO3 soln. (50 mL). EtOAc (50 mL) was added, and the layers were separated. The aqueous layer was further extracted with EtOAc (2 x 50 mL). The organic extracts were combined, washed with brine (1 x 100 mL), dried (MgSO4). Excess solvent was removed under reduced pressure, and the resultant oil was purified via column chromatography (silica, EtOAc) to yield **4.72**.

To a round bottom flask was added **4.56** (844 mg, 1.561 mmol), anhydrous THF (25 mL) and anhydrous MeOH (6 mL). The solution was cooled to 0 °C, and added portion wise over 5 mins was $NaBH_4$ (714 mg, 19.34 mmol). At t = 0.5 h, TLC analysis (silica, EtOAc:C_6H_{14}, 1:1) indicated complete consumption of **4.56**, at which point, EtOAc (100 mL) and H_2O (50 mL) were both added. The layers were separated, and the aqueous layer was further extracted with EtOAc (3 × 50 mL). The organic extracts were combined, washed with brine (1 × 100 mL), dried ($MgSO_4$), and excess solvent was removed under reduced pressure.

To the residual oil was added anhydrous MeCN (15 mL), and **4.72** (400 mg, 1.486 mmol) and TFA (0.1 mL). The mixture was stirred at r.t. for 0.5 h, before being diluted with anhydrous MeCN (90 mL). Added to the solution was: AgOTf (590 mg, 2.29 mmol), $Zn(OAc)_2$ (2.10 g, 11.45 mmol) and 2,2,6,6-TMPi (4 mL). The solution was

brought up to 90 °C and stirred for 20 h. Excess solvent was removed at reduced pressure, and the residue was taken up in CH_2Cl_2 and the major green band was eluted on a silica plug (EtOAc:CH_2Cl_2, 1:9). The crude product was further purified via column chromatography (silica, $CHCl_3$:EtOAc, 5:95) 95), and precipitated from $CHCl_3$:C_6H_{14} to yield the desired **4.75** as a green powder (82 mg, 106.5 µmol, 7%)

^{1}H NMR (DMSO-D_6, 400 MHz): δ = 8.97 (s, 1H), 8.72 (s, 1H), 8.70 (d, *J* = 4.5 Hz, 1H), 8.61 (s, 1H), 8.59 (d, *J* = 4.5 Hz, 1H), 8.54 (d, *J* = 8.6 Hz, 2H), 8.31 (d, *J* = 4.4 Hz, 1H), 8.13 (d, *J* = 8.6 Hz, 2H), 8.00 (d, *J* = 4.4 Hz, 1H), 7.26 (s, 2H), 4.50 (s, 2H), 3.94 (s, 3H), 3.86 (s, 6H), 1.98 (s, 6H).ppm. ^{13}C{^{1}H} NMR (DMSO-D_6, 101 MHz): δ = 170.7, 160.2, 153.6, 151.1, 150.7, 148.9, 147.4, 146.4, 145.8, 137.7, 137.0, 134.1, 133.0, 128.5, 122.7, 121.6, 120.2, 117.9, 111.8, 97.1, 94.0, 68.5, 60.4, 56.1, 55.8, 49.7, 30.7.ppm. R_F = 0.72 (silica, EtOAc/C_6H_{14}, 1:1). UV–Vis (THF) λ_{abs} (log ε) = 418 (5.37), 520 (3.84), 574 (3.98), 585 (4.02), 618 (4.73) nm. λ_{em} (THF): 622, 676 nm. M.P. 239–240 °C (dec.)

[17,18-dihydro-18,18-dimethyl-3-bromo-5-(4-nitrophenyl)-10-(3,4,5-trimethoxyphenyl)-13-bromoporphyrinato]zinc(II) – 4.75b/ZnC^2-Br

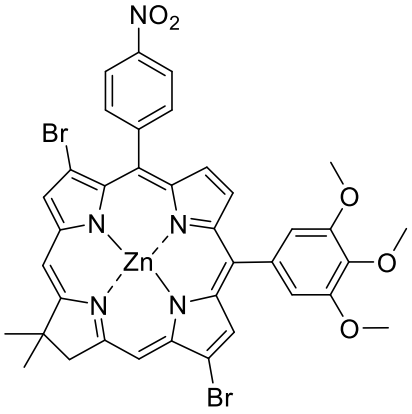

4.75b / **ZnC^2-Br**

Isolated as a by-product from the synthesis of **4.75** (12 mg, 14 µmol, 0.3%)

^{1}H NMR (DMSO-D_6, 400 MHz): δ = 9.00 (s, 1H), 8.71 (s, 1H), 8.65 (s, 1H), 8.63 (s, 1H), 8.54 (d, *J* = 8.7 Hz, 2H), 8.30 (d, *J* = 4.4 Hz, 1H), 8.12 (d, *J* = 8.6 Hz, 2H), 8.00 (d, *J* = 4.5 Hz, 1H), 7.25 (s, 2H), 4.54 (s, 3H), 3.94 (s, 3H), 3.86 (s, 6H), 1.98 (s, 6H) ppm. ^{13}C{^{1}H} NMR (DMSO-D_6, 101 MHz): δ = 171.5, 160.5, 151.1, 147.3, 146.7, 143.8, 137.8, 134.1, 123.2, 121.7, 111.6, 94.7, 93.8, 68.5, 60.4, 56.1, 55.8, 44.9, 30.6. R_F = 0.74 (silica, EtOAc/C_6H_{14}, 1:1). UV–Vis (THF) λ_{abs} = 421, 522, 578, 589, 624 nm.

5,15-bis(3,4,5-trimethoxyphenyl)-10,20-bis(4-nitrphenyl)porphyrin – 4.76/H_2P

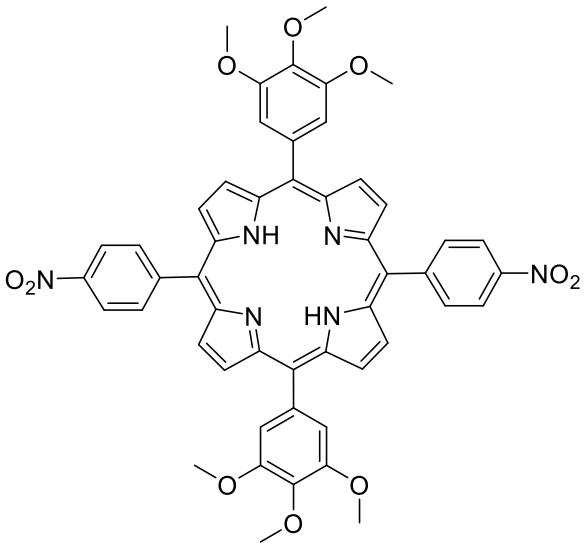

4.76 / H_2P

To a round bottom flask was added 5-(3,4,5-trimethoxyphenyl)dipyrromethane **4.52** (1.712 g, 3.7 mmol), anhydrous THF (55 mL) and anhydrous MeOH (17 mL). Added portion wise was $NaBH_4$ (7.60 g, 200 mmol), and the solution was stirred at r.t. for 15 mins. TLC (silica, EtOAc:C_6H_{14}, 1:1, v/v) indicated complete consumption of **4.52** and subsequently the reaction was quenched with H_2O. To this was added CH_2Cl_2 and the layers were separated. The aqueous layer was extracted with CH_2Cl_2 (2 × 200 mL). The organic layers were combined, washed with brine (1 × 200 mL), dried ($MgSO_4$) and excess solvent was removed under reduced pressure to yield the dipyrromethane carbinol as a vibrant orange oil. Added directly to this was MeCN (790 mL), followed by TFA (2.5 mL). The solution instantly became purple and darkened over the course of 5 mins. DDQ (2.0 g, 8.81 mmol) was then added, and the solution was allowed to stir for 1 h, followed by Et_3N (5 mL). Excess solvent was then removed at reduced pressure. The crude porphyrin was transferred onto a silica plug and the DDQ adducts were eluted with CH_2Cl_2. Once this ran clear, the desired porphyrin was eluted with $CHCl_3$:EtOAc 3:1, v/v. Excess solvent was removed at reduced pressure and the porphyrin was precipitated from MeOH to yield the desired **4.76** as a purple powder (422 mg, 0.477 mmol, 25%)

^{1}H NMR ($CDCl_3$, 400 MHz): δ = 9.02 (d, *J* = 4.7 Hz, 4H), 8.77 (d, *J* = 4.8 Hz, 4H), 8.66 (d, *J* = 8.6 Hz, 4H), 8.40 (d, *J* = 8.5 Hz, 4H), 7.46 (s, 4H), 4.19 (s, 6H), 3.98 (s, 12H), -2.79 (s, 2H). ^{13}C{^{1}H} NMR ($CDCl_3$, 101 MHz): δ = 151.6, 148.9, 148.0, 138.2,

137.1, 135.2, 132.3, 130.9, 122.1, 121.1, 117.7, 113.0, 61.4, 56.5.ppm. Calcd for $C_{50}H_{41}N_6O_{10}$ $[M+H]^+$ 885.2878, found, 885.2883. R_F = 0.57 (silica, $CHCl_3$). UV–Vis (THF) λ_{abs} (log ε) = 423 (5.75), 515 (4.56), 551 (4.23), 592 (4.03), 648 (3.85) nm. λ_{em} (THF): 655, 722 nm. M.P.: = > 300 °C.

[5,15-bis(3,4,5-trimethoxyphenyl)-10,20-bis(4-nitrphenyl)porphyrinato]zinc(II) – 4.77/ZnP

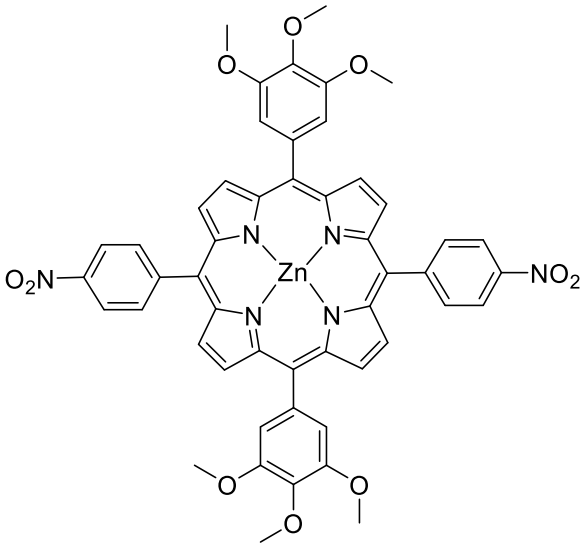

4.77 / ZnP

To a round bottom flask was added **4.76** (102 mg, 0.112 mmol) along with $CHCl_3$ (10 mL) and MeOH (10 mL). Added to this was $Zn(OAc)_2.2H_2O$ (225 mg, 1.03 mmol). The solution was heated to 70 °C for 4 h. The solution was washed with sat. $NaHCO_3$ soln. (1 × 50 mL), brine (1 × 50 mL), and dried ($MgSO_4$). Excess solvent was removed under reduced pressure. The crude **4.77** was passed through a silica plug ($CHCl_3$:EtOAc, 3:1, v/v) to yield the desired **4.77** as a green-purple powder (96 mg, 0.101 mmol, 90%).

^{1}H NMR ($CDCl_3$, 400 MHz): δ = 9.12 (d, *J* = 4.6 Hz, 4H), 8.87 (d, *J* = 4.6 Hz, 4H), 8.66 (d, *J* = 8.6 Hz, 4H), 8.40 (d, *J* = 8.6 Hz, 4H), 7.46 (s, 4H), 4.18 (s, 6H), 3.96 (s, 12H). ^{13}C{^{1}H} NMR (CDCl3, 101 MHz): δ = 151.5, 150.7, 149.7, 149.6, 147.9, 138.1, 137.8, 135.1, 133.1, 131.6, 122.1, 121.9, 118.8, 112.9, 61.4, 56.5 ppm. HRMS (MALDI-TOF): Calcd for $C_{50}H_{39}N_6O_{10}Zn$ $[M+H]^+$ 947.2013, found, 947.1836. R_F = 0.28 (silica, $CHCl_3$). UV–Vis (THF) λ_{abs} (log ε) = 428 (5.81), 558 (4.61), 602 (4.19) nm. λ_{em} (THF): 620, 656 nm. M.P.: = > 300 °C.

[5,15-bis(3,4,5-trimethoxyphenyl)-10,20-bis(4-nitrphenyl)porphyrinato]palladium(II) – 4.78/PdP

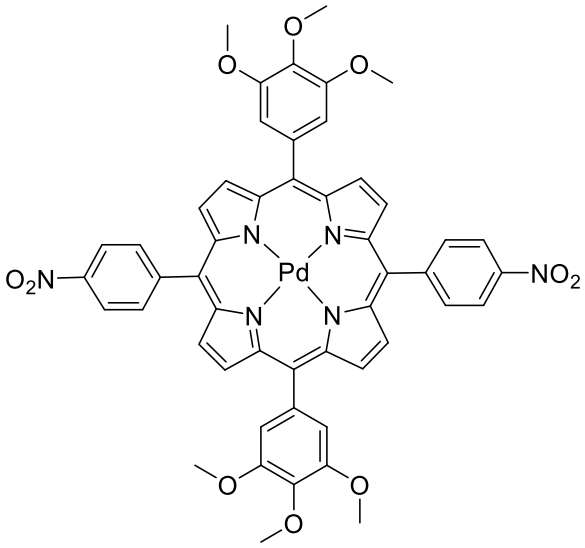

4.78 / PdP

To a round bottom flask was added **4.76** (102 mg, 0.112 mmol) along with $CHCl_3$ (10 mL) and MeOH (10 mL). Added to this was $Pd(OAc)_2$ (250 mg, 1.11 mmol). The solution was heated to 70 °C for 16 h. The solution was washed with sat. $NaHCO_3$ soln. (1 × 50 mL), brine (1 × 50 mL), and dried ($MgSO_4$). Excess solvent was removed under reduced pressure. The crude **4.78** was passed through a silica plug ($CHCl_3$:EtOAc, 3:1, v/v) to yield the desired 4.78 as an orange powder (84 mg, 0.849 mmol, 76%).

^{1}H NMR ($CDCl_3$, 400 MHz): δ = 8.98 (d, *J* = 4.9 Hz, 2H), 8.73 (d, *J* = 5.0 Hz, 2H), 8.65 (d, *J* = 8.6 Hz, 2H), 8.35 (d, *J* = 8.5 Hz, 2H), 7.42 (s, 2H), 4.18 (s, 3H), 3.96 (s, 6H). ^{13}C{^{1}H} NMR ($CDCl_3$, 101 MHz): δ = 151.6, 148.5, 148.0, 142.1, 140.9, 138.2, 136.7, 134.8, 132.1, 130.6, 122.6, 122.1, 119.4, 112.5, 61.4, 56.5 ppm. R_F = 0.23 (silica, $CHCl_3$). UV–Vis (THF) λ_{abs} (log ε) = 420 (5.59), 524 (4.61), 556 (3.86) nm. λ_{em} (THF): 655, 721 nm. M.P.: = > 300 °C.

1,1,2,2-Tetrakis(4'-(di(1H-pyrrol-2-yl)methyl)-[1,1'-biphenyl]-4-yl)ethylene – 5.40

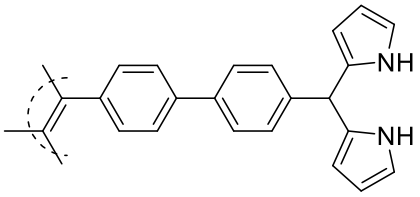

5.40

A solution of **5.39** (100 mg, 0.133 mmol, 1.0 equiv.) in pyrrole (3 mL) was degassed with argon for 5 min. The solution was stirred for 0.25 h at r.t. under argon in the presence of $InCl_3$ (118 mg, 0.534 mmol, 5.0 equiv.). The reaction mixture was diluted with CH_2Cl_2 (50 mL) and washed with 0.1 M NaOH solution, water and brine (1 × 25 mL each, in that order). The solvent was removed under reduced pressure to give a dark green oil crude product which was purified *via* flash column chromatography (silica ,EtOAc:C_6H_{14}, 1:1). The title compound was obtained as a grey solid upon rotary evaporation (90 mg, 0.074 mmol, 56%).

^{1}H NMR (400 MHz, $CDCl_3$): δ = 7.87 (s, 4H), 7.48 (d, *J* = 7.6 Hz, 8H), 7.34 (d, *J* = 8.0 Hz, 8H), 7.20 (t, *J* = 8.1 Hz, 8H), 7.17–7.11 (m, 8H), 6.66 (s, 8H), 6.15 (d, *J* = 2.7 Hz, 8H), 5.91 (s, 8H), 5.44 (s, 4H) ppm. ^{13}C{^{1}H} NMR (100 MHz, $CDCl_3$): δ = 142.8, 141.1, 140.5, 139.2, 138.5, 132.3, 132.0, 128.8, 127.0, 126.2, 117.3, 108.4, 107.2, 43.6 ppm; HRMS (MALDI) calcd. for $C_{86}H_{68}N_8$ [M^+]: 1212.5567; found 1212.5504. R_F = 0.51 (silica, EtOAc:C_6H_{14}, 1:1). M.P.= > 205–207°C (dec.).

1,1,2,2-Tetrakis(4'-(4,4-difluoro-4-bora-3 a,4 a-diaza-s–indacene)-[1,1'-biphenyl]-4-yl)ethylene – 5.33

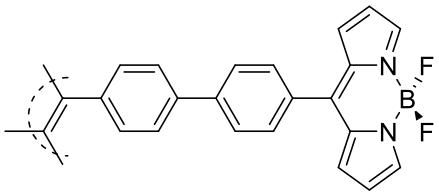

5.33

A solution of **5.40** (50 mg,0.04 mmol) in CH_2Cl_2 (5 mL) was degassed with Ar for 5 min. DDQ (37 mg, 0.164 mmol) was added and the reaction mixture was stirred for 5 min. Et_3N (80 µL, 0.618 mmol) was added and the solution was stirred for a further 3 min, before addition of $BF_3{\cdot}OEt_2$ (86 µL, 0.64 mmol). The reaction mixture was stirred for 35 min at room temperature and monitored via TLC. The reaction was quenched with water and the organic phase extracted with CH_2Cl_2 (3 × 50 mL). The organic phase was washed with water (2 × 25 mL), dried ($MgSO_4$) and solvent was removed at reduced pressure to yield a crude green product. This was purified via flash column chromatography(silica, EtOAc:C_6H_{14}, 1: 2) to yield **5.33** as an orange solid (19 mg, 32%).

^{1}H NMR (400 MHz, $CDCl_3$): δ = 7.94 (s, 8H), 7.75 (d, *J* = 8.2 Hz, 8H), 7.65–7.60 (m, 8H), 7.53 (d, *J* = 8.2 Hz, 8H), 7.29 (d, *J* = 8.2 Hz, 8H), 6.96 (d, *J* = 4.0 Hz, 8H), 6.54 (d, *J* = 2.9 Hz, 8H) ppm; ^{13}C{^{1}H} NMR (101 MHz, $CDCl_3$): δ=143.1(7), 143.1(4), 142.5(1), 142.5(0), 132.1, 132.0, 128.6, 121.9, 117.8, 117.6, 108.7, 108.3, 107.5, 44.0 ppm; ^{11}B NMR (128.4 MHz, $CDCl_3$): δ = 0.30 (t, $^1J_{B\text{-}F}$=28.7 Hz, 4B) ppm; ^{19}F NMR (376.5 MHz, $CDCl_3$): δ= - 145.06 ppm (q, $^1J_{F\text{-}B}$ = 28.6 Hz, 8F) ppm. HRMS (MALDI) calcd. for $C_{86}H_{56}B_4F_8N_8$ [M^+]: 1396.4872; found 1396.4917. M.P.= 208–210°C (dec.). R_F = 0.68 (silica, EtOAc:C_6H_{14} 1: 1).

1,1,2,2-Tetrakis(4-(4'-formylphenylethynyl)phenyl)ethylene – 5.41

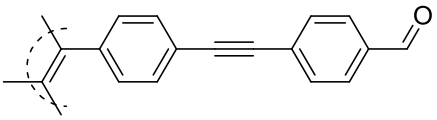

5.41

To an oven and flame dried Schlenk tube was added; **5.38** (215 mg, 501.7 μmol), 4-iodobenzaldehyde (1.0 g, 4.310 mmol, 8.6 eq.), PPh_3 (86 mg, 0.327 mmol), $Pd(PPh_3)_4$ (65 mg, 56.3 μmol), and CuI (53 mg, 278.3 μmol). The solids were dried under high vacuum (<0.1 mbar) for 2 h. Added to this was anhydrous 1,4-dioxane (8 mL) and anhydrous Et_3N (2 mL). The mixture underwent three freeze-pump-thaw cycles before being heated at 100°C for 25 h. Upon cooling to RT the mixture was passed through a pad of silica (EtOAc) and excess solvent was removed at reduced pressure. The product was adsorbed onto silica (THF) and purified via column chromatography (silica, EtOAc/Hex, 1/2, *v/v*). Excess solvent was removed under reduced pressure, and the residue was sonicated with Et_2O to yield the product as a brick orange solid (170 mg, 201.2 μmol, 40%).

^1H NMR ($CDCl_3$, 400 MHz): δ = 10.01 (s, 4H), 7.86 (d, *J* = 8.3 Hz, 8H), 7.64 (d, *J* = 8.2 Hz, 8H), 7.35 (d, *J* = 8.3 Hz, 8H), 7.06 (d, *J* = 8.3 Hz, 8H) ppm. ^{13}C NMR ($CDCl_3$, 101 MHz): δ = 191.5, 143.6, 141.3, 135.6, 132.2, 131.7, 129.8, 129.6, 121.4, 93.4, 85.9 ppm; HRMS (APCI) calcd. For $C_{62}H_{36}O_4$ [M^+] : 844.2630; found: 844.2619. M.P =158–160°C (dec.); R_F = 0.24 (silica, EtOAc:C_6H_{14}, 1: 2).

1,1,2,2-Tetrakis(4-((4-(di(1H-pyrrol-2-yl)methyl)phenyl)ethynyl) phenyl)ethylene – 5.42

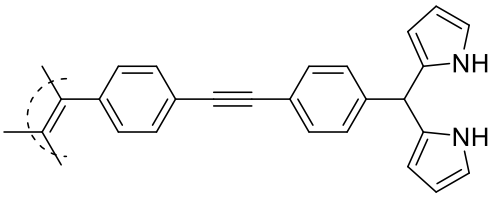

5.42

To a round bottom flask was added **5.41** (102 mg, 120.7 µmol) and freshly distilled pyrrole (5 mL). The solution was purged with argon and $InCl_3$ was added (134 mg, 605.8 µmol) and the mixture was stirred under argon until TLC indicated complete consumption of **5.41** (*c.a.* 20mins). The reaction mixture was diluted with CH_2Cl_2 (50 mL) and subsequently washed with H_2O, 0.1 M NaOH and brine (1 × 25 mL each, in that order). The organic extract was dried ($MgSO_4$) and excess solvent was removed at reduced pressure. The product was purified via column chromatography (silica, EtOAc/Hex, 1/1, *v/v*) to yield the desired product as a grey solid (40 mg, 30.5 µmol, 25%).

^{1}H NMR ($CDCl_3$, 400 MHz): δ = 7.93 (br s, 8H), 7.45 (d, *J* = 8.2 Hz, 8H) 7.30 (d, *J* = 8.3 Hz, 8H), 7.18 (d, *J* = 8.2 Hz, 8H), 7.01 (d, *J* = 8.3 Hz, 8H), 6.70–6.71 (m, 8H), 6.15–6.18 (m, 8H), 5.91 (s, 8H), 5.47 (s, 4H) ppm; ^{13}C{^{1}H} NMR ($CDCl_3$, 400 MHz): δ = 143.2, 143.1, 142.5(1), 142.5(0), 132.1, 132.0, 128.6, 121.9, 117.8, 117.6, 108.7, 108.3, 107.5, 44.0 ppm; HRMS (MALDI-TOF): calcd. For $C_{94}H_{68}N_8$ [M^+]: 1308.5567; found 1308.5552. M.p.= >300 °C (dec.) ; R_F = 0.65 (EtOAc:C_6H_{14} 1:1).

1,1,2,2-Tetrakis(4-((4-(4,4-difluoro-4-bora-3a,4a-diaza-s–indacene)phenyl)ethynyl)phenyl)ethene – 5.34

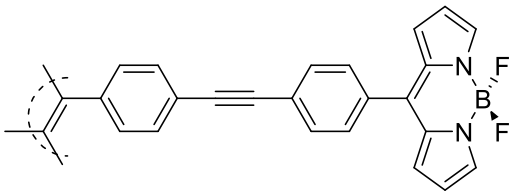

5.34

A solution of **5.42** (50 mg, 0.04 mmol) in CH_2Cl_2 (5 mL) was degassed with argon for 5 min. DDQ (32 mg, 0.164 mmol) was added and the reaction mixture was stirred for 5 min. Et_3N (75 µL, 0.62 mmol) was added and the solution was stirred for a further 3 min before addition of $BF_3{\cdot}OEt_2$ (78 µL, 0.64 mmol). The reaction mixture was stirred for 35 min at room temperature and monitored via TLC. The reaction was quenched with H_2O and the organic phase extracted with CH_2Cl_2 (2 × 25 mL). The organic phase was washed with water (2 × 25 mL), dried ($MgSO_4$), and the solvent evaporated to yield a crude green product which was purified via flash column chromatography (EtOAc:Hex, 1: 2, v/v) to yield an orange solid (11 mg, 7.37 µmol,19%).

^{1}H NMR (400 MHz, $CDCl_3$): δ = 7.96 (s, 8H), 7.68 (d, *J* = 8.3 Hz, 8H), 7.57 (d, *J* = 8.3 Hz, 8H), 7.52 (d, *J* = 8.2 Hz, 8H), 7.22 (d, *J* = 8.2 Hz, 8H), 6.95 (d, *J* = 4.1 Hz, 8H), 6.56 (m, 8H) ppm. ^{13}C NMR (101 MHz, CDCl3): δ=144.5, 141.6, 134.9, 133.6, 132.2, 131.8(9), 131.8(6), 131.7, 131.5, 130.8, 130.7, 129.3, 126.4, 118.9 ppm ^{11}B NMR (128.4 MHz, $CDCl_3$): δ = 0.28 (t, $^1J_{B\text{-}F}$=28.7 Hz, 4B) ppm. ^{19}F NMR (376.5 MHz, $CDCl_3$): δ= -145.08 ppm (q, $^1J_{F\text{-}B}$=28.6 Hz, 8F) ppm. HRMS (MALDI) calcd. for $C_{102}H_{74}B_3F_6N_8O_4Na$ [M-BF_2+2H+2EtOAc+Na+]: 1644.5914; found 1644.5953. M.P.= >150°C (dec.); R_F = 0.72 (silica, EtOAc:C_6H_{14}, 1:1).

7.3 Crystallographic Data

*Crystal Data for **3.36a**, **3.41a**, **4.55**, **4.65**, **5.37** and **5.39** were collected, solved and refined by Dr. B. Twamley. Crystal Data for **4.57**, **4.59**, **4.60**, **4.62**, **4.63**, **4.67**, **4.68**, and **H_2P** were collected, solved and refined by Dr. C. J. Kingsbury.*

Diffraction data for all compounds were collected on a Bruker APEX 2 DUO CCD diffractometer by using graphite-monochromated MoKα radiation (λ = 0.71073 Å) and Incoatec IμS CuKα radiation (λ = 1.54178 Å). Crystals were mounted on a MiTeGen MicroMount and collected at 100(2) K by using an Oxford Cryosystems Cobra low-temperature device. Data were collected by using omega and phi scans and were corrected for Lorentz and polarization effects by using the APEX software suite.[448] The structures were solved with Direct Methods and refined against $|F^2|$ with XL using least squares minimization.[126,449] Non-hydrogen atoms were refined with anisotopical thermal parameters. Hydrogen atoms were generally placed into geometrically calculated positions and refined using a riding model. The N–H hydrogen atoms were located using different maps and refined using the standard riding model. All images were prepared by using Olex2.[126]

Crystal Data for **3.36a**: $C_{29.08}H_{23.51}BrCl_{0.1}N_4Zn$ (M = 577.77 g mol^{-1}): triclinic, space group P-1 (No. 2), *a* = 16.5765(9) Å, *b* = 16.9003(10) Å, *c* = 16.9698(10) Å, α = 119.694(3)°, β = 102.715(3)°, γ =93.421(3)°, V = 3947.8(4) Å^3, Z = 6, T = 100(2) K, μ(Cu Kα)= 3.349 mm^{-1}, D_{calc} = 1.458 g cm^{-3}, 48448 reflections measured (5.576° ≤ 2θ ≤ 137.21°), 14460 unique (R_{int} = 0.0794, R_{sigma} = 0.0738) which were used in all calculations. The final R_1 was 0.0692 (I > 2σ(I)) and wR_2 was 0.2044 (all data). In **3.36a** the asymmetric unit consists of three independent molecules and 0.5 hexane, which was modelled over two sites, at 25 % occupancy each, using a mixture of rigid group model and restraints, SIMU, DFIX, SADI and a partially occupied CH_2Cl_2 (0.15%), fitted using a rigid group using restraints (SIMU).

Crystal Data for **3.41a**: $C_{28}H_{22.95}Br_{1.03}N_4$ (M = 497.96 g mol^{-1}): monoclinic, space group P*2$_1$/n* (No. 14), *a* = 15.2041(9) Å, *b* = 9.8625(5) Å, *c* = 31.7167(18) Å, α = γ =

90°, β = 97.607(4)°, V=4714.1(5) Å^3, Z = 8, T=100(2) K, μ(Cu Kα)= 2.615 mm^{-1}, D_{calc} = 1.403 g cm^{-3}, 33238 reflections measured (5.622° ≤ 2θ ≤ 118.526°), 6800 unique (R_{int} = 0.1542, R_{sigma} = 0.1132) which were used in all calculations. The final R_1 was 0.0729 (I > 2σ(I)) and wR_2 was 0.2115 (all data). Crystals of 3.41 were poorly diffracting at low temperatures with long exposures collected to a resolution of d = 0.90 Å. Partially substituted with Br (Br3 = 3% and Br4 = 3% occupied) and refined with geometric (DIFX, SADI) and displacement (SIMU) restraints. The atomic displacements of the low occupancy Br3 and Br4 were restrained to be equal (EADP).

Crystal Data for **4.55**: $C_{12}H_8N_2O_3S$ (M = 260.26 g mol^{-1}): orthorhombic, space group P*na2$_1$* (No. 33), *a* = 23.0774(11) Å, *b* = 12.5622(5) Å, *c* = 3.8498(2) Å, α = β = γ = 90°, V = 1116.07(9) Å^3, Z=4, T=100(2) K, μ(Cu Kα)= 2.621 mm^{-1}, D_{calc} = 1.549 g cm^{-3}, 8764 reflections measured (3.831° ≤ 2θ ≤ 69.798°), 1759 unique (R_{int} = 0.0616, R_{sigma} = 0.0469) which were used in all calculations. The final R_1 was 0.0434 (I > 2σ(I)) and wR_2 was 0.1215 (all data).

Crystal Data for **4.57**: $C_{25}H_{19.60}Br_{1.40}N_3O_6$ (M = 570.05 g mol^{-1}): monoclinic, space group P*2$_1$/n* (No. 14), *a* = 10.328(2) Å, *b* = 17.309(3) Å, *c* = 13.364(3) Å, α = γ = 90°, β = 107.117(7)°, V = 2283.2(8) Å^3, Z = 4, T = 100(2) K, μ(Mo Kα)= 2.553 mm^{-1}, D_{calc} = 1.658 g cm^{-3}, 9068 reflections measured (8.000° ≤ 2θ ≤ 8.000°), 3711 unique (R_{int} = 0.1733, R_{sigma} = 0.2614) which were used in all calculations. The final R_1 was 0.0752 (I > 2σ(I)) and wR_2 was 0.1345 (all data).

Crystal Data for **4.59**: $C_{12}H_{10}BrNO_3S$ (M = 328.18 g mol^{-1}): orthorhombic, space group P*2$_1$2$_1$2$_1$* (No. 19), *a* = 4.8436(5) Å, *b* = 13.9149(13) Å, *c* = 18.5479(17) Å, α = β = γ = 90°, V = 1250.1(2) Å^3, Z = 4, T = 100(2) K, μ(Cu Kα)= 3.454 mm^{-1}, D_{calc} = 1.744 g cm^{-3}, 23296 reflections measured (3.660° ≤ 2θ ≤ 62.000°), 3972 unique (R_{int} = 0.0283, R_{sigma} = 0.0214) which were used in all calculations. The final R_1 was 0.0206 (I > 2σ(I)) and wR_2 was 0.0450 (all data).

Crystal Data for **4.60**: $C_{13}H_{11}BrN_2O_4S$ (M = 371.21 g mol^{-1}): triclinic, space group P-1 (No. 2), *a* = 6.8904(4) Å, *b* = 8.3224(4) Å, *c* = 12.8763(7) Å, α = 83.423(3)°, β = 80.393(3)°, γ = 85.693(3)°, V = 722.06(7) Å^3, Z = 2, T = 100(2) K, μ(Cu Kα)= 5.403 mm^{-1}, D_{calc} = 1.707 g cm^{-3}, 7190 reflections measured (7.000° ≤ 2θ ≤ 136.400°), 2617 unique (R_{int} = 0.0416, R_{sigma} = 0.0448) which were used in all calculations. The final R_1 was 0.0491 (I > 2σ(I)) and wR_2 was 0.1423 (all data).

Crystal Data for **4.62**: $C_{19}H_{23}BrN_2O_5S$ (M = 471.36 g mol^{-1}): monoclinic, space group P$2_1/c$ (No. 14), *a* = 7.7375(2) Å, *b* = 15.9728(3) Å, *c* = 16.7621(3) Å, α = γ = 90°, β = 93.0550(10)°, V = 2068.68(8) Å^3, Z = 4, T = 100(2) K, μ(Mo Kα)= 2.120 mm^{-1}, D_{calc} = 1.513 g cm^{-3}, 226885 reflections measured (3.520° ≤ 2θ ≤ 93.040°), 18433 unique (R_{int} = 0.0306, R_{sigma} = 0.0132) which were used in all calculations. The final R_1 was 0.0274 (I > 2σ(I)) and wR_2 was 0.0761 (all data).

Crystal Data for **4.63**: $C_{19}H_{23}BrN_2O_2S$ (M = 423.26 g mol^{-1}): monoclinic, space group C*2/c* (No. 15), *a* = 24.3927(8) Å, *b* = 12.4282(4) Å, *c* = 16.3832(5) Å, α = γ = 90°, β = 126.1600(10)°, V = 4010.0(2) Å^3, Z = 8, T = 100(2) K, μ(Mo Kα)= 2.168 mm^{-1}, D_{calc} = 1.403 g cm^{-3}, 81626 reflections measured (1.940° ≤ 2θ ≤ 36.230°), 9654 unique (R_{int} = 0.0663, R_{sigma} = 0.0453) which were used in all calculations. The final R_1 was 0.0525 (I > 2σ(I)) and wR_2 was 0.1239 (all data).

Crystal Data for **4.65**: $C_{26}H_{24}Br_2N_4O_8S_2$ (M = 744.43 g mol^{-1}): orthorhombic, space group P*bca* (No. 61), *a* = 13.9764(7) Å, *b* = 17.8228(9) Å, *c* = 23.0590(11) Å, α = β = γ = 90°, V = 5744.0(5) Å^3, Z = 8, T = 100(2) K, μ(Cu Kα)= 5.434 mm^{-1}, D_{calc} = 1.722 g cm^{-3}, 55114 reflections measured (7.668° ≤ 2θ ≤ 139.89°), 5407 unique (R_{int} = 0.0395, R_{sigma} = 0.0199) which were used in all calculations. The final R_1 was 0.0304 (I > 2σ(I)) and wR_2 was 0.0795 (all data).

Crystal Data for **4.67**: $C_{16}H_{24}N_2O_2$ (M = 276.37 g mol^{-1}): monoclinic, space group P$2_1/n$ (No. 14), *a* = 12.4967(6) Å, *b* = 6.5479(3) Å, *c* = 18.6946(9) Å, α = γ = 90°, β = 90.285(2)°, V = 1529.71(13) Å^3, Z = 4, T = 100(2) K, μ(Cu Kα)= 0.630 mm^{-1}, D_{calc}

= 1.200 g cm^{-3}, 11544 reflections measured (9.415° ≤ 2θ ≤ 138.300°), 2836 unique (R_{int} = 0.0393, R_{sigma} = 0.0272) which were used in all calculations. The final R_1 was 0.0775 (I > 2σ(I)) and wR_2 was 0.2234 (all data).

Crystal Data for **4.68**: $C_{16}H_{23}BrN_2O_2$ (M = 355.27 g mol^{-1}): monoclinic, space group P$2_1/c$ (No. 14), a = 15.1619(7) Å, b = 16.6014(7) Å, c = 6.8043(3) Å, α = γ = 90°, β = 102.657(2)°, V = 1671.08(13) $Å^3$, Z = 4, T = 100(2) K, μ(Cu Kα)= 3.401 mm^{-1}, D_{calc} = 1.412 g cm^{-3}, 12664 reflections measured (5.975° ≤ 2θ ≤ 139.400°), 3047 unique (R_{int} = 0.0435, R_{sigma} = 0.0361) which were used in all calculations. The final R_1 was 0.0352 (I > 2σ(I)) and wR_2 was 0.0916 (all data).

Crystal Data for **H_2P**: $C_{54}H_{44}Cl_{12}N_6O_{10}$ (M = 1362.35 g mol^{-1}): triclinic, space group P-*1* (No. 2), a = 10.7409(3) Å, b = 13.8709(4) Å, c = 20.1721(5) Å, α = 92.6170(10)°, β = 91.1040(10)°, γ = 95.9460(10)°, V = 2985.20(14) $Å^3$, Z = 2, T = 100(2) K, μ(Cu Kα)= 5.617 mm^{-1}, D_{calc} = 1.516 g cm^{-3}, 47088 reflections measured (2.190° ≤ 2θ ≤ 69.940°), 11167 unique (R_{int} = 0.0438, R_{sigma} = 0.0331) which were used in all calculations. The final R_1 was 0.0633 (I > 2σ(I)) and wR_2 was 0.1759(all data).

Crystal Data for **5.37**: $C_{23}H_{26}OSi_2$ (M = 374.62 g mol^{-1}): orthorhombic, space group P*ccn* (No. 56), a = 33.9086(9) Å, b = 5.5681(2) Å, c = 11.6573(3) Å, α = β = γ = 90°, V = 2200.97(11) $Å^3$, Z = 4, T = 100(2) K, μ(Cu Kα)= 1.514 mm^{-1}, D_{calc} = 1.131 g cm^{-3}, 15541 reflections measured (2.606° ≤ 2θ ≤ 69.836°), 2057 unique (R_{int} = 0.0423, R_{sigma} = 0.0251) which were used in all calculations. The final R_1 was 0.0404 (I > 2σ(I)) and wR_2 was 0.1152 (all data).

Crystal data for **5.39**: $C_{54}H_{36}O_4$ (M=748.83 g mol^{-1}): monoclinic, space group C*2/c* (No. 15), a = 35.8085(13) Å, b = 9.0237(3) Å, c = 34.1519(11) Å, α = γ = 90°, β = 120.7872(19)°, V = 9480.2(6) $Å^3$, Z = 8, T = 100(2) K, μ(Cu Kα)= 0.514 mm^{-1}, D_{calc} = 1.049 g cm^{-3}, 35951 reflections measured (2.873° ≤ 2θ ≤ 58.986°), 6752 unique (R_{int} = 0.0602, R_{sigma} = 0.0486) which were used in all calculations. The final R_1 was 0.1168 (I > 2σ(I)) and wR_2 was 0.3682 (all data). The crystals obtained for **5.39**

showed poor diffraction, resolution was limited to d = 0.9 Å. Two terminal carboxy phenyl groups were modelled as disordered in two locations using rigid groups, occupancies C37, 56%; C37B 44% and C51, 85%; C51b, 15%. Refined with restraints (DFIX, SIMU, RIGU and ISOR). It was not possible to refine the solvents in the lattice voids and their contribution to the diffraction data was removed using the SQUEEZE routine in PLATON. The solvent accessible volume (SAV) is 2025 $Å^3$ and there are 636 electrons found in this SAV. This is a mixture of CH_2Cl_2 and F_3CCO_2H.

8. References

[i] G. P. Moss, *Eur. J. Biochem.* **1988**, *178*, 277–328.

[ii] J. S. Lindsey, *Chem. Rev*. **2015**, *115*, 6534–6620.

[iii] M. Taniguchi, J. S. Lindsey, *Chem. Rev.* **2017**, *117*, 344–535.

[iv] J.-P. Strachan, D. F. O'Shea, T. Balasubramanian, J. S. Lindsey, *J. Org. Chem.* **2000**, *65*, 3160–3172.

[1] E. Sternberg, D. Dolphin, *Curr. Med. Chem.* **1996**, *3*, 239–252.

[2] E. Sternberg, D. Dolphin, *Tetrahedron* **1998**, *54*, 4151–4202.

[3] T. Maisch, *Mini-Rev. Med. Chem.* **2009**, *9*, 974–983.

[4] T. Maisch, R.-M. Szeimies, G. Jori, C. Abels, *Photochem. Photobiol. Sci.* **2004**, *3*, 907–917.

[5] P. Calzavara-Pinton, M. T. Rossi, R. Sala, M. Venturini, Photochem. Photobiol. **2012**, *88*, 512–522.

[6] A. Wiehe, J. M. O'Brien, M. O. Senge, *Photochem. Photobiol. Sci.* **2019**, *18*, 2565–2612.

[7] R. L. Edelson, *Sci. Am.* **1998**, *259*, 68–75.

[8] O. Raab, *Z. Biol.* **1900**, *39*, 524–546.

[9] H. von Tappeiner, A. Jesionek, *Munch Med. Wochenschr.* **1903**, *47*, 2042–2044.

[10] N. R. Finsen, La Photothérapie, Georges Carré et C. Naud, Paris, **1899**.

[11] K. I. Møller, B. Konigshoj, P. A. Philipsen, V. O. Thomsen, H. C. Wulf, *Photodermatol., Photoimmunol. Photomed.* **2005**, *21*, 118–124.

[12] R. Roelandts, *Photodermatol., Photoimmunol. Photomed.* **2005**, *21*, 115–117.

[13] The Nobel Prize in Physiology or Medicine 1903. NobelPrize.org. Nobel Prize Outreach AB 2021. Sun. 14 Nov 2021. <https://www.nobelprize.org/prizes/medicine/1903/summary/>

[14] F. Meyer-Betz, *Dtsch. Arch. Klin. Med.* **1913**, *112*, 476–503.

[15] http://dx.doi.org/10.1039/9781839164149-00252 - Zois chapter, cite properly

[16] R. Bonnett, *Chem. Soc. Rev.* **1995**, *24*, 19–33.

[17] J. Moan, *J. Photochem. Photobiol. B: Biol.* **1990**, *5*, 521–524.

[18] R. T. Aroso, F. A. Schaberle, L. G. Arnaut, M. M. Pereira, *Photohcem. Photobiol. Sci.* **2021**, *20*, 1497–1545.

[19] Herzberg, G. Spectra of Diatomic Molecules; Van Nostrand Reinhold: New York, 1950.

[20] N. Lane, Oxygen: The molecule that made the world., Oxford University Press, Oxford, 2002.

[21] M. Ackermann, F. Biaume, G. Kockarts, *Planet Space Sci.* **1970**, *18*, 1639–1651.

[22] R. S. Mulliken, *Nature* **1928**, *122*, 505.

[23] R. S. Mulliken, *Rev. Mod. Phys.* **1932**, *4*, 1–86.

[24] The Nobel Prize in Chemistry 1966. NobelPrize.org. Nobel Prize Outreach AB 2021. Mon. 22 Nov 2021. <https://www.nobelprize.org/prizes/chemistry/1966/summary/>

[25] D. Weldon, T. D. Poulsen, K. V. Mikkelsen, P. R. Ogilby, *Photochem. Photobiol.* **1998**, *70*, 369–379.

[26] Frimer, A. A., Ed. Singlet oxygen; CRC Press: Boca Raton, FL, 1985.

[27] C. S. Foote, S. Wexler, *J. Am. Chem. Soc.* **1964**, *86*, 3879–3880.

[28] A. A. Ghogare, A. Greer, *Chem. Rev.* **2016**, *116*, 9994–10034.

[29] E. L .Clennan, *Acc. Chem. Res.* **2001**, *34*, 875–884.

[30] P. R. Bolduc, G. L. J. Goe, *J. Org. Chem.* **1974**, *39*, 3178–3179.

[31] P. R. Ogilby, *Photochem. Photobiol. Sci*. **2010**, *9*, 1543–1560.

[32] J. Moan, K. Berg, *Photochem. Photobiol.* **1991**, *53*, 549–553.

[33] A. Baker, J. R. Kanofsky, *Photochem. Photobiol.* **1992**, *55*, 523–528.

[34] J. S. Dysart, M. S. Patterson, *Phys. Med. Biol.* **2005**, *50*, 2597–2616.

[35] C. Tanielian, R. Mechin, *Photochem. Photobiol.* **1994**, *59*, 263

[36] A. Michaeli and J. Feitelson, *Photochem. Photobiol.* **1994**, *59*, 284–289.

[37] D. Magda, M. Wright, R. A. Miller, J. L. Sessler, P. I. Sansom, *J. Am. Chem. Soc.* **1995**, *117*, 3629–3630.

[38] S. Callaghan, M. O. Senge, *Photochem. Photobiol. Sci.* **2018**, *17*, 1490–1514.

[39] S. Callaghan, M. A. Filatov, E. Sitte, H. Savoie, R. W. Boyle, K. J. Flanagan, M. O. Senge, *Photochem. Photobiol. Sci.* **2017**, *16*, 1371–1374.

[40] R. R. Allison, C. H. Sibata, *Photodiagn. Photodyn. Ther.* **2010**, *7*, 61–75.

[41] Q. Yao, H. Li, L. Xian, F. Xu, J. Xia, J. Fan, J. Du, J. Wang, X. Peng, *Biomaterials*, **2018**, *177*, 78–87.

[42] Q. Yao, J. Fan, S. Long, X. Zhao, H. Li, J. Du, K. Shao, X. Peng, *Chem*, **2022**, *8*, 1–13.

[43] G. Martini, E. Martinelli, G. Ruggeri, G. Galli, A. Pucci, *Dyes Pigm.* **2015**, *113*, 47–54.

[44] E. A. Halabi, Z. Thiel, N. Trapp, D. Pinotsi, P. Rivera-Fuentes, *J. Am. Chem. Soc.* **2017**, *139*, 13200–13207.

[45] Z. E. Dance, M. J. Ahrens, A. M. Vega, A. B. Ricks, D. W. McCamant, M. A. Ratner, M. R. Wasielewski, *J. Am. Chem. Soc.* **2008**, *130*, 830–832.

[46] V. Martinez, M. Henary, *Chem. Eur. J.* **2016**, *22*, 13764–13782.

[47] P.-C. Lo, M. S. Rodríguez-Morgade, R. K. Pandey, D. K. P. Ng, T. Torres, F. Dumoulin, *Chem. Soc. Rev.* **2020**, *49*, 1041–1056.

[48] R. S. Singh, R. P. Paitandi, R. K. Gupta, D. S. Pandey, *Coord. Chem. Rev.* **2020**, *414*, 213269.

[49] R. S. Singh, R. P. Paitandi, R. K. Gupta, D. S. Pandey, *Coord. Chem. Rev.* **2020**, *421*, 213404.

[50] S. Monro, K. L. Colón, H. Yin, J. Roque III, P. Konda, S. Gujar, R. P. Thummel, L. Lilge, C. G. Cameron, S. A. McFarland, *Chem. Rev.* **2019**, *119*, 797–828.

[51] A. Gandoslo, K. Purkalt, G. Gasser, *Chimia*, **2021**, *75*, 845–855.

[52] B. J. Hohlfeld, B. Gitter, C. J. Kingsbury, K. J. Flanagan, D. Steen, G. D. Wieland, N. Kulak, M. O. Senge, A. Wiehe, *Chem. Eur. J.* **2021**, *27*, 6440–6459.

[53] S. G. Keller, M. Kamiya, Y. Urano, *Molecules* **2020**, *25*, 5964.

[54] H. Mohr, B. Lambrecht, A. Selz, *Immunol. Invest.* **1995**, *24*, 73–85.

[55] R. Santus, P. Grellier, J. Schrével, J. C. Mazière, J. F. Stoltz, *Clin. Hemorheol. Microcirc.* **1998**, *18*, 299–308.

[56] M. Wainwright, *Chem. Soc. Rev.* **2002**, *31*, 128–136.

[57] V. Pérez-Laguna, I. García-Luque, S. Ballesta, L. Pérez-Artiaga, V. Lampaya-Pérez, S. Samper, P. Soria-Lozano, Y. Gilaberte, *Photodiagn. Photodyn. Ther.* **2018**, *21*, 211–216.

[58] J. B. Grimm, A. N. Tkachuk, L. Xie, H. Choi, B. Mohar, N. Falco, K. Schaefer, R. Patel, Q. Zheng, Z. Liu, J. Lippincott-Schwartz, T. A. Brown, L. D. Lavis, *Nat. Methods* **2020** *17*, 815–821.

[59] C. Spagnul, J. Greenman, M. Wainwright, Z. Kamil, R. W. Boyle, *J. Mater. Chem. B*. **2016**, *4*, 1499–1509.

[60] T. A. Theodossiou, J. S. Hothersall, P. A. De Witte, A. Pantos, P. Agostinis, *Mol. Pharmaceutics*, **2009**, *6*, 1775–1789.

[61] Y. Zhang, K. Shang, X. Wu, S. Song, Z. Li, Z. Pei, Y. Pei, *RSC Adv.* **2018**, *8*, 21786–21792.

[62] H. Falk, *Angew. Chem. Int. Ed.* **1999**, *38*, 3116–3136; *Angew. Chem.* **1999**, *111*, 3306–3326.

[63] J. M. O'Brien, E. Sitte, K. J. Flanagan, H. Kühner, L. J. Hallen, D. Gibbons, M. O. Senge, *J. Org. Chem.* **2019**, *84*, 6158–6173.

[64] E. Sitte, M. O. Senge, *Eur. J. Org. Chem.* **2020**, 3171–3191.

[65] N.I.H. – U.S. National Library of Medicine. Efficacy and Safety Study of TOOKAD® Soluble for Localised Prostate Cancer Compared to Active Surveillance. (PCM301). Tues. 15th Mar. 2022. <https://clinicaltrials.gov/ct2/show/NCT01310894>

[66] D. Hanaha, R. A. Weinberg, *Cell* **2011**, *144*, 646–674.

[67] J. L. Connolly, S. J. Schnitt, H. H. Wang, J. A. Longtine, A. Dvorak, H. F. Dvorak. Tumor Structure and Tumor Stroma Generation. In: D. W. Kufe, R. E. Pollock, R. R. Weichselbaum, et al., editors. Holland-Frei Cancer Medicine. 6th edition. Hamilton (ON): BC Decker; 2003. Available from: https://www.ncbi.nlm.nih.gov/books/NBK13447/

[68] P. C. Nowell, *Cancer Res*. **1986**, *46*, 2203–2207.

[69] P. Yan, L.-H. Liu, P. Wang, *ACS Appl. Bio Mater.* **2020**, *3*, 3456–3475.

[70] G. Shafirstein, D. Bellnier, E. Oakley, S. Hamilton, M. Potasek, K. Beeson, E. Parilov, *Cancers* **2017**, *9*, 12.

[71] M. Taniguchi, J. S. Lindsey, *Photochem. Photobiol.* **2018**, *94*, 290–327.

[72] M. Taniguchi, H. Du, J. S. Lindsey, *Photochem. Photobiol.* **2018**, *94*, 277–289.

[73] S. Schwartz, *Univ. Minn. Med. Bull.* **1955**, *7*, 7–13.

[74] M. Nencki, J. Zaleski, *Ztschr. Physiol. Ch.* **1900**, *30*, 384–435.

[75] R. L. Lipson, Masters Thesis, University of Minnesotta, July 1960.

[76] R. L. Lipson, E. Baldes, *Archiv. Dermatol.* **1961**, *82*, 508–516.

[77] J. G. Gray, R. L. Lipson, J. Macek, P. Parker, D. Romeyn, *Am. J. Obstet. Gynecol.***1967**, *99*, 766–771.

[78] R. L. Lipson, In Proceedings o/the 9th International Cancer Congress, Tokyo, Japan, 1966, 393.

[79] I. Diamond, A. F. McDonagh, C. B. Wilson, S. G.. Granelli, S. Nielsen, R. Jaenicke, *Lancet* **1972**, 1175–1177.

[80] T. J. Dougherty, *J. Natl. Cancer Inst.* **1974**, *51*, 1333–1336.

[81] T. J. Dougherty, G. Lawrence, J. H. Kaufman, D. Boyle, K. R. Weishaupt, A. J. Goldfarb, *Natl. Cancer Inst.* **1979**, *62*, 231–237.

[82] T. J. Dougherty, K. R. Weishaupt, W. Potter, United States Patent No. 4649151, 1987.

[83] T. J. Dougherty, T. S. Mang, *Photochem. Photobiol*. **1987**, *46*, 67–70.

[84] D. A. Bellineier, Y.-H Ho, R. K. Pandey, J. R. Missert, T. J. Dougherty, *Photochem. Photobiol.* **1989**, *50,* 221–228.

[85] R. K. Pandey, M. M. Siegel, R. Tsao, J. H. McReynolds, T. J. Dougherty, *Biomed. Environm. Mass Spectrom.*, **1990**, *19*, 405–414.

[86] A. Mironov, A. Nizhnik, A. Nochel, *Photochem. Photobiol.* **1990**, *4*, 297–306

[87] D. Kessel, P. Thompson, B. Musselman, C. K. Chang, *Photochem. Photobiol.* **1987**, *46*, 563–568.

[88] T. J. Dougherty, *Photochem. Photobiol.* **1987**, *46*, 569–573.

[89] S. Y. Yap, H. Savoie, I. Renard, B. P. Burke, H. C. Sample, S. Michue-Seijas, S. J. Archibald, R. W. Boyle, G. J. Stasiuk, *Chem. Commun*. **2020**, *59*, 11090–11093.

[90] K. J. Lorenz, H. Maeir, HNO, 2008, 56, 402 – 409.

[91] R. Bonnett, R. D. White, U. J. Winfield, M. C. Berenbaum, *Biochem. J.* **1989**, *261*, 277–280.

[92] M. O .Senge, *Photodiagn. Photodyn. Ther.* **2012**, *9*, 170–179.

[93] D. Lecerof, M. Fodje, A. Hansson, M. Hansson, S. Al-Karadaghi, *J. Mol. Biol.* **2000**, *297*, 221–232.

[94] A. M. del C. Battle, *J. Photochem. Photobiol. B: Biol.* **1993**, *20*, 5–22.

[95] I. E. Furre, S. Shahzidi, Z. Luksiene, M. T. N. Moller, E. Borgen, J. Morgan, K. Tkacz-Stachowska, J. M. Nesland, Q. Peng, *Cancer. Res.* **2005**, *65*, 11051–11060.

[96] C.-N. Lee, R. Hsu, H. Chen, T.-W. Wong, *Molecules* **2020**, *25*, 5915.

[97] F. Bryden, H. Savoie, E. V. Rosca, R. W. Boyle, *Dalton Trans*. **2015**, *44*, 4925–4932.

[98] T. L. Mindt, H. Struthers, L. Brans, T. Anguelov, C. Schweinsberg, V. Maes, D. Tourwe´ and R. Schibli, *J. Am. Chem. Soc.* **2006**, *128*, 15096–15097.

[99] J. Funkhouser, *Curr. Drug. Discovery*, **2002**, *2*, 17–19.

[100] L. C. Gomes-da-Silva, O. Kepp, G. Kroemer, *OncoImmunology* **2020**, 1841393.

[101] P. Gierlich, A. I. Mata, C. Donohoe, R. M. M. Brito, M. O. Senge, L. C. Gomes-da-Silva, *Molecules* **2020**, *25*, 5317.

[102] M. B. Ericson, A.-M. Wennberg, O. Larkö, *Ther. Clin. Risk. Manag.* **2008**, *4*, 1–9.

[103] D. F. Janssen, *Med. Oncol. (N. Y., NY, U. S.)* **2021**, *38*, 22.

[104] The top 10 causes of death, World Health Organization, 2020. Thurs. 18th Nov. 2021. <https://www.who.int/news-room/fact-sheets/detail/the-top-10-causes-of-death>

[105] Cancer, World Health Organization, 2022. Wed. 16th Mar. 2022. <https://www.who.int/en/news-room/fact-sheets/detail/cancer>

[106] R. A. Smith, *J. Chem. Educ.* **1998**, *75*, 420–420.

[107] D. Mansuy, *Comp. Rend. Chim.* **2007**, *10*, 392–413.

[108] T. D. Lash, S. A. Jones, G. M. Ferrence, *J. Am. Chem. Soc.* **2010**, *132*, 12786–12787.

[109] M. Moulin, A. G. Smith, *Biochem. Soc. Trans.* **2005**, *33*, 737–742.

[110] J.-L. Soret, *Compt. rend.Acad. sci.*, **1883**, *97*, 1269–1270.

[111] M. J. Gouterman, *J. Mol. Spectrosc.* **1961**, *6*, 138–163.

[112] J. R. Reimers, Z.-L. Cai, R. Kobayashi, M. Rästep, A. Freiberg, E. Krausz, *Sci. Rep.* **2013**, *3*, 2761.

[113] S. Ozawa, Y. Watanabe, I. Morishima, *J. Am. Chem. Soc.* **1994**, *116*, 5832–5838.

[114] C. Brückner, J. R. McCarthy, H. W. Daniell, Z. D. Pendon, R. P. Ilagan, T. M. Francis, L. Ren, R. R. Birge, H. A. Frank, *Chem. Phys.* **2003**, *294*, 285–303.

[115] H. L. Kee, C. Kirmaier, Q. Tang, J. R. Diers, C. Muthiah, M. Taniguchi, J. K. Laha, M. Ptaszek, J. S. Lindsey, D. F. Bocian, D. Holten, *Photochem. Photobiol.* **2007**, *83*, 1125–1143.

[116] K. Aravindu, H.-J. Kim, M. Taniguchi P. L. Dilbeck, J. R. Diers, D. F. Bocian, D. Holten, J. S. Lindsey, *Photochem. Photobiol. Sci.* **2013**, *12*, 2089–2109.

[117] J. Pelletier, J. Caventou, *Ann. Chim. Phys.* **1817**, *3*, 486–491.

[118] J. Pelletier, J. Caventou, *Ann. Chim. Phys.* **1818**, *9*, 194–196.

[119] M. Délepine, *J. Chem. Educ*, **1951**, *28*, 454–461.

[120] G. G. Stokes, *Proc. R. Soc. London* **1864**, *13*, 144–145.

[121] M. Tswett, *Ber. Dtsch. Bot. Ges.* **1906**, *24*, 384–393.

[122] R. Willstätter, M. Isler, *Justus Liebigs Ann. Chem.* **1912**, *390*, 269–339.

[123] H. Fischer, *Naturwissenschaften* **1940**, *28*, 401–405.

[124] R. B. Woodward, W. .A Ayer, J. M. Beaton, F. Bickelhaupt, R. Bonnett, P. Buchschacher, G. L. Closs, H. Dutler, J. Hannah, F. P. Hauck, S. Itô, A. Langemann, E. Le Goff, W. Leimgruber, W. Lwowski, J. Sauer, Z. Valenta, H. Volz, *J. Am. Chem. Soc.* **1960**, *82*, 3800–3802.

[125] H-C. Chow, R. Serlin, C. E. Strouse, *J. Am. Chem. Soc.* **1975**, *97*, 7230–7237.

[126] O. V. Dolomanov, L. J. Bourhis, R. J. Gildea, J. A. K. Howard, H. Puschmann, *J. Appl. Cryst.* **2009**, *42*, 339–341.

[127] M. Chen, *Annu. Rev. Biochem.* **2014**, *83*, 317–340.

[128] M. Schliep, G. Cavigliasso, R. G. Quinnell, R. Stranger, A. W. Larkum, *Plant, Cell Environ.* **2013**, *36*, 521–527.

[129] Y. Kashiyama, H. Miyashita, S. Ohkubo, N. O. Ogawa, Y. Chikaraishi, Y. Takano, H. Suga, T. Toyofuku, H. Nomaki, H. Kitazato, T. Nagata, N. Ohkouchi *Science* **2008**, *321*, 658–658.

[130] T. Tsuchiya, T. Mizoguchi S. Akimoto, T. Tomo, H. Tamiaki, M. Mimuro, *Plant Cell Physiol.* **2012**, *53*, 518–527.

[131] M. Chen, M. Schliep, R. D. Willows, Z.-L. Cai, B. A. Neilan, H. Scheer, *Science* **2010**, *329*, 1318–1319.

[132] M. Chen, Y. Li, D. Birch, R. D. Willows *FEBS Lett.* **2012**, *586*, 3249–3254.

[133] S. Akutsu, D. Fujinuma, H. Furukawa, T. Watanabe, M. Ohnishi-Kameyama, H. Ono, S. Ohkubo, H. Miyashita, M. Kobayashi, *Photomed. Photobiol.* **2011**, *33*, 35–40.

[134] R. D. Willows, H. Scheer, M. Chen, *Org. Lett.* **2013**, *15*, 1588–1590.

[135] Y. Li, N. Scales, R. E. Blankenship, R. D. Willows, M. Chen, *Biochim. Biophys. Acta, Bioenerg*. **2012**, *1817*, 1292–1298.

[136] K. E. Borbas, 181 Chlorins. In *Handbook of Porphyrin Science*. 2016, pp. 1–149.

[137] Oelze, J. Analysis of Bacteriochlorophylls. In Methods in Microbiology; Academic Press: London, 1985; Vol. 18, pp 257−284.

[138] K. Vogl, M. Tank, G. S. Orf, R. E. Blankenship, D. A. Bryant, *Front. Microbiol.* **2012**, *3*, 298.

[139] C. Brückner, *Acc. Chem. Res.* **2016**, *49*, 1080–1092.

[140] P. Rothemund, *J. Am. Chem. Soc.* **1935**, *57*, 2010–2011.

[141] P. Rothemund, A. R. Menotti, *J. Am. Chem. Soc.* **1941**, *63*, 267–270.

[142] A. D. Adler, F. R. Longo, J. D. Finarelli, J. Goldmacher, J. Assour, L. Korsakoff, *J. Org. Chem.* **1967**, *32*, 476–476.

[143] J. S. Lindsey, H. C. Hsu, I. C. Schreiman, *Tetrahedron Lett.* **1986**, *27*, 4969–4970.

[144] J. S. Lindsey, *Acc. Chem. Res.* **2010**, *43*, 300–311.

[145] E. J. Tarlton, S. F. MacDonald, E. Baltazzi, *J. Am. Chem. Soc.* **1960**, *82*,4389–4395.

[146] C. Brückner, J. J. Posakony, C. K. Johnson, R. W. Boyle, B. R. James, D. Dolphin, *J. Porphyrins Phthalocyanines* **1998**, *2*, 455–465.

[147] W. W. Kalisch, M. O. Senge, *Angew. Chem. Int. Ed.* **1998**, *37*, 1107–1109; *Angew. Chem.* **1998**, *110*, 1156–1159.

[148] H. Fischer, W. Neumann, *Justus Liebigs Ann. Chem.* **1932**, *494*, 225–245.

[149] U. Eisner, A. Lichtarowicz, R. P. Linstead, *J. Chem. Soc.* **1957**, 733–739.

[150] H. Whitlock, R. Hanauer, *J. Org. Chem.* **1969**, *33*, 2169–2171.

[151] J. B. Paine III, W. B. Kirshner, D. W. Moskowitz, D. Dolphin, *J. Org. Chem.* **1976**, *41*, 3857–3860.

[152] J. L. Sessler, A. Mozaffari, M. R. Johnson, *Org. Synth.* **1998**, *70*, 68–77.

[153] H. H. Inhoffen, *Naturwissenschaften* **1968**, *55*, 457–462.

[154] G. Quinkert, *Eur. J. Org. Chem.* **2004**, *2004*, 3727–3748.

[155] S. Aronoff, M. Calvin, *J. Org. Chem.* **1943**, *8*, 205−223.

[156] M. Calvin, R. H. Ball, S. Aronoff, *J. Am. Chem. Soc.* **1943**, *65*, 2259–2259.

[157] R. H. Ball, G. D. Dorough, M. Calvin, *J. Am. Chem. Soc.* **1946**, *68*, 2278−2281.

[158] H. Fischer, P. Halbig, B. Walach, B. *Justus Liebigs Ann. Chem.* **1927**, *452*, 268−302.

[159] H. Fischer, K. Platz, H. Helberger, H. Niemer, *Justus Liebigs Ann. Chem.* **1930**, *479*, 26–42.

[160] H. Fischer, F, Baláž, *Justus Liebigs Ann. Chem.* **1942**, *553,* 166–186.

[161] W. Schlesinger, A. H. Corwin, L. J. Sargent, *J. Am. Chem. Soc.* **1950**, *72*, 2867−2871.

[162] H. H. Inhoffen, W. Nolte, *Liebigs Ann. Chem.* **1969**, *725*, 167−176.

[163] H. H. Inhoffen, *Pure Appl. Chem.* **1968**, *17*, 443−460.

[164] H. W. Whitlock Jr., R. Hanauer, M. Y. Oester, B. K. Bower, *J. Am. Chem. Soc.* **1969**, *91*, 7485–7489.

[165] N. J. Cusack, C. B. Reese, A. C. Risius, B. Roozpeikar, *Tetrahedron* **1976**, *32*, 2157−2162.

[166] E. E. van Tamelen, R. S. Dewey, R. J. Timmons, *J. Am. Chem. Soc.***1961**, *83*, 3725−3726.

[167] A. C. Tomé, P. S. S. Lacerda, M. G. P. M. S. Neves, J. A. S. Cavaleiro, *Chem. Commun,* **1997**, 1199–1200.

[168] A. M. G. Silva, A. C. Tomé, M. G. P. M. S. Neves, A. M. S. Silva, J. A. S. Cavaleiro, *Chem. Commun.* **1999**, 1767–1768.

[169] A. M. G. Silva, A. C. Tomé, M. G. P. M. S. Neves, J. A. S. Cavaleiro, *Tetrahedron Lett.* **2000**, *41*, 3065−3068.

[170] A. M. G. Silva, A. C. Tomé, M. G. P. M. S. Neves, A. M. S. Silva, J. A. S. Cavaleiro, *J. Org. Chem.* **2005**, *70*, 2306–2314.

[171] X. Li, J. Zhuang, Y. Li, H. Liu, S. Wang, D. Zhu, *Tetrahedron Lett.* **2005**, *46*, 1555–1559.

[172] N. A. M. Pereira, A. C. Serra, T. M. V. D. Pinho e Melo, *Eur. J. Org. Chem.* **2010**, 6539–6543.

[173] I. Meunier, R. K. Pandey, M. O. Senge, T. J. Dougherty, K. M. Smith, *J. Chem Soc., Perkin Trans 1*, **1994**, 961–969.

[174] A. R. Morgan, N. C. Tertel, *J. Org. Chem.* **1986**, *51*, 1347−1350.

[175] J. B. Conant, W. W. Moyer, *J. Am. Chem. Soc.* **1930**, *52*, 3013−3023.

[176] H. H. Inhoffen, J.-H. Fuhrhop, H. Voigt, H. Brockman, *Liebigs Ann. Chem.* **1966**, *695*, 133–143.

[177] Jackson, A. H. Structure, Properties and Distribution of Chlorophylls. In Chemistry and Biochemistry of Plant Pigments; Goodwin, T. W., Ed.; Academic Press: London, 1976; Vol. 1, pp 1−63.

[178] Y. Liu, S. Zhang, J. S. Lindsey, *Nat. Prod. Rep.* **2018**, *35*, 879–901

[179] P. A. Jacobi, S. Lanz, I. Ghosh, S. H. Leung, F. Löwer, D. Pippin, *Org. Lett.* **2001**, *3*, 831–834.

[180]. W. G. O'Neal, W. P. Roberts, I. Ghosh, P. A. Jacobi, *J. Org. Chem.* **2005**, *70*, 7243 – 7251.

[181] P. A. Jacobi, H. L. Brielmann, M. Chiu, I. Ghosh, S. I. Hauck, S. Lanz, S. Leung, Y. Li, H. Liu, F. Löwer, W. G. O'Neal, D. Pippin, E. Pollina, B. A. Prat, F. Robert, W. P. Roberts, C. Tassa, H. Wang, *Heterocycles* **2011**, *82*, 1029–1081.

[182] W. G. O'Neal, P. A. Jacobi, *J. Am. Chem. Soc.* **2008**, *130*, 1102–1108.

[183] W. G. O'Neal, W. P. Roberts, I. Ghosh, H. Wang, P. A. Jacobi, *J. Org. Chem.* **2006**, *71*, 3472–3480.

[184] M. J. Costello, C. Emblow, R. J. White, (Ed.) (2001). European register of marine species: a check-list of the marine species in Europe and a bibliography of guides to their identification. *Collection Patrimoines Naturels*, 50. Muséum national d'Histoire naturelle: Paris. ISBN 2-85653-538-0, pp. 463.

[185] L. Berec, P. J. Schembri, D. S. Boukal, *Oikos*, **2005**, *108*, 473–484.

[186] F.-P. Montforts, *Angew. Chem. Int. Ed.* **1981**, *20*, 778–779; *Angew. Chem.* **1981**, *93*, 795–796.

[187] G. M. Badger, R. L. N. Harris, R. A. Jones, *Aust. J. Chem.* **1964**, *17*, 1002–1012.

[188] R. B. Woodward, *Pure Appl. Chem.* **1968**, *17*, 519–547.

[189] R. B. Woodward, *Pure Appl. Chem.* **1971**, *25*, 283–304.

[190] R. B. Woodward, *Pure Appl. Chem.* **1973**, *33*, 145–178.

[191] A. Eschenmoser, *Naturwissenschaften* **1974**, *61*, 513–525.

[192] A. Eschenmoser, C. E. Winter, *Science* **1977**, *196*, 1410–1420.

[193] C. J. Dutton, C. J. R. Fookes, A. R. Battersby, *J. Chem. Soc., Chem. Commun,* **1983**, 1237–1238.

[194] A. A. Ryan, M. O. Senge, *Photochem. Photobiol. Sci.* **2015**, *14*, 638–660.

[195] T. Tumolo, U. M. Lanfer-Marquez, *Food Res. Int.* **2012**, *46*, 451–459.

[196] J. Usuda, H. Kato, T. Okunaka, K. Furukawa, H. Tsutsui, K. Yamada,Y. Suga, H. Honda, Y. Nagatsuka, T. Ohira, M. Tsuboi, T. Hirano, *J. Thorac. Oncol.* **2006**, *1*, 489–493.

[197] J. Usuda, S. Ichinose, T. Ishizumi, H. Hayashi, K. Ohtani, S. Maehara, S. Ono, N. Kajiwara, O. Uchida, H. Tsutsui, T. Ohira, H. Kato, N. Ikeda, *J. Thorac. Oncol.* **2010**, *5*, 62–68.

[198] J. Son. G. Yi, M.-H. Kwak, S. M. Yang, J. M. Park, B.-I. Lee, M.-G. Choi, H. Koo, *J. Nanobiotechnol.* **2019**, *17*, 50.

[199] A. Amirshaghaghi, L. Yan, J. Miller, Y. Daniel, J. M. Stein, T. M. Bush, Z. Cheng, A. Tsuorkas, *Sci. Rep.* **2019**, *9*, 2613.

[200] D. Zhang, M. Wu, Y. Zeng, L. Wu, Q. Wang, X. Han, X. Liu, J. Liu, *ACS Appl. Mater. Interfaces* **2015**, *7*, 8176–8187.

[201] N. J. Razum, A. B. Snyder, D. R. Doiron, *Proc. SPIE*, **1996**, *2675*, 43–XXX.

[202] N. V. Kudinova and T. T. Berezov*, Biochem. Mosc. Suppl. Ser. B Biomed. Chem*. **2010**, *4*, 95–843.

[203] T. S. Mang, R. Allison, G. Hewson, W. Snider, R. Moskowitz, *Cancer J. Sci. Am.* **1998**, *4*, 378–384.

[204] R. Baskaran, J. Lee, S.-G. Yang, *Biomater. Res*. **2018**, *22*, 25.

[205] R. K. Pandey, D. A. Bellnier, K. M. Smith, T. J. Dougherty, *Photochem. Photobiol.* **1991**, *53*, 65–72.

[206] NIH, U.S. National Library of Medicine, ClinicalTrials.gov, https://clinicaltrials.gov/ct2/show/NCT03757754, (assessed January 2022).

[207] D. A. Bellnier, W. R. Greco, H. Nava, G. M. Loewen, A. R. Oseroff, T. J. Dougherty, *Cancer Chemother. Pharmacol.* **2006**, *57*, 40–45.

[208] F. Segatta, L. Cupellini, M. Garavelli, B. Mennucci, *Chem. Rev.* **2019**, *119*, 9361–9380.

[209] D. Narzi, D. Bovi, P. De Gaetano, L. Guidoni, *J. Am. Chem. Soc.* **2016**, *138*, 257–264.

[210] J. S. Moore, *Acc. Chem. Res.* **1997**, *30*, 402–413.

[211] L. Wu, C. Huang, B. P. Emery, A. C. Sedgwick, S. D. Bull, X.-P. He, H. Tian, J. Yoon, J. L. Sessler, T. D. James, *Chem. Soc. Rev.* **2020**, *49*, 5110–5139.

[212] X. Zhang, Y. Xiao, X. Qian, *Angew. Chem. Int. Ed.* **2008**, *47*, 8025–8029; *Angew. Chem.* **2008**, *120*, 8145–8149.

[213] M. Bio, P. Rajaputra, Y. You, *Bioorg. Med. Chem. Lett.* **2016**, *26*, 145–148.

[214] J. Gutknecht, *J. Membr. Biol.* **1981**, *61*, 61–66.

[215] The Nobel Prize in Chemistry 2022. NobelPrize.org. Nobel Prize Outreach AB 2021. Mon. 24 Oct 2022. <https://www.nobelprize.org/prizes/chemistry/2022/summary/>

[216] M. Villa, P. Ceroni, A. Fermi, *ChemPlusChem* **2022**, *87*, e202100558

[217] M. Marchini, A. Luisa, G. Bergamini, N. Armaroli, B. Ventura, M. Baroncini, N. Demitri, E. Iengo, P. Ceroni, *Chem. – Eur. J.* **2021**, *27*, 16250–16259.

[218] B. Khurana, P. Gierlich, A. Meindl, L. C. Gomes-da-Silva, M. O. Senge, *Photochem. Photobiol. Sci.* **2019**, *18*, 2613–2656.

[219] C. Vera, F. Tulli, C. D. Borsarelli, *Front. Bioeng. Biotechnol.* **2021**, *9*, 655370.

[220] F. Bryden, A. Maruani, J. M. M. Rodridgues, M. H. Y. Cheng, H. Savoie, A. Beeby, V. Chudasama, R. W. Boyle, *Bioconjugate Chem.* **2018**, *29*, 176–181.

[221a] A. Maruani, H. Savoie, F. Bryden, S. Caddick, R. W. Boyle, V. Chudasama, *Chem. Commun.* **2015**, *51*, 15304–15307.

[221b] F. Bryden, A. Maruani, H. Savoie, V. Chudasama, M. E. B. Smith, S. Caddick, R. W. Boyle, *Bioconjugate Chem.* **2014**, *25*, 611–617.

[222] G. N. Murshudov, A. I. Grebenko, V. Barynin, Z. Dauter, K. S. Wilson, B. K. Vainshtein, W. Melik-Adamyan, J. Bravo, J. M. Ferrán, J. C. Ferrer, J. Switala, P. C. Loewen, I. Fita, *J. Biol. Chem.* **1996**, *271*, 8863–8868.

[223] I. Belevich, V. B. Borisov, A. A. Konstantinov, M. I. Verkhovsky, *FEBS Lett.* **2005**, *579*, 4567–4570.

[224] S. P. D. Turner, M. H. Block, Z-C. Sheng, S. C. Zimmerman, A. R. Battersby, *J. Chem. Soc. Chem. Commun*, **1985**, 583–585.

[225] Müller, G.; Deeg, R.; Gneuss, K. D.; Gunzer, G. On the Methylation Process in Cobyrinic Acid Biosynthesis. In Vitamin B12, Proceedings of the Third European

Symposium on Vitamin B12 and Intrinsic Factor, Zurich, Switzerland, March 5−8, 1979; Zagalak, B., Friedrich, W., Eds.; Walter de Gruyter: Berlin, 1979; pp 279−291.

[226] M. R. Prinsep, F. R. Caplan, R. E. Moore, G. M. L. Patterson, C. D. Smith, *J. Am. Chem. Soc.* **1992**, *114*, 385–387.

[227] W. Gul, P. Carvalho, D. W. Berberich, M. A. Avery, M. A. ElSohly, *Acta Crystallogr., Sect. E: Crystallogr. Commun.* **2008**, *E64*, o1686.

[228] R. Adams, C. Cain, W. D. McPhee, R. B. Wearn, *J. Am. Chem. Soc.* **1941**, *63*, 2209–2213.

[229] D. Crowfoot, C. W. Bunn, B. W. Rogers-Low, A. Turner-Jones, The Chemistry of Penicillin, 1949, 310, DOI: 10.1515/9781400874910

[230] J. Li, H. Renata, *J. Org. Chem.* **2021**, *86*, 11206–11211.

[231] Q. Dan, S. A. Newmister, K. R. Klas, A. E. Fraley, T. J. McAfoos, A. D. Somoza, J. D. Sunderhaus, Y. Ye, V. V. Shende, F. Yu, J. N. Sanders, W. C. Brown, L. Zhao, R. S. Paton, K. N. Houk, J. L. Smith, D. H. Sherman, R. M. Williams, *Nat. Chem*. **2019**, *11*, 972–980.

[232] T. T. Talele, *J. Med. Chem.* **2018**, *61*, 2166–2210.

[233] E. N. Hancock, J. M. Wahl, M. K. Brown, *Nat. Prod. Rep.* **2019**, *36*, 1383–1393.

[234] J.-P. Strachan, D. F. O'Shea, T. Balasubramanian, J. S. Lindsey, *J. Org. Chem.* **2000**, *65*, 3160–3172.

[235] A. R. Battersby, C. J. R. Fookes, R. J. Snow, *J. Chem. Soc., Perkin Trans. 1* **1984**, 2725–2732.

[236] A. R. Battersby, S. P. D. Turner, M. H. Block, Z.-C. Sheng, S. C. Zimmerman, *J. Chem. Soc., Perkin Trans. 1* **1988**, 1577–1586.

[237] M. Taniguchi, D. Ra, G. Mo, T. Balasubramanian, J. S. Lindsey, *J. Org. Chem.* **2001**, *66*, 7342–7354.

[238] M. Ptaszek, J. Bhaumik, H.-J. Kim, M. Taniguchi, J. S. Lindsey, *Org. Process Res. Dev.* **2005**, *9*, 651–659.

[239] T. Balasubramanian, J.-P. Strachan, P. D. Boyle, J. S. Lindsey, *J. Org. Chem.* **2000**, *65*, 7919–7929.

[240] A. M. van Leusen, H. Siderius, B. E. Hoogenboom, D. van Leusen, *Tetrahedron Lett.* 1972, **52**, 5337–5340.

[241] H. Fischer, K. Zeile, *Liebigs Ann. Chem.* **1929**, *468*, 98–116.

[242] H. Fischer, A. Kirstahler, *Liebigs Ann. Chem.* **1928**, *466*, 178–188.

[243] J. P. Nagarkatti, K. R. Ashley, *Synthesis*, **1974**, *3*, 186–187.

[244] C.-H. Lee, J. S. Lindsey, *Tetrahedron* **1994**, *50*, 11427–11440.

[245] B. J. Littler, M. A. Miller, C.-H. Hung, R. W. Wagner, D. F. O'Shea, P. D. Boyle, J. S. Lindsey, *J. Org. Chem.* **1999**, *64*, 1391–1396.

[246] J. K. Laha, S. Dhanalekshmi, M. Taniguchi, A. Ambroise, J. S. Lindsey, *Org. Process Res. Dev.* **2003**, *7*, 799–812.

[247] M. Ptaszek, B. E. McDowell, J. S. Lindsey, *J. Org. Chem.* **2006**, *71*, 4328–4331.

[248] H.-J. Kim, D. K. Dogutan, M. Ptaszek, J. S. Lindsey, *Tetrahedron* **2007**, *63*, 37–55.

[249] J. S. Lindsey, *Chem. Rev.* **2015**, *115*, 6534–6620.

[250] M. Ptaszek, B. E. McDowell, M. Taniguchi, H.-J. Kim, J. S. Lindsey, *Tetrahedron* **2007**, *63*, 3826–3839.

[251] Y. Abel, I. Vlassiouk, E. Lork, S. Smirnov, M. R. Talipov, F.-P. Montforts, *Chem. Eur J.* **2020**, *26*, 17120–17127.

[252] Y. Liu, J. S. Lindsey, *J. Org. Chem.* **2016**, *81*, 11882–11897.

[253] M. Ptaszek, D. Lahaye, M. Krayer, C. Muthiah, J. S. Lindsey, *J. Org. Chem.* **2010**, *75*, 1659–1673.

[254] M. O. Senge, *Chem. Commun,* **2011**, *47*, 1943–1960.

[255] O. Mass, M. Ptaszek, M. Taniguchi, J. R. Diers, H. L. Kee, D. F. Bocian, D. Holten, J. S. Lindsey, *J. Org. Chem.* **2009**, *74*, 5276–5289.

[256] R. Xiong, A. I. Arkhypchuk, K. Eszter Borbas, *J. Porphyrins Phthalocyanines*, **2019**, *23*, 589–598.

[257] M. Krayer, M. Ptaszek, H.-J. Kim, K. R. Meneely, D. Fan, K. Secor, J. S. Lindsey, *J. Org. Chem.* **2010**, *75*, 1016–1039.

[258] A. I. Arkhypchuk, R. Xiong, K. E. Borbas, *J. Inorg. Biochem.* **2020**, *205*, 110979.

[259] R. Giovannetti, *Macro to Nano Spectrosc.* **2012**, *1*, 87–108.

[260] D. Marsh, L. Mink, *J. Chem. Educ.* **1996**, *73*, 1188–1190.

[261] A. M. Brouwer, *Pure Appl. Chem.* **2011**, *83*, 2213–2228.

[262] R. Bonnett, P. Charlesworth, B. D. Djelal, S. Foley, D. J. McGarvey, T. G. Truscott, *J. Chem. Soc. Perkin Trans. 2* **1999**, 325–328.

[263] W. P. Helman, A. B. Ross, F. Wilkinson, *J. Phys. Chem. Ref. Data* **1993**, *22*, 113–262.

[264] E. F. F. Silva, F. A. Schaberle, C. J. P. Monteiro, J. M. Dąbrowski, L. G.Arnaut, *Photochem. Photobiol. Sci.* **2013**, *12*, 1187–1192.

[265] E. G. Azenha, A. C. Serra, M. Pineiro, M. M. Pereira, J. Seixas de Melo, L. G. Arnaut, S. J. Formosinho, A. M. d. A. R. Gonsalves, *Chem. Phys.* **2002**, *280*, 177–190.

[266] J. Zhao, W. Wu, J. Sun, S. Guo, *Chem. Soc. Rev.* **2013**, *42*, 5323–5351.

[277] M. Taniguchi, H.-J. Kim, D. Ra, J. K. Schwartz, C. Kirmaier, E. Hindin, J. R. Diers, S. Prathapan, D. F. Bocian, D. Holten, J. S. Lindsey, *J. Org. Chem.* **2002**, *67*, 7329–7342.

[278] C. B. Gairaud, G. R. Lappin, *J. Org. Chem.* **1953**, *18*, 1–3.

[279] J. S. Yadav, S. Abraham, B. V. S. Reddy, G. Sabitha, *Tetrahedron Lett.* **2001**, *42*, 8063–8065.

[280] J. K. Laha, S. Dhanalekshmi, M. Taniguchi, A. Ambroise, J. S. Lindsey, *Org. Proc. Res. Dev.* **2003**, *7*, 799–812.

[281] M. Liu, M. Ptaszek, O. Mass, D. F. Minkler, R. D. Sommer, J. Bhaumik, J. S. Lindsey, *New J. Chem.* **2014**, *38*, 1717–1730.

[282] C. Muthiah, M. Ptaszek, T. M. Nguyen, K. M. Flack, J. S. Lindsey, *J. Org. Chem.* **2007**, *72*, 7736–7749.

[283] M. Taniguchi, M. N. Kim, D. Ra, J. S. Lindsey, *J. Org. Chem.* **2005**, *70*, 275–285.

[284] C. Muthiah, D. Lahaye, M. Taniguchi, M. Ptaszek, J. S. Lindsey, *J. Org. Chem.* **2009**, *74*, 3237−3247.

[285] J. K. Laha, C. Muthiah, M. Taniguchi, B. E. McDowell, M. Ptaszek J. S. Lindsey, *J. Org. Chem.* **2006**, *71*, 4092–4102.

[286] G. Zheng, M. Aoudia, D. Lee, M. A. Rodgers, K. M. Smith, T. J. Dougherty, R. K. Pandey, *J. Chem. Soc., Perkin. Trans. 1.* **2000**, 3113–3121.

[287] M. Ptaszek, J. Bhaumik, H.-J. Kim, M. Taniguchi, J. S. Lindsey, *Org. Proc. Res. Dev.* **2005**, *9*, 651–659.

[288] M. Krayer, T. Balasubramanian, C. Ruzié, M. Ptaszek, D. L. Cramer, M. Taniguchi, J. S. Lindsey, *J. Porphyrins Phthalocyanines* **2009**, *13*, 1098–1110.

[289] R. Xiong, A.-B. Bornhof, A. I. Arkhypchuk, A. Orthaber, K. E. Borbas, *Chem. – Eur. J.* **2017**, *23*, 4089–4095.

[290] R. Xiong, A. I. Arkhypchuk, D. Fovacs, A. Orthaber, K. E. Borbas, *Chem. Commun.* **2016**, *52*, 9056–9058.

[291] Z. Yu, C. Pancholi, G. V. Bhagavathy, H. S. Kang, J. K. Nguyen, M. Ptaszek, *J. Org. Chem.* **2014**, *79*, 7910–7925.

[292] A. Meares, G. V. Bhagavathy, S. R. Zik, T. Gallagher, M. Ptaszek, *J. Org. Chem.* **2018**, *83*, 9076–9087.

[293] R. Xiong, D. Mara, J. Liu, R. V. Deun, K. E. Borbas, *J. Am. Chem. Soc.* **2018**, *140*, 10975–10979.

[294] C. Ruzié, M. Krayer, J. S. Lindsey, *Org. Lett.* **2009**, *11*, 1761–1764.

[295] D. Ra, K. A. Gauger, K. Muthukumaran, T. Balasubramanian, V. Chandrashaker, M. Taniguchi, Z. Yu, D. C. Talley, M. Ehudin, M. Ptaszek, J. S. Lindsey, *J. Porphyrins Phthalocyanines* **2015**, *19*, 547–572.

[296] A. Meares, A. Satraitis, N. Santhanam, Z. Yu, M. Ptaszek, *J. Org. Chem.* **2015**, *80*, 3858–3869.

[297] B. Uthe, A. Meares, M. Ptaszek, M. Pelton, *J. Chem. Phys.* **2020**, *153*, 074302.

[298] M. K. Kuimova, G. Yahiogllu, P. R. Ogilby, *J. Am. Chem. Soc.* **2009**, *131*, 332–340.

[299] A. Z. Muresan, J. S. Lindsey, *Tetrahedron* **2008**, *64*, 11440–11448.

[300] K. E. Borbas, P. Mroz, M. R. Hamblin J. S. Lindsey, *Bioconjugate Chem.* **2006**, *17*, 638–653.

[301] L. Rogers, N. N. Sergeeva, E. Paszko, G. M. F. Vaz, M. O. Senge, *PLOS One* **2015**, 0125372.

[302] M. H. Staegemann, S. Gräffe, R. Haag, A. Wiehe, *Org. Biomol. Chem.* **2016**, *14*, 9114–9132.

[303] K. Urbańska, M. Pawlicki, *J Org. Chem.* **2020**, *85*, 8196–8202.

[304] F. Guintini, C. M. A. Alonso, R. W. Boyle, *Photochem. Photobiol. Sci.* **2011**, *10*, 759–791.

[305] K. Karikis, E. Georgils, G. Charalambidis, A. Petrou, O. Vakuliuk, T. Chatziioannou, I. Raptaki, S. Tsovola, I. Papakyriacou, A. Mitraki, D. T. Gryko, A. G. Coutsolelos, *Chem. – Eur. J.* **2016**, *22*, 11245–11252.

[306] J. Sandland, R. W. Boyle, *Bioconjugate Chem.* **2019**, *30*, 975–993.

[307] J. Laakso, G. A. Rosser, C. Szijjártó, A. Beeby, K. E. Borbas, *Inorg. Chem.* **2012**, *51*, 10366–10374.

[308] M. Liu, C.-Y. Chen, A. K. Mandal, V. Chadnrashaker, R. B. Evans-Storms, J. B. Pitner, D. F. Bocian, D. Holten, J. S. Lindsey, *New. J. Chem.* **2016**, *40*, 7721–7740.

[309] C. Donohoe, F. A. Schaberle, F. M. S. Rodrigues, N. P. F. Goncalves, C. J. Kingsbury, M. M. Pereira, M. O. Senge, L. C. Gomes-da-Silva, L. G. Arnaut, *J. Am. Chem. Soc.* **2022**, *144*, 15252–15265.

[310] P. Mroz, Y.-Y. Huang, A. Szokalska, T. Zhiyentayev, S. Janjua, A.-P. Nifli, M. E. Sherwood, C. Ruzié, K. E. Borbas, D. Fan, M. Krayer, t. Balasubramanian, E. Yang,

H. L. Kee, C. Kirmaier, J. R. Diers, D. F. Bocian, D. Holten, J. S. Lindsey, M. R. Hamblin, *FASEB J.* **2010**, *24*, 3160–3170.

[311] Y. Y. Huang, P. Mroz, T. Zhiyentayev, S. K. Sharma, T. Balasubramanian, C. Ruzié, M. Krayer, D. Fan, K. E. Borbas, E. Yang, H. L. Kee, C. Kirmaier, J. R. Diers, D. F. Bocian, D. Holten, J. S. Lindsey, M. R. Hamblin, *J. Med. Chem.* **2010**, *53*, 4018–4027.

[312] F. Ogata, T. Nagaya, Y. Maruoka, J. Akhigbe, A. Meares, M. Y. Lucero, A. Satraitis, D. Fujimura, R. Okada, F. Inagaki, P. L. Choyke, M. Ptaszek, H. Kobayashi, *Bioconjugate Chem.* **2019**, *30*, 169–183.

[313] H. L. Kee, R. Nothdurft, C. Muthiah, J. R. Diers, D. Fan, M. Ptaszek, D. F. Bocian, J. S. Lindsey, J. P. Culver, D. Holten, *Photochem. Photobiol.* **2008**, *84*, 1061–1072.

[314] Z. Yu, M. Ptaszek, *J. Org. Chem.* **2013**, *78*, 10687–10691.

[315] J. S. D. Mieog, F. B. Achterberg, A. Zlitni, M. Hutteman, J. Burggraaf, R.-J. Swijneburg, S. Gioux, A. L. Vahrmeijer, *Nat. Rev. Clin. Oncol.* **2022**, *19*, 9–22.

[316] O. Mass, J. S. Lindsey, *J. Org. Chem.* **2011**, *76*, 9478–9487.

[317] S. Y. Yap, H. Savoie, I. Renard, B. P. Burke, H. C. Sample, S. Michue-Seijas, S. J. Archibald, R. W. Boyle, G. J. Stasiuk, *Chem. Commun.* **2020**, *56*, 11090–11093.

[318] M. Hagras, A. MA. Mandour, E. A. Mohamed, E. B. Elkaeed, I. M.M. Gobaara, A. B. M. Mehany, N. S. M. Ismail, H. M. Refaat, *RSC Adv.* **2021**, *11*, 39728–39741.

[319] A. S. Negi, Y. Gautam, S. Alam, D. Chanda, S. Luqman, J. Sarkar, F. Khan, R. Konwar, *Bioorg. Med. Chem.* **2015**, *23*, 373–389.

[320] H. L. Smith, *Lancet*, **1913**, *181*, 846–846.

[321] A. Mariani, A. Bartoli, M. Atwal, K. C. Lee, C. A. Austin, R. Rodriguez, *J. Med. Chem.* **2015**, *58*, 4851–4856.

[322] T. M. Kosak, H. A. Conrad, A. L. Korich, R. L. Lord, *Eur. J. Org. Chem.* **2015**, *34*, 7460–7467.

[323] P. Brough, e-EROS Encycl. Reagents Org. Synth. 2001, https://doi.org/10.1002/047084289X.rn031

[324] A. Masashi, S. Shigeru, T. Hisashi, M. Teruaki, *Bull. Chem. Soc. Japan,* **1974**, *47*, 1777–1780.

[325] P. D. Rao, B. J. Littler, G. Richard Geier, J. S. Lindsey, *J. Org. Chem.* **2000**, *65*, 1084–1092.

[326] M. L. Perrin, F. Prins, C. A. Martin, A. J. Shaikh, R. Eelkema, J. H. van Esch, T. Briza, R. Kaplanek, V. Kral, J. M. van Ruitenbeek, H. S. van der Zant, D. Dulić, *Angew. Chem. Int. Ed.* **2011**, *50*, 11223–11226; *Angew. Chem.* **2011**, *123*, 11419–11422.

[327] A. Hamdan, J.W. F. Wasley, *Synth. Commun.* **1985**, *15*, 71–74.

[328] M. Krayer, T. Balasubramanian, C. Ruzié, M. Ptaszek, D. L. Cramer, M. Tainguchi, J. S. Lindsey, *J. Porphyrins Phthalocyanines*, **2009**, *13*, 1098–1110.

[329] H. J. Anderson, S.-F. Lee, *Can. J. Chem.* **1965**, *43*, 409–414.

[330] D. Bahulayan, S. K. Das, J. Iqbal, *J. Org. Chem.* **2003**, *68*, 5735–5738.

[331] H. Jing, P. Wang, B. Chen, J. Jiang, P. Vairaprakash, S. Liu, J. Rong, C.-Y. Chen, P. Nalaoh, J. S. Lindsey, *New. J. Chem.* **2022**, *46*, 5534–5555.

[332] D. T. M. Chung, P. V. Tran, K. C. Nguyen, P. Wang, J. S. Lindsey, *New J. Chem.* **2021**, *45*, 13302–13316.

[333] J. Jiang, P. Vairaprakash, K. R. Reddy, T. Sahin, M. P. Pavan, E. Lubian, J. S. Lindsey, *Org. Biomol. Chem.* **2014**, *12*, 86–103.

[334] H. L. Kee, J. R. Diers, M. Ptaszek, C. Muthiah, D. Fan, J. S. Lindsey, D. F. Bocian, D. Holten, *Photochem. Photobiol.* **2009**, *85*, 909–920.

[335] C. Muthiah, H. L. Kee, J. R. Diers, D. Fan, M. Ptaszek, D. F. Bocian, D. Holten, J. S. Lindsey, *Photochem. Photobiol.* **2008**, *84*, 786–801.

[336] E. B. Fleischer, A. M. Schachter, *Inorg. Chem.* **1991**, *30*, 3763–3769.

[337] T. E. O. Screen, K. B. Lawton, G. S. Wilson, N. Dolney, R. Ispasoiu, T. Goodson III, S. J. Martin, D. D. C. Bradley, H. L. Anderson, *J. Mater. Chem.* **2001**,*11*, 312–320.

[338] K. Rajesh, M. Somasundaram, R. Saiganesh, . K. Balasubramanian, *J. Org. Chem.* **2007**, *72*, 5867–5869.

[339] F. L. Lambert, W. D. Ellis, R. J. Parry, *J. Org. Chem.* **1965**, *30*, 304–306.

[340] J. Duan, L. H. Zhang, W. R. Dolbier, Jr. *Synlett*, **1999**, *8*, 1245–1246.

[341] A. S. Cannon, B. M. Foxman, D. J. Guarrera, J. C. Warner, *Crystal Growth & Design*, **2005**, *5*, 407–411.

[342] K. Ogawa, S. Tanaka, K. Shimura, *RSC Adv.* **2020**, *10*, 9657–9662.

[343] D. C. Batesky, M. J. Goldfogel, D. J. Weix, *J. Org. Chem.* **2017**, *82*, 9931–9936.

[344] C. J. Kingsbury, M. O. Senge, *Coord. Chem. Rev.* **2021**, *431*, 213760.

[345] M. O. Senge, *Chem. Commun.* **2006**, 243–256.

[346] W. Jentzen, J.-G. Ma, J. A. Shelnutt, *Biophys. J.* **1998**, *74*, 753–763.

[347] J. Karges, *ChemBioChem* **2020**, *21*, 3044–3046.

[348] A. Noweski, A. Roosen, S. Lebdai, E. Barret, M. Emberton, F. Benzaghou, M. Apfelbeck, B. Gaillac, C. Gratzke, C. Stief, A. R. Azzouzi, *Eur. Urol. Focus* **2019**, *5*, 1022–1028.

[349] A. M. Bugaj, *World J. Methodol.* **2016**, *6*, 65–76.

[350] M. Taniguchi, J. S. Lindsey, D. F. Bocian, D. Holten, *J. Photochem. Photobiol., C.* **2021**, *46*, 100401.

[351] R. Schmidt, C. Tanielian, R. Dunsbach, C. Wolff, *J. Photochem. Photobiol., A*, **1994**, *79*, 11–17.

[352] C. Würth, M. Grabolle, J. Pauli, M. Spieles, U. Resch-Genger, *Nat. Protoc.* **2013**, *8*, 1535–1550.

[353] J. Deng, H. Li, M. Yang, F. Wu, *Photochem. Photobiol. Sci.* **2020**, *19*, 905–912.

[354] M. A. Filatov, S. Baluschev, I. Z. Ilieva, V. Enkelmann, T. Miteva, K. Landfester, S. E. Aleshchnkov, A. V. Cheprakov, *J. Org. Chem.* **2012**, *77*, 11119–11131.

[355] D. Eastwood, M. Goutermann, *J. Mol. Spec.* **1970**, *35*, 359–375.

[356] D. J. Gibbons, A. Farawar, P. Mazzella, S. Leory-Lhez, R. M. Williams, *Photochem. Photobiol. Sci.* **2020**, *19*, 136–158.

[357] W.-P. To, Y. Liu, T.-C. Lau, C.-M. Che, *Chem. – Eur. J.* **2013**, *19*, 5654–5664.

[358] M. C. Daza, M. Doerr, S. Salzmann, C. M. Marian, W. Thiel, *Phys. Chem. Chem. Phys.* **2009**, *11*, 1688–1696.

[359] M. Segado, M. Reguero, *Phys. Chem. Chem. Phys.* **2011**, *13*, 4138–4148.

[360] J. Arnbjerg, M. J. Paterson, C. B. Nielsen, M. Jørgensen, O. Christiansen, P. R. Ogilby, *J. Phys. Chem. A*, **2007**, *111*, 5756–5767.

[361] L. V. Lutkus, S. S. Rickenbach, T. M. McCormick, *J. Photochem. Photobiol., A*, **2019**, *378*, 131–135.

[362] A. Barbieri, E. Bandini, F. Monti, V. K. Praveen, N. Armaroli, *Top. Curr. Chem.* **2016**, *374*, 47.

[363] H. Mori, T. Tanaka, A. Osuka, *J. Mater. Chem. C*, **2013**, *1*, 2500–2519.

[364] J.-X. Liu, S.-L. Mei, X.-H. Chen, C.-J. Yao, *Crystals*, **2021**, *11*, 155.

[365] B. A. Pulaski, S. Ostrand-Rosenberg, *Curr. Protoc. Immunol.* **2001**, *39*, 20.2.1-20.2.16.

[366] B. Schöra, S. Boegel, C. Albrecht, T. Bukur, V. Bukur, C. Holsträter, C. Ritzel, K. Manninen, A. D. Tadmor, M. Vormehr, U. Sahin, M. Löwer, *Front. Oncol.* **2020**, *10*, 1195.

[367] P. Kaur, G. M. Nagaraja, H. Zheng, D. Gizachew, M. Galukande, S. Krishnan, A. Asea, *BMC Cancer*, **2012**, *12*, 120.

[368] B. D. Lehmann, A. Colaprico, Tiago C. Silva, J. Chen, H. An, Y. Ban, H. Huang, L. Wang, J. L. James, J. M. Balko, P. I. Gonzalez-Ericsson, M. E. Sanders, B. Zhang, J. A. Pietenpol, X. S. Chen, *Nat. Commun.* **2021**, *12*, 6276.

[369] P. N. Munshi, M. Lubin, J. R. Bertino, *The Oncologist*, **2014**, *19*, 760–765.

[370] F. Schaberle, *Photodiagn. Photodyn. Ther.* **2018**, *23*, 75–77.

[371] M. Taniguchi, M. Ptaszek, B. E. McDowell, J. S. Lindsey, *Tetrahedron*, **2007**, *63*, 3840–3849.

[372] A. I. S. B. Villaverde, J. Netherton, M. A. Baker, *Antioxidants*, **2018**, *8*, 616.

[373] E. Paszko, C. Ehrhard, M. O. Senge, D. P. Kelleher, J. V. Reynolds, *Photodiagn. Photodyn. Ther.* **2011**, *8*, 224–231.

[374] D. Kessel, *Int. J. Clin. Pract.* **1997**, *53*, 263–267.

[375] D. D. La, S. V. Bhosale, L. A. Jones, S. V. Bhosale, *ACS Appl. Mater Interfaces* **2018**, *10*, 12189–12216.

[376] P. D. Boissieu, *J. Chem. Soc., Abstr.* **1888**, *54*, 928–972.

[377] There may be more information in the original publication (*Bull. Soc. Chim.,***1888**, *49*, 681–682) however we have not been able to access this.

[378] J. Schmidlin, *Ber. Dtsch. Chem. Ges.* **1907**, *40*, 2136–2329.

[379] A. Behr, *Ber. Dtsch. Chem. Ges.* **1872**, *5*, 970–972.

[380] H. Wuyts, *Ber. Dtsch. Chem. Ges.* **1903**, *36*, 863–870.

[381] Manchot, Krische, *Justus Liebigs Ann. Chem.* **1904**, *337*, 200.

[382] L. H. Cone, C. S. Robinson, *Ber. Dtsch. Chem. Ges.* **1907**, *40*, 2160–2166.

[383] E. Bergmann, D. Wagenberg, *Ber. Dtsch. Chem. Ges.* **1930**, *63*, 2585–2592.

[384] Orechow, *Bull. Soc. Chim. Fr.* **1919**, *4*, 188.

[385] W. E. Bachmann, *J. Am. Chem. Soc.* **1933**, *55*, 3857–3859.

[386] W. Schlenk, E. Bergmann, *Justus Liebigs Ann. Chem.* **1928**, *463*, 1–97.

[387] J. Schmidlin, R. von Escher, *Ber. Dtsch. Chem. Ges.* **1910**, *43*, 1153–1161.

[388] K. V. Sajna, V. Srinivas, K. C. K. Swamy, *Adv. Synth. Catal.* **2010**, *352*, 3069–3081.

[389] Y. Tezuka, A. Hashimoto, K. Ushizaka, K. Imai, *J. Org. Chem.* **1990**, *55*, 329–333.

[390] W. Wang, T. Lin, M. Wang, T.-X. Liu, L. Ren, D. Chen, S. Huang, *J. Phys. Chem. B* **2010**, *114*, 5983–5988.

[391] M. Teruaki, S. Toshio, H. Junichi, *Chem. Lett.* **1973**, *2*, 1041–1044.

[392] S. Tyrlik, I. Wolochowicz, *Bull. Soc. Chim. Fr.*, **1973**, 2147.

[393] J. E. McMurry, M. P. Fleming, *J. Am. Chem. Soc.* **1974**, *96*, 4708–4709.

[394] J. E. McMurry, M. P. Fleming, K. L. Kees, L. R. Kepski, *J Org. Chem.* **1978**, *43*, 3255–3266.

[395] H. Tong, Y. Hong, Y. Dong, M. Häußler, J. W. Y. Lam, Z. Li, Z. Guo, Z. Guo, B. Z. Tang, *Chem. Commun.* **2006**, 3705–3707.

[396] B. Z. Tang, H. Xu, J. W. Y. Lam, P. P. S. Lee, K. Xu, Q. Sun, K. K. L. Cheuk, *Chem. Mater.* **2000**, *12*, 1446–1455.

[397] J. Luo, Z. Xie, J. W. Y. Lam, L. Cheng, H. Chen, C. Qiu, H. S. Kwok, X. Zhan, Y. Liu, D. Zhu, B. Z. Tang, *Chem. Commun.* **2001**, 1740–1741.

[398] T. Förster, K. Kasper, *Z. Phys. Chem. (Muenchen, Ger.)* **1954**, *1*, 275– 277.

[399] Photophysics of Aromatic Molecules; Birks, J. B., Ed.; Wiley: London, 1970.

[400] A. Hoekstra, A.Vos, *Acta Crystallogr., Sect. B: Struct. Sci., Cryst. Eng. Mater.* **1975**, *31*, 1716–1721.

[401] G. Yu, S. Yin, Y. Liu, J. Chen, X. Xu, X. Sun, D. Ma, X. Zhan, Q. Peng, Z. Shuai, B. Tang, D. Zhu, W. Fang, Y. Luo, *J. Am. Chem. Soc.* **2005**, *127*, 6335–6346.

[402] A. Camerman, J. Trotter, *Proc. R. Soc. Lond. A.* **1964**, *279*, 129–146.

[403] C. J. Bongale, C.-W. Chang, C.-S. Lee, E. W.-G. Diau, C.-S. Hsu, *J. Phys. Chem. B*. **2005**, *109*, 13472–13482.

[404] Z. Zhao, B. He, B. Z. Tang, *Chem. Sci.* **2015**, *6*, 5347–5365.

[405] Y. Liu, Y. Tang, N. N. Barashkov, I. S. Irgibaeva, J. W. Y. Lam, R. Hu, D. Birimzhanova, Y. Yu, B. Z. Tang, *J. Am. Chem. Soc.* **2010**, *132*, 13951–13953.

[406] J. Mei, N. L. C. Leung, R. T. K. Kwok, J. W. Y. Lam, B. Z. Tang, *Chem. Rev.* **2015**, *115*, 11718–11940.

[407] Z. He, C. Ke, B. Z. Tang, *ACS Omega*, **2018**, *3*, 3267–3277.

[408] J. Mei, Y. Hong, W. Y. Lam, A. Qin, Y. Tang, B. Z. Tang, *Adv. Mater.* **2014**, *26*, 5429–5479.

[409] N. Grover, M. O. Senge, *Synthesis*, **2020**, *52*, 3295–3325.

[410] N.Shustova, A.F.Cozzolino, M. Dinca, *J. Am. Chem. Soc.* **2012**, *134*, 19596–19599.

[411] H. Ding, J. Li, G. Xie, G. Lin, R. Chen, Z. Peng, C. Yang, B. Wang, J. Sun, C. Wang, *Nat. Commun.* **2018**, *9*, 5234.

[412] L. Bian, Y. Liang, Z. Liu, *ACS Appl. Nano Mater.* **2022**, doi.org/10.1021/acsanm.2c01250.

[413] H.-T. Feng, J.-H. Wang, Y.-S. Zheng, *ACS Appl. Mater. Interfaces* **2014**, *6*, 20067–20074.

[414] S. Song, Y.-S. Zheng, *Org. Lett.* **2013**, *15*, 820–823.

[415] W. Dong, Z. Ma, P. Chen, Q. Duan, *Mater. Lett.* **2019**, *236*, 480–482.

[416] J. Shi, J. Huang, R. Tang, Z. Chai, J. Hua, J. Qin, Q. Li, Z. Li, *Eur. J. Org. Chem.* **2012**, *27*, 5248–5255.

[417] D. P. Hagberg, T. Edvinsson, T. Marinado, G. Boschloo, A. Hagfeldt, L. Sun, *Chem. Commun.* **2006**, 2245–2247.

[418] L. Zhu, W. Xie, L. Zhao, Y. Zhang, Z. Chen, *RSC Adv.* **2017**, *7*, 55839–55845.

[419] N. Zarrabi, C. Agatemor, G. N. Lim, A. J. Matula, B. J. Bayard, V. S. Batista, F. D'Souza, P. K. Poddutoori, *J. Phys. Chem. C* **2019**, *123*, 131–143.

[420] Z. Liu, Z. Jiang, M. Yan, X. Wang, *Front. Chem.* **2019**, *7*, 712.

[421] Z. Li, Y. Chen, X. Lv, W.-F. Fu, *New J. Chem.* **2013**, *37*, 3755–3761.

[422] Y. Zhao, S. He, J. Yang, H. Sun, X. Shen, X. Han, Z. Ni, *Opt. Mater.* **2018**, *81*, 102–108.

[423] C. F. A. Gomez-Duran, R. Hu, G. Feng, T. Li, F. Bu, M. Arseneault, B. Liu, E. Peña-Carbrera, B. Z. Tang, *ACS Appl. Mater. Interfaces* **2015**, *7*, 15168–15176.

[424] B. Dhokale, T. Jadhav, S. M. Mobin, R. Misra, *J. Org. Chem.* **2015**, *80*, 8018–8025.

[425] R. Hu, C. F. A. Gómez-Durán, J. W. Y. Lam, J. L. Belmonte-Vázquez, C. Deng, S. Chen, R. Ye, E. Peña-Carbrera, Y. Zhong, K. S. Wong, B. Z. Tang, *Chem. Commun.* **2012**, *48*, 10099–10101.

[426] J. Zou, Z. Yin, K. Ding, Q. Tang, J. Li, W. Si, J. Shao, Q. Zhang, W. Huang, X. Dong, *ACS Appl. Mater. Interaces* **2017**, *9*, 32475–32481.

[427] A. Kamkaew, S. H. Lim, H. B. Lee, L. V. Kiew, L. Y. Chung, K. Burgess, *Chem. Soc. Rev.* **2013**, *42*, 77–88.

[428] M. A. Filatov, S. Karuthedath, P. M. Polestshuk, H. Savoie, K. J. Flanagan, C. Sy, E. Sitte, M. Telitchko, F. Laquai, R. W. Boyle, M. O. Senge, *J. Am. Chem. Soc*. **2017**, *139*, 6282–6285.

[429] M. A. Filatov, S. Karuthedath, P. M. Polestshuk, S. Callaghan, K. J. Flanagan, M. Telitchko, T. Wiesner, F. Laquai, M. O. Senge, *Phys. Chem. Chem. Phys.* **2018**, *20*, 8016–8031.

[430] N. Kiseleva, M. A. Filatov, M. Oldenburg, D. Busko, M. Jakoby, I. A. Howard, B. S. Richards, M. O. Senge, S. M. Borisov, A. Turshatov, *Chem. Commun.* **2018**, *54*, 1607–1610.

[431] G. M. Locke, K. J. Flanagan, M. O. Senge, *Beilstein J. Org. Chem.* **2020**, *16*, 763–777.

[432] J. Wang, J. Mei, E. Zhao, Z. Song, A. Qin, J. Z. Sun, B. Z. Tang, *Macromolecules* **2012**, *45*, 7692–7703.

[433] Y. Xu, D. Chang, S. Feng, C. Zang, J.-X. Jiang, *New J. Chem.* **2016**, *40*, 9415–9423.

[434] Z. Wang, C.-Y. Zhu, J.-T. Mo, P.-Y. Fu, Y.-W. Zhao, S.-Y. Yin, J.-J. Jiang, M. Pan, C.-Y. Su, *Angew. Chem. Int. Ed.* **2019**, *58*, 9752–9757; *Angew. Chem.* **2019**, *131*, 9854–9859.

[435] For halogen = F: S. J. Maginn, R. J. Davey, *Acta Cryst.* **1994**, *C50*, 254–255.

[436] For halogen = Cl: a) V. V. Mitkevich, V. G. Lirstman, M. A. Strzhemechny, A. A. Avdeenko, V. V. Eremenko, *Acta Cryst.* **1999**, *B55*, 799–906; b) W. Manthey, K. Plieth, A. Singewald, *Ber. Bunsenges. Phy. Chem.* **1952**, *56*, 690–694.

[437] For halogen = Br: B. Peric, B. Kojic-Prodic, *Acta Cryst.* **2000**, *C56*, 211–212.

[438] For halogen = I: G. P. M. Van Der Velden, J. H. Noordik, *J. Cryst. Mol. Struct.* **1979**, *9*, 283–294.

[439] S.-Y. Jiang, S.-X. Gan, X. Zhang, H. Li, Q.-Y. Qi, F.-Z. Cui, J. Lu, X. Zhao, *J. Am. Chem. Soc.* **2019**, *141*, 14981–14986.

[440] A. F. M. EL-Mahdy, M. G. Mohamed, T. H. Mansoure, H.-H. Yu, T. Chen, S.-W. Kuo, *Chem. Commun.* **2019**, *55*, 14890–14893.

[441] K. Tanaka, D. Fujimoto, T. Oeser, H. Irngartinger, F. Toda, *Chem. Commun.* **2000**, 413–414.

[442] F. M. Amombo Noa, S. A. Bourne, L. R. Nassimbeni, *Cryst. Growth Des.* **2015**, *15*, 3271–3279.

[443] A. Loudet, K. Burgess, *Chem. Rev.* **2007**, *107*, 4891–4932.

[444] H. Yang, M. Li, C. Li, Q. Luo, M.-Q. Zhu, H. Tian, W.-H. Zhu, *Angew. Chem. Int. Ed.* **2020**, *59*, 8560–8570; *Angew. Chem.* **2020**, *132*, 8638–8648.

[445] H. Rosen, S. J. Klebanoff, *J. Biol. Chem.* **1977**, *252*, 4803–4810.

[446] J. A. S. Cavaleiro, H. Gorner, P. S. S. Lacerda, J. G. MacDonald, G. Mark, M. G. P. M. S. Neves, R. S. Nohr, H.-P. Schuchmann, C. von Sonntag, A. C. Tomé, *J. Photochem. Photobiol. A* **2001**, *144*, 131–140.

[447] Z. Melissari, H. C. Sample, B. Twamlet, R. M. Williams, M. O. Senge, *ChemPhotoChem* **2020**, *4*, 601–611.

[448] a) in *Saint*, Version 8.37a ed., Bruker AXS, Inc., Madison, WI, **2013**; b) in *SADABS*, version 2016/2 ed., Bruker AXS, Inc, Madison, WI,, **2014**; c) in *APEX3*, Version 2016.9-0 ed., Bruker AXS, Inc., Madison, WI, **2016**.

[449] G. Sheldrick, *Acta Cryst. Sect. A* **2015**, *71*, 3–8.